JOURNAL AerospaceLab

ONERA
THE FRENCH AEROSPACE LAB

return on innovation

Issue 7
June 2014

DOI : 10.12762/2014.AL07

Aeroacoustics

Publisher
Pierre Touboul

Editor in Chief
Alain Appriou

Editorial Board
Alain Appriou
Philippe Bidaud
Alain Merlen
Pierre Touboul

Production
Onera Scientific
Information Department

On line
www.aerospacelab-journal.com
Webmaster Onera

Contact
E-mail: aerospacelab@onera.fr

Produced by
Onera - BP 72
29 avenue de la Division Leclerc
92322 Châtillon CEDEX
France
www.onera.fr

ISSN: 2107-6596

Aeroacoustics: an Overview for Air Vehicle Applications

D. Gély
Head of the Aeroacoustics Research Unit
CFD and Aeroacoustics Department, Deputy Director

L. Leylekian
Director of the Iroqua Program
CFD and Aeroacoustics Department

DOI : 10.12762/2014.AL07-00

This issue of Aerospace Lab is dedicated to Aeroacoustics, the field of science that deals with sound generated by air flows and possible interaction with solid bodies. As noise issues became a major environmental challenge over the past decades, the aerospace industries have paid great attention to Aeroacoustics for the design of aircraft, as well as helicopters. An environmentally efficient air vehicle offers a competitive advantage. The worldwide air traffic is expected to double every 15 years and the annoyance to the population living in the vicinity of airports should at least remain the same and even decrease in the midterm. In this context, it is obvious that more flights might be allowed if silent aircraft were used instead of noisier aircraft from a former generation.

Reducing aircraft noise is a major component of the environmental policy on air transport. Over the last 30 years, aircraft noise has been dramatically reduced. This great improvement has resulted from combining technological innovations and international policies on aircraft noise.

The International Civil Aviation Organization (ICAO) has enacted more stringent certification limits since its “Chapter 3” in 1977. The current Chapter 4 (applicable as from 2006) involves a stringency of 10 EPNdB. A recent increase in stringency of 7 EPNdB for Chapter 14 (17 EPNdB cumulative to Chapter 3) will be applicable to aircraft submitted for certification after December 2017. These mandatory requirements come moreover within a comprehensive framework of noise reduction strategies known as the so-called “balanced approach”, a resolution adopted in October 2001 that included 4 pillars: noise reduction at the source, operational procedures, land use and planning management, and aircraft operation restrictions.

In order to cope with the corresponding social demand, both the European Commission and its member States – and especially France, which has a strong aerospace industry – launched ambitious research programs on aircraft noise and notably on noise at the source, thus encompassing in-depth aeroacoustics developments. Of course, most of this work has been conducted under strong coordination, through supportive expert networks: X-Noise at the European level (led by Snecma) and Iroqua at the French initiative (led by Onera).

The articles introduced in this issue of Aerospace Lab often describe work performed within these frameworks. Most of them address numerical simulations and the thorough understanding of noise generation, topics which are directly linked to this “noise reduction at the source”, probably the most conventional axis for noise reduction among those promoted by the “balanced approach”.

A variety of noise sources to be reduced

Several noise sources at takeoff or landing are considered: engine, airframe and installation effects. For high-bypass ratio engines, fan noise has been identified as a major noise source, especially at takeoff, but jet noise again becomes more and more important as fan noise reduction technologies progress. In addition, combustion noise, which is a recent topic as this emerging noise source, is still "inaudible" but would be noticeable when the former sources are mitigated enough. Beyond these sources due to the engines, airframe noise is induced by the turbulence due to the interaction between the aircraft and the flow. Protruding parts, such as the landing gear or high-lift devices, are the major sources of such an airframe noise. Last, forthcoming aircraft or engine architectures could lead to new noise sources. It is a well-known issue for Open Rotors, which are often thought of (and feared) in this regard.

All of these noise components differ by their features, in terms of frequency range and directivity. They are possibly modified by some strong interactions known as "installation effects": for instance, jet noise sources are modified by the presence of the wing or by the fuselage. Acoustic propagation is also affected by reflection and diffraction on these surfaces. If well-used, these effects could be advantageously used for shielding but, on the contrary, they can lead to noise reinforcement.

As is often the case, the ability to derive some reduction technologies for such a wealth of sources stemmed from actual progress in the basic understanding of the phenomena. Therefore, many problems were initially addressed by aeroacoustics through analytical or semi-analytical techniques. As illustrated by some articles in this issue of Aerospace Lab, this tradition is still alive and useful, not only for the advancement of science, i.e., for the understanding of basic mechanisms, but also for its ability to provide industry with fast and somehow reliable sizing methods.

High Performance computing, strong numerical and experimental expertise

However, most of the time, analytical derivations are only suitable for "basic" geometries, such as academic cylindrical jets, simplified airfoils representing wings, or cylinders representing landing gear struts. Indeed, with regard to the sophistication of involved physical interactions and with regard to the complex geometries of actual aeronautical parts, aeroacoustics, maybe more than other sciences, greatly resorts to advanced computational techniques. Nowadays, CAA (Computational AeroAcoustics) is commonly used in the industry and in research centers, and CAA combined with CFD (Computational Fluid Dynamics) is the key tool for accurate acoustic simulations. Thus, the articles presented hereafter strongly insist on particular numerical issues, specific numerical schemes, dissipation and dispersion, new meshing techniques, or innovative formulations for ancient problems.

Comparison with measurements is the second leg required to address the issue of aircraft noise. However, experimental characterization remains essential, either to confirm and drive the numerical simulation or to validate some actual noise reduction technologies. In this domain, France and Europe remain in the lead, with a large set of wind tunnel facilities and especially anechoic wind tunnels dedicated to acoustic tests in the presence of flow. New trends in the experimental domain would be to strive to successfully make simultaneous acoustical and aerodynamic measurements in conventional wind tunnels. This would be a major step, both from a scientific standpoint and from the point of view of competitiveness: scientifically speaking, it would allow us to record correlated acoustic and aerodynamic measurements, paving the way for a better validation of numerical simulations. For industry, it would mean shorter, swifter and cheaper validation processes. In France, Onera is currently working on this new way, through strong developments in de-convolution and de-reverberation techniques.

Aeroacoustics at the crossroad: prospect for integrating engineering and social science

Additionally, regardless of the progress made in the reduction of noise at the source, it is now more and more clearly understood that noise reduction is not only an engineering issue: although dramatic improvements have objectively been achieved over the past 15 years, sensitivity to noise and the related annoyance have increased, at least in Europe, thus triggering a huge amount of work on perception, non-acoustical factors assigned to noise and psychoacoustics.

A new synergetic approach would be to bring these perceptive approaches closer to the technological methods, for instance to precisely determine which patterns or features of noisy events are considered as really annoying, how they are related to physical noise sources and how to deal with them within a genuine acoustic design process. The aviation industry cannot economize on sound design.

These new multidisciplinary ways to address noise issues, beyond aeroacoustics, are also addressed by dedicated French and European experts and especially within the aforementioned networks, X Noise and Iroqua. They may be worthy of being discussed in a future issue of Aerospace Lab ■

L. Leylekian
(Onera)
M. Lebrun [1]
(Aircelle)
P. Lempereur
(Airbus)

E-mail : laurent.leylekian@onera.fr

DOI : 10.12762/2014.AL07-01

An overview of aircraft noise reduction technologies

The aim of this article is to provide a broad overview of current and future noise reduction technologies used in aircraft industries. It starts by recalling the regulation framework and the European incentives that have triggered efforts in this domain, as well as the major dedicated EU research programs. Then, technologies are introduced in four parts: engine nacelle, fan, jet and exhaust technologies and finally the airframe noise. The article concludes by giving some indications about the present capacity of these technologies to meet the noise reduction requirements and future trends to improve them.

Introduction

This paper is aimed at providing an updated outlook on aircraft noise reduction technologies. However, these technologies are not to be considered alone. They are not add-ons or gadgets that can be plugged into given aircraft architectures irrespective of any regulation context. On the contrary, they have arisen as output from a continuous effort intended to give the most suitable response to a vast regulation framework and high community expectations.

In this paper, we will first provide an outlook on the existing regulations and recommendations, focusing on the International Civil Aircraft Organization's (ICAO) balanced approach. Therefore, we will explain how industrial countries or regional blocks, such as the European Union, initiated comprehensive programs that encourage aerospace industries and related research centers to develop innovative parts or subsets leading to low noise aircraft. Then, we will detail these technologies, starting by the engine and nacelles – which have traditionally been associated with noise issues in people's mind – and ending with the airframe, which up until recently was not thought to be a major noise source, though it is the case in modern aircraft. The paper concludes by giving some clues about future trends, such as open rotors or/and flying wings and their expected performances with regard to these very significant noise issues.

Contextual regulations and recommendations

Aircraft noise has become, at least in Europe, a major concern for communities around airports. This concern has led to great societal pressure on policy-makers, thus giving rise to stacked legislations and regulations at various levels. In Europe, two directives address noise issues, the first from a general standpoint [1] and the second one specifically in regard to noise-related operating restrictions at community airports [2].

Both of these EC directives refer to notions that are now commonly handled by the aerospace industries – such as noise mapping, L_{den} or dose-response curves [3] – but they are also based on the famous "balanced approach" popularized in the fall of 2001 by the 33rd General Assembly of the ICAO [4]. This so-called balanced approach establishes that the reduction of perceived noise and of the subsequent annoyance should stem from advances in Air Traffic Management and land-use policies around airports, but also on technologies aimed at lowering the noise at the source, i.e., on aircraft. This incentive came with more mandatory policies – such as the progressive hardening of certification procedures – the famous successive "chapters" of Appendix 16 to the Convention on International Civil Aviation [5].

ICAO's regulations and local policies

As a matter of fact, "Chapter 2" of ICAO's Annex 16 was superseded by Chapter 3, which became mandatory for new design in 1978 and by Chapter 4, which became mandatory for new design in 2006. As an outcome, "Chapter 2" aircraft were completely phased-out in developed countries as early as April 2002, but some Chapter 3 aircraft are still in operation. Currently, Chapter 3 defines the maximum effectively-perceived noise levels (in EPNdB) for approach, take-off / sideline and take-off / cutback depending on the maximum take-off weight of airplanes. Basically, Chapter 4 has implemented the additional requirement of achieving a 10 dB cumulative margin – i.e., on the sum of the three certification measurements – compared to Chapter 3. This provision associates to the increased stringency some flexibility in the way to achieve the noise reduction, for instance

[1] Maxime LEBRUN was head of the Snecma Acoustics Department at the time when this paper was starting to be written

more substantial noise reduction under take-off conditions than on approach. It is worth noting that this stringency will be further reinforced, since ICAO adopted the new "Chapter 14", which will become mandatory for new design on the 31st of December 2017 and which will demand future aircraft to prove a 17 dB cumulative margin compared to Chapter 3 [6].

These global regulatory requirements are even strengthened by some local airport rules, such as noise exposure limits, noise charges, curfews, operating quotas, operational noise limits, restrictions on Chapter 3 aircraft, noise abatement procedures and preferential runways. In this regard, the famous "Quota Count" system enforced in London airports is one of the most stringent and surely the most critical for large airplanes, considering the importance of this international hub [7, 8]. In this system, aircraft are ranked in eight 3 EPNdB-span noise categories. For each category, the quota count doubles according to the following table. The critical point is that this classification is applicable irrespective of the aircraft take-off weight (TOW).

Cat. (dB)	<84	84 to 87	87 to 90	90 to 93	93 to 96	96 to 99	99 to 102	>102
Weight	0	0.25	0.5	1	2	4	8	16

Table 1 : Noise category according to the British "Quota Count" system

Aircraft are then sorted according to these categories, both at departure (averaged at sideline and cutback) and arrival (referring to the certified approach noise level). Since London airports have yearly revised operating quotas, airlines are strongly urged to use low-quota aircraft. This has led aircraft manufacturers to prioritize noise concerns in their design and the most significant example is the Airbus A380, whose design has achieved QC/0.5 at arrival and QC/2 at departure, whereas Boeing B747 achieves QC/2 and QC/4 under the same respective conditions. Since the operation of QC/4 and above airplanes is not allowed at nighttime, there is a strong incentive to use low QC aircraft when operating at all three of the London airports.

EU recommendations and technical agenda

Each of the aforementioned regulations triggered an ongoing effort by aircraft and engine manufacturers and by their associated research centers to define and follow a path toward more silent aircraft. This ambition was concretized by explicit targets set forth in 2001 (published in 2002) by the Advisory Council for Aeronautics Research in Europe (ACARE) [9] and regularly updated since then [10,11]. These targets were endorsed by the official European bodies and especially by the European Commission: its political demand to lower by half the noise stemming from civil aviation was finally given a more technical wording, i.e., to achieve between 2000 and 2020 a 10 dB reduction in the noise perceived by the community per plane and per operation (take-off and landing) (see figure 1).

This clear and widely shared expectation pushed the European Commission, as well as national agencies, to upgrade support for various technological research projects. In particular the European Commission fostered a great number of projects through its successive Framework Research Programs (FP) [12].

In fact, several Level 1 projects – so-called "technological bricks" – were granted to address various technological challenges related to aircraft noise reduction, for various specific devices or technologies, or to achieve a better understanding of their underlying physical mechanisms. For instance, projects such as TEENI [13], FLOCON [14], TIMPAN, LAGOON [15, 16] or COJEN [17] respectively addressed Turboshaft Engine Exhaust noise, Flow Control for Fan Broadband Noise, Landing Gear and High Lift Devices Airframe Noise or Jet noise. A good review of these projects and of the associated progress is provided by the X-Noise network [12]. For the sake of simplicity, these technological bricks are often split and referred to as NRT1 and NRT2 (first and second generation Noise Reduction Technologies respectively), according to whether they are able to reach TRL 6 before 2010 or between 2010 and 2020.

Moreover, these kinds of component-oriented projects are still supported and carried out but they have been superseded since 2001 by demonstration platforms and integrated programs aimed at synthesizing the advances made on individual components. Silencer was the first of these programs and was then followed by Openair [18] and CleanSky [19].

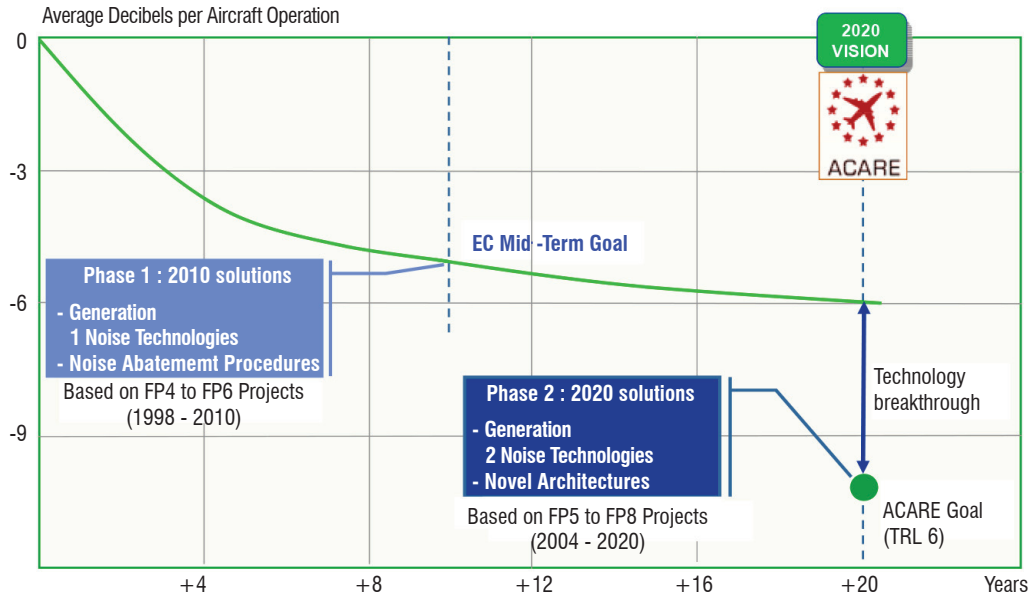

Figure 1 - Expected advances on noise reduction with NRT1 and NRT2, as well as the Noise Abatement Procedure [21]

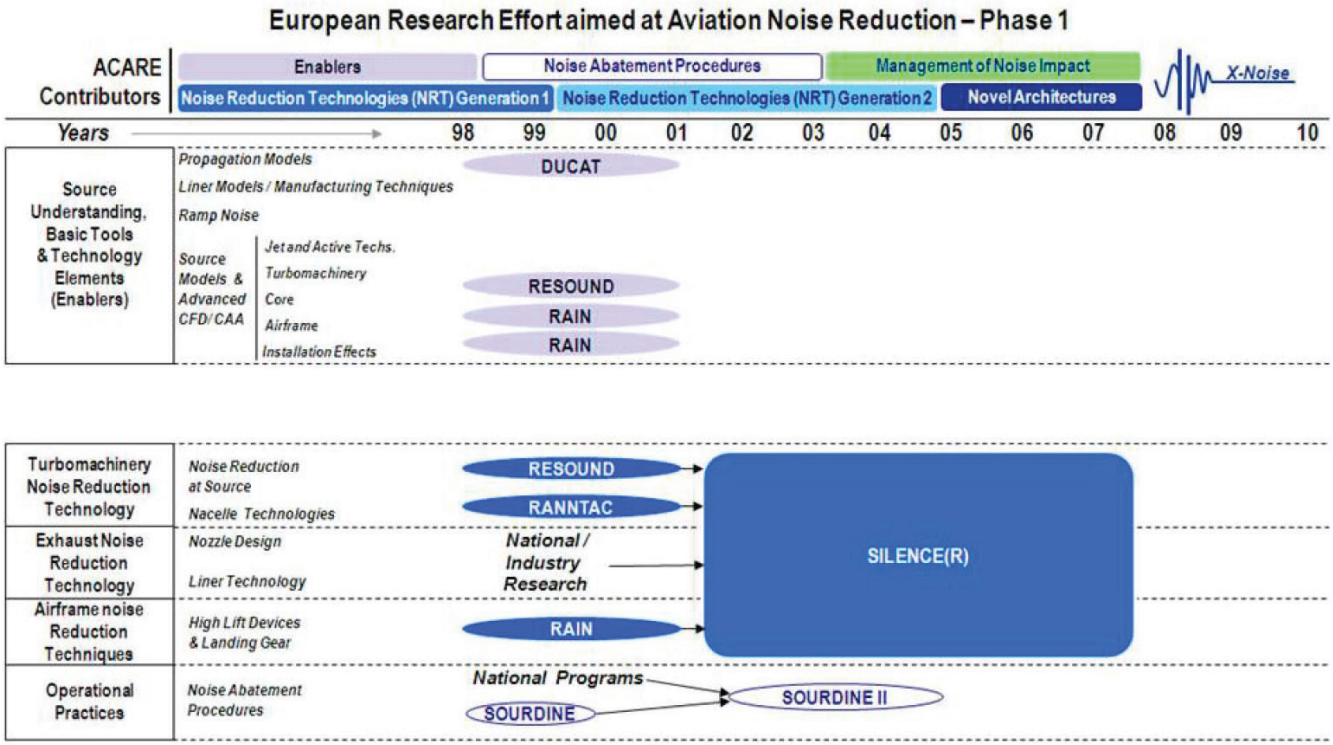

Figure 2 - European Research Effort aimed at Aviation Noise Reduction – Phase 1 [21]

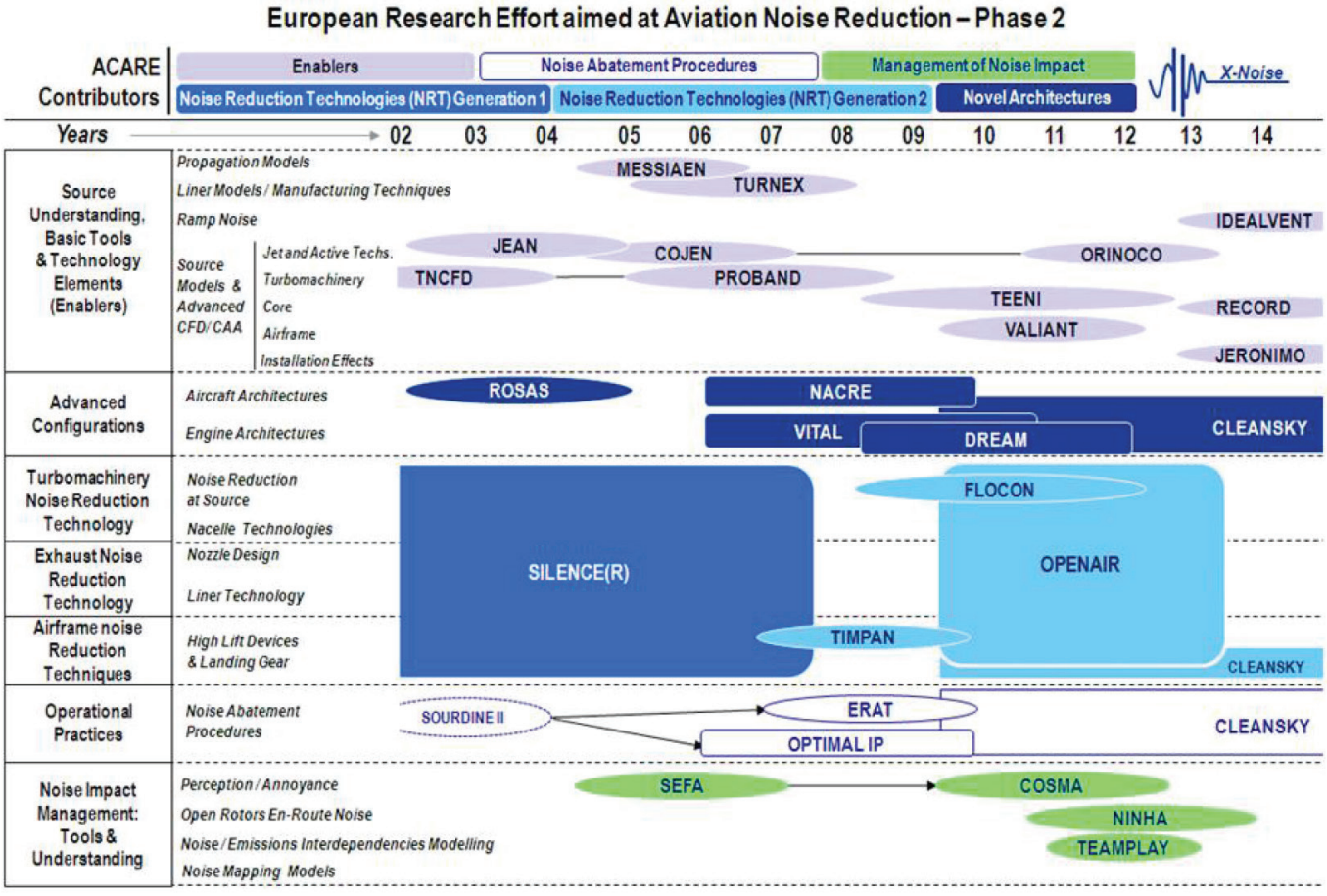

Figure 3 - European Research Effort aimed at Aviation Noise Reduction including Noise impact Management – Phase 2 [21]

A glimpse of such research programs at the European level is provided by the figures 2 and 3, which classify them by addressed technology streams and by year. The two most noteworthy differences between these two charts, which do not address the same time span, is the emergence of new categories dealing with "advanced configurations" on the one hand and "noise impact management" on the other hand. It clearly illustrates the extent to which the integration of various technologies into single platforms is an issue by itself and to what extent aircraft noise is now dealt with not only as a technological issue, but also as a perceptive one.

Beyond programmatic details, one can notice that both the 2020 ACARE horizon and the 2017 ICAO cut-off date more or less fit very concrete industrial milestones, at least in Europe: the development of the A350, a new long-range aircraft and of the A320 single aisle aircraft family with a New Engine Option (NEO), such as the CFMI LEAP1A. However, the entry into service of these two families of aircraft is foreseen between 2015 and 2016. Therefore, in the following parts of this article, we will often refer to this so-called "reference configuration" – to discriminate between NRT1, which will probably be embedded therein, and the most advanced NRT2 technologies that will not.

In this article, we will give a wide overview of NRT1 and NRT2 technologies, classified by components – such as nacelle, engine or airframe – as well as an assessment of their respective benefits. As an outcome, we will also recapitulate the overall gain stemming from all of these technologies – whether NRT1 or NRT2 – and from the associated Noise Abatement Procedures (NAP) compared to the Acare target. Finally, we will conclude by giving some trends about the current research aimed at providing more advanced technologies and solutions for low-noise architectures beyond 2020.

NRT1 and NRT2 technologies

It is well-known that most noise reduction achievements have been made so far by reducing the jet noise. In comparison to aircraft dating back to the 70s, current engines display a dramatically increased bypass ratio (BPR), up to 10-12. This means that most of the thrust is currently due to the moderately-compressed secondary flow. As a result, the jet noise, which fits a strong power law with the jet velocity $(\sim v_{thrust}^{\ 8})$, has been dramatically reduced. Therefore, previously minor noise sources, such as the tonal and broadband components of fan noise, have become comparable to – and now may overtake – the residual jet noise even at take-off. More precisely, the larger the fan, the stronger this noise source, since it stems from various phenomena, all correlated to this fan size [20] :

- interactions of the rotor fan blade-tip with the turbulent boundary layer on the inlet-duct, (rotor boundary layer interaction noise) ;
- turbulent eddies convected in the rotor boundary layer with the rotor trailing edge (rotor self-noise) ;
- interactions between the rotor wake and the downstream outlet guide vanes (OGV interaction noise) ;
- Turbulent eddies convected in the vane boundary layer and the vane trailing edge (OGV self-noise).

On the other hand, during the landing phase, the engine regime decreases so that the airframe noise becomes comparable to – or sometimes dominates – the overall remaining engine noise. Among its various contributors, landing gear on the one hand and flaps and slats on the other hand are predominant (see figure 4).

Beyond those remarks on the relative weight of each contributor, it is commonly admitted that the process of correlative noise reduction with BPR increase will probably come to an end in the forthcoming years: the nacelles, so far considered as a major support of turbomachinery noise reduction through acoustic liners, would become so large and so heavy that they generate both a spurious drag and an unbearable additional weight, therefore annihilating the possible gains in both consumption and noise. Consequently, the nacelles of Ultra High Bypass Ratio (UHBR) engines are to be considerably reduced in length and volume, leading to a dramatic reduction of potential turbomachinery noise absorption by acoustic liners and making the noise produced by the fan system and the jet mixing much more sensitive to the flow around the aircraft (detrimental installation effects).

In between, as shown by figure 5, present turbofans, future Ultra High Bypass Ratio (UHBR) and Open Rotors (OR) [23].

Nacelles

In order to lighten the nacelle, aerospace industries are currently trying to shorten it both upstream and downstream. Therefore the fan noise and other internal noises are less absorbed by shortened nacelle ducts and various technologies are considered to limit this drawback.

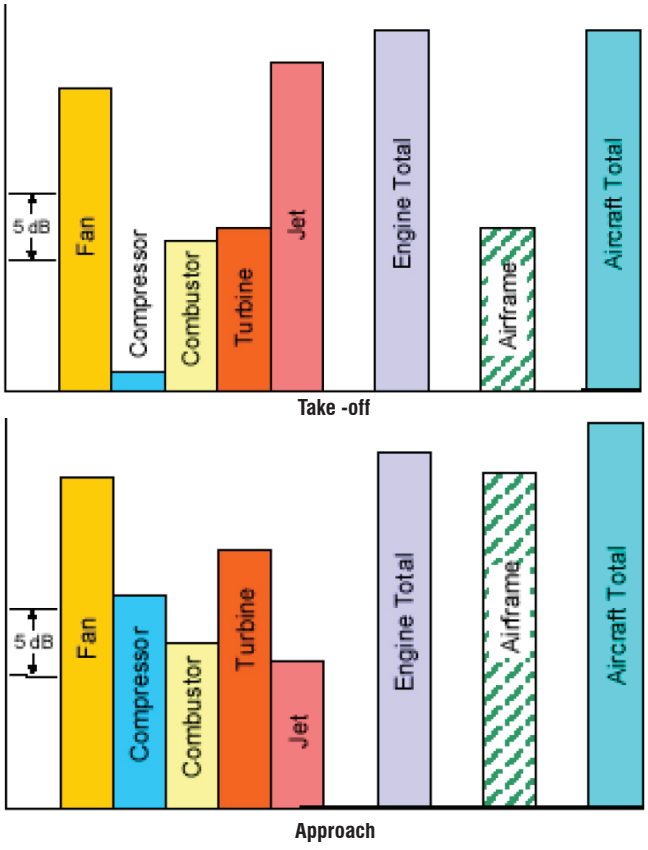

Figure 4 - Relative weights of noise sources at take-of and landing according to [22]

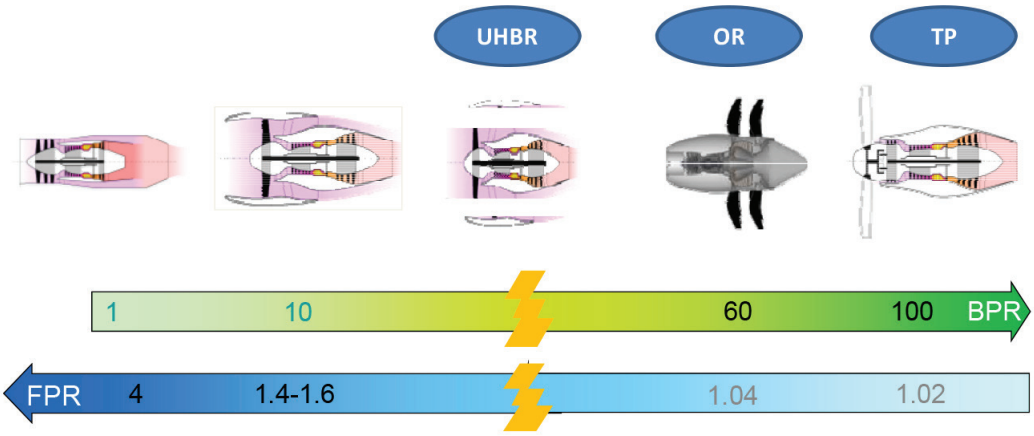

Figure 5 - BPR and FPR (Fan Pressure ratio) from simple flux turbojets to turboprops (TP)

As a first trend, further optimization of noise absorbers – the so-called "liners" – is considered. Currently, those materials consist of classical honeycombs, where the outer plate is porous or perforated as illustrated by figure 6. Basically, these liners behave like Helmholtz resonators, i.e., they allow noise to be reduced within an optimized frequency range. Therefore, they are well suited to fan noise, which is basically a tonal noise. Quite often, superimposed layers or such liners – called "2 degrees of freedom" (2DOF) or even "3 degrees of freedom" (3DOF) – are used in order to broaden the absorption frequency range.

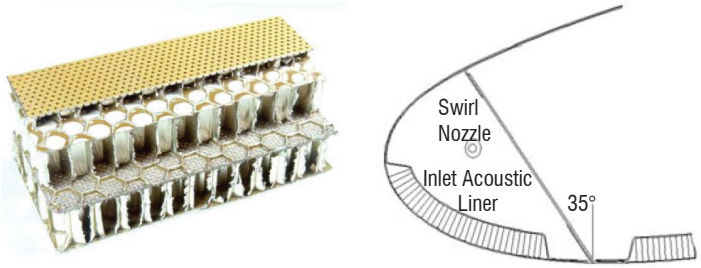

Figure 6 - A 3 DOF Honeycomb liner sample (left) and a sketch of extended lip treatment (right)

Lip treatments

Optimization could mean an extension of the surfaces treated with such absorbers. More precisely, computations and experiments have proven that treating up to the inlet lip is quite efficient. However, this ambition challenges the current concept of the nacelle, since this zone is used for de-icing and since de-icing techniques and noise techniques are not necessarily compatible [24]. Currently, there are two kinds of de-icing techniques, which can be either pneumatic (hot air blowing pipes) or thermoelectric. However, intake liners are often made of glass-fiber composites, i.e., insulating materials. Two kinds of technologies are currently under study to overcome this compatibility issue, pneumatic (hot air blowing pipes are the conventional technology on most of current aircraft) or thermoelectric. An acoustically treated lip technology integrating a pneumatic anti-ice system has been developed and its efficiency has been shown at full scale by in-flight experiments on an A380. A lip acoustic lining technology compatible with thermoelectric anti-ice systems is still a very low TRL.

Smart liner distribution

Beyond the lip treatment, much expectation also arises from smarter liners or smarter liner distribution. For instance, current air intake treatments are usually split by longitudinal splices bordering separate treated parts. This technological limitation entailed sharp azimuthal variations within the acoustical impedance of the intake and thus limited acoustical performance, especially when facing shock waves generated by the fan tip leading edge at transonic speed. Some "zero-splice" liners [28] (figure 7) have been developed and used for the first time on the Airbus A380 and they are being used on the new A350 XWB, on the SSJ100 and will be available on the new Silvercrest engine. The challenges lie in the very accurate design and production processes required just in front of the fan, in order to keep the 0-splice benefit available.

Figure 7 - True zero-spliced liners as tested (left) and mounted on the A380 (right) from [28] ; reprinted by permission of the American Intitute of Aeronautics and Astronautics Inc.

To move forward, it is now envisaged to use more finely-tuned liners in order to optimize the absorption process [24] (figure 8). More precisely, some work is currently being carried out to modulate the liner inner thickness along the intake. This modulation must be computed to optimize the impedance matching, as long as the acoustic wave gets out of the intake. This concept borders another one that considers sophisticated impedance distributions. Ideally, such smart distributions would favor acoustic modes with an upward directivity, in order to spare the community. This concept is aimed at achieving the same goal as the so-called negatively-scarfed air intake, i.e., orienting outgoing waves toward the sky. Though quite old, these ideas remain up to now at TRL6 in the case of the first one and at lower TRL for the other and have not led yet to an industrial design.

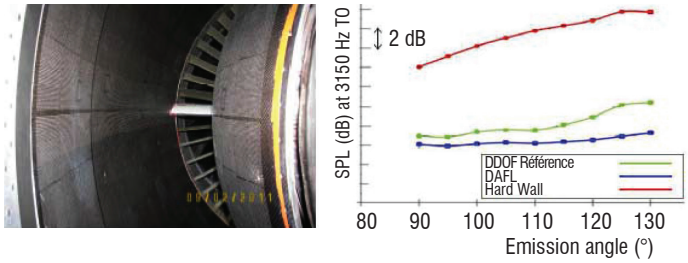

Figure 8 - Distributed Aft Fan Liners and their dramatic effects on noise reduction as tested in [24]; reprinted by permission of Snecma.

Fan noise

Although nacelle technologies may be seen as external devices to treat the fan noise (and the core noise too), some technologies are also being developed for the fan components themselves. However, these parts are directly involved in the thermodynamic processes ruling the efficiency and the consumption of the engine. Therefore, any optimization of the fan components will be will first and foremost assessed in this last regard. Moreover, little information is publicly disclosed by engine manufacturers on the implementation of these inner technologies, since they directly challenge their competitiveness.

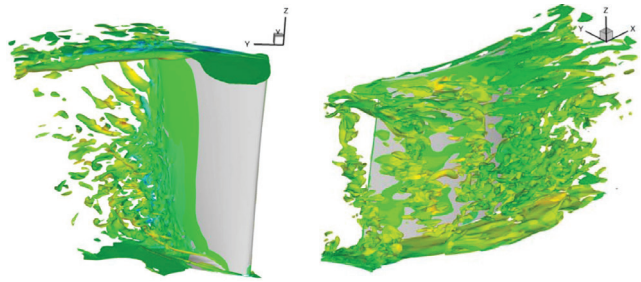

Figure 9 - LES-computed isosurfaces of the axial component of vorticity on rotor (left) and stator (right) blades [20]

Shape optimization and other passive technologies

As previously mentioned, rotating parts generate two kinds of noise, i.e., self-noises and interaction noises, both of which are enhanced when the rotation speed increases: fan broadband noise is proportional to $u_{tip}^{5/2}$ [20]. Basically, two general strategies are being experimented with to reduce fan noise : attempting to optimize the blades, or to directly act on the air flow. Generally, the first technological route does not use liners or absorbing materials because their implementation on 3D rotating parts is quite delicate and challenges their structural properties.

Thus, the actual challenge is rather to optimize the 3D blade shape. Through this route, engine efficiency is expected to be optimized over a wide range of regimes. Geometries stemming from this kind of trade-off provide good results at cruise and take-off conditions, when aero performance is crucial, but they suffer some drawbacks on approach, hence affecting the noise performance under this latter condition. Several works are still under investigation to address this issue, but most of them remain confidential since any step forward in this technical domain could provide decisive advantages to manufacturers in the commercial competition.

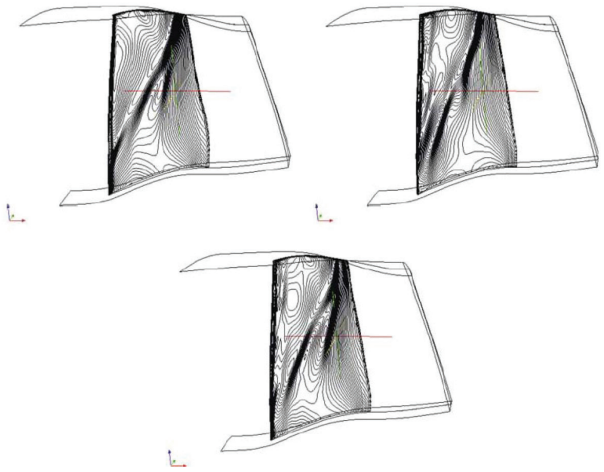

Figure 10 - Suction side density contours of variously-optimized blades: initial geometry (left), aerodynamic optimization (center), and aeromechanical optimization [25]

Another well-explored way to reduce the fan noise is to regularize the air flow and to reduce its velocity. This is especially important for large fans, since the blade tip velocity could become transonic. To reduce this speed, fans can be de-coupled from the primary shaft with the help of gearboxes. This solution has, for instance, been used on the Pratt & Withney PW1100G, whereas it has not been implemented on the CFM LEAP-1A, though both were designed for single aisle midrange aircraft such as the Airbus A320. The choice is strategic and has led to different optimized solutions where weight, temperature and low pressure turbine performance are key parameters. Finally, there are different sizes of engines: the PW1100G measures 2.057 m, whereas the Leap-1A measures only 1.981m. The blade tip speeds are respectively 60m/s using the gearbox and 75m/s in direct drive. One can thus say that one company chose to push conventional technologies up to their limits, whereas the other preferred to integrate a new optimized component. The trade-off between the two solutions may be carefully assessed, since the additional gearbox also induces and increased weight. This remark applies to any additional technology. For instance, for the same sake of optimizing the air flow through optimal pressure conditions, Pratt & Withney tested Variable Area Fan Nozzle (VAFN), i.e., sliding flaps that focus on pressure discharge, versus the regime downstream of the fan. Although the manufacturer claims some genuine performance gain, it avoided implementing this technology on the PW1100G family, probably because of the increased weight and complexity that it would have induced [26].

Beside this effort, some attempts have also been made to reduce the fan noise downstream, through liners. Past endeavors to implement porous materials on OGV did not show any evidence of actual benefit. However, recent experimental tests made with carefully-computed Distributed Aft Fan Liners (DAFL) in the secondary duct of a full scale demonstrator achieved very significant noise reduction [24]. According to the data presented, the aft fan broadband noise reduction was of up to 5 dB and important blade passing frequency tonal noise almost completely disappeared. It is still unclear whether this performance stems from standard absorption processes, or from more subtle modal redistribution mechanisms.

Active stators

A longstanding effort has also been conducted to reduce the fan noise - both forward and rearward - through active devices. The idea is basically the same as that in any feedback loop, i.e., measuring the residual signal and acting in order to nullify the latter. Thus, the technology requires measurement microphones, or sensors, and speakers, or actuators. Efforts regarding these technologies were made within national and European programs. Low TRL advances achieved, for instance, in EU-funded programs such as RANTAC or RESOUND, led to integrations attempts in SILENCER and OPENAIR [27].

Two competing technologies tested in SILENCER used inlet wall-mounted and OGV-integrated actuators respectively. It is worth noting that SILENCER tests were performed on a large-scale mockup at the RACE and ANECOM anechoic fan noise facilities. In addition to this program, it appears that active stator technology with OGV-integrated actuators is better suited, both because their presence does not affect the passive liners that can be implemented additionally and because their intrinsic efficiency is higher since they are closer to the noise source.

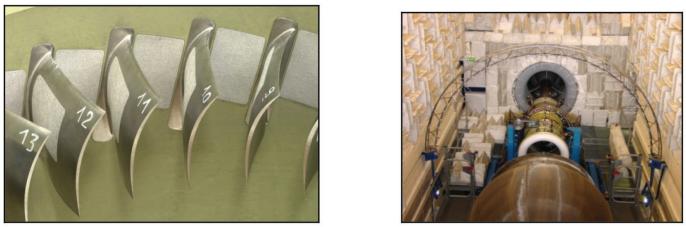

Figure 11 - Active fan stator and 3D measurement fitted with Piezo Actuator System on and between blades at the RACE Anechoic Facility [21]

These preliminary integration works have been extensively continued in OPENAIR with a special focus on the most significant fan contribution, i.e., its rearward noise (whereas SILENCER focused on the forward noise). At the beginning of OPENAIR, the project was aimed at reaching TRL 5 for this technology. Currently, it reaches only TRL 4 because of both severe integration issues and limited achievements in related control and signal processing. Moreover, some related issues arise, such as the energy supply for these devices and trade-off considerations for balancing rearward and forward noise reduction. However, the proven benefits of these active stator technologies are significant enough to pursue the effort in forthcoming research programs [21].

New engine architectures

Beyond these local improvements, some attempts have been made to experiment far more dramatic modifications of the engine architectures. Preliminary studies to probe various technologies have already been conducted, or are being conducted, both for Ultra High Bypass Ratio engines and for Open Rotors. These two technological tracks are both presumed to lower fuel consumption and to reduce noise emission (at least jet noise, since tonal noise may dramatically increase for Open Rotors).

For instance, from 2008 to 2011, within the DREAM project (EC 7th framework program), preliminary campaigns were led to compare noise measurements and numerical simulations on some Open Rotor configurations. Computational Fluid Dynamic (CFD) and Computational AeroAcoustics (CAA) made by Onera (France) appeared to be in good agreement with the measurements performed by Tsagi (Russia) [29, 30].

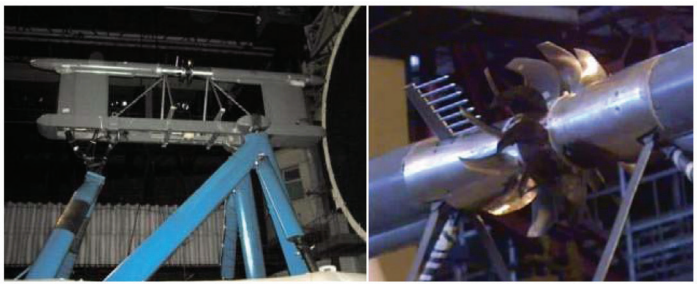

Figure 12 - VP107 test vehicles in TsAGI T104 low speed wind tunnel. The mock-up is a 0.6373 m diameter propeller at model scale with 12 blades on the front propeller and 10 on the rear one [29]

Extensions of these works are now conducted within the CleanSky Framework: In France for instance, Snecma's Hera test vehicle underwent preliminary testing in Onera's S1 wind tunnel in July 2013. Full-scale propeller tests are expected in 2015.

Figure 13 - Snecma's Hera test vehicle mounted in Onera's S1 wind tunnel facility

Further new technological research programs have already been launched. Especially, it is worth mentioning COBRA, a new EU-Russia cooperation program that started in October 2013 and that is considered as the continuation of VITAL and DREAM. Actually, COBRA is dedicated to the consolidation of Ultra High Bypass Ration (UHBR) ContraRotating TurboFan (CRTF) that was once explored by Kuznetsov – one of the Russian partners – in the early 90s and further explored within VITAL. CRTFs associate two contrarotating fans in a nacelle and thus appear as a kind of hybrid between turbofans and Open Rotors.

CRTFs envisaged by COBRA strongly differ from those experimented with within the VITAL program and by the Russian engine manufacturer. Kuznetsov's NK-93 (BPR $\sim$ 16.5) depicted in the picture above highlight the good behavior in term of performance of this concept,

but the design was made over more than 20 years ago without the current computational tools and free from present environmental constraints. At the time being indeed, first NK-93 full scale tests showed that noise performances of such UHBR CRTFs were not so bad and that the combustion chamber has been up to now one of the most efficient among the Russian ones. Compared to VITAL, COBRA plans to explore a higher bypass ratio (BPR ~ 11 within VITAL) with the obligation to use a gear box in order to reduce the fan speed. This reduction will directly impact the tip velocity and thus will allow the fan noise to be reduced. Within the COBRA project, the BPR investigated is from 15 up to 25, according to the detailed specifications proposed by the partners in charge of this activity (Snecma and Kuznetsov). A specific conception/optimization will be proposed by European research centers (Onera and DLR) and by Russian partners (CIAM, Kuznetsov, AEROSILA and MIPT). Both designs will be manufactured by COMOTI and tested at CIAM's C3-A test rig facility.

Jet noise and nozzle exhaust technologies

Though jet noise has been significantly reduced within double flux engines, it remains an important source of noise, especially at take-off. Towards the end of the 20th century, new momentum was given to research aimed at its reduction, especially through US programs. Phases 1 (2000-2005) and 2 (2005-2010) of the Quiet Technology Demonstrator Program gave evidence that the so-called chevrons lead to some jet noise reduction [32].

Chevrons

Chevrons are geometrical corrugations of the cylindrical exhaust of either the primary jet (core chevrons) or the secondary one (fan chevrons). The detailed mechanisms through which chevrons act are still under investigation. Actually, there is evidence that several mechanisms may contribute to the efficiency of this kind of device and that these mechanisms are strongly affected by the chevron geometry. For instance, core chevrons are directed inward with respect to the jet and are known to lower mainly the take-off noise. On the other hand, fan chevrons are generally parallel to the engine axis and reduce shock-cell noise, so they are rather efficient during cruising, when this phenomenon appears [33].

Currently, several computations and experimental works are being carried out to improve the understanding of the impact of chevrons on noise and especially to quantify this impact. However, while current numerical simulations - mostly based on Computational Fluid Dynamic and Acoustic Analogy – can provide qualitative ranking of various geometries, or can lead to a good noise reduction impact, they have not been able to provide reliable absolute noise levels in some cases. This is especially true when considering installation effects, which are now the big challenge for chevron computations. In addition, these effects will become more significant as engine BPR increases and as engines get closer to the wing. Complex effects such as the loss of jet axisymmetry, jet instability and appearance of new noise sources due to jet interaction with the wing or the pylon are then to be taken into consideration.

However, despite their efficiency or the challenges that they entail and though they have actually reached TRL 8-9, chevrons are not always considered as mandatory from the standpoint of end-users and thus they have not been generalized on all engines and all aircraft. Some regulation issues may indeed interfere with the trade-off: Since the chevron can be considered as an optional kit, it can help to achieve few decibels in order to be compliant with the most stringent regulations; for instance, chevrons lead to a 2 EPNdB additional cumulative margin necessary for the A321 to be compliant with Chapter 4. As far as the A320NEO is concerned, the jet noise is sufficiently reduced for chevrons to not achieve a sufficiently large enough global aircraft noise reduction compared with the aero performance penalty that they generate when cruising.

Virtual chevrons

The true reason behind this reluctance to systematically add chevrons is that they are suspected to increase the aircraft overall weight and, above all, they lead to additional drag, which downplay their interest with regard to fuel consumption. Therefore, current research is being conducted to develop what is known as "virtual chevrons", i.e., microjet devices that would blow pressurized air into the main jet and that are supposed to act as physical geometrical chevrons. Most advanced works are now dealing with continuous jets, which are easier to implement, whereas low TRL works are carried out on pulsed jets. In France, these works have been performed through various programs, such as OSCAR, ORINOCO or REBECCA, in connection with European collaborations such as OPENAIR or even with international cooperations with JAXA. However, few results have been published [34, 35].

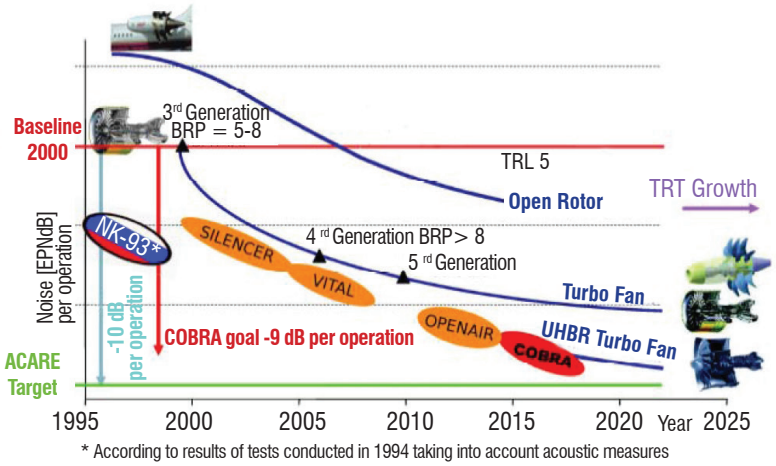

Figure 14 - The 1980 s Kuznetsov NK-93 on a flight test bed (left) and expected position of COBRA's deliveries on a noise roadmap (right)

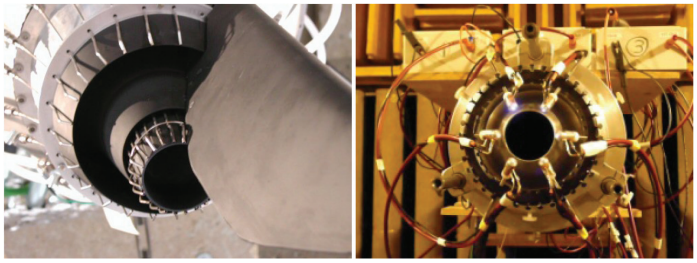

Figure 15 - Double-stream nozzle with continuous microjets at the Martel facility (Poitiers) within the framework of a French-Japanese cooperation (left. A plasma-based pulsed microjet developed at Onera and tested at the Ecole Centrale de Lyon (right)

For continuous microjets, several experiments have been made by various teams, testing rings of several microjets (typically between 10 and 40) obtained with flaps and hatches scooping the main jet. These tests have helped to explore various parametric configurations, varying the number of microjets, the microjet nozzle shape and orientation, the jet mass flow, or its pressure gradient. In particular, a large-scale cooperation between France and Japan within this framework is worth mentioning [36]. This cooperation, involving JAXA and IHI in Japan, and Snecma and Onera in France features a large facility providing experimental simulation of microjets, the STA-R (Système de Technologie Active Réduit). Measurement campaigns performed under various conditions in the Onera's anechoic wind tunnel CEPRA 19 have shown that continuous microjets could lead to nearly 1 EPNdB reduction, even under take-off conditions at Mach 0.3. This reduction effect is measurable from 90 degrees (lateral side of the exhaust nozzle) to 150 degree (i.e., downstream of the jet).

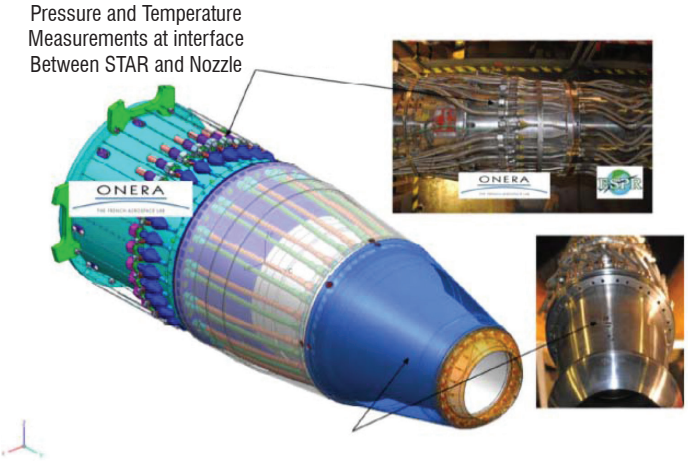

Figure 16 - sketch of the Japanese test rig mounted on the STA-R as described in [36]; reprinted by permission of Nozomi Tanaka.

Additionally, several other integration technologies have been carried out within the Level 2 EU-funded program OpenAir. As for the STA-R, these tests basically showed that the order of magnitude of the overall gain achievable from continuous virtual chevrons is roughly 1 dB, i.e., similar to physical chevrons.

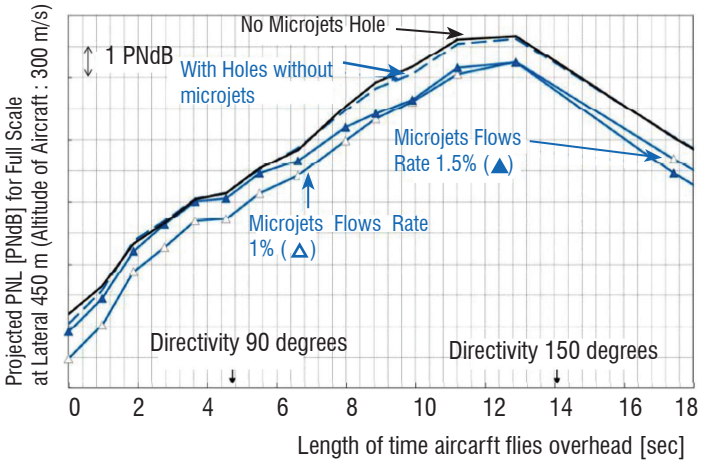

Figure 17 - overall noise reduction with additional microjet flows. According to [36],roughly 1 EPNdB is achievable .

Some complementary work is also being carried out, mainly by research centers, on pulsed jets. This work tends to prove a potential increase of efficiency compared to continuous microjets, though the physical mechanisms are still unclear. What is clear however, is that this expected increased efficiency requires a fine control of the microjet relative phases and frequencies, otherwise spurious additional noises nullify the expected benefit. It is also worth mentioning that both the continuous and the pulsed microjets act on the broadband jet noise and not on its possible tonal components, such as the screech noise. When using pulsed jets, the broadband noise reduction is achieved at the expense of the appearance of a tonal noise. The frequency of this tonal noise is the frequency of the pulsed jets – usually some kilohertz – and care must be taken to ensure that its magnitude does not balance the gain stemming from the broadband noise reduction at a lower frequency.

Airframe

The airframe is the other major source of noise. As for the engine noise, this category may be divided into several subcategories, among which the two main contributors are the landing gear and high-lift devices (HLD) [37]. As could be expected, the larger the plane, the more significant the effect of the landing gear is compared to that of the HLD. For instance, the HLD noise is dominant in regard to airframe noise for an Airbus A320, whereas the landing gear noise is more important for an A380. Therefore, this latter source of noise has been extensively studied and reduced on recent large carriers, especially with regard to the critical Quota Count policy enforced in London. One can even say that, in this regard, the A380 has specifically been designed to comply with this local regulation.

Nowadays, the physical mechanisms leading to landing gear noise are well understood, but remain quite hard to simulate or to lead to reliable quantitative estimations. These noises are due to complex phenomena of boundary layer separation, laminar-to-turbulent boundary layer transition, shear layer transition, laminar separation bubble and associated dynamic effects. Generally speaking, these sources account for some broadband noise, but are usually less noisy than high

intensity tonal noise due to resonating cavities and holes. Though easy to describe with academic geometries, these phenomena could lead to odd behaviors when complex shapes are involved and even more so in the case of interacting bodies. Predicting the overall airframe noise stemming from such geometries usually requires both deep physical analysis and massive computation facilities. A good example of such academic studies addressing both HLD and landing noises is provided by the program VALIANT [38]. However, in parallel with these scientific developments or even in their absence, some technical recipes may be applied to limit the sources of this noise.

Figure 18 - Flow computation in and around a wing-flap gap (left) and a two-strut landing gear (right) as performed in [38]. The computation on the left is a so-called DES computation, whereas the one on the right is a LES computation.

Landing gear

For instance, minimizing landing gear noise often requires the landing gear geometry to be simplified, in order to avoid spurious noise sources or interactions. Many experimental attempts have been performed in this regard, within programs such as RAIN, SILENCER and TIMPAN [39] or LAGOON [15, 16]. The preliminary work achieved in RAIN was conducted on a non-operable mockup that featured complete fairings. Though unrealistic from an industrial point of view, the concept proved to potentially lead to a more than 10 dB reduction over a wide span of frequencies. Work has thus been pursued within SILENCER, with both a nose landing gear (NLG) and a main landing gear (MLG). Tests were performed on A340 1/10 scaled mockups in the German DNW LLF facility and some actual flight tests were also performed at Tarbes (France).

These flight tests just featured “simple” bogie fairings, which allowed a significant overall reduction of 2.0 EPNdB for the landing gear noise and of 0.4 EPNdB for the aircraft as a whole. The tests done in the DNW-LLF facility were performed on more advanced (but non-operational) configurations, both for the NLG and the MLG. These innovations proved to account for a 4.1 EPNdB noise reduction in the LG noise itself and 1.6 EPNdB for the whole aircraft.

Efforts on the landing gear noise have been pursued in TIMPAN and OPENAIR. Since this latter program has not ended yet, a summary of the progress made is not available yet. However, these new programs addressed the possible benefit of splitters between the bogie fairing and the strut. It is expected that such fairing could attenuate

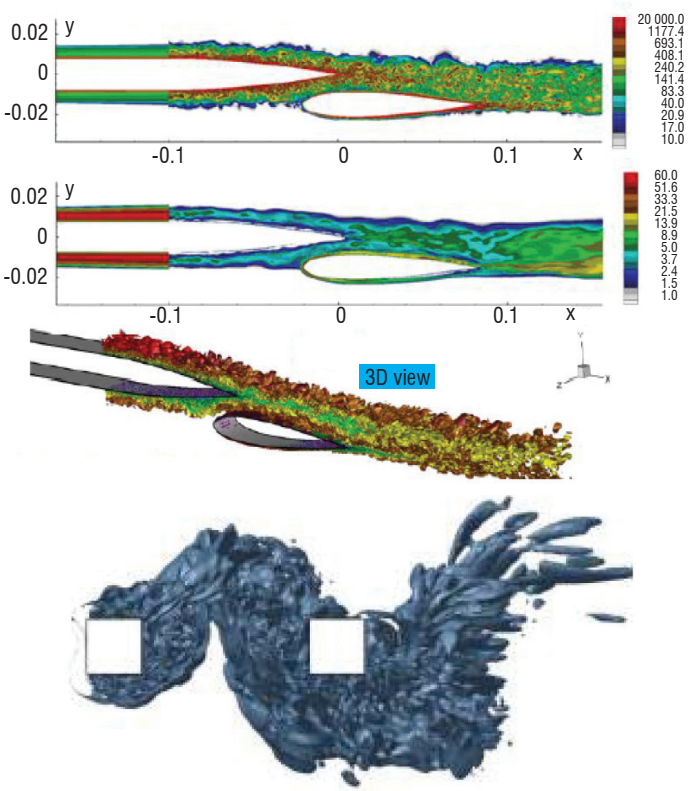

Figure 18 - Flow computation in and around a wing-flap gap (left) and a two-strut landing gear (right) as performed in [38]. The computation on the left is a so-called DES computation, whereas the one on the right is a LES computation.

communication between shear layers, thereby preventing the formation of large scale and noisy vortices. It is even expected to explore such splitters without fairings, the latter being quite unpopular among manufacturers, since they increase the LG weight.

In addition to this research, some technologies have been applied to the most recent aircraft, such as the Airbus A380 or A350: as previously mentioned, caps are used on cavities, for instance on inner and outer hubs, and rims are applied on wheels. Moreover, some smart dressing techniques are used in order to avoid putting cables, wires and accessories in the wake of high flows. It has been shown that this so-called “slow down flow” concept – i.e., putting bodies either in front of the main strut, where flow velocity goes to zero, or behind it in

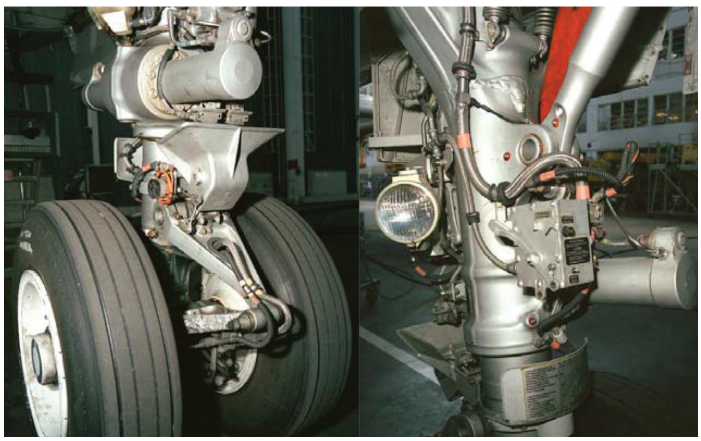

Figure 19 a - An actual landing gear with all its associated devices and commands

Figure 19 b - NLG and MLG fairings tested in SILENCER

the quiet zone – significantly reduce the downstream turbulence and noise. Optimizing this masking technique however requires advanced capacities in simulation, in order to predict, or at least to assess, the interaction between the involved parts and the bluff body and great efforts are currently being made in this regard within OPENAIR. However, caps, rims and the "slow down flow" concept, still enforced today on some modern aircraft, allow the global aircraft noise to be reduced at landing from 1 to 2 EPNdB. Moreover, it is expected that some 0.5 dB more can be gained from specific acoustic techniques, such as plain perforated or even porous fairings, which are now at TRL 5. More probably however, these techniques will be deployed only when absolutely required as, for instance in 2018-2019 for the forthcoming A350-1000, which is aimed at reaching the London QC/0.5 category with the help of such fairings.

High Lift Devices

Compared to landing gear, the progress made on flaps and slats noise reduction appears to be quite less mature. This is mainly due to the fact that known technologies to reduce this noise strongly reduce the lift performance. Currently, at landing, this degradation is so critical that it often forces the aircraft speed to increase, and therefore the regime, so that the expected gain is nullified. In addition to this technical limitation, HLD noise is quite complex to describe and to compute: it involves challenging mechanisms of unsteady vortex recirculation, free shear layer vortex flow reattachment, or edge scattering tone noise. The overall result is a broadband noise with some tonal components, the whole and especially the latter becoming more intense when the angle of attack increases. Overall, the slat component generally dominates in that of the flap and fits a strong power law with the aircraft velocity (v9/2). This slat component is rather rearward and accounts for the tones. On the contrary, flap noise is purely broadband but the flaps also account for strong spurious interactions: For instance, even though little is known about outboard spoiler deflection, these are known to modify the wing circulation and therefore the slat noise. In the same vein, flaps may interact with the wake of the main landing gear to produce a strong low frequency interaction noise [31].

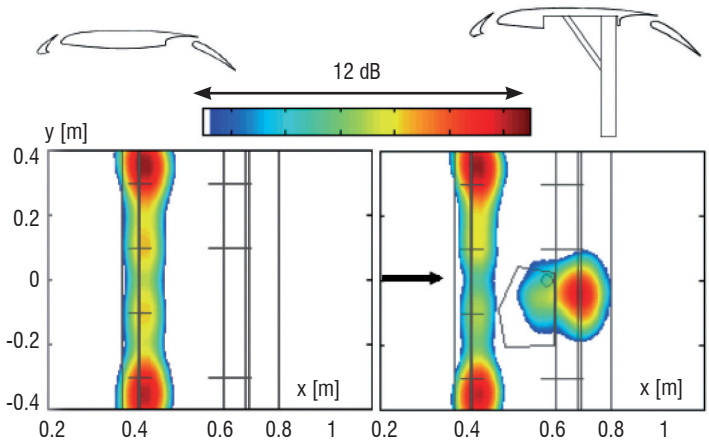

Figure 20 - Gear wake / flap interaction according to [31].

Currently, few technologies are used to limit HLD noise. On the recent A380 and A350, slats are tilted to avoid any gap between them and the wings, so that the flow cannot pass in between. It is quite effective, both from the acoustic and performance standpoints, even though this solution can be applied only on limited parts of the wing.

However, some more advanced solutions are envisaged, among which slat gap optimization or suppression (for instance with inflatable cuffs), HLD edges made of porous materials, slat chevrons or even fractal spoilers are included. All of these solutions have been studied within TIMPAN and are still under investigation within OPENAIR. For instance, slat gap optimization has proven to be neutral from the aerodynamic point of view, but beneficial for acoustics: 2D simulation made in TIMPAN showed that slat noise may be reduced up to 2 EPNdB with this technology. However, the TRL for this technology is currently only 3 and is expected to reach 4 or 5 by the end of OPENAIR.

As for porous materials or fractal edges, or brushed edges, the idea behind these concepts is always the same, i.e., to avoid sudden flow discontinuities. Up to now, however, porous materials have been too brittle to comply with the requested thinness of slat trailing edges and solutions based on grids or metallic meshes are suspected to generate additional tonal noise. Investigations with a Kevlar cloth cover are being continued in OPENAIR, but airworthiness considerations may still hinder this kind of technology in the future. Slat chevrons, i.e., corrugations on their trailing edges, will be experimented with also in OPENAIR, in order to suppress coherent vortex structures in the gap, as well as fractal spoilers to limit or suppress the noise presumably originating from both the spoiler side-edges and the interaction of the turbulent spoiler wake with the downstream flap.

Some much more advanced ideas have been suggested, such as adaptive leading edges (for instance with shape memory alloys or more probably through actuators) that would suppress slat gaps. However, safety concerns, which require traditional slats (in case of rear wind for example) have prevented advanced investigations of the concept up to now.

Globally speaking however, HLD noise reduction technologies are quite recent and substantial progress may be expected even though basic understanding is sometimes still lacking and though noise reduction may conflict with other requirements, such as performance or airworthiness. The table hereafter summarizes expectations in 2007 about these technologies. Though new official assessment is not available, these figures can reasonably be expected to remain true.
Airframe noise component Achievable with previous technologies
Overall gain including TIMPAN concepts.

Airframe noise component	Achievable with previous technologies	Overall gain including TIMPAN concepts
Landing gear	4.0 dB	6.0 dB
High Lift devices	0.2 dB	4.0 dB
Overall airframe noise	1.7 dB	5.0 dB
Overall aircraft noise	N/A	2.5 to 3 dB

Table 2 - expected gains for various devices before and after TIMPAN

Cavity noise

In addition to Landing gear and HLDs, cavities are also a matter of concern for noise. Actually, numerous devices are embedded in the surfaces of aircraft, which have surface irregularities (hatches, hooks, slits, holes) globally termed as "cavities". These cavities usually trigger detachments of the turbulent boundary layer, which act in turn as a noise source.

As for HLD and landing gear, the theoretical way to avoid this spurious noise source is well-known (i.e., basically filling the cavities!) though this harms their operational purpose. Therefore, recipes leading to the reduction of this noise source usually stem from compromises between the operational optimization and noise issues.

Future noise reduction technologies

What will the challenges beyond 2020 be? Previous sections presented different technologies applied, or to be applied, to still conventional engine architectures, i.e., so-called "tube and wings" equipped with turbofans. However, the challenge for reducing fuel consumption is so great that new architectures are requested. As previously mentioned, Ultra High ByPass Ratio engines (UHBR) are being studied, but with very hard integration issues, since the fan diameter is even greater than that presently used. With this option, noise reduction would basically entail pushing the same technologies further than those presented above.

However, it must be kept in mind that new noise sources could emerge from these more "open" engines, especially if traditional ones, such as fan and jet, are lowered. In this case, core machinery noise, such as compressor noise, turbine noise or even combustion noise would need to be considered. Currently, few things are known about these sources, but some preliminary work suggests that they could be more complex than expected. For instance, combustion noise is known to be divided into "direct noise" – i.e., sound directly stemming from the combustion process in the chamber – and "indirect noise", due to the conversion of vortices into sound waves through the turbine stages. "Direct noise" was thought to be more important than "indirect noise", however, a recent study tends to prove the contrary. Investigation work is still underway.

In addition to UHBR, another strategy could also be to continue increasing BPR using the Open Rotor architecture (OR). Noise is then the most critical issue, along with safety: Whereas single propellers radiate mostly tonal noise in the propeller plane, two counter-rotating rotors without nacelle radiate many tones over a wide frequency-range due to complex and intense noise interference mechanisms. Actually, the radiated frequencies combine all of the possible linear combinations between the two blade passing frequencies and this spectrum is propagated in all directions. Ongoing research activities are facing this drawback and several tricks are being investigated to lower this excessive noise: Tuning parameters, such as blades shape, blade length (especially differentiating the length between the first propeller and the second) and the gap between the two propellers, or even their respective rotating speeds or clocking, are among the various methods being experimented with [40]. Currently, there is reasonable confidence that Open Rotors will be able to meet the strictest regulation of Chapter 14 in a few years. From a programmatic standpoint, the main framework for such integrated research is the CleanSky research program, which will allow the engine manufacturer Snecma to produce a demonstrator by the end of the decade. Through this platform, new noise technologies, such as 3D-optimized blade design and pylon blowing in order to strongly reduce the interaction of the pylon wake with the blades, will be demonstrated. Current liner-based technologies will probably be used less, since they are both inefficient and impossible to insert into open architectures.

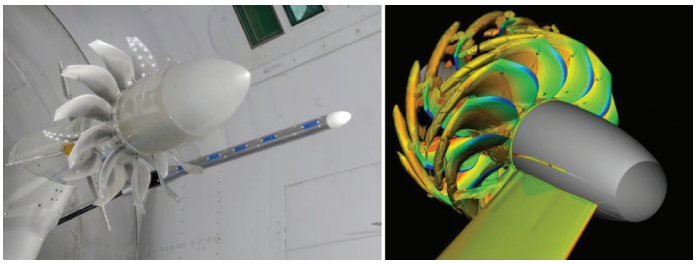

Figure 21 - Open Rotor mounted on Hera vehicle (Snecma) and under test at the S1 Onera wind tunnel and the simulation of interactions between the two propellers (Onera)

It is also worth mentioning that the most recent trends tend to locate these forthcoming Open Rotors rearward, near the empennage, between two vertical stabilizers, both to gain from the masking effect for community and to increase comfort and safety for passengers. Currently, aircraft manufacturers have not yet chosen between the two competitive technologies of UHBR and Open Rotors, but this critical choice is considered as imminent and is likely to arise before 2015. Neither the first nor the second technological route will be sufficient to meet the stringent new objectives defined by ACARE for 2050 [21]. It is generally assumed that though 2020 objectives will be reached through enforcing new Noise Abatement Procedures (NAP) in addition to NRTs, 2050 objectives will require a breakthrough in aircraft architectures.

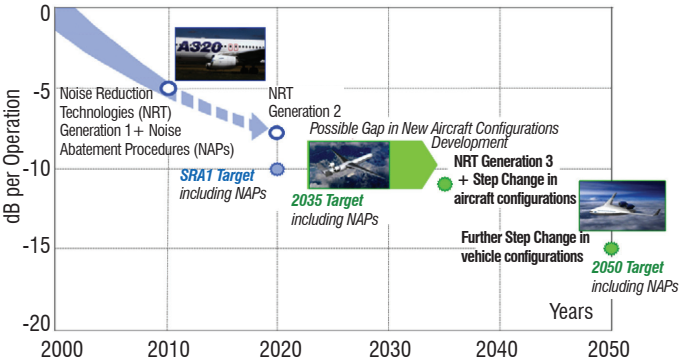

Figure 22 - Further ACARE objectives for 2050 [21]

Clearly, these most silent configurations would then involve integrating engines into the aircraft fuselage, or architectures where the engines would be completely shielded. Once again, these future configurations would strongly reduce both fuel consumption – through a dramatic reduction of the drag – and noise, with masking effects. Succeeding to build up such a configuration is a huge challenge, since it would involve fully reinventing the entire aircraft with unexplored aerodynamic effects and brand new propulsion systems. In particular, these engines would ingest air flows with intense distortion of the boundary layer, an unfamiliar configuration that remains to be addressed by research. However, the greatest challenge is probably not technical but commercial and psychological. Before engaging in such developments, manufacturers need to convince airliners of the expected benefits and the latter need to accustom their customers to the idea of embarking on such new aircraft. These are challenges that go far beyond technical issues ■

Figure 23 - Airbus views on a futuristic design for 2030 : rearward engines with or without Open Rotors (top) and embedded engines (bottom).

Figure 24 - The previous configurations could be ultimately superseded by flying wings in case of acceptance by the market

Acronyms

ACARE	(Advisory Council For Aeronautics Research in Europe)
BPR	(ByPass Ratio)
CAA	(Computational Aeroacoustics)
CFD	(Computational Fluid Dynamic)
CROR	(CountraRotating Open Rotor)
CRTF	(CountraRotating TurboFan)
DAFL	(Distributed Aft Fan Liners)
DOF	(Degree of Freedom)
EC	(European Commission)
EPNdB	(Effectively-Perceived Noise Decibels)
FP	(European Framework Programs)
HLD	(High-Lift Device)
ICAO	(International Civil Aviation Organisation)
IGV	(Inlet Guided Vane)
LG	(Landing Gear)
NAP	(Noise Abatment Procedure)
NEO	(New Engine Option)
NRT	(Noise Reduction Technology)
OGV	(Outlet Guided Vane)
OR	(Open Rotor)
QC	(Quota Count)
STAR-R	(Système de Technologie Active Réduit)
TOW	(Take-off Weight)
TRL	(Technological Readiness Level)
UHBR	(Ultra-High Bypass Ratio)
VAFL	(Variable Area Fan Nozzle)

References

[1] *Declaration by the Commission in the Conciliation Committee on the Directive relating to the assessment and management of environmental noise* - Directive 2002/49/EC of the European Parliament and of the Council of 25 June 2002 relating to the assessment and management of environmental noise.
[2] Directive 2002/30/EC of the European Parliament and of the Council of 26 March 2002 on the establishment of rules and procedures with regard to the introduction of noise-related operating restrictions at Community airports (Text with EEA relevance).
[3] *Position Paper on Dose Response Relationships Between Transportation Noise and Annoyance* - European Commission. February 2002.
[4] ICAO - *Guidance on the Balanced Approach to Aircraft Noise Management*. Doc 9829.
[5] ICAO - *Aircraft Noise to the Convention on International Civil Aviation.* Environmental Protection, Volume I, Annex 16.
[6] ICAO - *Environmental Protection Committee Delivers Progress on New Aircraft CO_2 and Noise Standards*.

[7] CAA ERCD - *Review of the Quota Count (QC) System: Re - Analysis of the Difference Between Arrivals and Departures*. Report 0204 (1999).
[8] CAA ECRD - *Quota Count Validation Study: Noise Measurements and Analysis.* Report 0205 (2003)
[9] ACARE - *Strategic Research Agenda 1*. October 2002.
[10] ACARE - *Strategic Research Agenda 2*. Volume 1 & Volume 2, October 2004
[11] European Commission, Flightpath 2050 - *Europe's Vision for Aviation*. March 2011
[12] X-Noise - *European Research Effort aimed at Aviation Noise Reduction*. Roadmaps.
[13] E. BOUTY, K. KNOBLOCH, D. BLACODON - *TEENI Turboshaft Engine Exhaust Noise Identification a brief overview*. Internoise Conference, Lisbon 2010.
[14] L. ENGHARDT - *The EU FP7 Research Project FLOCON*. *Objectives and first results*, Internoise Conference, Lisbon 2010.
[15] E. MANOHA, J. BULTÉ, V. CIOBACA, B. CARUELLE - LAGOON - *Further Analysis of Aerodynamic Experiments and Early Aeroacoustics Results*. 15th AIAA/CEAS Aeroacoustics Conference, Miami, May 2009, AIAA 2009-3277.
[16] L. SANDERS, E. MANOHA, S. BEN KHELIL, C. FRANÇOIS - LAGOON - *CFD / CAA Coupling for Landing Gear Noise and Comparison with Experimental Database*. 17th AIAA/CEAS Aeroacoustics Conference, Portland, June 2011, AIAA 2011-2822.
[17] See for instance C. BOGEY, S. BARRÉ, D. JUVÉ, C. BAILLY - *Simulation of a Hot Coaxial Jet: Direct Noise Prediction and Flow-Acoustics Correlations*. Physics of Fluids 21, 035105, 2009.
[18] E. KORS - *OPENAIR Aerodays*. Madrid, March 2011.
[19] Cleansky website
[20] L. ENGHARDT - *PROBAND - Improvement of Fan Broadband Noise Prediction : Experimental Investigation and Computational Modeling - Selected Final Results*. CEAS Broadband noise Workshop 2008, Bilbao.
[21] ACARE - Introduction - Aviation Noise Research Context ACARE SRA 2020 / SRIA 2050, Unpublished.
[22] AIRBUS - *Getting to Grips with Aircraft Noise*. December 2003.
[23] C. LAVANDIER, L. LEYLEKIAN, C. COLLIN - *Réduire les nuisances sonores engendrées par l'aéronautique civile*. AAAF Conference, June 2013.
[24] J. MARDJONO, G. RIOU, J.M. BOITEUX, F. BOUBILA - *EPSL Static Tests Demonstration of Liners Noise Reduction Concepts*. AIAA 2013-2174.
[25] S. PIERRET, R. FILOMENO COELHO, H. KATO - *Multidisciplinary and Multiple Operating Points Shape Optimization of Three-Dimensional Compressor Blades*. Struct Multidisc Optim (2007) 33: 61–70.
[26] Data taken from The Flying Engineer, Pratt and Whitney PW1100G Geared Turbofan Engine.
[27] H. LISSEK, A. S. MOREAU - *Design of Electroacoustic Absorbers for Use as Semi-Active Acoustic Liners*. 15th ASC-CEAS Workshop, 1st Workshop on X-noise EV.
[28] P. FERRANTE, D. COPELIO, M. BEUTKE - *Design and Experimental Verification of "True Zero-Splice" Acoustic Liners in the Universal Fan Facility Adaptation (UFFA)*. Modular Rig AIAA-2011-2728.
[29] R.BOISARD, G. DELATTRE, F. FALISSARD - *Assessment of Aerodynamics and Aero-Acoustics Tools for Open Rotors*. 9th European Conference on Turbomachinery, Istanbul, Turkey, 2011.
[30] I. LEPOT, M. LEBORGNE, R. SCHNELL, J. YIN, G. DELATTRE, F. FALISSARD, J. TALBOTEC - *Aero-Mechanical Optimization of a Contra-Rotating Open Rotor and Assessment of its Aerodynamic and Acoustic Characteristics*. Proceedings of the Institution of Mechanical Engineers, Part A: Journal of Power and Energy, 225-7, 850-863 (2011).
[31] D. GÉLY, J. DELFS - *Aeroacoustic Installation Effects on Transport Aircraft Research at Onera and DLR*. 16th workshop of the Aeroacoustics Specialist Committee of CEAS and 2nd workshop of the European X-Noise EV network, Braunschweig, October 2012.
[32] W. HERKES, R. F. OLSEN, AND S. UELLENBERG - *The Quiet Technology Demonstrator Program: Flight Validation of Airplane Noise*. AIAA Paper 982611, no. 2006-2720.
[33] C. HENRY, C. BAILLY, G. BODARD - *Statistical Modeling of BBSAN Including Refraction Effects*. AIAA paper 2012-2163.
[34] R. MAURY, A.V.G. CAVALIERI, P. JORDAN, J. DELVILLE AND J.P. BONNET - *A Study of the Response of a Round Jet to Pulsed Fluidic Actuation*. 17th AIAA/CEAS Aeroacoustics Conference, Portland (Oregon), AIAA 2011-2750.
[35] R. MAURY - *A Study of the Response of a Subsonic Round Jet to Steady and Pulsed Fluidic Actuation*. Journées Iroqua, Ecole Centrale de Lyon, 22th November 2012.
[36] N. TANAKA, T. OISHI, O. PICCIN, D. GÉLY, K. YAMAMOTO, S. ENOMOTO - *Jet Noise Reduction Using Microjet Configurations Experimental Characterization in CEPRA19 Anechoic Wind Tunnel*.18th AIAA/CEAS Aeroacoustics Conference, Colorado Springs, 2012, AIAA 2012-2300.
[37] W. DOBRZYNSKI - *Almost 40 Years of Airframe Noise Research : What Did We Achieve?* Journal of Aircraft 2010 47:2, 353-367.
[38] Valiant program - Final Publishable Summary Report.
[39] W. DOBRZYNSKI, L.C. CHOW, S. MALCOM, A. BOILLOT, O. DEREURE, N. MOLIN - *Experimental Assessment of Low Noise Landing Gear Component Design.* AIAA/CEAS Aeroacoustics Conference, Miami, 2009.
[40] L. SOULAT, I. KERNEMP, S. MOREAU, R. FERNANDO - *Assessment and Comparison of Tonal Noise Models for Counter-Rotating Open Rotors*. AIAA

2013-2201.

AUTHORS

Laurent Leylekian graduated from the Ecole Nationale Supérieure de Physique de Grenoble (now PHELMA) in 1990 and received his PhD in Solid State Physics from the Université Paris XI-Orsay in 1993. He started his career at the Commissariat à l'Energie Atomique (CEA) and joined the French Aerospace Lab (Onera) in 1994. After working for 15 years on functional materials, he joined the aeroacoustics department to lead the Iroqua program structuring the national effort in this discipline.

Maxime Lebrun graduated from Ecole Catholique des Arts et Métiers (ECAM) in 1997 and received his PhD in Aeroacoustics from Ecole Centrale de Lyon in 2002. Then he worked in the Acoustics department at Snecma, Safran group, on research programs, advanced low noise fan blade design and new engine developments (SaM146, Silvercrest and Leap). He managed this department from 2009 to 2013. He recently became head of the Product Support engineering department at Aircelle, Safran Group.

Pierre Lempereur is the technical advisor in the field of Acoustics for Airbus Engineering, in charge of noise research strategy and of supervising the acoustic design of project aircraft. He obtained his Aeronautical Engineer Degree from the Ecole Nationale Supérieure d'Ingénieurs de Constructions Aéronautiques (ENSICA), then took post graduate training courses in acoustics at the University of Sherbrooke. He joined the acoustics department of Airbus Engineering in 1984. He conducted the acoustic integration of the A320, A330 and A340. He initiated and conducted noise reduction technology research programs in the areas of high speed propeller aeroacoustics, turbofan nacelle acoustic treatment, airframe noise and advanced noise abatement procedures He supervised the implementation of novel noise technologies and the acoustic design of the A380 and A350 aircraft. He has been a member of the ICAO/CAEP expert work group developing aircraft noise standards since 1993.

Y. Delrieux
(Onera)

E-mail : yves.delrieux@onera.fr

DOI : 10.12762/2014.AL07-02

From design to flight testing : overview of rotorcraft acoustic research at Onera for industrial applications

The reduction of noise emission has become a key commercial argument for helicopter manufacturers, such as Airbus Helicopters. For years, Airbus helicopters has placed emphasis on the good acoustic behavior of its helicopters, as proven by its communication on the fenestron concept, the acceptance of its aircraft for the Grand Canyon tours and the presentation of its recent Bluecopter™ Technology. Thus, Airbus helicopters has become one of leaders in the manufacture of low noise helicopters. Some of its advances in this field have been made thanks to its cooperation with Onera. The paper is aimed at presenting the way in which Onera has become a reliable partner for industry to face the challenge. Partly thanks to wind tunnel tests, Onera has developed a set of numerical tools and acquired a physical understanding of the noise emitted by the rotors of helicopters. These tools have been used to design new main rotor blades, optimized to reduce the vibration, to improve the aerodynamic performances and to reduce the noise emission for specific flight conditions. Both active devices and passive design have been developed and tested at model scale, before being provided to the industry for scale one developments and for implementation on actual helicopters and to be tested in flight. For the tail rotor, fenestron noise has also been studied numerically and during flight tests, in order to determine noisy flight conditions and to improve the tools and methodology for future definition and optimization.

Introduction

In the early 70s, acoustics became a key parameter for the design of new helicopters. One of the main arguments, among others such as safety, for the fenestron concept [16], developed by Sud-Aviation (integrated into Aérospatiale and then merged with Daimler-Benz AG to give birth to Eurocopter, which was renamed Airbus helicopters in 2014) was the reduction of the noise emission. At the same time, the first measurements of the noise emitted by helicopters were performed by Aérospatiale and Onera. The first studies have shown that noise is emitted by the engines predominantly under take-off conditions. Turboméca and Onera have thus worked on the determination of the noisy parts of the engines, by means of static bench tests. Nevertheless, for most flight conditions, the rotors (main and tail rotors) have been shown to be the main sources of noise.

In the 80s, Onera and the US Army started to collaborate within the framework of a MoU (Memorandum of Understanding) to study noise emission, by means of high and moderate speed flight tests and by means of wind tunnel tests in CEPRA19, in descent flight [1]. Onera then tested various different blades of a main rotor provided by Aérospatiale in descent flight in CEPRA19 [2] and at high speed in S2Ch [3].

In parallel to these experimental studies, the HSI noise was numerically analyzed using CFD/CAA or CFD/Kirchhoff methods. Thanks to the wind tunnel tests and to the numerical tools, some blade tip geometries have been proposed to reduce the HSI noise in forward flight.

To answer to the industrial demand, the main emphasis was thus placed on the understanding and acquisition of numerical tools for the prediction of the most penalizing noise source during the landing of helicopter (penalizing for implementation of helipads in urban areas): the so called BVI noise. The computational chain (composed initially of comprehensive codes and secondly by CFD/CAA) developed at Onera was validated by comparison with two different databases [4]. The first one is the HART database [5], obtained in 1994 by testing a four bladed BO105 rotor trimmed with HHC, within the framework of a multinational research cooperation (between NASA, the US Army, the DLR, the DNW and Onera), including aerodynamic measurements (blade pressure, vortex positions, field velocities, etc.), dynamics (elastic deformations) and acoustics. The second one is the ERATO [6] database, obtained in 1998 within the framework of the bilateral French-German cooperation between Onera, DLR and Airbus helicopters.

The tools have been used to design and optimize new blades, which were first tested at model scale in a wind tunnel, before being provided to industrialists for the scale one design and for flight tests on real helicopters.

Another noise source, the BWI noise, which may be dominant under some climb configurations, was studied at Onera mainly within the framework of two PhD theses [7;8]; however, at the present time, no activities are being carried out in this topic at Onera. As for HSI noise, it could be possible to launch new activities, in the event of renewed interest by industry or the international community, especially for flight conditions where BWI is more important than BVI in terms of intensity, in a frequency domain between BVI noise and turboshaft engine noise (around 1 to 3 kHz). BWI was studied during the HART wind tunnel test campaigns and some climb configurations were also analyzed. Onera showed that BWI was not related to isotropic turbulence, but rather to the blade interactions with coherent large-scale structures present in the flow, and linked these structures to short-wave vortex instabilities. These instabilities occur when an external strain field deforms the vortex core elliptically. The deformation induces the resonant coupling of two vortex modes (Kelvin modes). Thus, similarly to BVI noise, the reduction of BWI noise could be obtained by an appropriate control of the vortex generation.

For the reduction of BVI noise, both passive rotor blade design (ERATO) and active control concepts have been studied and optimized numerically and experimentally, such as active trailing edge flaps, which have been tested at high speeds in the S1 Modane wind tunnel and active twist (within the framework of French contracts and European programs), which will be tested in the DNW-LLF wind-tunnel. These solutions have been proven, both numerically and experimentally, to be efficient for high BVI noise reduction, the challenge being to implement them on actual helicopters by solving the unavoidable difficulties: adapting the model technologies to full scales blades and solving the problems linked to vibrations, weight or electrical consumption. In this second phase, the role of Onera is to provide support to industry for the transfer from this model scale to full scale (like the Blade 2005 program for the passage from ERATO to Blue Edge™ [15]).

At Airbus helicopters, new rotor technologies resulting from these helicopter main rotor BVI noise reduction studies have been developed within the framework of Bluecopter®: Blue Pulse™ active rotor, which is based on piezo-driven flap modules on the trailing edge, for both external noise and vibration reduction, and Blue Edge™, a passive concept, derived from the double-swept shape of the ERATO project. The full-scale developments of such technology have been supported by the DGAC and tested in flight.

The Fenestron™, a technology used for helicopter tail rotors, has been evaluated during a joint Airbus helicopters/Onera program including CFD/CAA computations and flight tests, where onboard and ground noise measurements were performed.

In parallel to these different programs aimed at reducing the noise at the emission, the computer codes have also been adapted to take into account maneuver flight conditions (such as decelerating or turning flights) in order to study low noise flight procedures (mainly within the framework of EU contracts). The purpose is to provide flight procedures to the pilots, in order to avoid noisy configurations during specific missions.

Experimental work in helicopter noise assessment

Two main kinds of helicopter tests are conducted. The first kind of tests is generally performed on model rotors mainly for the purpose of validating the numerical tools and showing the efficiency of the proposed technical solutions. These solutions are mounted on a mock-up, using dedicated technologies that may not be directly transposable to actual full scale helicopters. The second kind of the tests is performed by the industrialist on ground equipment, such as whirl towers or static benches, and then validated in flight.

Several testing facilities have been used for the characterization of helicopter rotor noise. For the analysis of the HSI noise, tests have been conducted in both the Onera S2Ch and S1MA wind tunnels.

The tests in the S2Ch (In Chalais-Meudon, near Paris) were conducted in the wind tunnel fitted with removable acoustic lining [9]. The test section had a diameter of 3 meters and the maximum wind speed was 110 m/s. Two different rotors were tested, a straight-tip one and a second one equipped with a sweptback tip, in order to compare the transonic effects between the two kinds of blades (figure 1). The measured dramatic increase of noise level when the tip Mach number goes over a value of around 0.9 was linked to the phenomenon of delocalization shown by aerodynamic computations. The sweptback tip was shown to induce much lower noise levels, thanks to the delay of the delocalization towards higher tip Mach numbers.

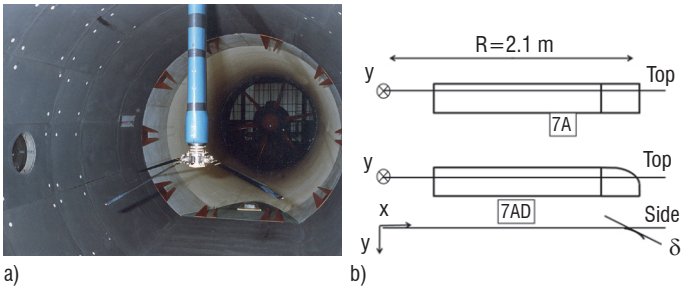

Figure 1 - a) S2Ch two bladed rotor tests [9]. b) 7A and 7AD blade shapes

The conclusions were confirmed during a second test campaign [10] conducted in the 8 m diameter S1 Modane wind tunnel, where two rotors provided by Airbus helicopters were tested, the 7A and 7AD rotors, which differ in their blade tip, the second one having a parabolic tip. The tests showed that at very high tip Mach numbers, the delocalization phenomenon can be dramatically reduced with suitable tip geometries, leading to noise reductions of up to 8 dBA, and also showed the influence of the rotation speed.

Several test campaigns have been conducted for the BVI noise analyses. During the first years of the studies on BVI noise, since no computation was available, the tests performed in CEPRA19 [2] led to a first quantitative characterization of the noise in descent flight.

Afterwards, the HART campaign in the DNW, ERATO in S1MA and DNW and RPA in S1MA enabled both the development of numerical methods and the validation of new rotor noise reduction concepts.

Due to the wind tunnel capabilities, noise measurements are generally devoted to high speed noise in the S1 Modane wind tunnel (figure 2) closed section facility, while BVI noise is studied in the open room of DNW-LLF (figure 3).

a)

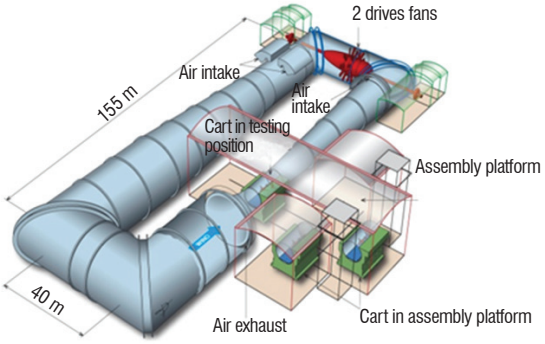

b)

Figure 2 - a) Onera S1 Modane wind tunnel, b) Helicopter main rotor tests in the S1 Modane wind tunnel (active rotor)

Both passive design (ERATO) [11] and the active rotor RPA have been tested in the S1 Modane wind tunnel [12, 13,14].

For the active flap rotor (figure 2b), a wind-tunnel test was first performed in September 2004 in the S1 Modane facility, to check the behavior of the active flaps under realistic aerodynamic loads. High speed noise and thickness noise can be evaluated in the S1 Modane wind tunnel, by means of in-plane microphones and the loading noise and BVI noise in level flight can be evaluated using microphones located below the rotor. Despite the unfitted geometry of the measurement in the S1 Modane wind tunnel, thanks to an acoustic liner and to the fact that the noise component of interest is tonal noise, the BVI noise was shown to be extractable by using synchronous time averaging of the signal, so that any background noise not synchronic with the harmonics of the rotor rotation could be removed. The tests were first conducted with a reference rotor and then using the studied rotor equipped with active flap, under the same flight conditions, to quantify the potential advantages of the concepts. Unfortunately, the expected tests in DNW-LLF to confirm these first results have not yet been conducted.

The DNW-LLF wind tunnel is particularly well suited to BVI noise measurement, since it has a very wide open section, in which a translating array of microphones can be implemented below the rotor, to obtain noise contours in a horizontal plane, including the maximum BVI noise zones on both sides of the rotor, as shown in figure 3b. It also allows the acoustics to be linked to the wake and the vortices, by means of PIV measurements performed simultaneously.

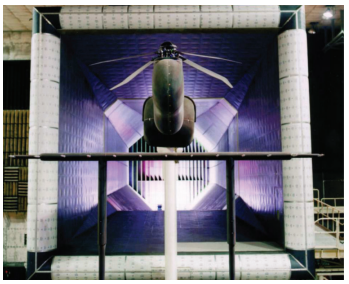

a)

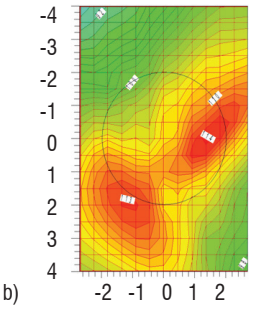

b)

Figure 3 - a) Helicopter main rotor tests in the DNW-LLF (passive design). b) Typical BVI noise measurements at DNW obtained with 13 mic. (vertical lines) at 17 streamwise locations (horizontal lines).

Complementarily to the wind tunnel tests, flight tests can be conducted. These are generally performed by industry once the new concepts or design have proven to be efficient for the objectives set. For example, the BlueEdge™ rotor [15] was successively tested in the laboratory for fatigue tests, then to check the main structural characteristics of the blade and to identify the blade modes and to cross-check the blade elastic model, then on a whirl tower to analyzethe dynamic behavior of the blades and finally in flight on an EC155 helicopter [15]. The rotor was tested during more than 75 hours. The performance of the rotor in terms of figure of merit, power consumption, vibration levels and dynamic loads was analyzed under different flight conditions and the noise reductions expected during the ERATO program were confirmed.

Onera and Airbus helicopters estimated that flight tests were appropriate for the study of the noise emission of a Fenestron because of the difficulty of having access to a wind tunnel that is able to simulate actual flight conditions, including a complete helicopter (with the fuselage and both rotors). A specific study was launched by Onera and Airbus helicopters, with support from the French Ministry of Civil Aviation (DGAC), to acquire an experimental comprehensive database to validate aerodynamic and aeroacoustic simulation tools that are accurate for Fenestron noise predictions.

The tests were conducted on a Dauphin 6075 [16, 17, 18] equipped with a first generation 13-blade Fenestron. It was equipped with steady wall pressure sensors on the rear part of the fuselage and tail, and with unsteady wall pressure sensors in the duct (figure 4). The blade pressures were measured by pairs of upper/lower thin layer unsteady transducers, mounted on four blades. Two series of flight tests were performed in 2009 and 2010, one for inboard noise measurements and the other one for ground noise measurements. For the first campaign, onboard acoustic measurements were performed using four microphones located on the horizontal empennage. For the ground measurements, eleven microphones were uniformly spaced on a 500 m linear antenna perpendicular to the direction of flight. Ground noise footprints were plotted for various flight conditions: level flights, approach and take-off. The recorded signals were processed in order to enable their comparison with CFD/CAA computations, by taking into account flight measurement specifications, such as the Doppler effect, propagation delays and aircraft location variation. By means of frequency analyzes, the Fenestron noise components were emphasized as function of the flight conditions and compared to computed ones.


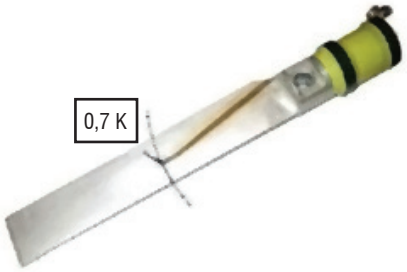

a) b) c)

Figure 4 - a) Fenestron set-up. b) Microphone settings - c) Instrumented blade

Modeling tools for rotor design and optimization

Over the years, Onera has developed a set of prediction tools aimed at the computation of the noise radiated by the rotors as a function of the flight conditions and the corresponding kind of noise source. Indeed, there is a dominant type of noise source for each flight condition, which must be treated in a different way (typically quadrupolar noise at high speed, BWI noise in climb, BVI noise in descent etc..).

Moreover, even for a given flight condition, different phenomena are involved when considering the noise radiation at different microphone locations relative to the helicopter. This is due to the different noise radiation directivities, partly because of the nature of the noise (monopole, dipole or quadrupole, etc.) and because of the noise source displacement relative to the observation point. For example, during the flyover in descent flight at moderate speed, several noise sources may successively be dominant for a microphone on the ground close to the flight pass: first the main rotor thickness noise, then low frequency main rotor loading noise, then main rotor BVI noise, possibly engine noise and finally tail rotor thickness and loading noise. The common point of the various tools is the requirement of suitable prediction of the aeromechanics, of the aerodynamic field (strongly coupled) and then of the acoustic radiation.

For high speed noise predictions, the acoustic codes are based both on Lightill Acoustic Analogy (LAA) and Kirchhoff formulation. At the beginning of the studies at Onera, the aerodynamics were determined using a full potential code (FP3D) or an Euler solver (WAVES) and the acoustics were obtained with a LAA code and a Kirchhoff code (KARMA) [19], [20], [21]. In the LAA formulation, the determination of the quadrupole terms requires a volume integration of the Lighthill stress tensor. Using Kirchhoff integration, the difficulty of the volume integration is avoided thanks to the use of a prescribed surface, over which the pressure field must be provided. HSI noise can now be solved by the elsA solver [22, 23] followed by the Kirchhoff formulation of KIM [24], both presented further on.

As mentioned in the introduction, Onera and Airbus helicopters have mainly directed their efforts towards the prediction of BVI noise. The computational method used at Onera for the prediction of BVI noise [25] was implemented progressively between 1990 and 1995. The wind tunnel tests have shown that the radiated BVI noise is a consequence of several interactions between the vortices (generally tip vortices, but not always) emitted by the blades and the following blades; these interactions generate pressure fluctuations on the blades, which are the source of the BVI noise. The goal of the computational method is to accurately compute the unsteady pressure fluctuations encountered by the blades during their rotation. A key point is the good prediction of the wake convection between the emission of the vortices and the interactions; a change in miss-distance by a quarter-chord can lead to a variation of more than 5 dB (mid-frequency range, i.e., 6th to 40th bpf). At the beginning of these developments, the CFD methods (Euler or Navier-Stokes methods) were not accurate enough to convect vortices over large distances (more than one rotor revolution), so it was decided to develop a chain of comprehensive codes that could compute the wake characteristics and the resulting blade pressure fluctuations separately.

Actually, the computational method consists of five main steps: the rotor trim, the wake prediction, the roll-up model, the calculation of blade pressure and finally the noise radiation. The first step of the computational chain is to determine the rigid and aero-elastic dynamic response of the blades, depending of the flight conditions that must be simulated (advancing speed, rotor thrust, flapping piloting law, etc.). Up to 1996, this was done by the R85 code developed by Airbus helicopters for isolated rotor simulations. A more general tool (the HOST code), applicable not only to isolated rotors but also to a complete helicopter, has been developed since then by Airbus helicopters.

The wake model is computed by the METAR code and is defined by a prescribed helicoidal geometry described by vortex lattices. A coupling between R85/HOST and METAR [26,27] is made until convergence is reached on induced velocities at the rotor disk level. The flexibility of the blades is also taken into account by solving the Lagrange equations. The rigid and aero-elastic blade motion being known, a second step is necessary to iteratively distort the initial wake geometry under its own aerodynamic influence. This is performed by the MESIR code, which computes (using the Biot&Savart law) the velocities induced by all vortex lattices at each discretization point of the wake and modifies the wake geometry accordingly. First, comparisons between computation and experimental data have shown the necessity of an intermediate step between wake and pressure calculations. Indeed, the vorticity carried by the last lattice is generally not representative of the actual rolled-up vorticity. Due to the blade motion, the tip vortex may slide inboard and multiple vortices may appear. The vorticity roll-up code [28], called MENTHE, identifies the portions of the MESIR predicted vortex sheets whose intensity is sufficient to result in a roll-up. The intensities and radial locations of the rolled-up vortices, which constitute the interacting vortices, are determined at the emission azimuths. One important point is that this code (possibly adapted) is mandatory to determine the actual vortex roll-up for any kind of design resulting in unconventional vortex roll-up, such as trailing edge flaps, vane tip, active twist, etc...

Blade pressure distribution is then calculated by the unsteady singularity method ARHIS. This code assumes that the flow around the rotor is inviscid and incompressible. It performs 2D-by-slices calculations. Subsonic compressibility effects are included by means of Prandtl-Glauert corrections, combined with local thickening of the airfoil. In addition, finite span effects are introduced through an elliptic-type correction of the pressure coefficients. The interacting vortices are modeled as freely convecting and deforming clouds of vortex elements. The main advantage of this method is its ability to take into account the vortex deformation during strong blade-vortex interactions. A variable azimuthal step is used, depending on the impulsiveness of the interaction. Finally, the noise radiation is computed by the Paris code, starting from the blade pressure distribution provided by ARHIS[28]; PARIS is based on the Ffowcs Williams-Hawkings equations and predicts the loading and thickness noise. It uses a time domain formulation. One of the aspects of interest of Paris [29], is the ability to link the acoustic pressure peaks for a given microphone to the blade pressure fluctuations and to the blade-vortex interactions, which means that the vortices responsible for the noisiest interactions can be identified, as well as the blade portion that radiates most noise. This is a very efficient tool for rotor optimization, since it greatly helps to alleviate the noisiest phenomena. It was used, for example, to define the backwards and forward sweeps of the ERATO blade, which provide the main part of the noise reductions.

This numerical chain has been validated with the experimental data from HART (1 and 2) in terms of wake convection, vortex characteristics (number of roll-up vortices, spanwise location close to the emission, vortex strength versus azimuth, vortex core radius, etc.), blade deformations, blade loads and finally acoustics. Onera has participated in a large number of workshops for code validation and comparisons, within the framework of the HART programs, as well as within the framework of the NASA Ames 80- by 120-Foot Wind Tunnel, called the Caradonna tests [30]. Thanks to this, each step of the chain has been evaluated, validated or improved.

Thanks to its low CPU consumption, the comprehensive chain has been widely used for rotor design and the optimization explained in the following chapters; as from the year 2000, CFD methods began to be able to preserve the vorticity of the vortices, from their emission up to the interactions. Within the framework of the French-German cooperation CHANCE (2001-2006) [31], the Chimera techniques were developed and used for automatic mesh generation and adaptation in the *elsA* solver. In 2004, these methods were applied to the HART Baseline test-case, but no BVI was simulated due to excessively coarse blades and background grids. During the French-German program SHANEL, thanks to the use of higher order schemes, matrix dissipation and efficient vorticity confinement techniques, it became possible for CFD to capture the BVI and, when coupled with a Ffowcs-Williams and Hawkings (FW-H) code (KIM code at Onera), to provide a correct far field acoustic radiation compared to wind tunnel measurements. Nevertheless, these CFD/FW-H methods are still too costly to be intensively used for rotor design or optimization.

The *elsA* code gives a solution of the 3D compressible Euler equations in a reference frame attached to the rotating blade. A space-centered Jameson scheme is used for the spatial discretization and the time integration uses a four-stage Runge-Kutta explicit scheme. Onera developed a module called Cassiopée, which generates and refines the Cartesian background grids around the blades automatically and allows sophisticated methods to be used, such as high-order schemes, matrix dissipation and Vorticity Confinement. The Vorticity Confinement [32] method is a numerical technique that is aimed at reducing the artificial diffusion of vortices by numerical resolution schemes for the Euler/RANS equations. It was first introduced and developed for the incompressible formulation of the Navier-Stokes equations. During the SHANEL program, it was introduced in *elsA* and applied to helicopter BVI configurations.

The CFD field is treated by the integral method code KIM [24], which uses either the FW-H solid or porous surface formulations or the Kirchhoff formulation.

CFD/CAA methods are also used for the Fenestron noise predictions. The aerodynamic flow over the entire helicopter is obtained by solving the URANS equations over the complete aircraft, using the *elsA* solver. The main rotor is modeled using a non-uniform actuator disk method accounting for the load of the rotor over one revolution, in order to reduce the cost of the unsteady computation to densify the grid in the Fenestron area (figure 5a). The Fenestron blade motion is taken into account using the Chimera method developed at Onera [33] (figure 5 b). The far field acoustic radiation is computed using KIM code, by placing porous acoustic surfaces in such a way that they contain all of the acoustic sources of the Fenestron and that they account for any reflection or diffraction occurring in the shroud (figure 5c). This prediction method has been validated by comparison with acoustic measurements obtained during the Fenestron flight test.

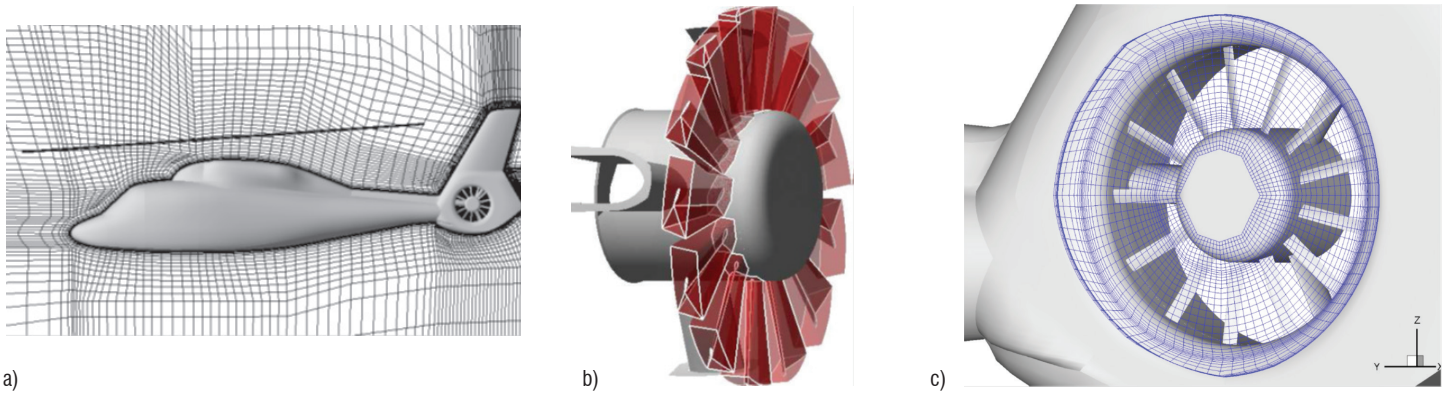

Figure 5 - Fenestron noise computation. a) Helicopter geometry. b) Chimera grids around the blades. c) Acoustic integration surfaces

Complementarily to these numerical tools, Onera has been developing simplified models, mainly for the conception and pre-design of new concepts [33].

Rotor optimization and design

HSI noise

Some experimental (S2Ch and S1 Modane wind tunnels tests) and numerical analyzes of the HSI were performed and different blade tips were proposed to reduce the Shock-like sound wave phenomenon called delocalization, which is responsible for a dramatic increase in the noise level, when the tip speed reaches Mach numbers close to 0.9. No specific studies on HSI have been performed at Onera for a long time, since this topic has not been identified as a priority recently.

BVI Noise

Passive design

The BlueEdge™ rotor was first designed at Onera and DLR during the ERATO program, which was a cooperative project between Onera and the DLR with the involvement of Airbus helicopters (France and Germany). The ERATO rotor was designed using the tools described further on and the physical understanding of the BVI phenomenon. It was than tested in two wind tunnels (DNW-LLF and S1MA). In view of scale-one application to a 4-to-6 ton helicopter, the ERATO program was aimed at designing, building and testing a quiet model rotor, which would be 6 dBA less noisy (in terms of averaged ground noise level) than a current technology reference rotor under ICAO descent flight certification conditions, that is, 6 degree descent at 125 km/h. Moreover, since the descent angle and the flight speed may vary in a real landing approach , some stability of the noise level improvement was sought with respect to the descent angle and to the flight speed. Significant noise reductions were also envisaged for medium and high-speed level flight. This ambitious goal was to be accomplished with the constraint of minimum penalties with respect to rotor vibrations and performance.

The main phase consisted in the continuation of the parametric studies, comprising refined rotor geometry parameters such as the airfoil, twist and chord length spanwise distributions and the quarter-chord line geometry. The goals of this new design were to reduce the blade vortex interactions, by modifying some of their characteristics. Indeed, the HART tests and the Caradonna experiment, as well as the numerical analyses, made it possible to rank the different parameters responsible for the BVI noise radiation. The design was thus performed by means of the parametric analysis of the effect of the selected parameters on the BVI noise.

One of the key features of ERATO is the double-swept planform (figure 6).

An inboard forward sweep is followed by an outboard backward sweep. The goal of this shape is to phase shift the impulsive pressure fluctuations occurring in the span direction and leading to constructive pressure accumulations for a given microphone. Moreover, the spanwise chord, twist and thickness distributions were optimized to reduce the intensity of the emitted vortices. An increased chord length was defined to accelerate the vortex convection, from its emission up to the interaction, in order to increase the blade vortex miss distance, which was shown to be one of the most influent parameters. The combination of the entire design parameter optimization was checked, in order not to alter the expected benefits of each of them taken separately.

The last phase comprised the structural design and manufacture of the instrumented optimized rotor blades, the S1 Modane and DNW-LLF wind tunnel tests and a thorough analysis of the test results for validation of the design methodology.

At the end of 2000, Airbus helicopters signed a research agreement with Onera that was supported by the DGAC, in order to develop a full-scale blade for flight testing. Afterwards, Airbus helicopters, with the support of Onera, starting from the ERATO design, took into account the full scale constraints in terms of stability, deformation, structures, etc... to design a new blade, keeping the main features and advantages of ERATO, but able to fly on a real EC 155 helicopter. The design was finally validated in terms of vibration, performance and acoustics during flight tests.

Active design

Complementarily to passive design, active control solutions are expected to be more efficient, since it is possible to adapt the control laws depending on the flight conditions and closed loop controls can be expected to be efficient. The main constrains of this kind of solution

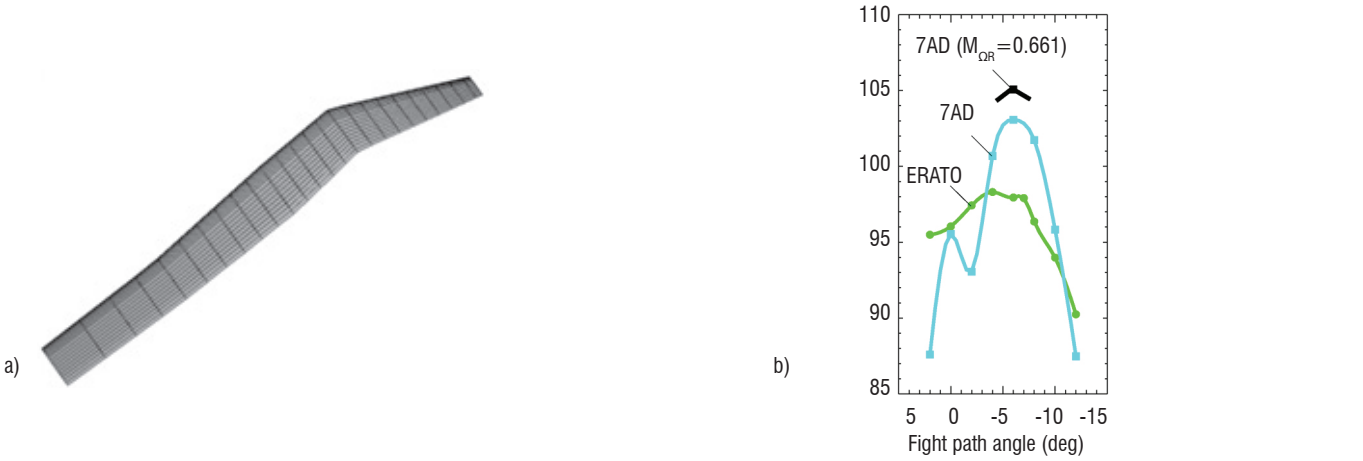

Figure 6 - a) ERATO blade shape. b) Noise reduction with ERATO blade measured at DNW (dBA) versus the descent angle at $M_{\Omega R}$=0.617.

are the cost, the weight increase, the additional power consumption and the maintenance. Nevertheless, it was judged important for industry and research centers to develop their competences in the field of active rotors. Thus, a project funded by the French Civil Aviation Authority, called the DTP RPA, also known as ABC, was launched in France at the end of 1998, involving Airbus helicopters and Onera. Similar activities were being addressed in Germany by the DLR and Airbus helicopters Deutschland, within the framework of ADASYS. Three main objectives were targeted: to decrease the BVI noise radiated during descent flight, to decrease the vibration level generated by the rotor and, finally, to increase the aerodynamic performance of the rotor, by either alleviating the dynamic stall effect, or decreasing the consumed power in fast cruise flight. Since one of the key parameters of the BVI noise emission are the blade vortex miss distances, the aim was to dramatically increase the vortex convection, from their emission up to the interaction, by means of the blade trailing edge flaps, so that the close interactions could be avoided. For a given rotor, the maximum noise is generally obtained at around 6° or 7° of descent angle. The level decreases very fast, by more than 6 dB (mid-range frequency, 6^{th} to 40^{th} bpf) for a change of $\pm 2°$ in the descent angle. A $\pm 2°$ modification in the slope corresponds to only around a half chord in the vertical position relative to the blade. It means that a gain of more than 6 dB can be expected by increasing (or decreasing) the wake convection between the emission and the interaction by 7cm for a model rotor. This can be performed by activating the flap for a range of blade azimuths corresponding to the travel of the vortices on the advancing side. Computations have shown that this effect can theoretically be easily achieved if the flap is sufficiently large and deep and can be activated with a sufficient deflection angle.

The flap is also expected to be able to reduce the vortex intensity at their emission, by means of adapted flap control laws. Numerical simulations have shown the efficiency of both effects. The main challenge remains to be able to implement efficient flaps (which means large ones, with strong deflections) on actual model rotor and full scale rotors.

As for ERATO, two wind-tunnel test campaigns were planned, one in the S1 Modane wind tunnel, mainly focused on dynamic aspects and one in DNW-LLF mainly dedicated to acoustic issues. During the first phase, the comprehensive code chain was adapted to take into account the trailing edge flap. Both the dimensions and locations of active flaps were determined, by means of numerical studies carried out on a full-scale ATR blade geometry provided by Airbus helicopters Deutschland. Since the efficiency of the flaps, in terms of noise reduction or vibration reductions, were obtained for different flap locations and dimensions, it was decided to keep the capability to choose three spanwise locations of 15% chord flaps, depending of the expected benefits: more inboard (70-80% R) for vibration, more outboard (80-90% R) for noise, for example (figure 7).

For each flight condition and flap geometry, optimal flap deflection laws were numerically determined at both full and wind-tunnel scales. In parallel, an active flap device was defined that could be implemented on the model scale blades to be tested in both wind tunnels. The second phase of the project, which started in 2001, was devoted to the manufacturing of a prototype blade by Onera and of a set of 5 "series" blades by the DLR for the tests in S1 Modane and DNW-LLF wind tunnels. The test campaign began in December 2005 in the S1 Modane wind-tunnel. Fourteen microphones were available for the acoustic measurements. Six of these were located on a vertical strut in front of the rotor shaft, for the determination of the thickness noise and eight were located below the rotor on the advancing blade side to determine loading noise (including BVI).

Measurements were carried out for different parametric sweeps of the phase actuation, for a given maximum flap deflection. For all of the flight conditions and for both flap positions, noise reductions were obtained with every flap deflection frequency for certain values of the phase. An example is provided in figure 8 for two different flap amplitudes in various phases, the flap being actuated at a frequency of 4-per-rev. By increasing the flap amplitude from 0.7° (figure 8a), to 1°, the noise reduction is increased from -1.2 dBA to -2.7 dBA.

For the active flap, noise reductions of up to 3 dBA have been obtained on the BVI component, although the flight conditions were not a descent flight with high BVI levels, showing the capability of the active flap concept for BVI reduction.

Blue Pulse™ technology, based on active flaps, has been flying since 2005, showing a noise reduction of up to 5 EPNDB [15]. Airbus helicopter evaluations with Blue Pulse™ are continuing on an EC145, while the development of a miniaturized system for production applications is advanced.

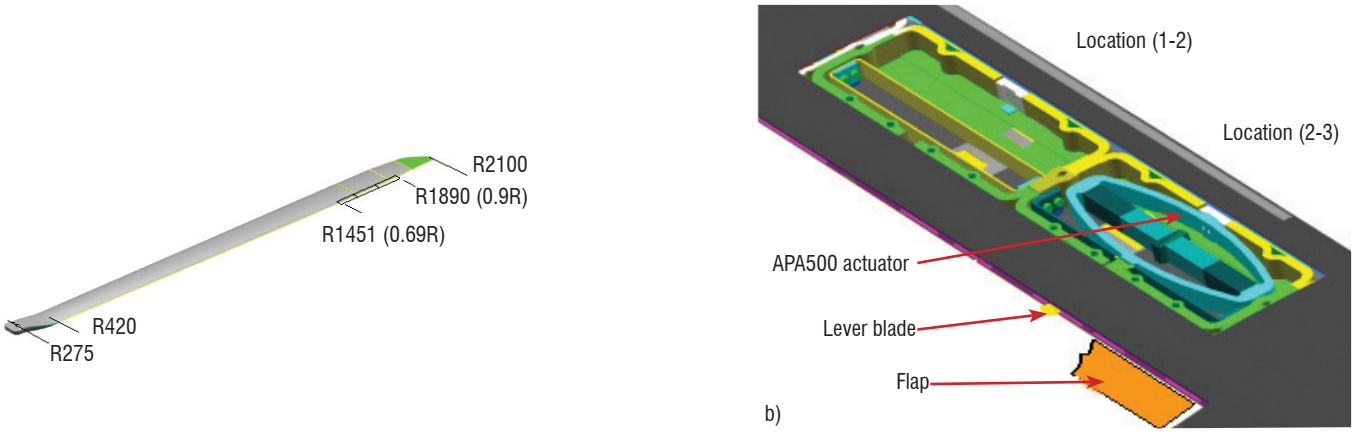

Figure 7 - a) ABC blade dimensions and b) flap positions [13]

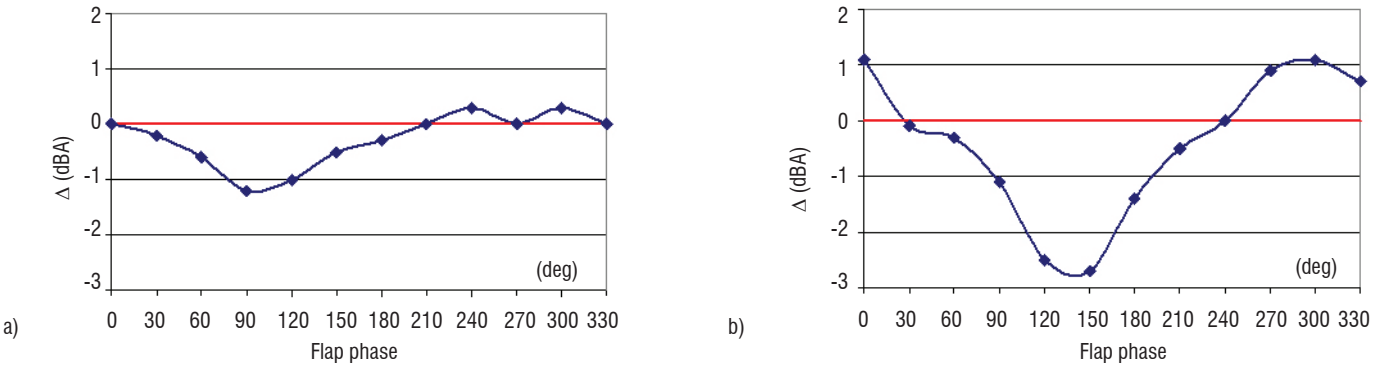

Figure 8 - Noise reduction versus the phase of actuation. 4w - a) 0.7° of amplitude. b) 1° of amplitude

With the same objective as for the active flaps, a theoretically very promising way of reducing the BVI noise consists in modifying the spanwise twist distribution over the blade, in order to modify either the vortex generation or its convection. As for trailing edge flaps, numerical studies have been performed to show the theoretical efficiency of such a solution. The challenge is once again the capability to make blades equipped with active twist devices. Thanks to suitable twist laws, it is theoretically possible to dramatically decrease the BVI by increasing the induced velocities in a selected blade azimuth range. Onera performed an optimization of the twist laws within the framework of the European project Friendcopter and during an Onera/Airbus helicopter program [35]. The GADO optimizer was used to couple the R85 aero-elastic code with objective function of the induced velocity maximization near the blade tip on the leading edge. Thanks to the optimized law, the vortices are convected faster and a gain of more than 7 dBA is obtained on the maximum noise, which is even more important if only the leading edge is considered (right hand part of the contour plot in figure 9).

Low noise flight procedures

Complementary to the previous studies, numerous activities have been carried out using the codes developed (including simplified models [34] or using the Onera chain adapted to unsteady flight conditions [36]), in order to provide low noise flight procedures to the pilots for given missions, in terms of speed, rate of descent, etc.

Concluding remarks

Among the studies performed at Onera (with close cooperation from the DLR) within the framework of helicopter acoustics, several have led to industrial applications. To gain the confidence of industrialists in the proposed solutions and the numerical tools, research centers must prove the accuracy of their tools, using wind tunnel tests and thanks to international cooperation, within the framework of workshops. Onera has proven its capability to face this ambitious challenge, thanks to its efficient numerical tools and wind tunnel facilities ■

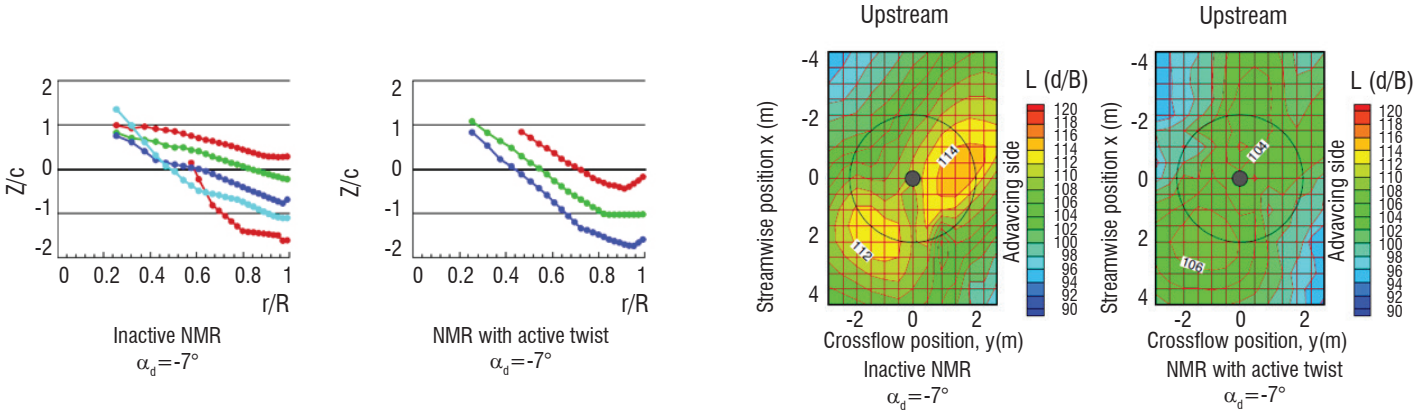

a) Blade-vortex miss-distances (Z/c) as a function of the blade span (r/R) at the azimuth of interaction

b) Noise contours (mid-range frequencies, 6th to 40th bpf)

Figure 9 - Noise reduction using active twist (New Model Rotor, NMR). Numerical simulations.

Acknowledgements

The author would like to thank all of the Onera teams that have been involved in the described activities and, in particular, the colleagues from the Applied Aerodynamics Department.

References

[1] C. DAHAN, C. LARNAUDIE, C. MALARMEY - *Synthèse des essais de rotors maquettes à la soufflerie CEPRA 19 dans le cadre du MoU*. Rapport de synthèse Onera 41/5094 PY, 1981.
[2] M. CAPLOT, A. DUPONT, C. LARNAUDIE - *Synthèse des essais de rotors maquettes de l'aérospatiale dans la soufflerie CEPRA 19.* Rapport de synthèse Onera 71/5094 PY, 1987.
[3] M. CAPLOT, P. LEBIGOT, P. LOOPUYT, J. PERRET-LIAUDET - *Essais acoustiques de maquettes de rotors d'hélicoptères de l'Aérospatiale dans la soufflerie S2Ch*. Rapport final Onera 81/5094 PY, 1988.
[4] P. SPIEGEL, G. RAHIER, B. MICHÉA - *Blade-Vortex Interaction Noise: Prediction and Comparison with Flight and Wind Tunnel Tests*. 18th European Rotorcraft Forum, Avignon, September 1992.
[5] R. KUBE, W. SPLETTSTOESSER, W. WAGNER, U. SEELHORST, Y. YU, A. BOUTIER, F. MICHELI, E. MERCKER - *Initial Results from the Higher Harmonic Control Aeroacoustic Rotor Test (HART) in the German–Dutch Wind-Tunnel.* 75th AGARD Fluid Dynamic Panel Meeting on Aerodynamics and Aeroacoustics of Rotorcraft, Berlin, October 1994.
[6] Y. DELRIEUX, J. PRIEUR, M. COSTES, P. GARDAREIN, P. BEAUMIER, H. MERCIER DES ROCHETTES, P. LECONTE, P. CROZIER, W.R. SPLETTSTOESSER, B. VAN DER WALL, B. JUNKER, K.-J. SCHULTZ, E. MERCKER, K. PENGEL, J-J. PHILIPPE, B. GMELIN - *The Onera-DLR Aeroacoustic Rotor Optimization Program ERATO: Methodology and Achievements*. AHS-Aerodynamics, Acoustics, and Test and Evaluation Technical Specialists Meeting, San Francisco, 2002.
[7] E. BOUCHET - *Étude du bruit d'interaction pale-sillage d'un rotor principal d'hélicoptère*. Thesis. Université du Havre, 2002.
[8] Y. MAUFFREY - *Contribution numérique à l'étude des mécanismes aéroacoustiques intervenant dans l'interaction pale-sillage d'un rotor d'hélicoptère*. Thesis. Université Pierre et Marie Curie, 2008.
[9] J. PRIEUR - *Experimental study of High Speed Impulsive Rotor Noise in a Wind Tunnel*. 16th European Rotorcraft Forum, Glasgow 1990.
[10] C. POLACSEK, P. LAFON - *High Speed Impulsive Noise and Aerodynamic Results for Rectangular and Swept Rotor Blade Tip Tests in S1-Modane Wind Tunnel*. 17th European Rotorcraft Forum, Berlin 1991.
[11] J. PRIEUR, W.R. SPLETTSTOESSER - *ERATO: an Onera-DLR Cooperative Programme on Aeroacoustic Rotor Optimisation*. 25th European Rotorcraft Forum Roma, 1999.
[12] P. CROZIER, P. LECONTE, Y. DELRIEUX, B. GIMONET, A. LE PAPE, H. MERCIER DES ROCHETTES - *Wind-Tunnel Tests of a Helicopter Rotor With Active Flaps*. 32nd European Rotorcraft Forum. Maastrricht 2006.
[13] Y. DELRIEUX, A. LE PAPE, P. LECONTE, P. CROZIER, B. GIMONET, H. MERCIER DES ROCHETTES - *Wind Tunnel Assessment of the Concept of Active Flaps on a Helicopter Rotor Model*. 63rd AHS Annual Forum. Virginia Beach, USA, 2007.
[14] A. LE PAPE, C. LIENARD, J. BAILLY - *Active Flow Control for Helicopters*. Aerospace Lab Issue 6, June 2013.
[15] P. RAUCH, M. GERVAIS, P. CRANGA, A. BAUD, J-F. HIRSCH, A. WALTER, P. BEAUMIER - *Blue Edge™: The Design, Development and Testing of a New Blade Concept*. 63rd AHS Annual Forum. Virginia Beach, USA, 2007.
[16] P. GARDAREIN, S. CANARD, J. PRIEUR - *Unsteady Aerodynamic and Aeroacoustic Simulations of a Fenestron Tail Rotor.* 62nd AHS Annual Forum, Phoenix, 2006.
[17] P. GARDAREIN, F. FALISSARD, L. BINET, J.-C. CAMUS - *Validation of Aerodynamic and Aeroacoustic Computations of a Fenestron in Real Flight Conditions*. 36th European Rotorcraft Forum. Paris, 2010.
[18] F. FALISSARD, F. DESMERGER, P. GARDAREIN, L. BINET, J.C. CAMUS - *Aeroacoustic Flight Test and Data Analysis for the Validation of Fenestron Noise Computations*. 67th AHS Forum, Virginia Beach 2011.
[19] J. PRIEUR - *Calculation of Transonic Rotor Noise Using a Frequency Domain Formulation.* AIIA Journal vol 26, 1988.
[20] C. POLACSEK, M. COSTES - *Rotor Aeroacoustics at High Speed Forward Flight Using a Coupled Full Potential/Kirchhoff Method.* 21st ERF, St Petersburg, 1995.
[21] C. POLACSEK, J. PRIEUR - H*igh-Speed Impulsive Noise Computation in Hover and Forward Flight Using a Kirchhoff Formulation*. 1st Joint CEAS/AIAA Aeroacoustics Conference, Munich, 1995.
[22] L. CAMBIER - *The elsA Solver*. 1st Onera-DLR aerospace symposium. Paris 1999.
[23] L. CAMBIER L, M. GAZAIX - *elsA : an Efficient Object-Oriented Solution to CFD Complexity*. AIAA Paper 2002-0108, 2002.
[24] G. RAHIER, J. PRIEUR - *An Efficient Kirchhoff Integration Method for Rotor Noise Prediction Starting Indifferently from Subsonically or Supersonically Rotating Meshes.* 53rd Annual Forum of the American Helicopter Society, Virginia Beach, USA 1997.
[25] P. BEAUMIER, Y. DELRIEUX - *Description and Validation of the Onera Computational Method for the Prediction of Blade-Vortex Interaction Noise*. Aerospace Science and Technology Journal. 2004.
[26] M. ALLONGUE, T. KRYSINSKI - *Aéroélasticité appliquée aux rotors d'hélicoptères - validation du code R85*. 27ème Colloque d'Aérodynamique Appliquée, AAAF, Marseille 1990.
[27] B. BENOIT, A.-M. DEQUIN, K. KAMPA, W. GRUNHAGEN, P-M. BASSET, B. GIMONET - *HOST, A general helicopter simulation tool for Germany and France*. 56th AHS Annual Forum. Virginia Beach, May 2000.
[28] G. RAHIER, Y. DELRIEUX - *Blade-vortex interaction noise prediction using a rotor wake roll-up model*. Journal of Aircraft, Vol.34, N° 4, 1997.
[29] P. SPIEGEL, G. RAHIER - *Theoretical Study and Prediction of BVI Noise Including Close Interactions*. AHS Technical Specialists Meeting on Rotorcraft Acoustics and Fluids Mechanics, Philadelphia, PA, October 1991.
[30] F. CARADONNA, C. KITAPLIOGLU, M. MCCLUER, J. BAEDER, G. LEISHMAN, C. BEREZIN, J. VISINTAINER, J. BRIDGEMAN, C. BURLEY, R. EPSTEIN, A. LYRINTZIS, E. KOUTSAVDIS, G. RAHIER, Y. DELRIEUX, J. RULE, D. BLISS - *A Review of Methods for the Prediction of BVI Noise.* Journal of the American Helicopter Society, Vol. 45, n° 4, pp 303-317, October 2000.
[31] M. COSTES, K. PAHLKE, A. D'ALSACIO, C. CASTELLIN, A. ALTMIKUS - *Overview of Results Obtained During the 6-year French-German CHANCE Project*. 61st AHS Annual Forum, Grapevine, USA 2005.
[32] M. COSTES - *Development of a 3rd-Order Vorticity Confinement Scheme for Rotor Wake Simulations.* 38th ERF, Amsterdam, 2005.

[33] C. BENOIT, G. JEANFAIVRE, E. CANONNE - *Synthesis of Onera Chimera Method Developed in the Frame of CHANCE Program.* 31st ERF, Florence, Italy, 2005.
[34] G. REBOUL and A. TAGHIZAD - *Semi-Analytical Modeling of Helicopter Main Rotor Noise*. 38th European Rotorcraft Forum, Amsterdam, 2012.
[35] J. BAILLY, Y. DELRIEUX - *Improvement of Noise Reduction and Performance for a Helicopter Model Rotor Blade by Active Twist Actuation.* 35th European Rotorcraft Forum, Hamburg, 2009.
[36] G. PEREZ, M. COSTES - *A New Aerodynamic and Acoustic Computation Chain for BVI Prediction in Unsteady Flight Conditions.* 60th Annual Forum Baltimore, 2004.

Acronyms

ABC (Active Blade Concept)
BVI noise (Blade Vortex Interaction noise)
BWI noise (Blade Wake Interaction noise)
CFD (Computational Fluid Dynamics)
CAA (Computational Aeroacoustics)
DNW-LLF (Deutsch-Niederländische Windkanäle-Large Low-speed Facility)
DTP RPA (Développement Technique Probatoire Rotor à Pale Active)
ERATO (Etude d'un Rotor Aéroacoustiquement et Technologiquement Optimisé)
FW-H (Ffowcs Williams-Hawkings)
HART (Higher harmonic control Aeroacoustics Rotor Test)
HHC (Higher Harmonic (pitch) Control)
HOST (Helicopter Overall Simulation Tool)
HSI noise (High Speed Impulsive noise)
LAA (Lightill Acoustic Analogy)
NMR (New Model Rotor)
STAR (Smart Twisting Active Rotor)
S1MA (Soufflerie 1 Modane Avrieux)

AUTHOR

Yves Delrieux has been a researcher at Onera since 1988. He leads the acoustics studies on rotors and propellers in the Computational Fluid Dynamics and Aeroacoustics Department. He obtained a PhD degree from Ecole Centrale de Lyon in 1991. He is mainly involved in noise prediction and optimization of rotary wings.

C. Polacsek, R. Barrier
(Onera)
M. Kohlhaas, T. Carolus
(Institute for Fluid and Thermodynamic)
P. Kausche, A. Moreau
(DLR)
F. Kennepohl
(MTU Aero Engines)

E-mail: cyril.polacsek@onera.fr

DOI : 10.12762/2014.AL07-03

Turbofan Interaction Noise Reduction Using Trailing Edge Blowing: Numerical Design and Assessment and Comparison with Experiments

This paper investigates the effect of a flow control device on turbofan sound generation, applied to a low-speed axial compressor model in a laboratory test rig. This treatment consists in a secondary mass flow ejected through the trailing edge of the rotor blades, designed to fill the velocity defect behind the rotor and to decrease the turbulent kinetic energy related to the wakes, so that broadband interaction noise should be reduced. The design and implementation of the blowing device is first briefly described, as well as the fan stage experiment. Then, the paper focuses on computation methods devoted to the capture of turbulent wakes and to the acoustic response of the stator (with and without blowing). 3D steady RANS and quasi-2D LES approaches are considered for the CFD, both coupled to an integral formulation based on the theory proposed by Amiet, aiming at calculating the in-duct sound power and estimating the acoustic performance of the treatment. Under optimal blowing conditions, significant sound power reductions are predicted by the simulations. First attempts to relate numerical predictions to available measurements, *i.e.*, hot-wire data and in-duct sound power spectra, are proposed and discussed.

Introduction

A major source of broadband turbofan noise results from the interaction of turbulent rotor blade wakes with the outlet guide vanes (OGV). The objective of this study is to assess the effect of a flow control device on sound generation, applied to a low-speed axial compressor model in a laboratory test rig and studied within the framework of the European project FLOCON. This treatment consists in a secondary mass flow ejected through the trailing edge of the rotor blades (Trailing Edge Blowing, TEB). It is designed to fill the velocity defect behind the rotor and to decrease the turbulent kinetic energy related to the wakes, so that interaction noise should be reduced. Tone noise reduction has been successfully investigated by Brookfield and Waitz [1] and by Sutliff et al. [2], with optimal PWL tone reduction measured in the NASA Glenn Aero-Acoustic Propulsion Laboratory (AAPL) of 5.4, 10.6, and 12.4 dB for the first three tones, respectively. Further investigations by Sutliff [3] focused on broadband noise, showing a 2-3 dB average reduction on the turbulent pressure spectrum measured over the stator vane surface. However, only 1 dB attenuation of broadband PWL in the aft arc was assessed by far-field measurements for optimal blowing rate, probably due to the rotor noise dominating the contribution in the Advanced Noise Control Fan (ANCF) test bed. Noise benefits of rotor TE blowing have been also investigated on an advanced model turbofan tested in the NASA Glenn 9- by 15-Foot Low Speed Wind Tunnel (9x15 LSWT) [4], confirming the acoustic performance of the TEB for the tones and indicating some broadband noise reductions, possibly attributed to a reduction of blade wake turbulence.

Another attempt is investigated here on a laboratory test rig with similar TEB technology and using extensive numerical simulations, focusing on the broadband noise component and only considering outlet duct acoustic measurements. Previous studies [5] showed that, for most loaded OGV conditions, the broadband sound power measured in the outlet duct was mainly attributed to the rotor-stator interaction mechanism. Compared to the 1.2 m diameter turbofan simulator used in [3], this laboratory experiment is quite limited by the size of the rig (0.45 m rotor diameter) and then by the thickness of the vanes (very thin) at the trailing edge. Thus, practical blowing mass flow rates can only be reached by increasing the jet velocity. As pointed out in [6], the turbulent mixing of high-speed blowing jets can cause additional broadband noise sources that might increase the PWL spectrum (particularly the high-frequency part), as is also discussed in this paper.

The design and implementation of the blowing device performed by the USI (University of Siegen), already detailed in a more dedicated communication [7], is first briefly described here, as well as the fan stage experiment. Then, the paper focuses on computation methods devoted to the capture of turbulent wakes and to the acoustic broadband response of the stator (with and without blowing). 3D steady RANS and quasi-2D LES approaches are considered for the CFD, both coupled to an integral formulation based on the theory proposed by Amiet, aiming at calculating the in-duct sound power and estimating the acoustic performance of the treatment. Although restricted to a thin radial extent, LES permits the turbulence spectrum content and the integral length scale to be locally assessed. These methodologies and the resulting blowing effect on turbulence characteristics and acoustic behavior are addressed. First attempts to relate numerical predictions to available measurements, *i.e.*, hot-wire data and in-duct sound power level (SPL) spectra are discussed.

Fan stage model and trailing edge blowing implementation

The measurements were performed in a laboratory scale fan rig located at DLR Berlin. For the design and the implementation of the blowing devices, a new fan with 18 blades containing internal passages for TEB was designed. Important design parameters are given in table 1 and figure 1. Two x-hot-wire probes located downstream of the rotor trailing edge plane are used to measure the wake characteristics and a microphone rake provides the acoustic spectra in the outlet duct.

Volume flow rate at the inlet $\dot{V}_{in}$	2.52	[m³/s]	Rotor speed, N	3159	[rpm]
Rotor diameter D_A	0.4524	[m]	No. of rotor blades, B	18	
Hub diameter D_I	0.286	[m]	No. of stator vanes, V	32	

Table 1 – Design parameters of the fan stage

For the rotor blade design, a NACA 6515-63 airfoil with span length L_{span} = 83.2 mm is used. The fan operates at its design flow rate coefficient:

$$\varphi_{in} \equiv \frac{\dot{V}_{in}}{\pi^2 D_A^3 N} = 0.21 \qquad (1)$$

The position of the reference plane corresponds to the stator leading edge. The wake velocity profiles and the turbulent quantities are evaluated at a relative blade height of:

$$h^* = \frac{h}{(D_A - D_I)/2} \qquad (2)$$

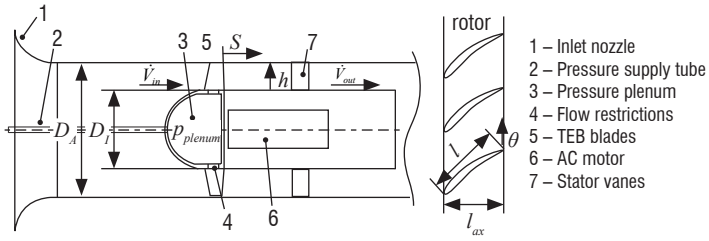

Figure 1 – Schematic drawing of the TEB fan stage: meridional section (left) and coaxial section of the cascade (right)

Figure 2 shows the internal passages with guide vanes, shaped carefully to avoid excessive pressure losses. The internal passages responsible for a specific blade height are connected to the pressure plenum in the hub via flow restrictions, which control the individual blowing mass flow rates. The inlet cross sections of the restrictions, as well as the plenum pressure, were optimized claiming a flat wake velocity profile. A pressure supply tube from the inlet nozzle to the plenum delivers the needed pressure, as well as the overall TEB mass flow.

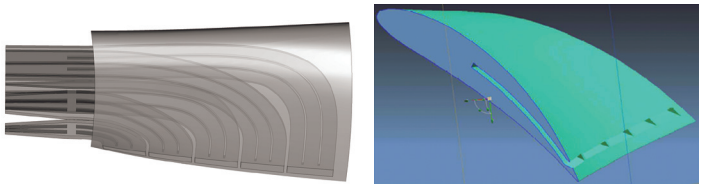

Figure 2 – Rotor blade with internal passages, guide vanes and flow restrictors at the passage entrances (left), and CAD geometry (right) provided by the USI

RANS-based and LES-based methodologies

3D RANS computations (USI)

RANS computations are mainly performed by the USI. The computational domain consists of 1/18th of the bladed annulus, from 1.0 D_A upstream to 1.0 D_A downstream of the rotor. It also covers the five internal blade passages including the guide vanes, from their inlet in the hub to their orifices, where the jet flow mixes with the main flow. General grid interface (GGI) boundary conditions were imposed in the circumferential direction. The inlet mass flow rate of the fan system was imposed on the upstream boundary according to the operation point of φ_{in} = 0.21, while an opening pressure boundary condition was set at the downstream boundary. At the entrance of each of the five internal blade passages, the flow restrictions and the pressure plenum inside the hub were modeled. Of course, no boundary conditions have to be specified at the exit of the channels (*i.e.*, the orifices), since the flow mixes with the main flow. To solve the RANS equations, ANSYS CFX with the standard SST-turbulence model and a 2nd order approximation (blend factor of 1) was employed [8]. The block structured numerical grid consists of 7.1 million nodes. Special attention was paid to the wake region, by using a very fine grid resolution of about 3 million nodes. Common grid quality criteria were considered in most of the fluid flow regions (grid angles > 20°). Due to geometrical restrictions, some grid angles in the TEB injection orifices were as small as 13°. In these regions, a finer grid was employed to ensure sufficient accuracy. For the simulation, the maximum value of y^+_{max} for the first node adjacent to the blade surface was < 6, whereas the area averaged y^+_{ave} at the blade was < 1. The convergence criteria were set to 1.10^{-6} MAX residuals.

3D RANS and quasi-2D LES computations (Onera)

3D RANS computations have been also performed on a baseline case, using the CFD Onera code elsA that solves the compressible equations in the relative frame with a cell-centered finite volume formulation. Space discretization is ensured using the Jameson second-order-centered scheme with the addition of an artificial viscosity. Turbulence closure is achieved using the k-l turbulence model proposed by Smith [9]. In this model, l (characteristic length scale of turbulence) is a transported quantity. The computation is performed on a single rotor passage using a multi-block grid of about 1 million nodes. Particular attention has been paid to the mesh downstream of the blade, to keep

a good description along the wake development zone. The mesh has 17 cells in the rotor tip gap. The exit plane is located approximately at 3 chord lengths from the rotor trailing edge.

Due to CPU and memory limitations, the LES approach is practically restricted to a quasi-2D computation [10,11] so that the simulation is only focused here on a thin strip (L_{strip}) of the full spanwise response. As in reference 10, the sub-grid scale viscosity is given by the WALE model (Wall Adapting Local Eddy-viscosity) [12]. The quasi-2D computation domain is a section in a circumferential plane at mid-span (corresponding precisely to a half height of the central injection slit for the blowing case) and extruded in the spanwise direction over 20% of the chord (figure 3, left). The full 3D test-case is thus converted to a cascade-like test-case for the LES simulation, assuming that flow physics of the fan rig remains well captured by this conversion. In the LES simulation, the incoming flow is perfectly laminar. Any "background" turbulence thus comes only from the unsteadiness created in the simulation (that is, from shear, even small, outside the boundary layer and the wake zone). The mesh size (Δx, Δy, Δz) near the airfoil must verify some criteria for the validity of the LES computation. The non-dimensional criteria used for this study are: $\Delta x^+ \leq 40$, $\Delta y^+ \leq 2$, $\Delta z^+ \leq 20$.

The blowing mass-flow in the central injection slit obtained from a 3D computation (USI) is translated in the quasi-2D LES as an equivalent mass-flow, by using uniform blowing along the entire extrusion of the blowing slit (figure 3, right). Optimal blowing conditions issued from USI computations were obtained with $\dot{m}_{blowing}$ = 142 g/s.

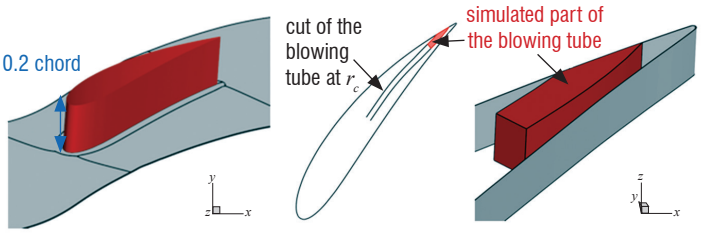

Figure 3 – LES spanwise extrusion (left) and simulated part of the blowing tube (right)

Acoustic post-processing based on the Amiet broadband noise theory

This section presents the Amiet-based theory [13] adopted here to predict broadband interaction noise, using either 3D RANS or 2D LES output data. A concise form of Onera formulation [14] providing the power density spectrum (PSD) of the acoustic power, S_{ww}, in the outlet duct can be written as:

$$S_{ww}(f) = V \sum_{m=-m_{\max}}^{+m_{\max}} \sum_{n=1}^{n_{\max}} \varphi_{mn}(r_s, f) \left| \mathcal{L}(r_s, K_c, 0) \right|^2 U_c \, \phi_{u_n u_n}(K_c, 0) \quad (3)$$

φ_{mn} is a kernel function related to the Green function (valid for an annular duct and a uniform mean flow), $\mathcal{L}$ is the aeroacoustic transfer function obtained from the aerodynamic response of an isolated (zero-thickness) stator vane. K_c and U_c are respectively the convection wave-number and the convection speed, taken equal to the streamwise velocity (U_s). $\phi_{u_n u_n}$ is the 2-wavenumber turbulence spectrum related to the upwash velocity component, u_n, and adjusted using standard Von-Karman model. $\phi_{u_n u_n}$ can be expressed versus the turbulent velocity spectrum, $S_{u_n u_n}$ and the spanwise correlation length scale, ℓ_y :

$$\phi_{u_n u_n}(K_c, 0) = \frac{U_c}{\pi} S_{u_n u_n}(\omega) \ell_y(\omega) \quad (4)$$

$\phi_{u_n u_n}$ requires the knowledge of the mean-square turbulent velocity, u_{turb} (also related to the kinetic energy, k) and the integral length scale, Λ. This information is usually obtained from a RANS calculation. In (4), the upwash turbulent velocity spectrum and spanwise correlation length scale may be directly post-processed from LES output data, as done here for $S_{u_n u_n}$. However, assessment of ℓ_y is practically not feasible, because the radial extent is too thin. An alternative approach is to use an analytical expression for ℓ_y, deduced from the Von-Karman spectrum and directly related to Λ, as discussed by Lynch [15]. CFD data extraction for RANS and LES output post-processing is sketched in figure 4. The inter-stage red plane in figure 4 (left) corresponds to the hot-wire position in the DLR rig. Inputs to (4) are taken at the stator leading edge (LE) position. In figure 4 (right), LES data is interpolated from the rotating frame to the fixed frame and uniformly distributed along a mean streamline assumed to represent the path of convected turbulent structures impacting the stator vane (chord aligned to this path). This allows us to calculate the turbulent velocity spectra and the integral length scale at mid span.

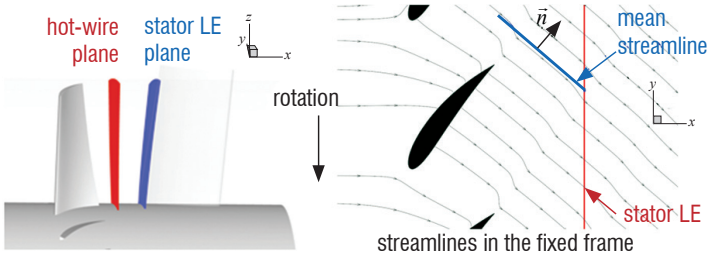

Figure 4 – CFD data extraction for aeroacoustic analyses: 3D RANS (left) and quasi-2D LES (right)

Aerodynamic and noise predictions, and comparison with experiment

Rotor wake characteristics

Firstly, wake characteristics in terms of velocity defect and turbulence intensity have been analyzed, in order to check the reliability of the CFD computations (by comparison to the experiment in a baseline case) and to estimate the effect of the blowing. Axial velocity profiles computed by USI RANS are compared to the measurements for two spanwise stations in figure 5. Predicted and measured blowing effects are similar, showing a significant reduction at 74% span but an overshoot at 44% span, revealing quite important radial effects. Although optimal blowing conditions assessed by RANS were estimated using a minimization process at several radial stations, wake filling performances achieved by a blowing distribution through the five slits and measured by the hot-wire probes reveal significant differences (compared to the simulations), particularly when moving towards the casing.

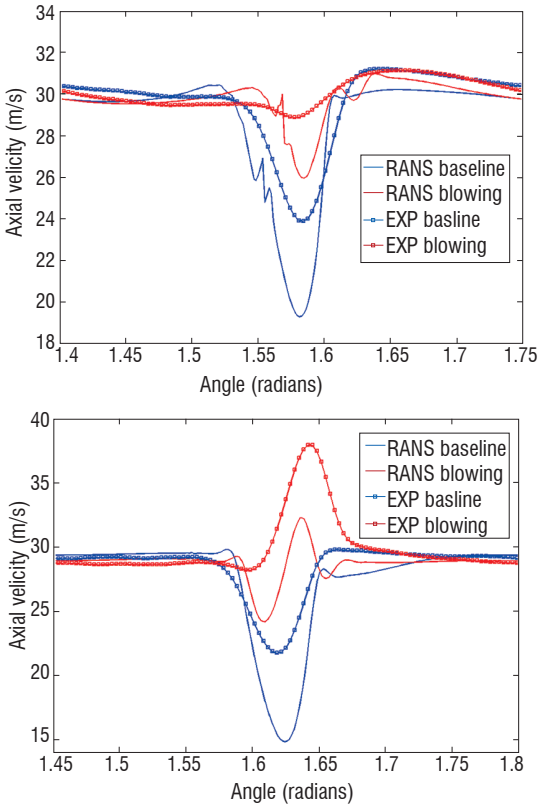

Figure 5 – Axial velocity profiles issued from USI RANS and experiment at 74% (top) and 44% (bottom) span

Turbulence intensity, T_u, scaled by axial, radial and tangential velocity components is defined as:

$$T_u = \frac{u_{turb}^{1/2}}{U_s} = \frac{u_{turb}^{1/2}}{\sqrt{U_x^2 + U_r^2 + U_t^2}}$$

$$u_{turb} = \frac{1}{3}\left(\left\langle u_x^2 \right\rangle + \left\langle u_r^2 \right\rangle + \left\langle u_t^2 \right\rangle\right) = \frac{2}{3}k \qquad (5)$$

T_u 360°-plots issued from USI RANS baseline computation (1 rotor blade channel) and from baseline and blowing experimental cases (18 blade passages) are compared in figure 6. The agreement between prediction and measurements is rather good, although the turbulent wake level is over estimated by RANS. Intense turbulence spots near the hub and casing can be also observed in the experiments. Measured T_u wakes are clearly attenuated when the blowing is active (figure 6, right), despite slight blade-to-blade irregularities. This effect is highlighted in figure 7, comparing the T_u plots over 1 blade channel (time-averaging using blade passing trigger in the experiment). The reduction of turbulence intensity due to the blowing is fairly well assessed by the CFD, but the levels are overpredicted, except near the blade foot region, where the measurements are higher.

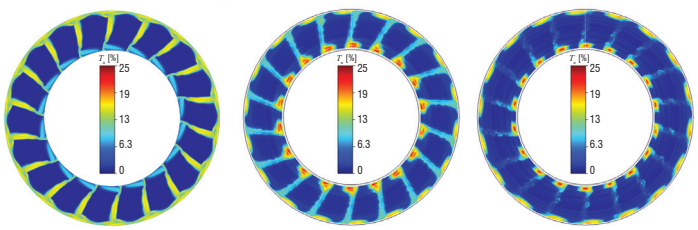

Figure 6 – Turbulent intensity plots: RANS-SST (baseline, left) and exp. (baseline, mid. and blowing, right)

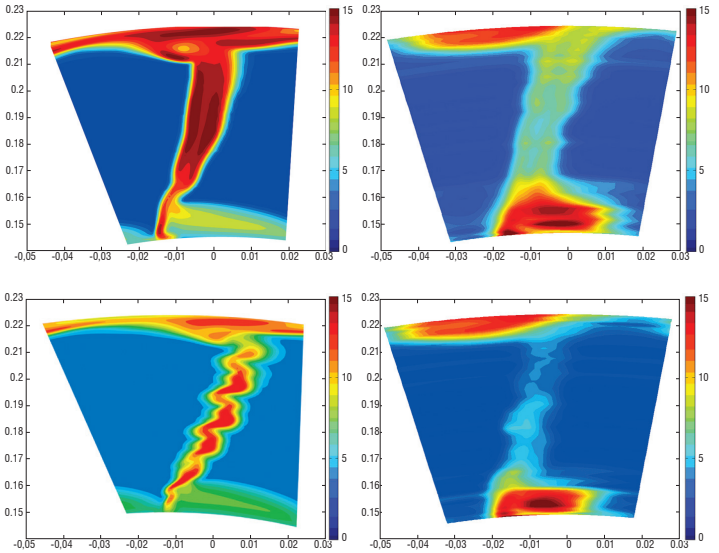

Figure 7 – Blade channel turbulent intensity plots provided by RANS-SST (left) and experiment (right): baseline (top) and blowing (bottom) cases

The LES simulation is useful to capture unsteady phenomena, as can be seen in figure 8, showing a snapshot of Mach number and Q-criterion isosurface (with/without blowing). While both computations show a separation with production of turbulent structures occurring on the suction side of the blade, separation seems to be much less massive in the blowing case. Downstream from the rotor, the turbulent structures are also smaller and restricted to a thinner wake when blowing is active. This phenomenon is highlighted in figure 9, related to the flow near the blowing slit, obtained by an average of the LES solution during a five rotor blade passage, which reveals a strong blowing effect that tends to delay the separation and reattachment points of the boundary layer almost up to the blowing slit. The turbulence kinetic energy in the blade wake region computed from velocity fluctuations during the five rotor blade passage is plotted in figure 10, for the baseline and blowing cases. A strong reduction in the turbulence kinetic energy can be clearly seen when the blowing is active.

These LES predictions were carefully checked by comparing the relevant averaged fields to those provided by RANS at the same spanwise position. Angular profiles of turbulence intensity deduced from LES (with/without blowing) at inter-stage position are plotted in figure 11 and compared to the RANS $k-\ell$ baseline solution. T_u is strongly reduced by the blowing and baseline solutions are found to be rather close to experiment, with an LES amplification that could be attributed to confined grid (quasi-2D) effects. It should be noted that the background turbulence level (about 2%) visible in figure 11 is contributing to the theta-averaged levels of T_u profiles discussed below. For reliability, we tried to obtain a similar value of this background turbulence level between RANS and measurements at the inlet boundary condition, as shown by the comparison addressed in figure 12.

Finally, the radial profiles of T_u obtained from a circumferential averaging of CFD solutions at the hot-wire plane are compared to the experimental values (blade passage trigger average) in the baseline case in figure 13, showing the best agreement for the RANS-SST model. Blowing efficiency provided by the USI RANS is found to be comparable to the measurements in terms of T_u reduction (figure 13, bottom). As already observed in figures 6 and 7, a strong turbulence activity is measured in the vicinity of the hub, attributed to a flow separation near the blade foot (laboratory test rig imperfections) and giving rise to vortex shedding not captured by RANS and not reduced by the blowing.

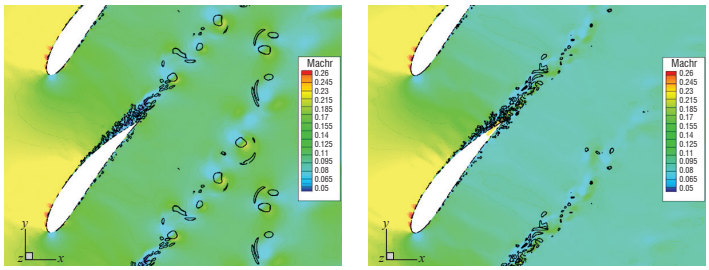

Figure 8 – Relative Mach number and iso-surface of the Q-criterion (LES snapshot): Baseline case, left, and blowing case, right

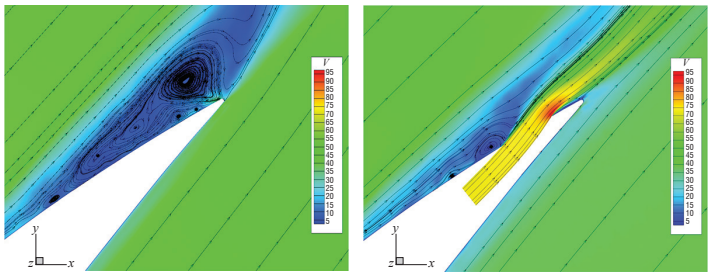

Figure 9 – LES-averaged relative velocity amplitude and streamlines near the blowing slit, without (left) and with (right) blowing

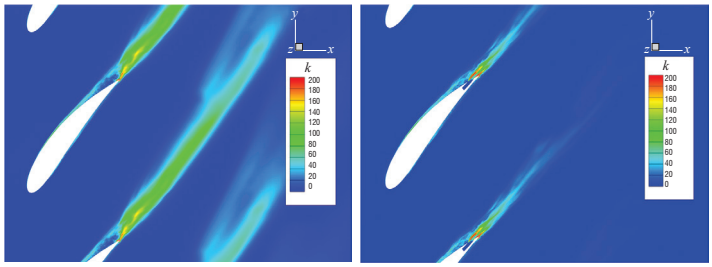

Figure 10 – Turbulence kinetic energy (m^2/s^2) from LES velocity fluctuation averaging: Baseline case, left, and blowing case, right

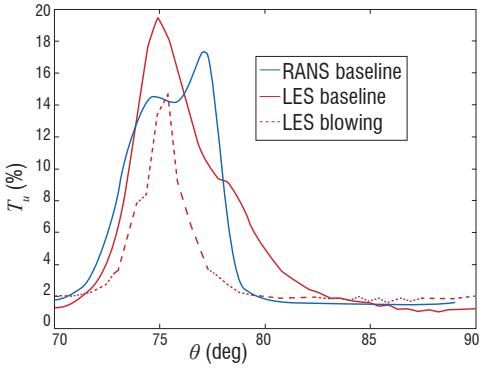

Figure 11 – LES T_u profiles compared to RANS $k-\ell$ at mid-span and hot-wire axial position

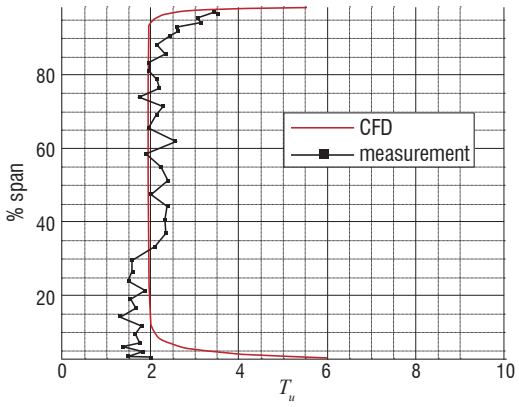

Figure 12 – T_u intensity (%) provided by RANS $k-\ell$ compared to measurement at the inlet

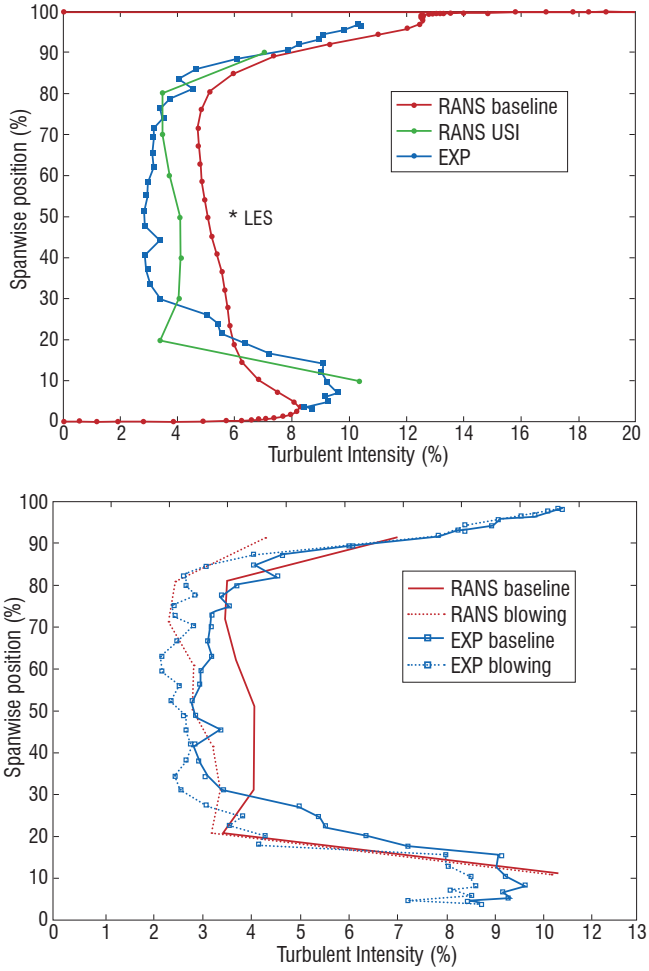

Figure 13 – T_u radial profiles: CFD *vs.* experiment in the baseline case (top), and blowing vs. baseline (bottom)

Turbulent velocity spectra and correlation scales

LES simulations data is post-processed, in order to assess the turbulent velocity spectra and correlation scales. PSD of the upwash velocity component ($S_{u_n u_n}$ in (4)) calculated at the inter-stage for the baseline and blowing cases are compared in figure 14 to the Von-Karman spectra (used in (3)). Slopes are similar, but a hump over a wide frequency range can be observed in the LES solutions. The streamwise 0-time shift cross-correlation function (applied to the streamwise velocity component) is compared for baseline case to the theoretical Gaussian solution [11] in figure 15 top, showing a very good agreement. The integral scale Λ (deduced by integration over x) is found to be close (at mid-span) to the RANS-based solutions plotted in figure 15 bottom. RANS-based solutions are obtained from a circumferential average of the integral length scale, directly extracted from the CFD for the Onera result, because this length is a transported quantity of the $k-\ell$ turbulence model. Turbulent (streamwise) velocity spectra measured by hot-wire probes at 74% and 44% span are plotted in figure 16 top and bottom, respectively. These are compared to the LES solution scaled in level (- 10 dB) and overplotted in figure 16 top, showing very close attenuation slopes and similar trends of blowing effects at 74%. However, blowing at 44% is much less efficient, with a level increase for frequencies beyond 4 kHz. Thus the OASPL obtained with blowing for this radial station would be just slightly lower than for the baseline case. A similar tendency for measured turbulence intensity profiles can be observed in figure 13, showing a lower level reduction around 45% span (discarding the spurious baseline oscillating point), compared to 75% span. The rise of turbulent velocity levels beyond 4 kHz (figure 16 bottom) should have a hard impact

on the noise level in this frequency range, as will be discussed in following section. The numerous peaks visible in the red spectra when the blowing is active (whereas only expected BPF tones are present without blowing) should also be noted. These might be attributed to small blowing jet variations from blade-to-blade (non-homogeneous wake filling), giving rise to multiple pure tones (rotor rotation harmonics). Such extra tones were pointed out in reference [4], when investigating alternate blade blowing.

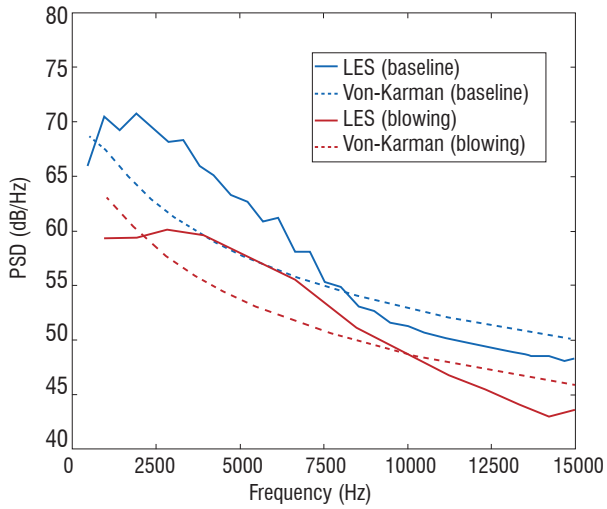

Figure 14 – PSD of upwash turbulent velocity resulting from LES and Von-Karman model

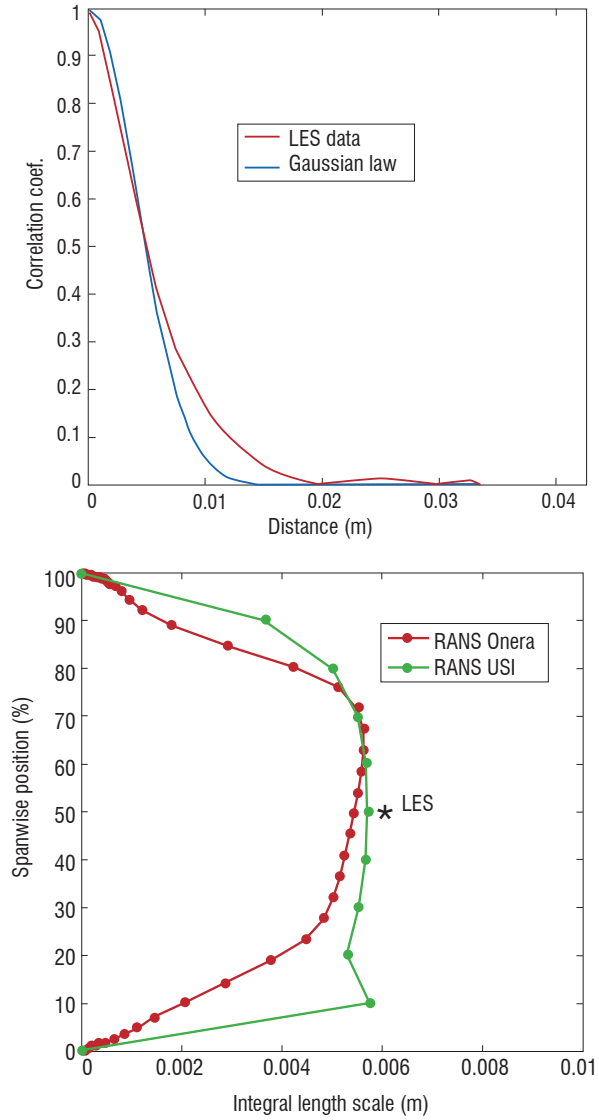

Figure 15 – LES-based streamwise correlation function (top) and integral length scale issued from RANS and LES (bottom)

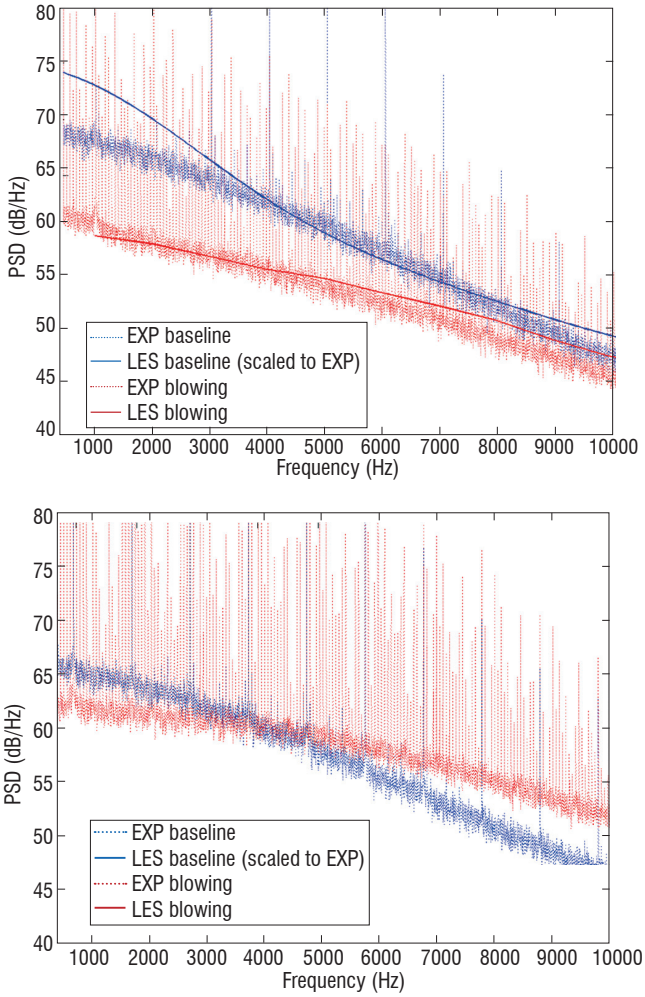

Figure 16 – PSD of streamwise turbulent velocity at 74% span (top) and at 44% span (bottom)

Assessment of sound power level broadband noise reduction

Previous RANS and LES analyses are used to estimate the PSD of acoustic pressure in the outlet duct (observer at outer wall), as shown in figure 17 for the baseline case. The LES-based prediction is achieved by applying a basic scaling correction $10\log\left(L_{span}/L_{strip}\right)$ on the sound pressure level (SPL). A satisfactory agreement is obtained for the RANS-based solutions, whereas the LES-based spectrum is over-predicted (certainly due to the quasi-2D approach restrictions). However, the frequency slope using LES seems better appraised. Finally, PSD of acoustic power (PWL spectra) using RANS-SST and LES input data are presented and compared in figure 18 top. Sound power (obtained by integrating acoustic intensity along the duct section) is more suited than sound pressure to estimate the acoustic performance of the TEB, and calculated PWL spectra have been smoothed for clarity. As expected from turbulent wake analyses, significant reductions are observed in the computation results, with relative level attenuations that are twice as large for LES compared to RANS (about 7 dB vs. 3.5 dB max), but with quite similar behavior with respect to frequency. This must be related to the experimental SPL spectra, measured by a microphone at the casing wall, in figure 18 bottom. Unfortunately, experimental results do not show any noise reduction, nor for the tones (see the non-filtered spectra), and moreover highlight a broadband level increase for frequencies beyond 4 kHz. This sound increase at high frequencies is certainly related to the rise of turbulent velocity spectra already observed from the hot-wire probe results at 44% span (figure 16 bottom). This is quite disappointing, since numerical simulations suggested significant acoustic performances of this TE blowing device, confirming the previous published results from NASA Glenn tests [3,4]. A few possible explanations of this test failure are addressed in the last section.

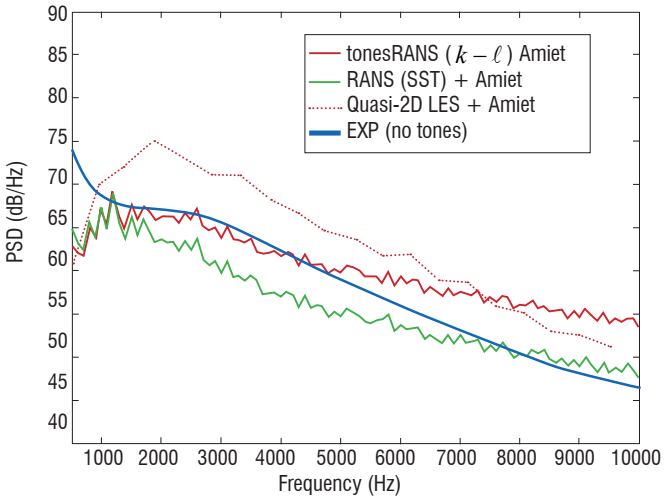

Figure 17 – SPL spectra (baseline) resulting from calculations and experiment

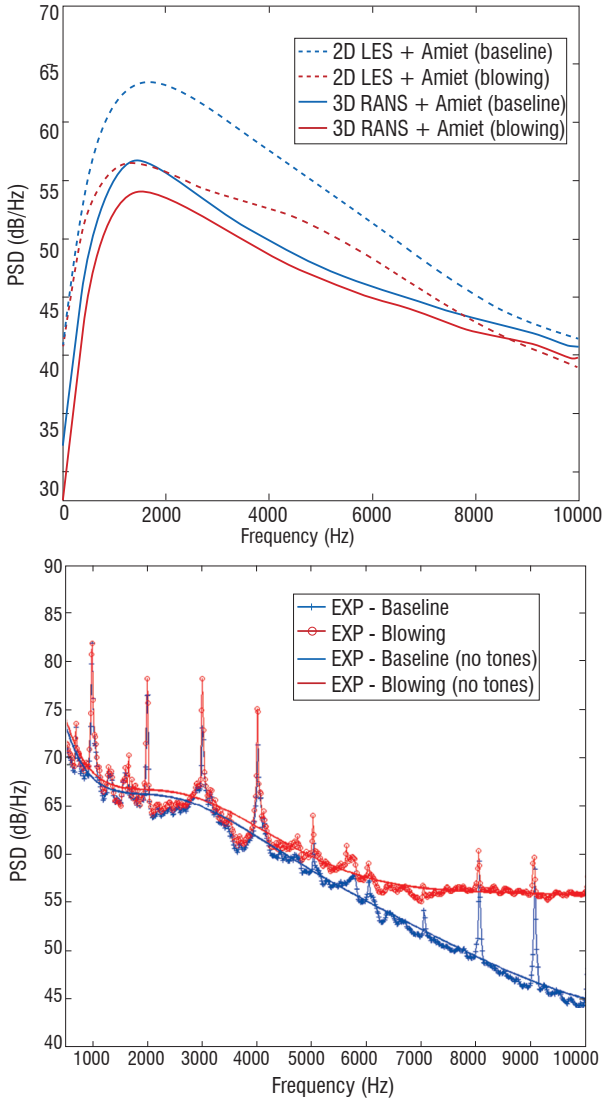

Figure 18 – Blowing effect on broadband noise spectra PWL predictions (smoothed, top) and SPL measurements (bottom)

Possible explanations of noise reduction failure in the experiments

Regarding CFD data and hot-wire probe analyzes, three main reasons can be argued for observing no noise reduction in the experiments:

- This laboratory axial compressor rig is characterized by intense turbulence structures in the vicinity of the hub and the casing, which largely contribute to the RSI broadband noise and are poorly affected by the blowing. The blowing mass flow rate was optimized assuming no separated flows at the blade foot and thus under-predicting these 3D effects in the spanwise direction. TE blowing in this test rig is certainly efficient with respect to turbulent wake reduction away from these regions. This decrease in the turbulent wake intensity is balanced by the interaction sources near the hub and casing. Similar spanwise dependency has been noticed for the velocity defects (reduction at 75% and overshoot at 45% span), limiting the tone noise reduction also;

- A non-homogeneous wake filling from blade-to-blade is suspected from rotor-clock average analyzes, revealing non fully periodic wakes in the (r-θ) planes and the presence of numerous tones in the hot-wire spectra when the blowing is active. This may also be responsible for minimizing the efficiency of the blowing, assumed to be fully homogeneous in the simulations;

- Due to the small size of the slits, the blowing jet speed is very high and jet mixing velocity fluctuations captured by hot-wire measurements at some radial positions may contribute to self jet noise, particularly at medium and high frequencies, as shown by the sound spectra.

Conclusions

A comprehensive study of turbofan broadband noise reduction using a trailing edge blowing device has been carried out numerically and experimentally in a laboratory axial compressor stage rig. The blowing design and optimal settings were obtained through extensive RANS computational studies. 3D RANS simulations have been supplemented by quasi-2D LES, in order to better assess the turbulent characteristics of the flow, and CFD post-processed data has been used as input to an Amiet-based acoustic calculation. Wake analyses have shown relevant reductions in the velocity defect and turbulent intensity, in good agreement with the hot-wire measurements performed in the inter-stage plane. These are responsible for significant SPL attenuations in the outlet duct spectra (up to 3.5 dB for RANS-based and up to 7 dB for LES-based solutions) with a similar response to frequency, which lets this methodology appear reliable. However, the acoustic measurements have not revealed any acoustic performance of the blowing (moreover, some noise increase was detected at high frequencies). This mismatch has been discussed at the end of the paper and can be attributed to a strong turbulence activity in the test rig duct wall hub and to a non-homogeneous wake filling from blade-to-blade. The contribution of mixing jet sources not considered in these simulations is also suspected ■

Acknowledgements

This work was supported by the European Commission (FLOCON).

References

[1] J.M. BROOKFIELD and I.A. WAITZ – *Trailing-Edge Blowing for Reduction of Turbomachinery Fan Noise*. Journal of Propulsion and Power, vol. 16, n°. 1, pp. 57-64, 2000.
[2] D.L. SUTLIFF, D.L. TWEEDT, E.B. FITE and E. Envia – *Low Speed Fan Noise Reduction with Trailing Edge Blowing*. NASA/TM-2002-211559, 2002.
[3] D.L. SUTLIFF – *Broadband Noise Reduction of a Low-Speed Fan Noise Using Trailing Edge Blowing*. NASA/TM-2005-213814 and AIAA-2005-3028, 2005.
[4] R.P. WOODMARK, E.B. FITE and G.G. PODBOY – *Noise Benefits of Rotor Trailing Edge Blowing for a Model Turbofan.* AIAA-2007-1241, 2007.
[5] V. JURDIC, A. MOREAU, P. JOSEPH, L. ENGARDT and J. COUPLAND – *A Comparison between Measured and Predicted Fan Broadband Noise Due to Rotor-Stator Interaction*. AIAA-2007-3692, 2007.
[6] M.L. LANGFORD, C. MINTON, W.F. NG, R.A. BURDISSO and C. HALASZ – *Fan Flow Control for Noise Reduction Part 3: Rig Testing of Optimal Design*. AIAA-2005-3027, 2005.
[7]M. KOHLHAAS and T. CAROLUS – *Trailing Edge Blowing for Reduction of Rotor-Stator Interaction Noise: Criteria, Design and Measurements*. ISROMAC-14, Honolulu (USA), 2012.
[8] ANSYS – *Ansys CFX-Solver, Release 10.0: Modelling.* Canonsburg, Pennsylvania, 2005.
[9] B.R. SMITH – T*he Near-Wall Model for the* $k-\ell$ *Two Equation Turbulence Model.* AIAA-94-2386, 25th Fluid Dynamics Conference, Colorado Springs (Colorado), 1994.
[10] J. RIOU, S. LÉWY and S. HEIB – *Large Eddy Simulation for Predicting Rotor-Stator Broadband Interaction Fan Noise*. Inter-noise 2007, Istambul, August 2007.
[11] G. ASHCROFT and D. NURNBERGER – *A Computational Investigation of Broadband Noise Generation in a Low-Speed Axial Fan*. AIAA-2009-3219, Miami, Florida, 2009.
[12] F. NICOUD and F. DUCORS – *Subgrid-Scale Stress Modelling Based on the Square of the Velocity Gradient.* Flow Turbulence and Combustion, vol. 62(3), pp. 183-200, 1999.
[13] R. K. AMIET – *High-Frequency Thin Airfoil Theory for Subsonic Flow*. AIAA Journal, 14(8), 1976.
[14] G. REBOUL, C. POLACSEK, S. LÉWY and S. HEIB – *Ducted-fan Broadband Noise Simulations Using Unsteady or Averaged Data*. Inter-noise2008, Shangaï, China, 2008.
[15] D.A. LYNCH, T.J. MUELLER and W.K. BLAKE – *A Correlation Length Scale for the Prediction of Aeroacoustic Response*. AIAA-2002-2569, 2002

Acronyms

AAPL	(Aero-Acoustic Propulsion Laboratory)
ANCF	(Advanced Noise Control Fan)
CFD	(Computational Fluid Dynamics)
GGI	(General Grid Interface)
LE	(Leading Edge)
LES	(Large Eddy Simulation)
LSWT	(Low Speed Wind Tunnel)
OASPL	(Over All Sound Pressure Level)
OGV	(Outlet Guide Vanes)
PSD	(Power Density Spectrum)
PWL	(sound PoWer Level)
RANS	(Reynolds-Average Navier-Stokes)
RSI	(Rotor Stator Interaction)
SPL	(Sound Pressure Level)
SST	(Steady State Turbulence)
TEB	(Trailing Edge Blowing)
USI	(University of Siegen)
WALE	(Wall Adapting Local Eddy-viscosity)

Cyril Polacsek graduated from the Ecole Nationale Supérieure d'Ingénieurs de Poitiers (ENSIP) in 1989, with a Masters Degree in aeroacoustics and signal processing. He started his career at Onera as a test engineer (rotorcraft test campaigns in S1-Modane wind tunnel facilities) and became a specialist in source modeling and numerical simulations related to turbomachinery noise. He is now in charge of turbofan noise activities in the "CFD and Aeroacoustics" Department.

Raphaël Barrier graduated from the École Centrale de Marseille and received a Masters Degree in mechanical and aerospace engineering at the Ecole Centrale Paris in 2005. An engineer at Onera since 2006, he is in charge of CFD studies and software development concerning analysis and design for turbomachinery components. He is also in charge of the technical and scientific aspects of the turbomachinery related studies in the Applied Aerodynamics Department.

Michael Kohlhaas graduated in 2009 from the University of Siegen, where he obtained his Diploma degree in Mechanical Engineering. Since 2009, he has been working as a doctoral student in the Turbomachinery Group of the Fluid und Thermodynamics Institute (Institut für Fluid und Thermodynamik, IFT) in Siegen. His current activities involve the reduction of rotor-stator interaction noise by trailing edge blowing.

Prof. Thomas Carolus is head of the Turbomachinery Group at the Fluid and Thermodynamics Institute (Institut für Fluid und Thermodynamik, IFT) of the University of Siegen, Germany. He received his Diploma, Master and Ph.D. degrees from the Universität (Technische Hochschule) Karlsruhe and the Georgia Institute of Technology in Atlanta, USA. Before joining the University of Siegen, he was senior research engineer for the German automotive supplier Bosch.

Philip Kausche studied Aeronautics and Astronautics at the Technical University of Berlin and graduated in 2008. He wrote his diploma thesis in the Engine Acoustics department at the German Aerospace Center (DLR) in Berlin. Since then, he has worked there as a research scientist on several European projects. Currently, he is working on the completion of his dissertation, which is about noise control in a turbomachine.

Antoine Moreau studied in Toulouse at the Ecole Nationale Supérieure d'Ingénieurs en Construction Aéronautique (ENSICA) and obtained his degree in Aerospace Engineering in 2005. Since then, he has been working at the Engine Acoustics Department of the German Aerospace Center (DLR) located in Berlin. His research is focused on fan and compressor acoustics and the development of low-noise aerodynamically efficient designs, based on experiments and theoretical prediction methods.

Fritz Kennepohl received his mechanical engineering diploma at the Technical University of Braunschweig in 1978. Since then he has been working for MTU Aero Engines in various positions, on acoustic design of aeroengine components, development of noise prediction methods, analysis of measurements, etc. His scientific focus has been on the generation and reduction of turbomachinery noise and particularly turbine noise. He retired in 2013, after the end of the European Research project FLOCON.

F. Simon
(Onera)
T. Haase, O. Unruh, M. Pohl
(DLR)
E. Tijs
(Microflown)
R. Wijntjes, H. van der Wal
(NLR)
G. L. Ghiringhelli
(Politecnico di Milano)

E-mail: frank.simon@onera.fr

DOI : 10.12762/2014.AL07-04

Activities of European Research Laboratories Regarding Helicopter Internal Noise

Although the acoustic comfort in helicopter cabins is not subject to European Recommendations regarding aeronautic environmental noise (ACARE 2020), helicopter manufacturers use many resources to improve internal acoustic comfort. This task is particularly difficult because, on the one hand, passengers are in close proximity to the disturbing sources and, on the other hand, the noise frequency range is located in the domain of high sensitivity of the human ear (500-5000 Hz). These activities are often conducted in conjunction with external laboratories specialized in the aeronautic domain.
The purpose of this paper is to describe how different European laboratories (affiliations of the authors), involved in a "Helicopter Garteur Action Group" (AG20), usually address this problem of helicopter internal noise, in particular in terms of design, characterization or active control of vibration applied to helicopter panels, in order to improve acoustic comfort.
Typical measurement techniques and applications of simulation methods are presented to illustrate the activities of laboratories, especially the characterization and optimization of the acoustic behavior of an isolated helicopter panel and, secondly, the evaluation of its effect in a cabin mock-up or in flight. In addition, procedures of active (or semi-active) control are described and applied to the vibro-acoustic transmission of an isolated panel, then to an anti-torque plate of a helicopter mock-up and finally in flight, in order to reduce the noise produced by gear-box vibrations.

Introduction

For several years, aeronautical industries have wished to improve internal acoustic comfort. This is particularly true within the cabin of a helicopter, where passengers are in close proximity to disturbing sources that contribute to interior noise: main and tail rotors, engines, main gearbox (tonal noise) and aerodynamic turbulence (broadband noise) (figure 1).

These sources generate bending vibrations of the entire tail boom, induced vibrations in the cabin at blade passing frequencies (up to 60 Hz), transient vibrations of rotor blades (2-10 Hz) and structure borne noise induced by gear meshing within gear-boxes (500-5000 Hz). External noise (up to 4000 Hz) is also transmitted by acoustic leakages between fuselage and doors.

For a safe, comfortable and healthy helicopter, the following requirements are decisive:

- cabin vibration levels below 0.05 g for steady flight and 0.11g for transition flight (derived from the EC Directive 2002/44/EC on whole-body vibrations);
- cabin noise levels between (80÷85) dBA for steady flight and 87 dBA for transition flight (derived from the EC Directive 2003/10/EC on interior noise).

It can be noted that these values are higher than in airliner cabins (i.e., 70 dBA) and don't correspond to jet smooth ride comfort (i.e., 0.02 g).

Several European projects have as objectives the reduction of cabin noise and vibration levels: i.e., RHINO (Reduction of Helicopter Interior NOise), FRIENDCOPTER (FRIENDly HeliCOPTER), CREDO (Cabin noise REduction by experimental and numerical Design Optimization) or HELINOVI (HELIcopter NOise and VIbration reduction).

It appears that conventional passive systems (trim panels and passive anti-resonance isolation systems, as well as classical vibration

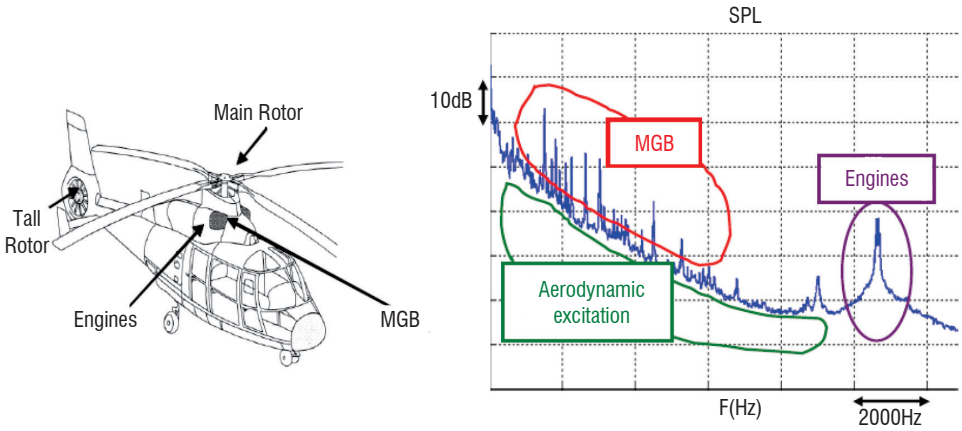

Figure 1 - Main sources with frequency ranges

absorbers and pendulum absorbers) are still the main way to control the acoustics of the cabin, whereas active systems (active vibration and noise control), despite many studies in laboratories since the 1990s, are really applied only in particular cases in complement to passive solutions (structure piezo control, strut vibration control, active noise reduction headrest, etc.). It is due to difficulties to provide algorithm robustness (instability of time convergence), with a spatial reduction (particularly in the medium and high frequency range) and due to a critical balance in terms of added mass and electrical power.

The purpose of this paper is to describe how different European laboratories usually address this problem of helicopter internal noise, in particular in terms of design, characterization or active control of vibration applied to helicopter panels, in order to improve the acoustic comfort. It is based on a think tank, "Helicopter Garteur Action Group", devoted to "Design and characterization of composite trim panels" (AG20).

The activities of the laboratories involved in this group (affiliations of the authors) are presented through the description of mature or in-progress measurement techniques and applications of simulation methods, firstly, to determine and optimize the acoustic behavior of an isolated passive and active helicopter panel and, secondly, to evaluate its effect in a cabin mock-up, or in flight. Finally, in order to reduce the pressure radiated by a helicopter cabin roof (mechanical deck), active control of vibration transmission through the anti-torque plate and cabin roof is also discussed.

Figure 2 - Business" configuration in the cabin of a Eurocopter EC 135

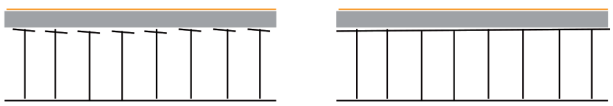

Figure 3 - Honeycomb sandwich panel, front side open (left) or closed (right), with absorption layer

Acoustic behavior of an isolated helicopter panel

With regard to passive systems, trim panels in helicopter cabins (figure 2) are generally provided with a core in honeycomb and external layers (laminates) in composite fibers, front side open or closed, sometimes with an absorptive layer (Figure 3)

This light trim assembly is not subjected to a high static force and must simply ensure sufficient stiffness to not be damaged during the helicopter life. Each material fulfills specific tests to be certified: behavior at high temperatures, with humidity, etc. Nevertheless, these components can worsen the internal acoustic comfort.

The Acoustic Transmission Loss (TL) of a trim panel (or fuselage) allows its acoustic efficiency to be quantified. It represents the ratio between incident acoustic power, produced by a diffuse acoustic field, and the acoustic power radiated by the panel (figure 4).

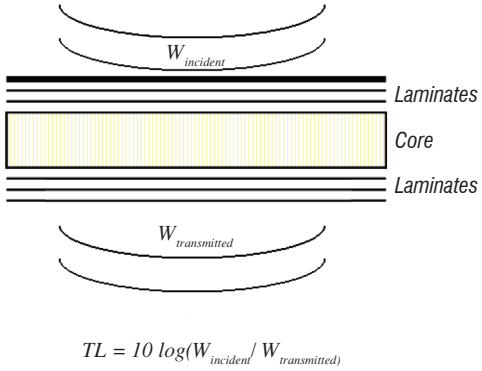

Figure 4 - Acoustic Transmission Loss applied to a trim panel

Measurement of TL (NLR)

This type of parameter is currently measured in a laboratory on an elementary panel, with a controlled excitation. The mounting conditions of the test objects are of great importance for the measured results. Due to practical reasons, the mounting can vary considerably between various labs.

At NLR, the panels tested, representative of a fuselage section are suspended on springs, free from the surrounding structure. The rea-

son for choosing a free-free set-up is to have well defined boundary conditions, in order to preclude possible difficulties in formulating the boundary conditions correctly in a FEM model. Flanking noise has been suppressed adequately by a specially designed panel support structure.

The TL is measured according to the method described in ISO Standard 15186-1, the TL in dB being determined from:

$$TL = SPL_{send} - 6 - SIL_n - 10\log\left(\frac{S_m}{S}\right)[dB] \quad (1)$$

where SPL_{send} is the sound pressure level in the sending room (in dB re 20 μPa), measured with a microphone on a rotating boom, SIL_n is the sound intensity level (in dB re 1 pW/m^2), normal to and averaged over the measuring surface S_m, and S is the area of the test specimen (i.e., the part radiating sound to the receiving room).

The NLR test set-up is shown in figure 5. The volume of the reverberation room is 33 m3, resulting in a diffuse sound field for frequencies of about 500 Hz and higher. In order to reduce the measuring error below 500 Hz due to insufficient diffusivity of the sound field, the TL is determined from successive measurements for different loudspeaker positions.

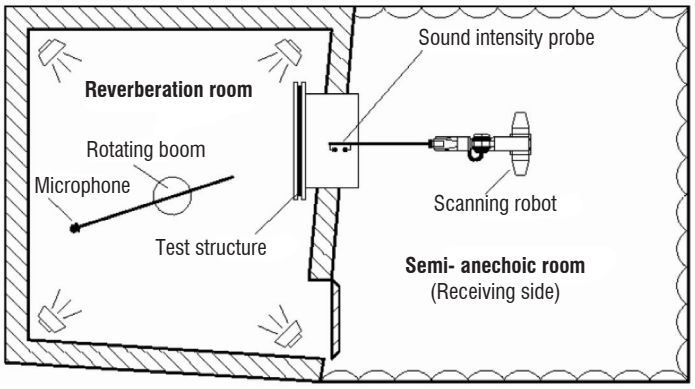

Figure 5 - Set-up for transmission loss measurements on panels (NLR)

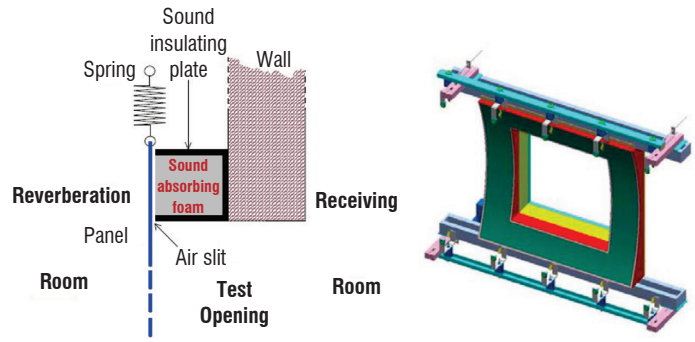

Figure 6 - Principle (left) and CATIA picture (right) of the NLR flanking noise suppression structure

Since the panels are mounted free from the surrounding structure, a special provision has been designed for adequate flanking noise suppression (Figure 6). On all four sides of the test opening, a U-shaped sound insulating structure is mounted, filled with sound absorbing foam.

The panel frames are suspended on springs, which are selected so as to obtain a mass spring resonance frequency of about 5 Hz. The 1m×1m test opening (niche) has a depth of about 1 m. The sound power radiated by the panel is determined from sound intensity measurements over the cross-section of the niche, using a robot to scan the measuring surface. To suppress the effect of reflections on the walls of the semi-anechoic receiving room, sound absorbing foam is installed around the test opening.

Simulation and passive optimization of TL (DLR / Onera)

In parallel, TL simulations, based on analytic modeling or FE / BE calculation, can be achieved to evaluate the effect of the main parameters or to optimize the nature and arrangement of layers, especially for trim panels.

The TL simulations performed, for example, by DLR, mainly focus on the frequency range from 0Hz up to 2000 Hz, where active and semi-active methods applied to panels can improve the TL. First of all, the TL simulation, which is based on a FE element calculation and a numerical modeling of the diffuse sound field, is described. One of the main interests of the FE method is to be able to take into account complex boundary conditions for finite panel sizes, which are present in technical applications such as helicopter cabins or aircraft cabins. The frequency constraint of 2000 Hz is due to the computational effort that is needed if the mesh size has to be increased for higher frequencies. Also, panels with foam cores are typically of a higher computational complexity. This is due to the modeling of the core, which must be done with solid elements that have more degrees of freedom than a shell element.

The computational effort is the most limiting method for the FE calculations done at DLR. The advantage of a FE simulation compared to the semi-analytical PIAMCO calculations is the ability to calculate detailed transfer functions of the structure in order to further investigate semi-active control methods.

The simulation of the TL can be described by three steps and is shown in figure 7:

- generating the diffuse sound field by modeling acoustic point sources that are placed on a hemisphere [1] and calculation of the nodal forces that are present on the FE-model;
- harmonic analysis with the FE software ANSYS© of the excited panel and calculation of the normal surface velocities;
- post-processing of the normal surface velocities by the radiation resistance matrix [2];
- calculation of the transmission loss from the incident and radiated sound power (figure 8).

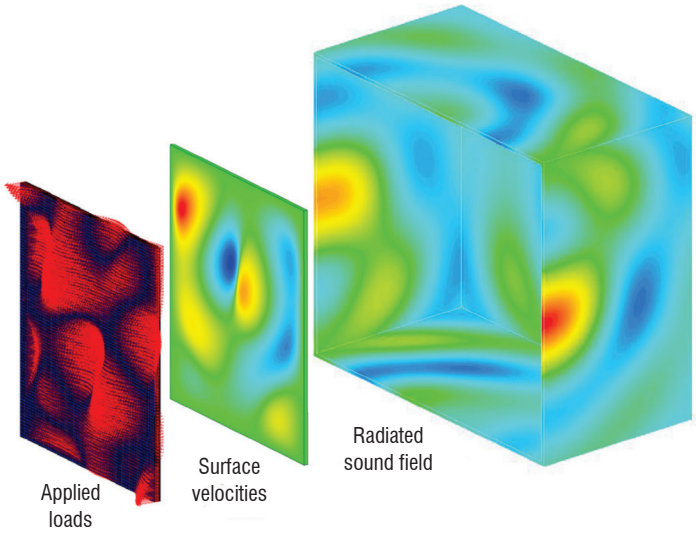

Figure 7 - Steps of the transmission loss simulation at DLR

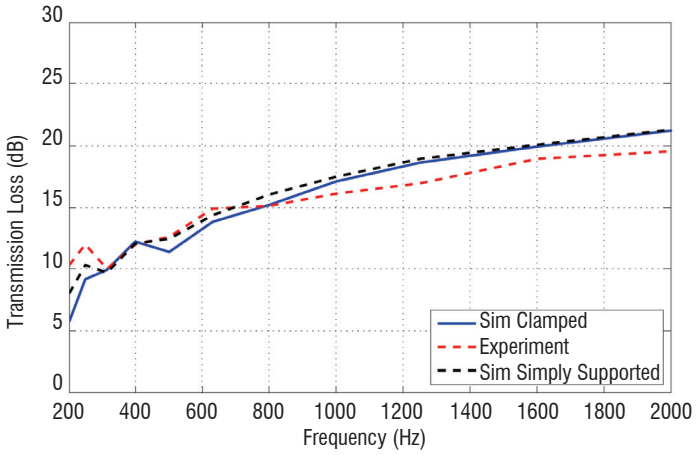

Figure 8 - Simulated (DLR) / experimented (Onera) TL (dB) of typical honeycomb sandwich panel

Nevertheless, to increase the frequency range of interest and because of the CPU time needed for an optimization process, analytical or semi-analytical models are widely used, although suited to an infinite panel size or a finite panel size with simple boundary conditions (simply supported, clamped or free conditions).

The following figure (figure 9) shows an example of a TL simulation result determined by Onera from an optimization process for a honeycomb sandwich pane [3], representative of a trim panel.

The assembly of materials has been defined from a fractional plan using a database, composed of several Nomex honeycomb (with variable thickness), fiber glass, Kevlar, carbon and viscoelastic materials.

The obtained optimal configuration, computed with a semi-analytical model (software PIAMCO [4]), has a maximum global TL in the frequency range of 500-5000 Hz [5] and complies with initial requirements, such as surfacic mass and thickness below 6 kg/m^2 and 20 mm, and presence of a viscoelastic layer on both sides of the core. The panel surfacic mass and thickness are 6 kg/m^2 and 8.2 mm, with a core of 5 mm thick.

It appears that, in the mentioned frequency band, the TL is similar to that produced by a steel panel of equal weight. The coincidence frequency, fc, and the double wall resonance frequency, fd (with a "dilatation effect" of the panel), appear beyond the band (12 and 18.4 kHz) [6]. Thus, the TL follows only the mass law. Moreover, the high damping provided by the viscoelastic layer (about 20 %) is not efficient beyond the coincidence frequency.

This type of result shows that other trim panel designs must be proposed to avoid the "mass effect", unfavorable to current cabins. For instance, it may be interesting to use foam with open cells, offering less stiffness than honeycombs, to decrease the double wall resonance frequency and to thereby generate a high TL form medium frequency range. Figure 10 shows the simulated and experimental TL of a sandwich panel with an "open cell foam", whose surfacic mass and thickness fulfill the previous requirements. In this case, the double wall resonance frequency of around 550 Hz leads to a TL of about 60 dB at 10 kHz, compared with figure 9. The influence of the transverse Young modulus of foam Ecz is brought to the fore to shift the double wall resonance frequency.

We would expect similar curves as in figure 9 and figure 10, up to 2000 Hz, with FE element calculations with DLR tools.

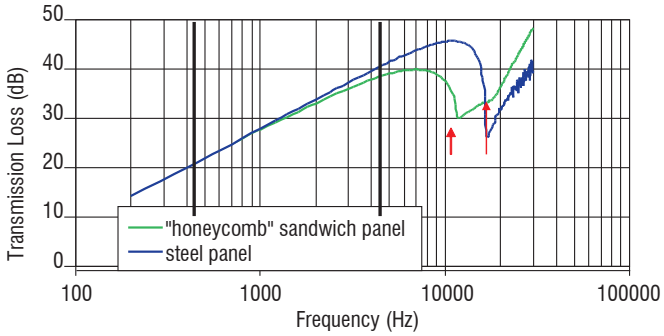

Figure 9 - Simulated TL of optimal "honeycomb" sandwich and steel panels [3] (Onera)

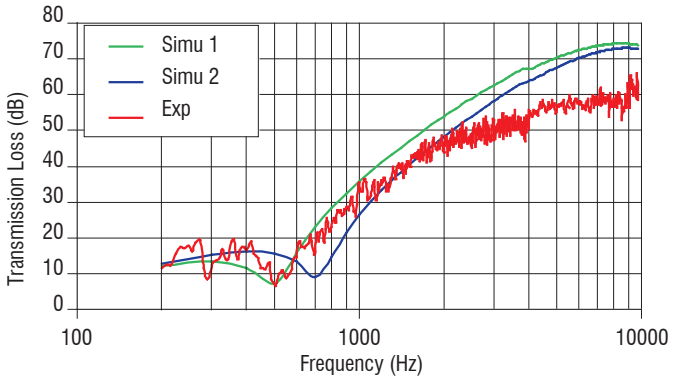

Figure 10 - Simulated / experimental TL of a sandwich panel with “open cell” foam - simu 1: Ecz=0.1 Mpa - simu 2: Ecz=0.2 Mpa [3] (Onera)

However, this type of concept proposed by Onera has led Eurocopter to propose improvements compatible to other constraints such as, for example, fire resistance (patent [7]).

Nevertheless using open cell foam can generate a significant reduction of mechanical stiffness. A multi-objective genetic algorithm can then be used to find an optimized panel with a good compromise between acoustical and mechanical properties [8]. That is to say, to perform a tri-objective optimization for a "lightweight stiff acoustic panel". The main drawback is the computing time, but the advantage is the quantity of information obtained.

Active or semi-active control of TL (Onera / DLR)

As a complement to the passive behavior of the optimized trim panel described previously, active or semi-active control techniques have been developed by laboratories to improve the TL of elementary panels in low frequencies (figure 11).

Active isolation is a good solution when a large part of the primary excitation is transmitted to the trim panels through structural attachment points. In helicopters, this is the case with the struts or the frames: the vibrations coming from the gear-box excite the trim panels through their attachment points. The idea is to reduce the incident vibration levels, which excite the trim panels.

The trim panels are usually mounted with soft rubber parts, which filter part of the incident energy. Nevertheless, these passive parts are not efficient enough to drastically reduce the incident vibration levels

and their efficiency is concentrated in the higher frequency range. Moreover, a soft mount induces suspension modes that are added to the primary excitation at low frequencies. An active isolation system is efficient at low frequencies and will complete the passive part.

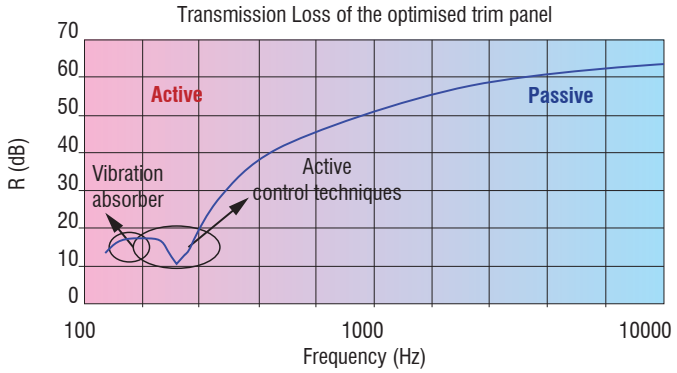

Figure 11- Complementarities of passive and active techniques

Active isolation system consists in replacing the attachments by actuators. The existent passive parts are usually kept. Depending on the vibration levels and the static forces, the actuators used in isolation system can be based on different technologies: hydraulic, magnetorheological or piezoelectric, for example.

In order to reduce the structural noise and vibrations coming from the trim panel, Active control methods with piezoelectric patches present another solution to add damping in the panel [9][10].

This control approach is termed active structural acoustic control (ASAC), in contrast to active noise control (ANC), where secondary sound sources are used to lower the initial sound field.

Recently, a new approach has been developed to keep the best of these two approaches: semi-passive, or semi-active techniques, according to appellations [11][12][13]. These techniques consist in connecting piezoelectric patches to an electronic circuit. In some cases, the energy of a piezoelectric patch is dissipated in a RLC (resistance, inductance and capacitance) electronic scheme, with a resonant frequency tuned to the target frequency to be reduced.

In DLR, for example, negative capacitance networks are applied to a vibrating panel, in order to increase the total damping: To achieve optimal results, due to the damping of negative capacitance networks, the ASAC pre-design tool [14] is extended by an objective function that calculates the performance of negative capacitance networks. Figure 12 shows a flow chart of the ASAC pre-design tool of the DLR.

The working principle of a shunt damped active structure is presented in figure 13. The piezoelectric patch actuator is used as an energy transducer, which transfers mechanical energy to electrical energy. The electrical energy is dissipated in the electrical domain and the vibrations are thereby damped. For a multi modal system with varying eigenfrequencies, the negative capacitance networks are well suited. The capacitive reactance of the piezoelectric patch transducer is compensated over a wide frequency range, in comparison to simple resonant shunts. This is achieved by a circuit of active impedance converters, which are presented for example in [15][16].

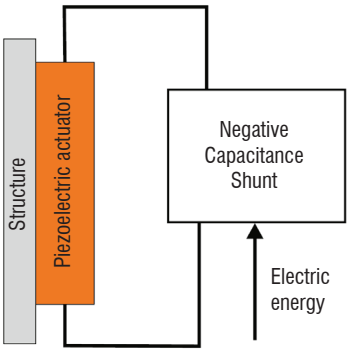

Figure 13 - Principle of a shunt damped structure (DLR)

To achieve a reasonable performance for a high number of modes that are present in plate structures, a custom actuator placement is needed. In a first study, a steel plate was equipped with actuators designed with the ASAC pre-design tool. The calculated actuator placement is presented in figure 14.

Further details of the design and simulation process can be found in [17]. The achieved modal damping improvement is presented in figure 15. It can be seen that an improvement in modal damping up to

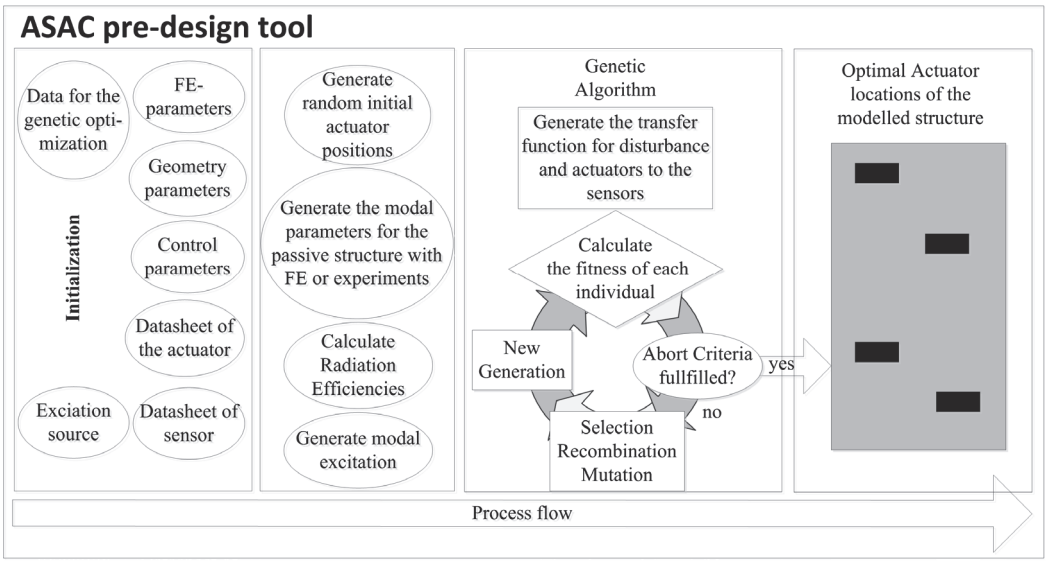

Figure 12 - Flow chart of the ASAC pre-design tool (DLR)

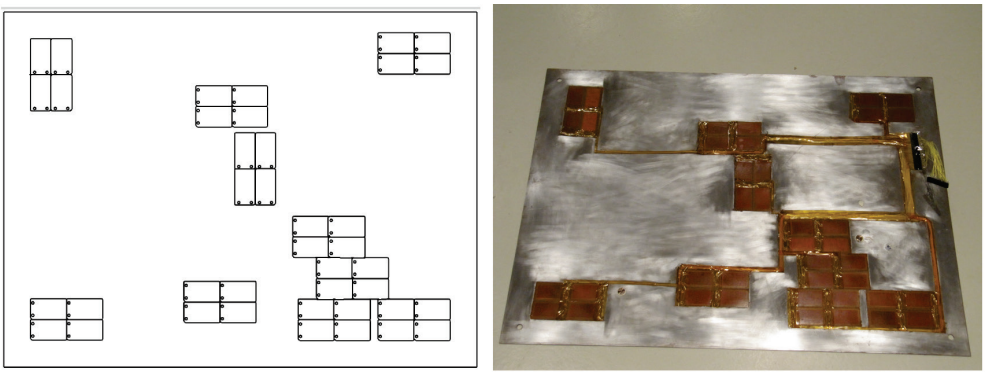

Figure 14 - Designed plate equipped with actuators, sketch and laboratory demonstrator (DLR)

17 dB can be achieved. Also, the prediction of the ASAC pre-design tool compared to the achieved reductions is very good. The applicability of negative capacitance networks to more damped structures must be studied in the GARTEUR AG 20.

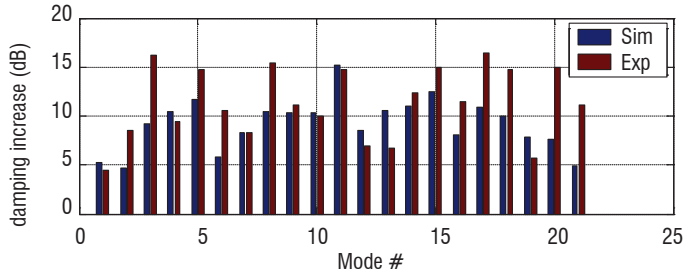

Figure 15 - Damping increase of the shunt damped plate (DLR)

Applications in a cabin mock-up or in a fuselage

Optimizing the configuration of an isolated panel does not guarantee a low noise level in a cabin. Using a cabin mock-up or a real fuselage allows real boundary conditions to be taken into account and allows a realistic loading to be reproduced. Nevertheless, the measured parameters must change: they will be, for instance, acoustic Insertion Loss or reciprocal Transmission Loss. Moreover, active control processes can also be extended to a particular area around the vibration sources: for instance, the mechanical deck that supports the gear-box struts.

Acoustic Insertion Loss in a cabin mock-up (Onera)

At Onera, a mock-up of NH90 cabin (figure 16), made up of carbon frames and Nomex honeycomb sandwich panels placed between fiber-glass and carbon laminates, is equipped with four electrodynamic shakers fixed on the roof of the cabin (mechanical deck), at the same locations as real gear-box struts, to simulate the vibration sources generated by a gear-box (figure 17).

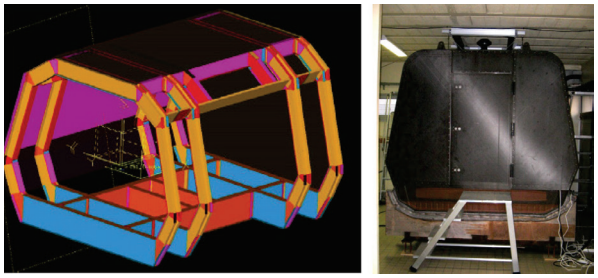

Figure 16 - Right: The strong frames of a cabin mock-up, right: cabin mock up (Onera)

Figure 17 - Mechanical deck of an Onera cabin mock-up, with shakers and loudspeaker

The structural intensity generated by local forces is measured on different composite multi-layered panels (separated by carbon frames) of the mechanical deck [18].

The magnitude of the structural intensity is shown in figure 18, in the case of excitation with 1 or 4 forces. In the 500-3000 Hz frequency band, the energies are propagated mainly towards the middle of the mechanical deck, from the excited source(s), with an important decrease in magnitude along the propagation path (due to high structural damping and the modal coupling).

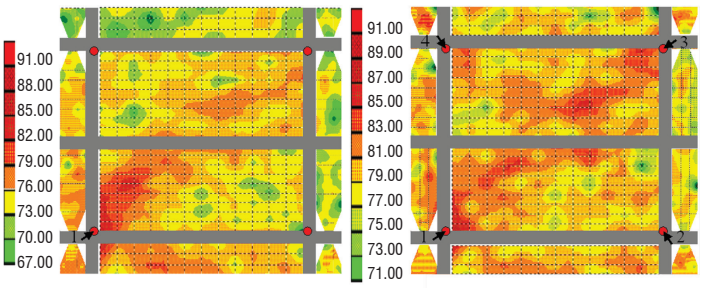

Figure 18 - Structural intensity field on the mechanical deck for the 500-3000 Hz frequency band - Magnitude in dB (ref: 10-12 W/m2) - Excitation by 1 shaker (left) and 4 shakers (right) [18] (Onera)

Figure 19 shows the acoustic pressure field in the cabin 0.2 m away from the mechanical deck, with the four sources between 500 and 3000 Hz. The maximum pressure is focused in the middle of the mechanical deck, which confirms the hypothesis of wave propagation towards the middle.

Nevertheless, a contribution of energy flow through external panels, which can produce side panel excitation and thus a radiating side pressure, can also be noted.

To evaluate the efficiency of a trim panel located under the mechanical deck (figure 20) facing the two main panels, Insertion Loss has

been measured under the ceiling with the acoustic power measurement procedure described in [19][20].

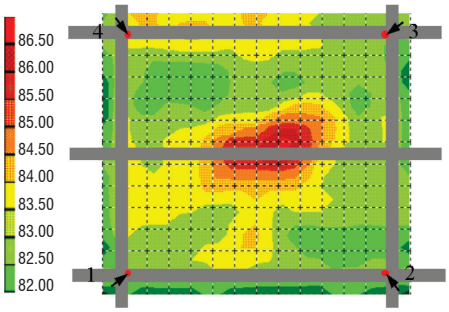

Figure 19 - Nearfield acoustic pressure under the mechanical deck for the 500-3000 Hz frequency band - Magnitude in dB (Ref: 2 10-5 Pa) - Excitation by 4 shakers [18] (Onera)

The Insertion Loss is defined by:

$$IL = L_{W_2} - L_{W_1} = 10\log_{10}\left(\frac{W_2}{W_1}\right) \quad [dB] \qquad (2)$$

where L_{W_2} and L_{W_1}, are the acoustic powers (dB) with and without panel, respectively.

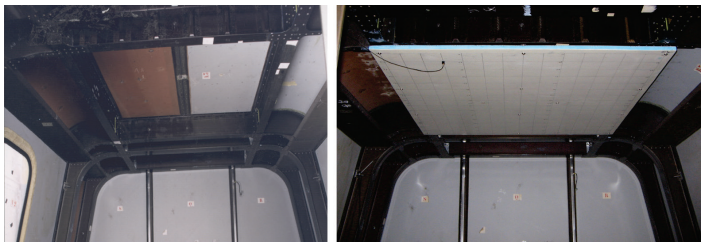

Figure 20 - Ceiling of Onera cabin mock-up without (left) and with trim panel (right)

Two types of trim panels have been tested, one called a "usual" trim panel with a honeycomb and the other called an "optimized" trim panel, with thick foam to have a "dilatation effect" in the medium frequency range (figure 21).

Comparisons are shown in figure 22, in the 1/3 octave frequency bands.

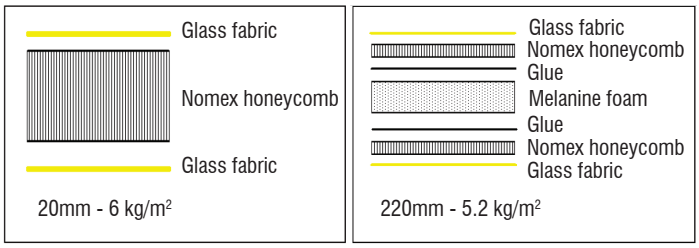

Figure 21 - Example of the usual trim panel (left) and optimized trim panel (right) (Onera)

First, we compare the acoustic powers without panel and with the "usual" helicopter panel. It can be noted that the Insertion Loss increases with the frequency. Nevertheless, from 1/3 octave 5000 Hz, acoustic power due to the presence of "usual" panel is negative. This can be explained by a contribution of external acoustic sources in the cabin (radiating from other panels) whose acoustic power is much higher than the acoustic power radiated by the panel. The behavior of the optimized panel, excited by the pressure radiation of the mechanical deck, is consistent compared to the simulated TL, with a decrease of radiated power from 1/3 octave 630 Hz. From 1/3 octave 1250 Hz, the acoustic power becomes too low to compensate for the external acoustic power produced by other sources.

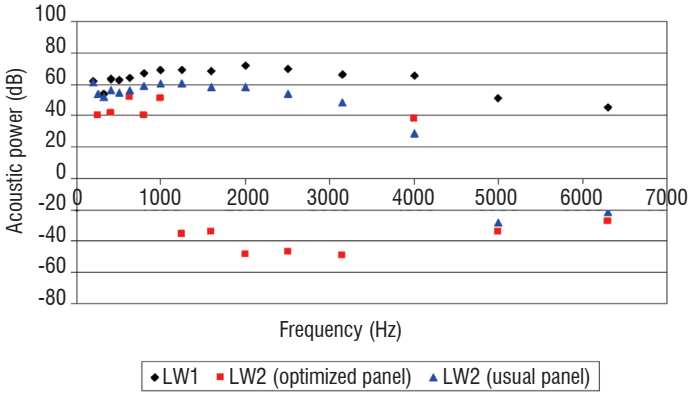

Figure 22 - Acoustic powers (dB) without and with trim panels (200-6300 Hz) (Onera)

We can deduce that the optimized panel can generate a higher Insertion Loss than the usual panel, for a similar thickness and surface mass (particularly from 1/3 octave 1250 Hz).

Nevertheless, these results show that the internal noise can come from pressure radiating from adjacent walls, even if only the mechanical deck is excited by vibration sources, which is consistent with structural intensity propagation.

Vibro-acoustic characterization in a real fuselage (NLR / Politecnico di Milano)

As seen previously, simplified mock-ups can be used for preliminary testing activities, but they may not be fully representative.

As in a laboratory set-up, the reciprocal TL measurement can be performed on a complete fuselage with a source inside the mock-up having a known volume velocity and microphones (normal derivatives) on the exterior side of (part of) the fuselage (figure 23).

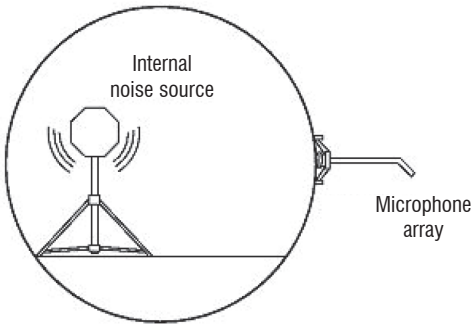

Figure 23 - Reciprocal TL measurement (NLR)

Figure 24 - Array configurations, left: arc, right: row (NLR)

In NLR, a dodecahedron is used as the sound source. The pressures on the exterior side of the fuselage can be measured with different array configurations, such as an arc around the fuselage, or a row of microphones turned around the fuselage (figure 24).

Similarly, Agusta-Westland and Politecnico di Milano built a ground based facility, suitable for experimental activities on internal noise, using an actual helicopter fuselage, although an old one, therefore not representative of current design and manufacturing technologies: it consists in the fuselage of an A109A [21], grounded at three points; main and tail rotors, as well as engines are not installed, while the actual gear-box is installed with actual structural fixtures; in order to naturally reproduce noise due to gear meshing, it is powered by means of electric engines and an aerodynamic brake is used to reproduce the loading effect of gear tooth meshing. The cabin is in green configuration, without any internal equipment and sound treatments.

Most experiments and data presented hereafter have been carried out and collected within the framework of the European IP Friendcopter.

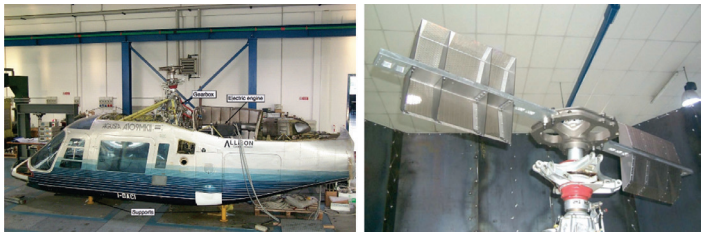

Figure 25 - Left: Helicopter mock-up, right: aerodynamic brake [21] (Politecnico di Milano)

Despite an installed power lower than the actual one, the dynamic behavior (medium-high frequency vibrations and noise) is quite similar as that for in-flight measurement, although still lower, as depicted in the following figure, which shows the acceleration at one of the attachments of the anti-torque plate at audio frequencies. Thus, the mock-up can be validated as a test-bench.

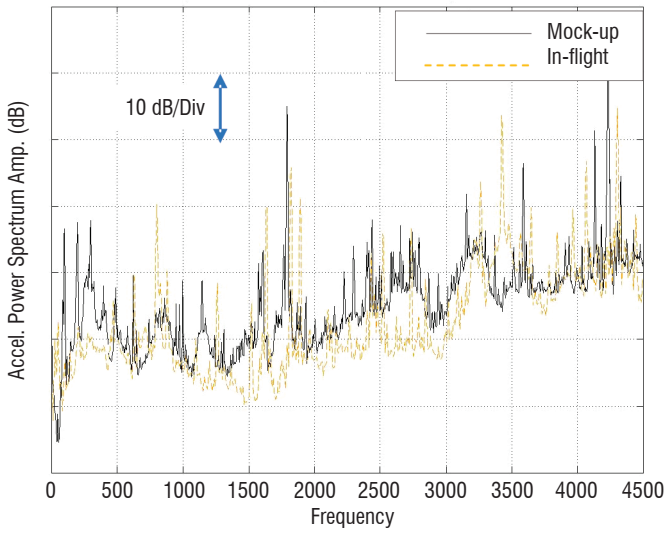

Figure 26 - Comparison of anti-torque plate attachment acceleration: in flight vs. mock-up (Politecnico di Milano)

Thanks to the availability of this test rig an extensive study can be carried out; some of these experiments aimed at understanding the complex dynamics of the cabin structure are described in the following page. Laser scanner measurement has been carried out, in order to identify operational deflection shapes of the cabin walls, with particular attention to the cabin roof.

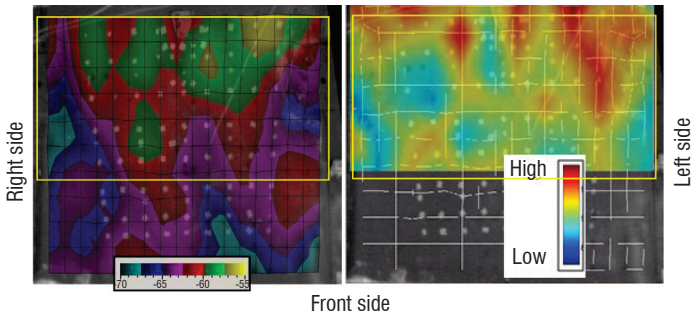

Figure 27 - Comparison between the wall speed (left) and the noise map (right) in the 1600 Hz band (Politecnico di Milano)

On the left side of Figure 27, the operational deflection shape of the rear part of the cabin roof is presented for a 1600 Hz frequency. It is compared with the acoustic map, measured 20 cm from the wall, in the same area.

Due to the interference of reflected waves in the closed field, the noise exhibits a very irregular behavior. This could make many actions critical, e.g., the placing of noise error sensors.

Application of the active control of gear-box vibration transmission (Politecnico di Milano)

The design and tuning of active control systems can also benefit from the availability of test rigs. The following figure shows an example of installation applied to the active control of acceleration, based on a MIMO FXLMS adaptive algorithm, with piezoceramic patches and accelerometers on the anti-torque plate.

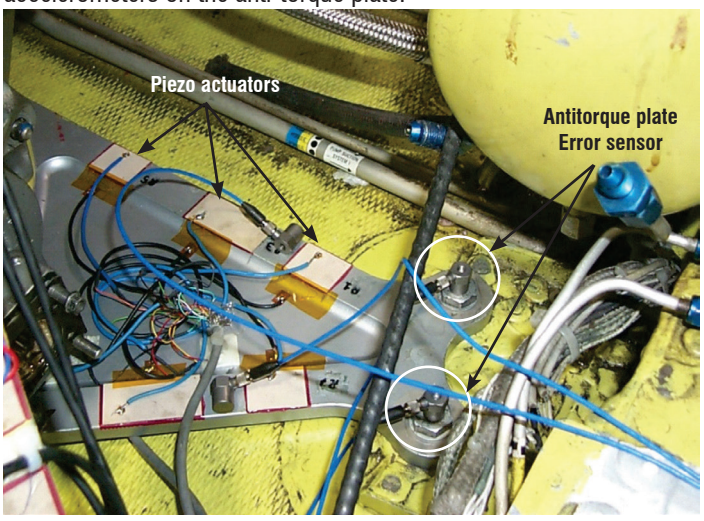

Figure 28 - Installation of piezoceramic patches on the anti-torque plate [21] (Politecnico di Milano)

Due to not yet fully solved problems in adopting noise - or mixed - error signals, structural control is adopted; the results confirm those of the literature experiments: a good structural effect, with a nearly complete rejection of the disturbance and a hardly relevant noise improvement.

As shown by figure 29 for the attachment points (strut and ATP), the error signal is reduced at the controlled frequencies.

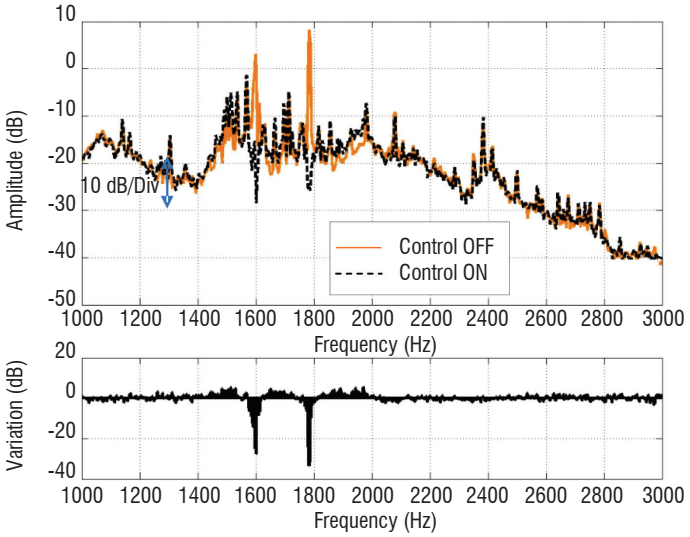

Figure 29 - Acceleration (Control On-Off) at error point – reference value for dB: 1m/s² (Politecnico di Milano)

In the acoustic map presented in figure 30, one can appreciate that, at the 1600 Hz tonal disturbances, most of the rear part of the cabin exhibits a reduction (up to 10 dB), while at a few points the noise level increases. The comparison of individual time averaged SPL levels at the measurement points (figure 31) shows that, at most of these, the noise is reduced; furthermore, it is possible to appreciate how the active control produces a smoother SPL behavior with smaller discrepancies between close points.

It can be noted in [21] that a mean reduction of 3 dB is obtained for each target frequency band, over the whole measurement area.

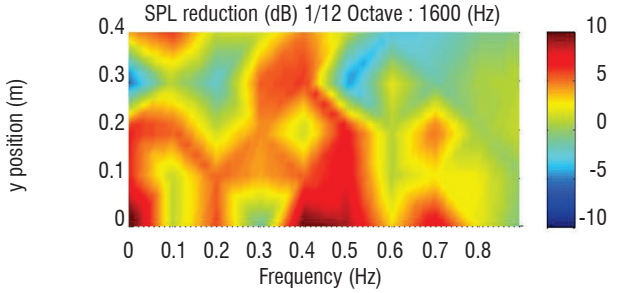

Figure 30 - Map of acoustic reduction due to active control at 1600 Hz (rear cabin)

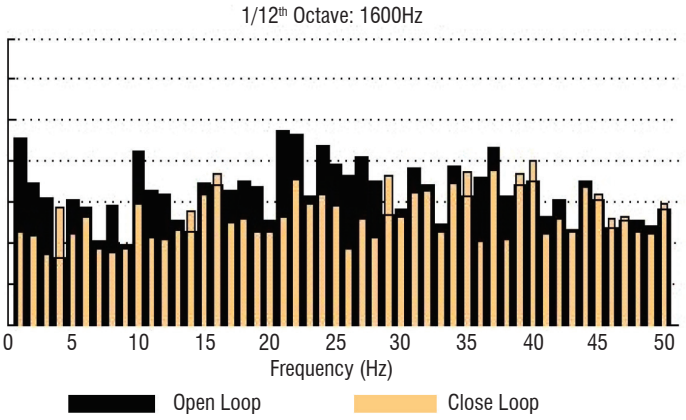

Figure 31 - Time averaged SPL (1600 Hz) (Control On-Off)

Applications in flight tests

Once the passive concepts, or active control techniques, have been tested in the laboratory or in a mock-up, new tests can be conducted in flight, with specific requirements (sound leaks, noise of the turbulent boundary layer, limited added weight, low coherence between signals, etc.). Some examples of application in flight are given below.

Integration of optimized trim panel and active control systems in a helicopter cabin (Onera)

In accordance with previous Onera simulations of TL, a helicopter trim roof is manufactured by Onera with "open cell" panel composition (figure 32,table 1).

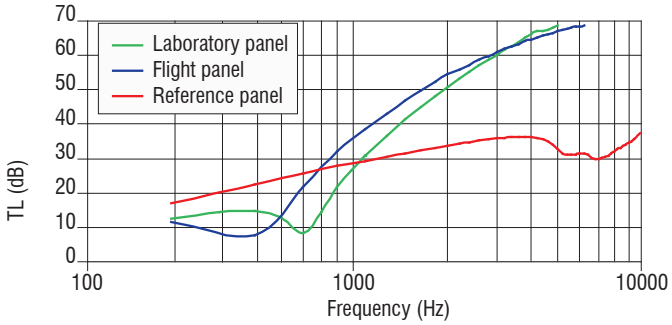

Figure 32 - Simulated TL of a laboratory panel/ flight panel [22] (Onera)

characteristics	Laboratory panel	Flight panel	Reference panel
Surfacic mass (kg/m²)	5.3	~5.4	~9
Thickness (mm)	10.5	18	10.7

Table 1 - Characteristics of laboratory, flight and reference panel (Onera)

This structure is mounted under the mechanical deck of an EC Dauphin, with elastomeric mounts to limit the transmission of vibration (figure 33). This panel must theoretically improve the TL between 400 and 4000 Hz. The TL of a heavier damped panel with, among other layers, a Nomex honeycomb core and a viscoelastic layer (9 kg/m² for 10.7 mm in thickness), is also presented. This reference panel, with its mass behavior, is less interesting from 700 Hz, with a difference of about 30 to 40 dB at high frequencies.

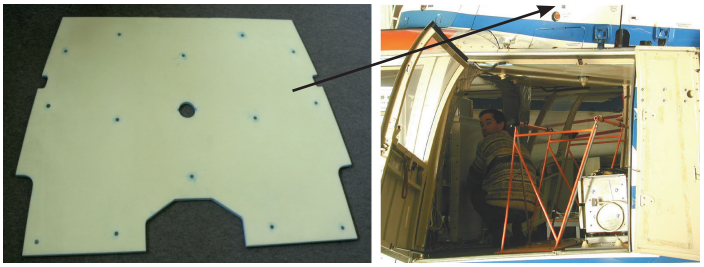

Figure 33 - Trim roof with location of the elastomeric mounts (left) and EC Dauphin cabin with trim roof (right) [22] (Onera)

In the Dauphin cabin, there is an acoustic pressure field with tones (fundamental and harmonic frequencies) produced by 6 main sources with gears, that is to say, 4 stages of the main gear-box, the rear "fenestron" and the fan [5].

We compare the acoustic level pressure, averaged from 6 microphones in cabin, without trim panel and with the “open cell” or “reference” panels (figure 34). The tests have been conducted by Onera for a stationary flight at 85 % of maximum torque.

In table 2, the acoustic reduction at the main tones and the global reduction between 300 and 5000 Hz are shown, with the presence of the “open cell” panel. It can be noted that, contrary to the simulations (table 1), the pressure level is similar with the two types of trim panel. These are efficient from 300 Hz and reduce the aerodynamic pressure and the gear tones (except for the rear “fenestron”). Nevertheless, the reduction reaches, globally, 6.5 dB, which is much lower than in the laboratory.

The “reference” panel, thanks to its high mass, and the “open cell” panel, because of the “double wall” effect, can be assumed to reduce the pressure in the cabin, up to the level produced by the other acoustic transmission paths, such as the side doors or the back surface, which are insufficiently treated by materials.

This type of result, in accordance with tests in the Onera Cabin Mock-up, has questioned the assumption of "major radiation from the roof panel excited by the mechanical deck" proposed in [5] and justify the development of a metrological tool, able to yield information on acoustic radiating areas in the cabin [23][24], in order to target appropriate acoustic passive or active solutions.

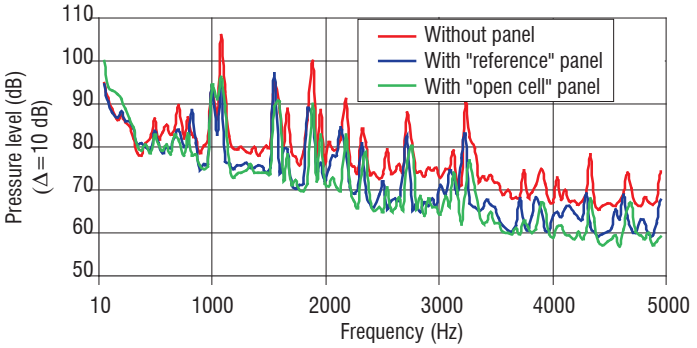

Figure 34 - Averaged pressure level in the Dauphin cabin (dB) - Stationary flight at 85 % of the maximum torque[22] (Onera)

	Tone 1	Tone 2 Fenestron	Tone 3 Stage 4	Tone 4 Stage 3	Tone 5 Stage 2	Tone 6 Stage 4	Tone 7	Global
Frequency (Hz)	708	1001	1074	1550	1880	2176	3235	300-5000
Reduction (dB)	5.3	-0.7	8	3	10	8.6	12.6	6.5

Table 2 - Reduction of the pressure level in the cabin with an "open cell" panel (dB)) - Stationary flight at 85 % of the maximum torque [22] (Onera)

However, recently, in order to study internal noise comfort improvement for an EC155 helicopter, Caillet et al. [25] determined the acoustic radiating of cabin panels with Nearfield Acoustic Holography applied in front of each cabin surface (to measure normal velocity field), coupled with a GRIM software (ICARE based on Neumann Green functions GV computed with a beam tracing algorithm [26]) to calculate the sound pressure at any point in the cabin (figure 35).

It appeared (figure 36) that, although the highest contribution in the dB SIL4 frequency range was due to the roof panels, contributions of rear, right and left side panels was significant. Moreover, dissymmetry of side contributions could be explained by the dissymmetry of the MGB struts loads and by significant leaks measured on the right-hand side panels.

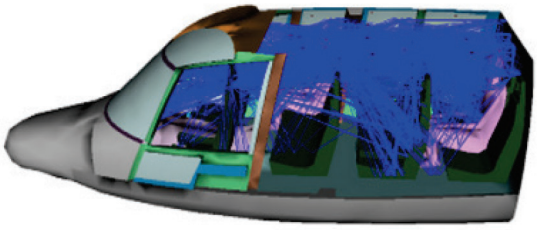

Figure 35 - Example of beam tracing calculation result with ICARE [25]

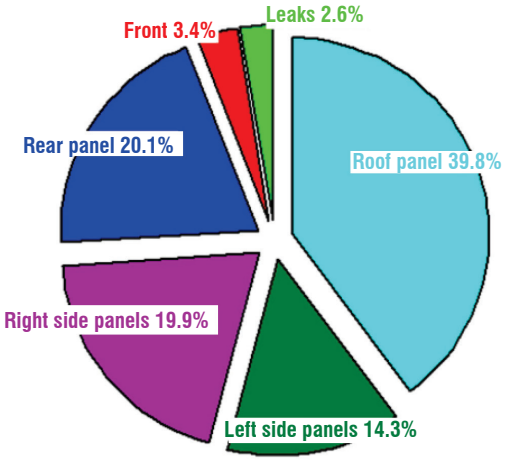

Figure 36 - Average contribution in the EC155 cabin dB SIL4 [25]

Finally, in parallel to tests conducted with an optimized trim panel under the mechanical deck, active control processes are applied by Onera in an EC Dauphin, for a level flight at 85 % of the maximum torque (speed of 140 kt), with 4 inertial actuators (PCB model 712-A02) and accelerometers placed, located on the mechanical deck, close to the 4 gear-box strut connections (figure 37).

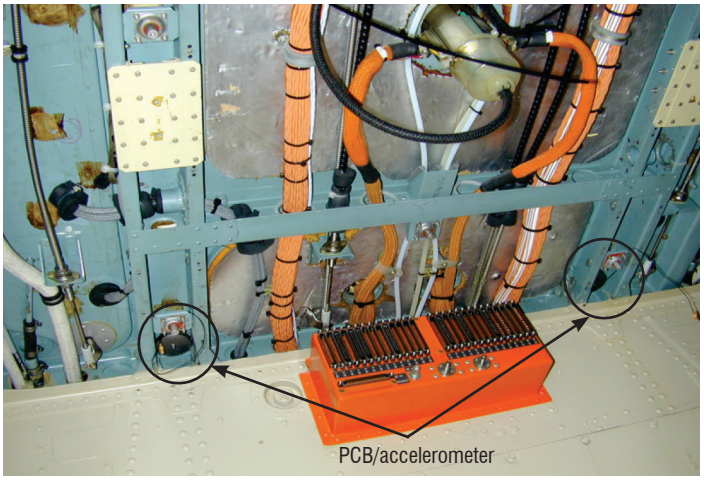

Figure 37 - Installation of inertial actuators with accelerometers placed (Onera)

Thus, an averaged reduction of 3 dB is obtained in the cabin from 6 microphones (i.e.,figure 38) at 1074 Hz (Stage 4 of the main gear-box), using 4 SISO FXLMS applied to the accelerometers (for -4.4 dB vibration).

It can be noted that these findings are similar to those obtained by the Politecnico di Milano in an A109A mock-up [21].

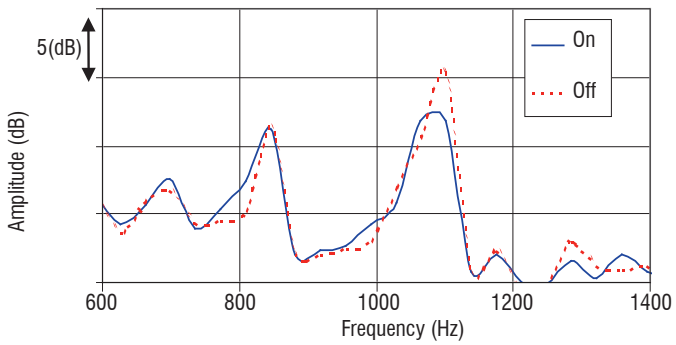

Figure 38 - Example of the acoustic pressure level in a Dauphin cabin (dB - relative value), Control On-Off - Level flight at 85 % of maximum torque (Onera)

Thus, while it is difficult to reduce the cabin noise with the optimization of only one panel (i.e., trim panel under the mechanical deck, as seen previously) because of contributions of other transmission paths, active control applied close to vibration sources ensures a reduction of several dB, even at medium frequencies. Nevertheless, as specified in the introduction, the " hard system added mass / electrical consumption" balance versus "efficiency of control" must be evaluated with industrial requirements.

Panel noise contribution (Microflown)

Although the sound level inside a cabin can be determined rather straightforwardly for a given position, it is harder to assess to which degree each radiating surface contributes to the perceived sound.

As seen previously, Nearfield Acoustic Holography [25] can be applied to estimate the sound radiated from each surface, using an array of sound pressure microphones. However, the radiation can also be determined straightforwardly with a single probe containing a particle velocity sensor. In this section, a procedure involving this sensor is described to measure, not only the radiation, but also the sound pressure contribution of each panel to a listener's position.

Although the history of sound pressure microphones goes back to 1876, it was not until 1994 that a convenient particle velocity sensor called the Microflown was invented [27]. The latter provides a direct measurement of the acoustic particle velocity and can be regarded as a point sensor, due to its sub-millimeter dimensions; much smaller than the wavelength of most frequencies of interest. Microflowns are usually combined with a conventional microphone in a so-called PU probe, where P stands for sound pressure and U for acoustic particle velocity. PU probes have been shown to have advantages because of their small size, wide operational frequency range [28] and the direct measurement of particle velocity.

Several unique applications of PU probes emerged over the past decade. Examples of applications for helicopter interior noise are in situ absorption measurements [29], transmission loss measurements without reverberant rooms and panel noise contribution: Contrary to traditional PP sound intensity probes consisting of a pair of microphones, particle velocity measurements in the near field are usually affected little by background noise and reflections [30]. Furthermore, PU probes can be extended easily to full 3D probes and can be used in environments with a high pressure-intensity index [28].

Microflown has shown the potential of its "panel noise contribution" method to measure the sound pressure contributions from certain interior panels to a reference listening position. The method consists of two parts: the source strength determination and the transfer path determination [31]. The contribution of each radiating section to the sound pressure at the reference position is determined by combining results from the two parts. The synthesized sound pressure at the reference position is finally obtained by summing all sound pressure contributions. The method has been shown to be accurate and fast, compared to existing methods.

Description of the method

The Helmholtz integral equation relates the acoustic pressure and normal velocity on a closed boundary surface S of a vibrating object to the radiated pressure field inside the fluid domain. With this equation, the sound pressure pr at the reference position can be defined as [31]:

$$p_r = \int_S \left(\frac{p_2}{Q_2} u_{n,1} - \frac{u_2}{Q_2} p_1 \right) dS \qquad (3)$$

where $u_{n,1}$ and p_1 are the normal particle velocity and sound pressure, respectively, at the surface boundary. Transfer functions and describe the propagation of sound from surface boundary to the reference position.

In the panel noise contribution method, the normal particle velocity and sound pressure at the surface, and the acoustic transfer functions are measured separately in two steps. First, the radiation of the test article in running conditions is determined. The surface is discretized by dividing it into a number of panels and $u_{n,1}$ and p_1 are obtained by measuring the particle velocity and sound pressure at each panel, with a PU probe. Second, the test article is stopped and the transfer functions from the panel to the reference position are acquired. Usually, it is convenient to determine these transfer function reciprocally, because a direct measurement requires separate tests for each panel with an omni-directional sound source radiating a known volume velocity Q_2 at the panel. Instead, the omni-directional sound source is positioned at the reference position and the resulting sound pressure p_2 and particle velocity u_2 at the panel are measured. This reciprocal approach allows all transfer paths to the panels to be measured at once.

Ultimately, the sound pressure at the reference position is obtained by summing the contributions from all panels. This synthesized sound pressure should equal the sound pressure measured by a microphone during step one, at the reference position. The measurement quality can be checked by comparing both values.

Examples of helicopter tests performed

Panel noise contribution measurements have been performed inside vehicles like cars, aircraft and trains. The following figure shows the results of a test in a Type W3 Swidnick helicopter, with a distributed array of 45 probes [32]. Such results show which panels should be treated to reduce the noise inside the cabin at certain frequencies.

Alternative to measurements at fixed positions, the surface radiation can also be mapped quickly and with high resolution using a scanning technique called Scan & Paint [30]. It involves a probe that is swept across a surface while a video of the measurement set-up is made.

The position of the probe is obtained from the video with dedicated software. The tracking procedure is automated, which speeds up the post-process procedure.

Conclusion

The acoustic characterization of helicopter structures, in terms of Transmission Loss (or a similar parameter), is dealt with differently in laboratories (experiments or simulations on isolated or integrated panels in a cabin). This is also true for approaches to increase the Transmission Loss (passive optimization or active process).

This is the reason why one of the objectives of the "Helicopter Garteur Action Group", devoted to the "design and characterization of composite trim panels", is to apply:

- different types of simulation methods to design and optimize composite trim panels according to common acoustic cost functions and to validate numerical approaches by laboratory tests;
- different types of experimental techniques to characterize composite trim panel acoustic radiation in both a standardized test set–up and a generic helicopter cabin.

These simulations and tests will constitute a benchmark to assess the appropriateness of tools for complex configurations (multiple anisotropic layers with various mechanical characteristics, effect of confined medium on internal noise, etc.). This benchmark will help helicopter manufacturers to select the right tools to simulate or quantify acoustic radiation from vibrating helicopter panels ■

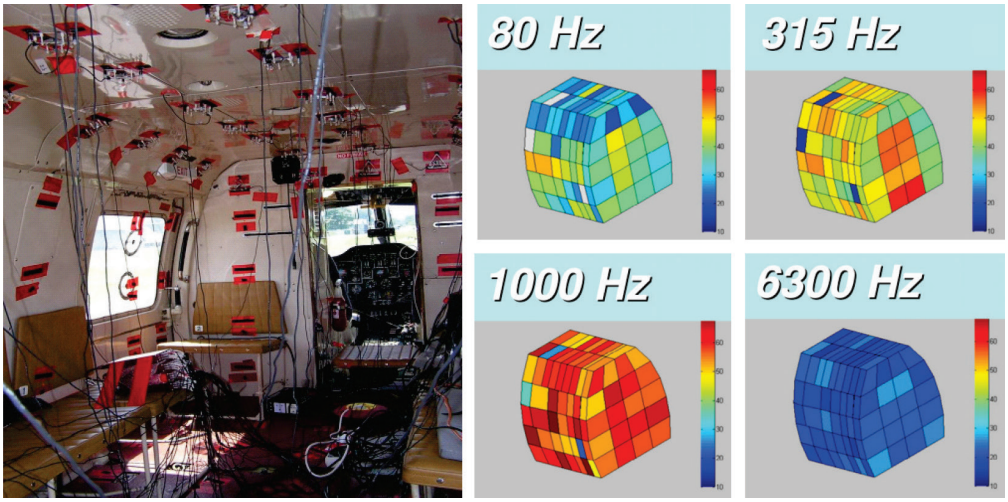

Figure 39 - Helicopter test. Left: probe installation on the roof section. Right: Example of panel contributions (Microflown)

Acknowledgements

We thank the GARTEUR (Group for Aeronautical Research and Technology in Europe) for allowing the cooperation between authors of different laboratories in the helicopter domain (GoR-HC).

Acronyms

ANC	(Active Noise Control)
ASAC	(Active Structural Acoustic Control)
IL	(Insertion Loss)
SPL	(Sound Pressure Level)
TL	(Transmission Loss)

References

[1] M. WITTING - *Modelling of Diffuse Sound Field Excitations and Dynamic Response Analysis of Lightweight Structures.* Herbert Utz. Verlag, 2000.

[2] F. FAHY, P. GARDONIO - *Sound and Structural Vibration.* Academic Press, 2nd Ed., 2007.

[3] F. SIMON, S. PAUZIN, D. BIRON - *Optimisation of Sandwich Trim Panels for Reducing Helicopter Internal Noise.* ERF30, Marseille, France, September 2004.

[4] Software PIAMCO-V1 (Prévision de l'Indice d'Affaiblissement de Matériaux COmposites) N° IDDN.FR.001.130043.001.S.P.2002.000.30805.

[5] M. DUSSAC et al. - *A Finite Element Method to Predict Internal Noise Levels at Discrete Frequencies for a Partially Composite Helicopter Fuselage.* Onera T.P. n°1989-49, AHS annual forum, Boston, USA, 1989.

[6] A.C. NILSSON - *Wave Propagation in and Sound Transmission Through Sandwich Plates.* J. Sound Vib., 138(1), 73-94, 1990.

[7] F. MARROT, H. SIBOIS - *Panneau insonorisant à cœur souple, procédé de fabrication d'un tel panneau insonorisant.* Patent Application FR08/06.828 filed on December 5th, 2008.

[8] P. LEITE, M. THOMAS, F. SIMON, Y. BRÉCHET - *Optimal Design of an Asymmetrical Sandwich Panel for Acoustical and Mechanical Properties Using a Genetic Algorithm.* 11th Biennial Conference on Engineering Systems Design and Analysis, Nantes, France, July 2012.

[9] F. SIMON, S. PAUZIN - *Active Vibration Control of the Acoustic Radiation of a Honeycomb Flat Panel.* Internoise 96, Liverpool, July 1996.

[10] B. PETITJEAN, I. LEGRAIN, F. SIMON, S. PAUZIN - *Active Control Experiments for Acoustic Radiation Reduction of a Sandwich Panel: Feedback and Feedforward Investigations.* J. Sound Vib., 252 (1),19-36, 2002.

[11] M. MISOL, S. ALGERMISSEN, H. MONNER - *Experimental Investigation of Different Active Noise Control Concepts Applied to a Passenger Car Equipped with an Active Windshield.* J. Sound Vib., 2012.

[12] T. HAASE, S. ALGERMISSEN, O. UNRUH, M. MISOL - *Active Control of Counter Rotating Open Rotor Interior Noise*", AIA-DAGA, Merano, Italy, 2013.

[13] R. H. CABELL, N. H. SCHILLER, F. SIMON - *Application of a Broadband Active Vibration Control System to a Helicopter Trim Panel.* Noise-Con 2013.

[14] O. HEINZE, M.ROSE, S. ALGERMISSEN, M.MISOL - *Development and Experimental Application of a Pre-Design Tool for Active Noise and Vibration Reduction Systems.* ACTIVE 2009, Ottawa, 2009.

[15] C. H. PARK, H. C. PARK - *Multiple-Mode Structural Vibration Control Using negative Capacitance Shunt Damping.* KSME International Journal, Vol. 17 No. 11, 1650-1658, 2003.

[16] C. H. PARK, A. BAZ - *Vibration Control of Beams with Negative Capacitive Shunting of Interdigital Electrode Piezoceramics.* Journal of Vibration and Control 11; 331, 2005.

[17] M. POHL, M. ROSE, T.HAASE - *Actuator Placement for Shunt Damping of Panel Structures – Numerical Simulation and Experimental Validation.* ICAST, Aruba, 2013.

[18] F. SIMON, S. PAUZIN - *Structural Intensity Formulation and Measurement Validation in the Case of Composite Multi-Layered Structures.* Acta Acustica, Vol. 92(2), 2006.

[19] NF EN ISO 3741 (S 31 022) - *Determination of Sound Power Levels of Noise Sources Using Sound Pressure - Precision Methods for Reverberation Rooms,* 2000.

[20] ISO 9614-1 - *Determination of Sound Power Levels of Noise Sources Using Sound Intensity - Part 1: Measurement at Discrete Points.* 1993.

[21] W. CORBETTA, E. VIGONI, A. TOSO, G.L. GHIRINGHELLI, L. DOZIO, F. CENEDESE - *Active Control of Helicopter's Gearbox Vibrations and Effects on the Cabin Noise.* 34th European Rotorcraft Forum 2008 (ERF34) , Liverpool, UK, 16-19 Sept. 2008, ISBN: 9781617821998, p. 2297-2326, Paper_10a2

[22] F. SIMON, S. PAUZIN, D. BIRON - *Modelization and Test of Composite Trim Panels for Reducing Helicopter Internal Noise.* ICSV9 - 9th International Congress on Sound and Vibration, Orlando, USA, July 2002.

[23] E. JULLIARD, F. SIMON, S. PAUZIN, D. BIRON - *Acoustic Localization into a Generic Helicopter Cabin.* Euronoise 2006, Tampere, USA, may 2006.

[24] G. MARTIN, F. SIMON, D. BIRON - *Detection of Acoustic Radiating Areas of a Generic Helicopter Cabin by Beamforming.* Acoustics '08, Paris, France, July 2008.

[25] J. CAILLET, F. MARROT, Y. UNIA, P-A. AUBOURG - *Comprehensive Approach for Noise Reduction in Helicopter Cabins.* Aerospace Science and Technology 23, 17–25, 2012.

[26] F. GAUDAIRE, N. NOE - *ICARE - Notice Technique.* CSTB, 15 Mars 2004.

[27] H.E. DE BREE, P. LEUSSINK, T. KORTHORST, H. JANSEN, T. LAMMERINK AND M. ELWENSPOEK - *The Microflown; a Novel Device Measuring Acoustic Flows.* Sensors and Actuators. 54 (1-3), 552-557. ISSN 0924-4247, 1996.

[28] F. JACOBSEN, H.E. DE BREE - *A Comparison of Two Different Sound Intensity Measurement Principles.* Journal of the Acoustical Society of America. 118 (3), 1510-1517. ISSN 0001-4966, 2005.

[29] J.D. ALVAREZ, F. JACOBSEN - *An Iterative Method for Determining the Surface Impedance of Acoustic Materials In Situ.* Internoise. 2008.

[30] H.E. DE BREE, W. DRUYVESTEYN - *A Particle Velocity Sensor to Measure the Sound from a Structure in the Presence of Background Noise.* Forum Acusticum conference. Budapest. Hungary, 2005.

[31] O. WOLFF - *Fast Panel Noise Contribution Analysis Using Large PU Sensor Arrays.* Internoise. 2007.

[32] O. WOLFF, H.E. DE BREE, J. DE BOER, W. HAKE - *In-Flight Panel Noise Contribution Analysis on a Helicopter of Type W3.* Technical Report www.microflown.com, 2008.

AUTHORS

Frank Simon, graduated from ENSICA Toulouse with a degree in Aeronautical Engineering (1989), from Supaero Toulouse with a PhD in Mechanical Engineering (Acoustics) (1997) and from the University of Toulouse with Authorization to supervise PhD students (2007). Research Master at Onera, specialized in the development of vibro-acoustic modelizations and measurement techniques, participation in various EC projects in the vibro-acoustic domains (RHINO, FACE, FRIENDCOPTER), in charge of internal noise in the Garteur group.

Thomas Haase graduated from Otto-von-Guericke University in Magdeburg in 2010, with a Diploma in Mechatronics. He joined the German aerospace center (DLR) in 2010 and is currently a scientist. His main interests are signal processing for active control and actuator/sensor placement for active structural acoustic control. He is an author of papers published in the conference proceedings of the 19th International Conference of Sound and Vibration (ICSV19) and the AIA-DAGA 2013 Conference on Acoustics 2013.

Oliver Unruh graduated from TU Berlin with a degree in Aerospace Engineering. He joined the German Aerospace Center (DLR) in 2009 and is currently working in the Department of Composite Structures and Adaptive Systems. He is part of a research group that deals with the design and realization of adaptive systems for active structural acoustic control. His research mainly concerns simulation methods in structural acoustics and sound propagation/radiation.

Martin Pohl graduated from TU Dresden in 2008 and joined the DLR in the same year. He currently works as a scientist focused on adaptive systems in structural dynamics, acoustics and electronics. There, he investigates piezoelectric shunt damping of shell structures for noise and vibration reduction of aircraft structures. He has published papers in the proceedings of ISMA, EURONOISE, ICAST and SMASIS conferences.

Emiel Tijs obtained his bachelor's degree in mechanical engineering at the Saxion Hogeschool Enschede in 2004 and has been working at Microflown Technologies ever since. He obtained his PhD developing an in situ method to measure sound absorption at Twente University in 2013. He is mainly involved in further developing sensors and applications for sound source localization and quantification, characterization of sound absorbing materials and underwater testing.

Rik Wijntjes graduated from Delft University in 2008, with a Master's degree in Applied Physics. He joined the National Aerospace Laboratory (NLR) in 2012 and is currently a R&D Engineer in Aeroacoustics, primarily involved in testing wall mounted sound absorbing materials. During these tests, the air flow effects over the surface of sound absorbing materials used in turbofan engine intake and exhaust ducts are simulated.

Henk van der Wal graduated from the University of Twente in 1973, with a Master's degree in Mathematics and informatics. He joined the National Aerospace Laboratory (NLR) in 1985 as a R&D Engineer in Aeroacoustics and retired in 2013. During his career he became an expert in the fields of noise insulation (aircraft fuselage barrels) and engine liner material testing. He has been the project manager of a large number of international (multi-partner) projects at the NLR and the work package leader for large European projects.

Gian Luca Ghiringhelli graduated from the Politecnico di Milano in Aeronautic Engineering (1980); He is a full professor at the Politecnico di Milano, in the Department of Aerospace Science and Technology. His past research fields include: structural dynamics and aeroelasticity, helicopter rotor modeling and analysis, aircraft design, composite structures, modeling and testing of smart structures (piezoelectric), and multibody modeling of complex systems; His current research fields include: vibration and noise in helicopters and aircraft (modelization and testing, materials and structures), active control and smart structures and materials (Piezo and MRF), and landing gear modeling and testing. Participation in the EC project FRIENDCOPTER.

I. Duran
(Cerfacs, Snecma)
S. Moreau
(Universite de Sherbrooke)
F. Nicoud
(Universite Montpellier)
T. Livebardon
(Cerfacs, Turbomeca)
E. Bouty
(Turbomeca)
T. Poinsot
(Institut de Mecanique
des Fluides de Toulouse)

E-mail: duran@cerfacs.fr

DOI : 10.12762/2014.AL07-05

Combustion Noise in Modern Aero-Engines

Combustion noise has recently been the subject of attention of both the aeroacoustic and the combustion research communities. Over the last decades, engine manufacturers have made important efforts to significantly reduce fan and jet noise, which increased the relative importance of combustion noise. Two main mechanisms of combustion-noise generation have been identified: direct combustion noise, generated by acoustic waves propagating to the outlet, and indirect combustion noise, caused by the acceleration of entropy waves (or hot spots) and vorticity waves through turbine blades. The purpose of this paper is to describe some of the predicting tools used in combustion noise, as well as to present an overview on some recent experimental studies.

Introduction

Noise emissions are a major concern for both aircraft and engine manufacturers. This is mainly caused by increasing restrictions and regulations regarding the global noise generated by aircraft during take-off and landing. At the same time, aircraft operators are concerned with passenger comfort and therefore demand a quieter cabin. Noise has become another pollutant source due to engines and airframe, which must be controlled both outside and inside aircraft and helicopters. For these reasons, the reduction of acoustic emissions is now a major field of research both for industry and research groups.

The first studies on the subject, carried out by Lighthill [32], showed the great importance of jet noise among the overall noise emissions. This was done in the context of the recently adopted jet engine, which was significantly louder than its helix-propelled predecessors. Lighthill showed that the jet-noise source scaled with the eighth power of the jet-exhaust speed, meaning that doubling the jet speed would lead to an increase of acoustic intensity level of nearly 50 dB. Jet speed reduction was at the time not only a noise concern, but also a performance requirement, since the propulsive efficiency increased significantly when the jet speed was reduced, increasing aircraft range and reducing cost. The turbofan engine used nowadays achieved these goals, reducing jet speed and maintaining the total thrust by increasing the mass-flow using a by-pass design. The increase in the propulsive efficiency and the noise reduction were significant, but the increase in air trafic and the construction of airports near residential areas forced aircraft manufacturers to further decrease the global noise emissions. At the same time, fuel costs and environmental concerns lead to further research on consumption reduction. The reduction of jet speed may reach a limit soon, since too high a by-pass ratio leads to heavier engines and therefore higher fuel consumption. Research on jet noise reduction continued in different directions, leading to solutions that were, in many cases, opposed to those reducing fuel consumption and for which a compromise had to be found. Chevrons, for example, were adopted to enhance the jet mixing at the outlet of the nozzle, in order to reduce jet noise, but this mechanism also had an impact on the propulsion, reducing the total thrust of the engine and therefore increasing the fuel consumption.

Other noise sources started to increase their relative contribution, as jet noise was significantly reduced. Firstly, the turbofan engine with high by-pass ratio reduced the jet noise, but at the same time added a significant contribution: the fan noise. As jet noise was being reduced, research on fan and turbomachinery noise increased, since there was still significant room for improvement. Airframe, landing gear, flap and slat noise were also considered, since they mostly contribute under approach conditions. Combustion noise was initially addressed in the work of Strahle [47], Chiu and Summerfield [5], Hassan [17], Marble and Candel [33], and Cumpsty and Marble [8], however, its relative contribution to the global aircraft acoustic emissions was still low. It was not until the development of the new low NOx-emission combustion chambers, such as lean premixed, rich-quench-lean or staged-injection combustion chambers, that noise emissions from the combustion chamber increased their relative contribution and started to be a major concern. These new

combustion chamber concepts have been adopted to reduce NOx emissions [40], but their design has two major issues. On the one hand, they can present combustion instabilities when the turbulent flame interacts with the acoustics of the chamber in a constructive way, increasing the acoustic energy, which can lead not only to high levels of noise but also to severe damage of the combustion system, where noise levels can exceed 200 dB. On the other hand, and as the main subject of this paper, the turbulent flame induces larger heat release fluctuations as the mixture approaches the lean extinction point. These heat release fluctuations generate two types of waves, acoustic and entropy, which are responsible for the two combustion noise generation mechanisms discussed in the following sections.

The rest of this paper is structured as follows: First, the two combustion noise generation mechanisms are presented. A description of computational methods to predict combustion noise in modern aero-engines is given and insights on previous, present and future experiments will follow. Conclusions and perspectives are finally drawn.

The two combustion noise generation mechanisms

Combustion noise is generated inside the combustion chamber and has to propagate through turbine blades. The problem of acoustic wave propagation through accelerating flows was first studied by Tsien [52] in a rocket engine combustion instability framework. It was Marble and Candel [33], however, who first included the propagation of entropy waves through accelerating subsonic and supersonic nozzles, explaining the two combustion noise generation mechanisms: direct and indirect, as seen in figure 1. Direct noise is generated by the acoustic waves produced in the flame region, which travel downstream through the turbine stages to the outlet. Indirect combustion noise is generated by the entropy waves induced by the unsteady combustion process. These waves generate noise when propagating through non-homogeneous flows, such as the turbine stages.

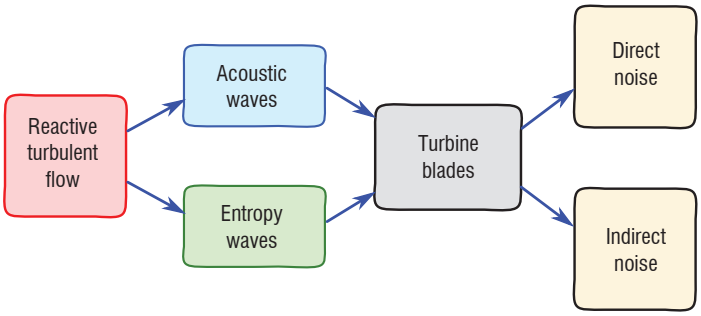

Figure 1: The two combustion noise mechanisms

Indirect combustion noise

Any heat release generates entropy, as described by the equation

$$\frac{\partial s}{\partial t}+\vec{u}\cdot\nabla s=\frac{\dot{Q}}{\rho T} \quad \text{with} \quad s=c_v\ln\left(\frac{p}{\rho^\gamma}\right) \tag{1}$$

where the usual definition of entropy is used. It is therefore straightforward to conclude that an unsteady heat release q' of this heat source (due to turbulence for example) generates a fluctuating entropy term, s', given by a linearization

$$\frac{\partial s'}{\partial t}+\vec{u}\cdot\nabla s'=\frac{q'}{\rho T}-\left(\frac{p'}{p}\vec{u}+\vec{u}'\right)\nabla s \quad \text{with} \quad \frac{s'}{c_p}=\frac{p'}{\gamma p}-\frac{\rho'}{\rho}, \tag{2}$$

as shown by Dowling et al. [9] where the mean steady quantities are represented by the non-primed variables for simplicity. This equation shows first that entropy fluctuations are generated by both the flame fluctuations (q') and by acoustic fluctuations in regions with mean heat release (second term on the right hand side). At the same time, it shows that once generated, in the region outside the flame where no mean or fluctuating heat release exists, the right-hand-side of Eq. (2) is zero and the entropy wave is just convected with the mean flow velocity $(\vec{u})$ when neglecting any flow mixing or diffusion. Marble and Candel [33] showed that a one-way coupling between entropy and acoustics appeared when a flow gradient existed in a quasi-1D nozzle. Using the quasi-1D linearized Euler equations for the flow through the nozzle (neglecting heat release and diffusion),

$$\left[\frac{\partial}{\partial t}+u\frac{\partial}{\partial x}\right]\left(\frac{p'}{\gamma p}\right)+u\frac{\partial}{\partial x}\left(\frac{u'}{u}\right)=0 \tag{3}$$

$$\left[\frac{\partial}{\partial t}+u\frac{\partial}{\partial x}\right]\left(\frac{u'}{u}\right)+\frac{c^2}{u}\frac{\partial}{\partial x}\left(\frac{p'}{\gamma p}\right)=\left[\frac{s'}{c_p}-2\frac{u'}{u}+(\gamma-1)\left(\frac{p'}{\gamma p}\right)\right]\frac{du}{dx} \tag{4}$$

$$\left[\frac{\partial}{\partial t}+u\frac{\partial}{\partial x}\right]\left(\frac{s'}{c_p}\right)=0 \tag{5}$$

the coupling between the entropy and acoustics appears on the right hand side of eq. (4), where the entropy wave appears multiplied by the velocity gradient, du/dx. If the flow is homogeneous with no acceleration, the right hand side of eq. (4) is zero and the well-known result for acoustic propagation in non-zero but constant-Mach-number flows is recovered from eqs. (3) and (4). However, when considering a mean flow gradient, the coupling between convective and acoustic waves appears: the entropy wave acts as a source term in the acoustic equation, generating entropy or indirect combustion noise. This mechanism, which converts entropy waves into acoustic noise, has been extensively studied from an experimental [2], analytical [53, 18, 44, 19, 31, 11, 20] and numerical point of view [24, 30, 50, 51].

Direct combustion noise

As seen in the second part of eq. (2), the entropy wave has an associated density fluctuation. In the near region of the flame, this density fluctuation is generated by the unsteady heat release and generates a velocity perturbation (acoustic wave) due to the mass conservation equation. This mechanism generates acoustic waves directly in the flame region as a monopole source [25], which propagate through the turbine stages, generating direct combustion noise. In free space, an acoustic analogy can be used to propagate this noise source. For example, when considering Phillips' analogy [38], which was extended to reactive flows by Chiu and Summerfield [5] and Kotake [25], the wave equation reads,

$$\frac{D^2\pi}{Dt^2}-\frac{\partial}{\partial x_i}\left(c^2\frac{\partial\pi}{\partial x_i}\right)=\frac{D}{Dt}\left[\frac{(\gamma-1)}{\rho c^2}\dot{\omega}_T\right] \tag{6}$$

where $\pi=(1/\gamma)\ln(p/p_\infty)$ and $\dot{\omega}_T$ is the heat release of the flame. Only this direct combustion noise contribution has been retained, for simplicity, to illustrate the monopole nature of combustion noise at low Mach numbers. Direct combustion noise has been studied analytically [46, 47], combining numerical simulations and acoustic analogies [22, 21, 48, 49] and experimentally [41]. These studies are mostly performed for free unconfined flames, a situation that is never observed in an engine.

The indirect mechanism can be of great importance in modern aero-engines due to the large accelerations of the flow in the turbine blades, as seen by [4, 36, 39]. Leyko et al. [28] showed that, for a 1D model combustor with a choked nozzle, indirect noise can be one order of magnitude larger than direct noise, depending on the mean Mach number in the combustion chamber. An order of magnitude can be useful here: sending a 10K temperature fluctuation through a choked nozzle can produce a pressure oscillation of up to 40 Pa at the outlet.

Both combustion noise generation mechanisms depend strongly on the propagation of waves through turbine stages: direct noise is shielded by the effect of the turbine blades and the successive accelerations and decelerations of the mean flow, while entropy noise is, on the other hand, generated by these accelerations and decelerations. For this reason, the study and the prediction of combustion noise has focused both on the generation of waves by the flame in the chamber and on the propagation of waves through non-uniform flows, which is typical of turbine stages.

Predicting combustion noise in modern aero-engines

The prediction of combustion noise through numerical methods is a challenging task. First, noise sources must be computed accurately in the combustion region, then propagated through turbine stages including the effects of velocity gradients where the entropy wave generates indirect noise and, finally, noise must be propagated in the far field. The hybrid method proposed here combines Large Eddy Simulations (LES) of the combustion chamber with analytical methods to resolve the propagation of waves through the turbine stages and is illustrated in figure 2.

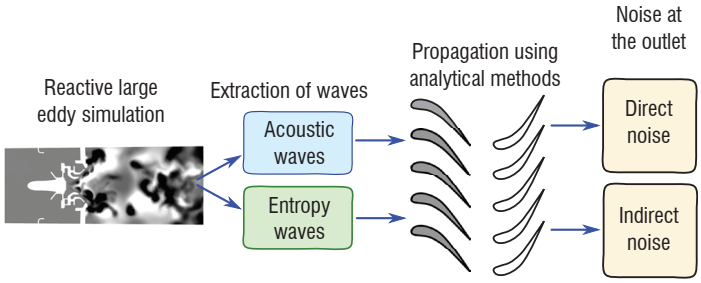

Figure 2 - CHORUS hybrid method to compute combustion noise

Since noise sources (in this case the flame dynamics) must be seized properly, RANS (Reynolds-Averaged Navier-Stokes) simulations are less suitable, since the unsteady features of the flow would have to be modeled. Indeed, the unsteadiness of the heat release is mainly caused by turbulence-flame interactions and acoustics-flame interactions, and thus a resolved compressible reactive LES is more suited. A proper LES simulation can resolve the large turbulent structures of the flow, which are responsible for the low-frequency wrinkling of the flame and therefore the unsteady heat release that generates noise. Small-scale turbulence is not resolved and must be modeled appropriately to consider its dissipation in the mean flow.

The flame model is of great importance also. The flame thickness is usually smaller than the grid size of any LES simulation and must be modeled or thickened artificially to be properly resolved in the computational mesh, thereby including an extra layer of modeling. The modeled flame must react properly to velocity, temperature and, in some cases, mixture fraction fluctuations in the flame front; therefore, the model can be a key element when computing combustion noise. The flamelet formulation has been used for non-premixed cases [21], while the G-equation [34, 23] has been used to model the flame in premixed combustion cases. A more general formulation is to use the thickened flame model [3], which has the advantage of dealing with both premixed and non-premixed flames. This is the case of modern aero-engines, where the flow is partially premixed and thus both premixed and diffusion (non-premixed) flames can be present. The idea behind this model is to artificially increase the flame thickness by multiplying the thermal diffusivity (D) by a factor F and dividing the pre-exponential constant (A) by the same factor. Since the flame thickness of premixed flames scales as $\delta \sim \sqrt{D/A}$ and the laminar flame speed as $s_l \sim \sqrt{DA}$, the new flame would be F times thicker (in order to be resolved by the mesh), while conserving the original laminar flame speed. The drawback of this formulation is that the Damköhler number, $D_a \sim \tau_t / \tau_c$, is also decreased by a factor F, meaning that vortices cannot wrinkle the thickened flame in the same way as they do with the real thin flame. The wrinkling of the flame by turbulent scales must be modeled through an efficiency function [7] obtained from canonical DNS simulations. The advantage of this formulation, however, is first that a multi-species combustion with different non-unity Lewis numbers can be considered, since the flame front is resolved in the mesh and not only as a discontinuity of the flow and, at the same time, the level of modeling tends to zero when the mesh size is reduced, which is not the case for the flamelet and the G-equation models. This last point is of great importance since, when performing resolved LES, one expects the numerical solution to tends to the real one when the mesh size tends to zero.

Next, once the noise sources are computed using LES, to obtain the direct and indirect noises generated, the acoustic and entropy waves must be propagated from the outlet of the combustion chamber to the outlet of the turbine. This propagation through a non-homogeneous flow is responsible, on the one hand, for the attenuation of the acoustic waves and, on the other hand, for the generation of indirect noise through the successive acceleration and deceleration of entropy waves in each turbine stage. However, including the turbine in the LES numerical simulation is not feasible using state-of-the-art computational codes and resources, and some kind of acoustic analogy or modeling should be used to account for the propagation and generation of indirect noise through the turbine. Acoustic analogies such as that of Lighthill [32] are widely used in the aeroacoustics community and easily applied with a low computational cost. When writing the complete acoustic analogy for reacting flows [1],

$$\frac{1}{c_\infty}\frac{\partial^2 p}{\partial t^2}-\frac{\partial 2 p}{\partial x_i^2}=\frac{\partial 2}{\partial x_i x_j}\left(\rho u_i u_j-\tau_{ij}\right)$$
$$+\frac{\partial}{\partial t}\left[\frac{\rho_\infty}{\rho}\frac{(\gamma-1)}{c^2}\left(\omega_T^{\cdot}+\sum_k h_k\frac{\partial J_k}{\partial x_k}-\frac{\partial q_i}{\partial x_i}+\tau_{ij}\frac{\partial u_i}{\partial x_j}+\dot{Q}\right)\right.$$
$$\left.+\rho_\infty\frac{D}{Dt}\ln r\right] \quad (7)$$
$$+\frac{1}{c_\infty}\frac{\partial}{\partial t}\left[\left(1-\frac{\rho_\infty c_\infty^2}{\rho c^2}\right)\frac{Dp}{Dt}-\frac{p-p_\infty}{\rho}\frac{D\rho}{Dt}\right]$$
$$+\frac{\partial^2}{\partial x_j t}\left(\rho_e u_j\right)$$

the indirect combustion noise source (last line) appears on the right hand side of the wave equation, in terms of the excess density, $\rho_e=(\rho-\rho_\infty)-(p-p_\infty)/c_\infty$, i.e, the density fluctuation that arises over and above isentropic acoustic contributions and associated with entropy fluctuations. A first drawback, however, is that the mean flow is considered at rest in the propagation region and therefore indirect noise, generated where velocity gradients are strong in the mean flow, cannot be predicted using this method and must be given in advance. Moreover, an acoustic analogy requires the medium to be broken down into a source region and a propagation zone, which can hardly be done in the indirect noise context. Assuming that the sound can be split into generation and propagation, the source term given by the excess density (right hand side of Eq(7)) must be part of the sources solved by LES to be propagated by the wave operator (left hand side of Eq(7)), which remains a daunting task.

The alternative is to solve analytically (under several assumptions) the propagation of waves through the non-homogeneous flow. Marble and Candel [33] first solved the propagation of waves through a quasi-1D subsonic and supersonic nozzle analytically using the compact assumption, where the wavelength of the waves is small compared to the nozzle transversal length (and therefore the result is valid in the low frequency range only). Thus, the linearized Euler equations (3)-(5) are assumed to be quasi-steady, giving three jump conditions between the inlet (i) and the outlet (o) corresponding to the mass, total temperature and entropy fluctuations, namely

$$\left(\frac{\dot{m}'}{\dot{m}}\right)_i=\left(\frac{\dot{m}'}{\dot{m}}\right)_o \quad (8)$$

$$\left(\frac{T_t'}{T_t}\right)_i=\left(\frac{T_t'}{T_t}\right)_o \quad (9)$$

$$\left(\frac{s'}{c_p}\right)_i=\left(\frac{s'}{c_p}\right)_o \quad (10)$$

These matching conditions are written as a function of the dimensionless upstream and downstream acoustic propagating waves w^+, w^- and entropy wave w^s defined in Eq((11), (12) and (13)) and solved analytically. Fully analytical solutions exist also when considering non-compact frequencies for a specific nozzle geometry [52, 33, 35, 15], for any nozzle geometry using an asymptotic expansion up to first order [45, 16] and, more recently, using the Magnus expansion for any frequency and any nozzle geometry [10]. These methods, however, are based on a quasi-1D formulation, neglecting the real 3D flow of the turbine and, in particular, the flow deviation imposed by the stator and rotor blades.

$$w^+=\frac{p'}{\gamma p}+\frac{u'}{\gamma c} \quad (11)$$

$$w^-=\frac{p'}{\gamma p}-\frac{u'}{\gamma c} \quad (12)$$

$$w^s=\frac{s'}{C_p} \quad (13)$$

Cumpsty and Marble [8] used the same compact assumption as Marble and Candel [33] to write the jump conditions of the acoustic and entropy waves, as well as vorticity waves w^v,

$$w^v=\frac{\xi'}{\omega} \quad (14)$$

where ξ' is a vorticity fluctuation, through a two-dimensional stator blade row combining Marble's equation's with the Kutta condition at the outlet of the row. This formulation is still based on the same compact assumption and is therefore only valid for low frequencies, but considers the 2D azimuthal component of the flow though neglecting radial effects, which are small below the radial cut-off frequency, which is typically of the order of 10^3-10^4 Hz. The model includes the effects of flow deviation, vorticity, the different azimuthal modes present in the combustion chamber and their cut-off frequencies, being therefore more suitable for the propagation and generation of combustion noise in turbine stages.

Finally, once the acoustic waves are obtained at the outlet of the aero-engine (direct and indirect), an acoustic analogy or a linearized 3D computation is used to obtain the far field combustion noise spectrum. The complete hybrid computation chain (named CHORUS) is illustrated in figure 2: The compressible unstructured reactive LES solver AVBP [42, 55] is used to compute the noise sources in the complex geometry of an actual combustion chamber. From this computation, the outgoing dimensionless waves defined above are extracted at the outlet of the combustion chamber and propagated through the blade rows using analytical method [8]. The waves at the outlet of the turbine can be finally propagated to the far-field using the acoustic solver AVSP-F, which solves the 3D linearized Euler equations in a quiescent flow in the frequency domain.

This hybrid method has been successfully applied in several state-of-the-art industrial aero-engines. The results of one of such simulations are presented here as an example. The LES simulations of the combustion chamber are performed on a single sector, using the unstructured compressible reactive code AVBP [42]. The waves at the outlet of the combustion chamber (acoustic, entropy and vorticity) are plotted in figure 3. It can be seen that the acoustic waves (figures 3(a) and 3(b)) are mainly longitudinal. It should be noted that, since the LES simulation is performed on a single sector, the low-order circumferential modes cannot be computed and only the plane mode will be taken into account. The circumferential mode in figure 3 corresponds to the first multiple of the number of sectors ($m=18$).

Using the analytical methods of Cumpsty and Marble [8], CHORUS is able to propagate these waves through the turbine stages and compute, on the one hand, direct combustion noise generated by acoustic waves and, on the other hand, the contribution from entropy and vorticity waves in indirect combustion noise. Below 8400 Hz, the azimuthal mode, visible at the outlet of the chamber in figure 3, is

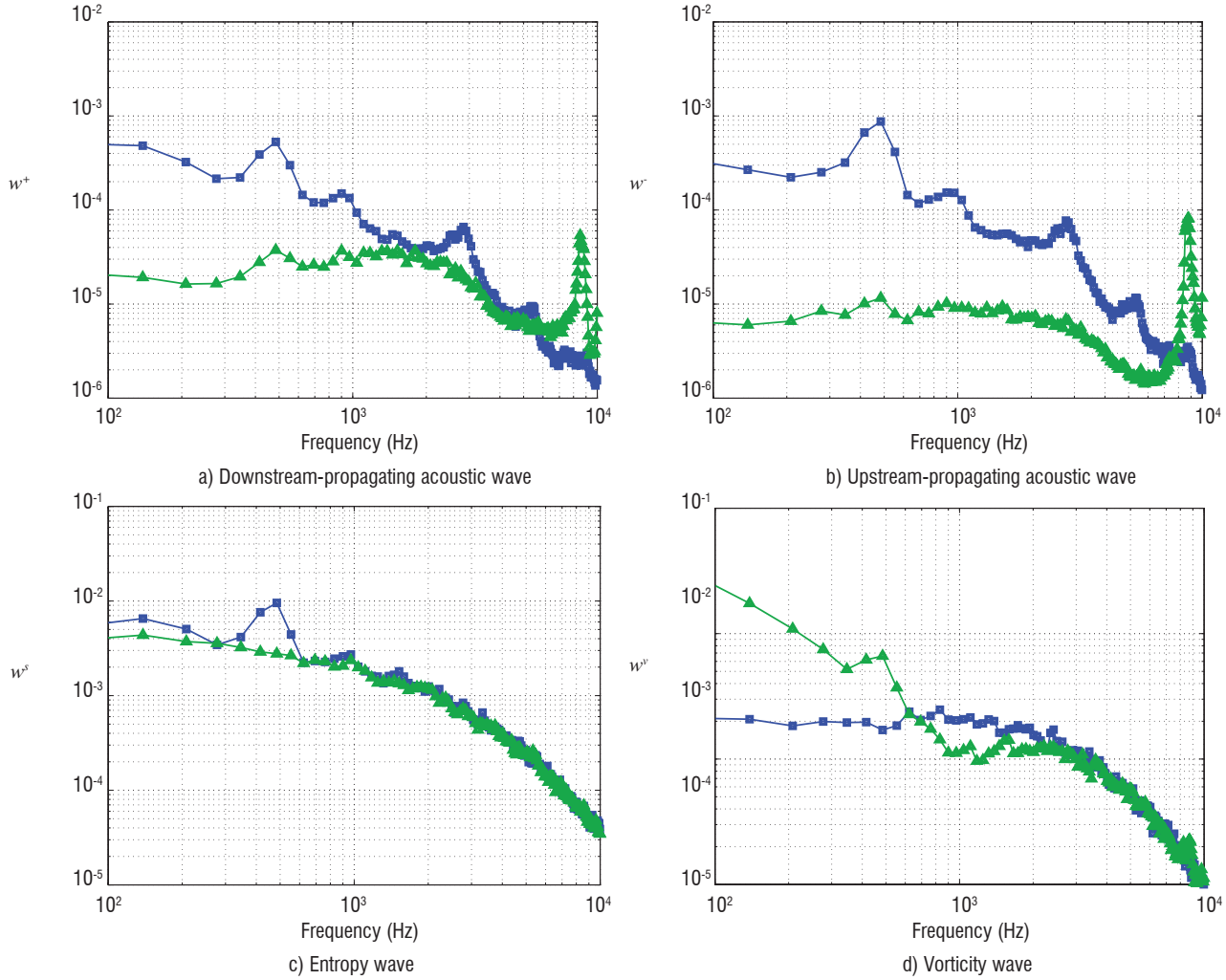

Figure 3 - Spectra of the waves at the outlet of the combustion chamber for the plane mode (■) and for the first circumferential mode of the sector, $m = 18$ (▲)

evanescent. As a consequence, in this computation, the plane mode is the only contributor to noise generation through the turbine. Noise terms are plotted in figure 4 in dB, showing that vorticity noise represents the weakest contribution and that indirect noise is stronger than direct combustion noise, though the latter is still significant and cannot be neglected.

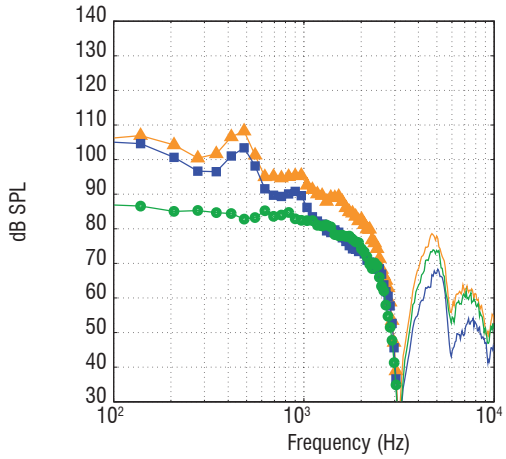

Figure 4 - Combustion noise at the outlet of the turbine stages induced by plane waves.Indirect noise (▲), direct noise (■) and vorticity noise (●)

Experiments on combustion noise

Strahle [46], Giammar and Putnam [13, 14] give reviews about experiments performed before the 1970s on combustion noise, mostly focused on direct combustion noise. Recent experiments have focused on indirect combustion noise, on the one hand to identify whether this mechanism is significant and, on the other hand, to assess the existing analytical theories for the prediction of this type of noise. Two of the most recent experiments are discussed here: the Entropy Wave Generator (EWG) and the Turboshaft Engine Exhaust Noise Identification (TEENI) experiments.

The entropy wave generator

Leyko et al. [30] showed, using the analytical theory of Marble and Candel [33] and a model 1D combustor, that indirect combustion noise could be stronger than direct noise, but only when large accelerations follow the combustion process. This is generally the case of aircraft aero-engines, where the turbine stages generate strong accelerations of the mean flow. Experiments on combustion performed in laboratories are, however, generally carried out at ambient pressure, with a low velocity exhaust, and therefore only produce direct combustion noise. The first successful experiment on indirect combustion noise was the entropy wave generator (EWG), carried out at the German Aerospace Center, DLR, by Bake et al. [2], and included an electrical heating device that

modeled the combustion process, followed by a convergent-divergent nozzle, allowing both subsonic and supersonic flows with a shock wave. Figure 5 shows a sketch of the experimental set-up, where the heating device and the convergent-divergent nozzle are shown. Table 1 presents the main geometrical parameters.

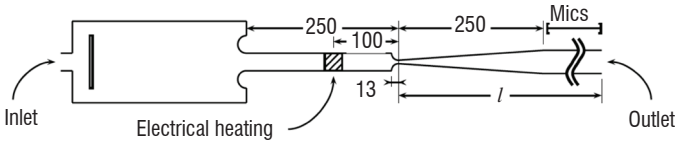

Figure 5 - Diagram of the Entropy Wave Generator experimental set-up (lengths are given in mm). Figure reproduced from Leyko [27]

Convergent length	Divergent length	Throat diameter	Inlet diameter	Exit diameter
13 mm	250 mm	7.5 mm	30 mm	40 mm

Table 1 - Main geometrical characteristics of the EWG nozzle

The flow through the nozzle could be either subsonic or supersonic with a shock wave, depending on the mass flow rate. Table 2 shows the main physical parameters of the EWG experiment for the supersonic case. When the heating device is triggered, it generates a temperature pulse shown in figure 6, due to the unsteady heat release. This unsteady heat release generates an entropy wave and an acoustic wave, as explained in § "The two combustion noise generation mechanisms".

Plenum pressure	Outlet pressure	Inlet Mach
117000 Pa	100800 Pa	0:037
Outlet Mach	Pulse duration, τ	Pulse amplitude
0.023	100 ms	9 K

Table 2 - Main physical parameters of the EWG experiment in the supersonic case with a shock wave.

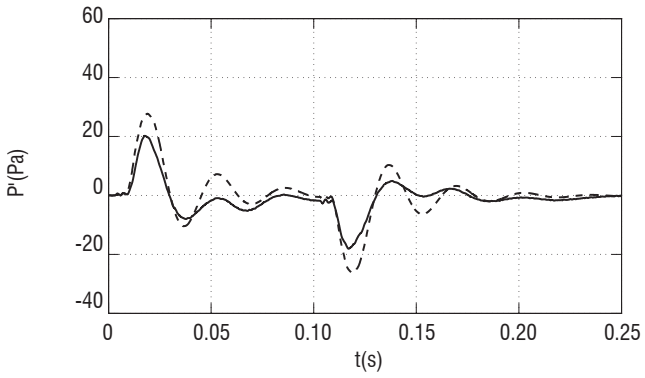

Figure 6 - Temperature pulse of the EWG in the supersonic case: experimental data (──) and numerical simulations (---) [31]

The experimental configuration has been studied for both the supersonic case [31] and the subsonic case [11, 15, 19, 29, 28]. For the supersonic case, the analytical model of Marble and Candel [33] was shown to correctly predict the entropy noise generated by the configuration, taking into account the propagation of waves through the nozzle and the interaction of these acoustic and entropy waves with the shock wave present in the divergent section [29, 31]. It was also shown that the main noise source in this case was the indirect mechanism. The pressure waves at the outlet of the EWG are shown in figure 7, showing a perfect agreement between numerical simulations and analytical methods. The slight disagreement with the experimental data is probably caused by the uncertainties on boundary conditions, as explained by Leyko et al. [31].

Howe [19] showed that, for the subsonic case, the large levels of pressure fluctuations measured experimentally at the outlet of the nozzle could not be attributed to the indirect mechanism. Duran et al. [11] showed that the heating device generated acoustic waves, due to the density fluctuations induced by the fluctuating heat release. These acoustic waves generated a direct noise contribution that was shown to be larger than the indirect source.

The EWG will be followed by the HAT nozzle with high pulsation energies, within the scope of the RECORD project funded by the Seventh Framework Program (FP7) of the European Commission. In this experiment, other aspects of indirect noise will be studied, such as non-linear effects, since entropy waves generated in real combustion chambers are expected to be large enough to present non-linear effects. This experiment will study the generation of noise by large-amplitude entropy waves and how the dissipation of entropy waves should be taken into account. The RECORD project will also focus on the understanding of core noise generation and transmission mechanisms, in real combustors and academic burners, using LES simulations coupled with low-order models and validated with experimental data.

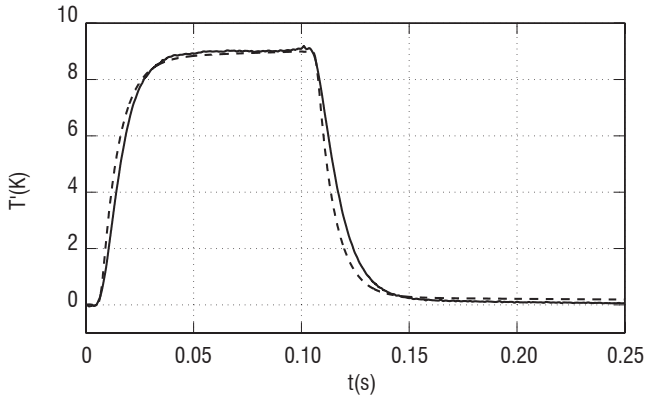

a) Comparison between experimental data (──) and numerical simulations (---)

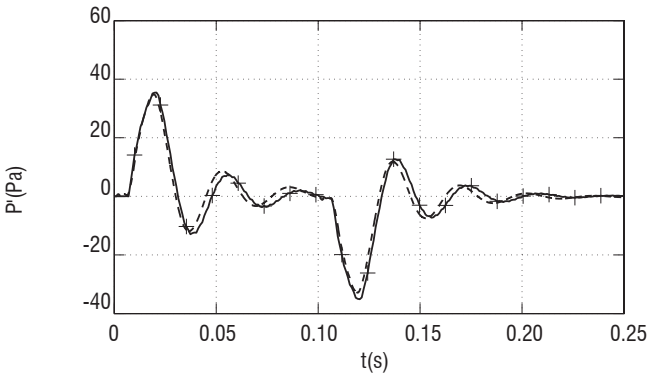

(b) Comparison between numerical simulations (---) and analytical methods (- + -)

Figure 7 - Indirect noise measured at the outlet of the EWG nozzle in the supersonic case [31]

TEENI: Full-scale combustion noise measurements

The TEENI program (Turboshaft Engine Exhaust Noise Identification) funded by the FP7 of the European Commission is focused on turboshaft engine noise, where jet-noise is negligible since the outlet flow speed is very low. The main aim of the project is to determine which of the other noise sources (turbine, combustion noise, etc.) is dominant in such engines. To do so, the objectives of the program are to:

- develop and test sensors that will allow the measurement of acoustic pressure and temperature fluctuations and are resistant to the engine environment (particularly high-temperatures);
- discriminate the origin of the sound field generated at the outlet of the turboshaft;
- understand the propagation of broadband noise through turbine blade rows;
- develop noise-source breakdown techniques, in order to locate the origin of the noise inside the engine.

Though the purpose of the project has a very wide scope, there is a particular interest in combustion noise identification. Experimental identification of other sources is relatively easy compared with combustion noise: turbine blades, for example, can be mounted in an experimental rig and tested individually; on the contrary, since combustion noise is generated both in the combustion chamber and caused by the propagation of entropy waves through turbine blades (generating indirect combustion noise), any aim at identifying combustion noise experimentally must be done in a complete engine test-rig, where other noise sources will add up interfering with combustion noise. Traditionally, in turbo-fan engines, combustion noise was measured indirectly by subtracting the individually tested noise contributions (such as compressor, turbine, fan and jet noise) from the noise of the complete test-rig, yielding what was usually known as 'excess noise', 'excess broadband noise' or sometimes simply 'core noise'. One of the goals of TEENI is to develop sensors and experimental procedures that will allow combustion noise to be identified accurately in a full scale aero-engine, performing cross-correlations of the pressure signal at the outlet with the pressure and temperature signals measured inside the combustion chamber.

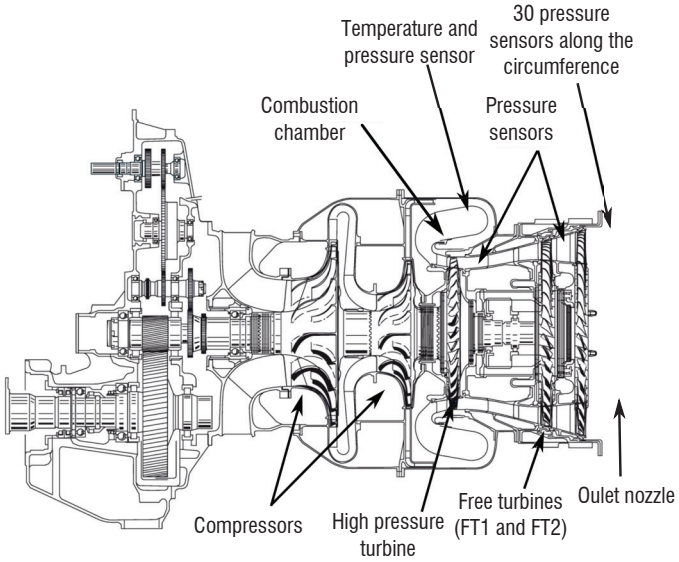

Figure 8 - Diagram of the TEENI experimental set-up

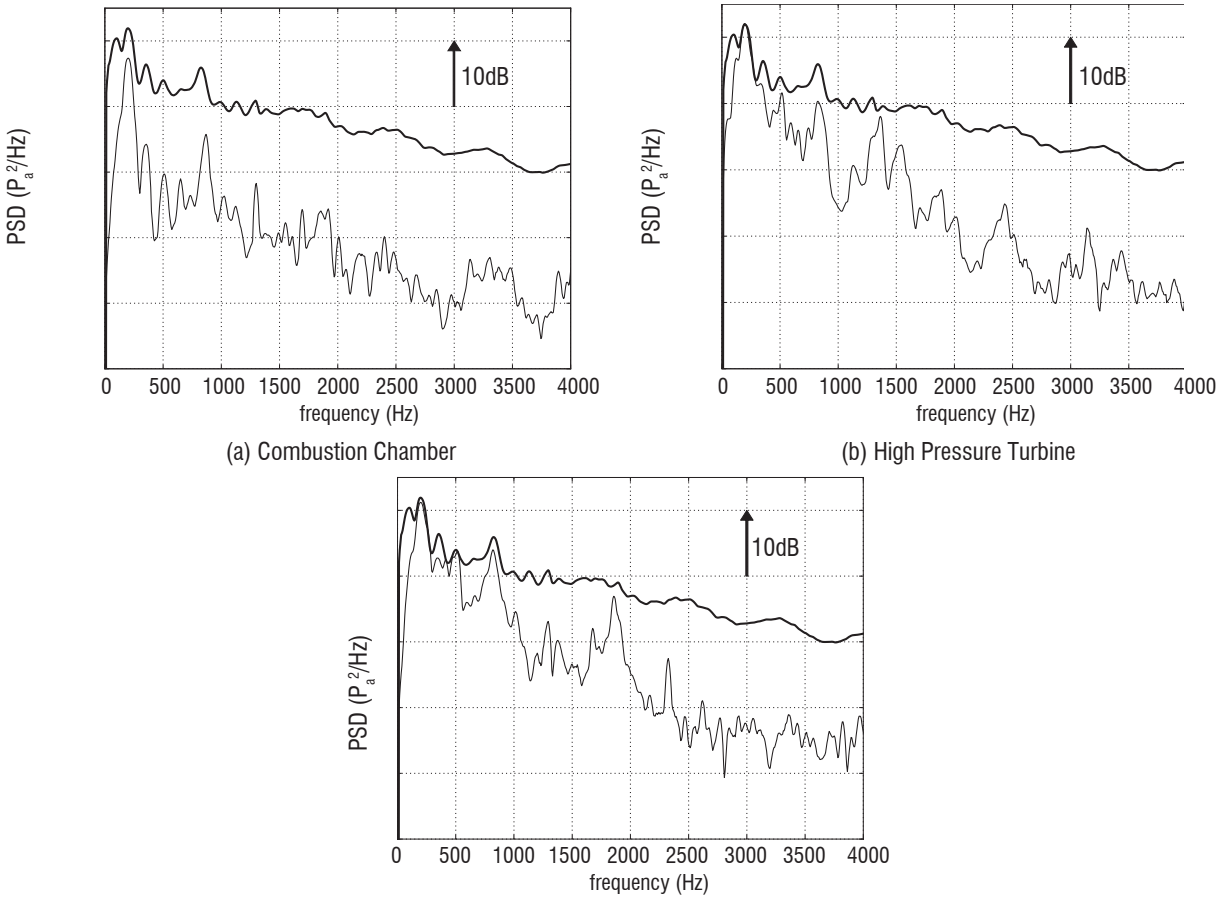

Figure 9 - PSD of pressure fluctuations (—) measured in the outlet nozzle and coherent PSD of pressure fluctuations correlated between different locations within the engine and this reference pressure probe using the three-sensor techniques (—).

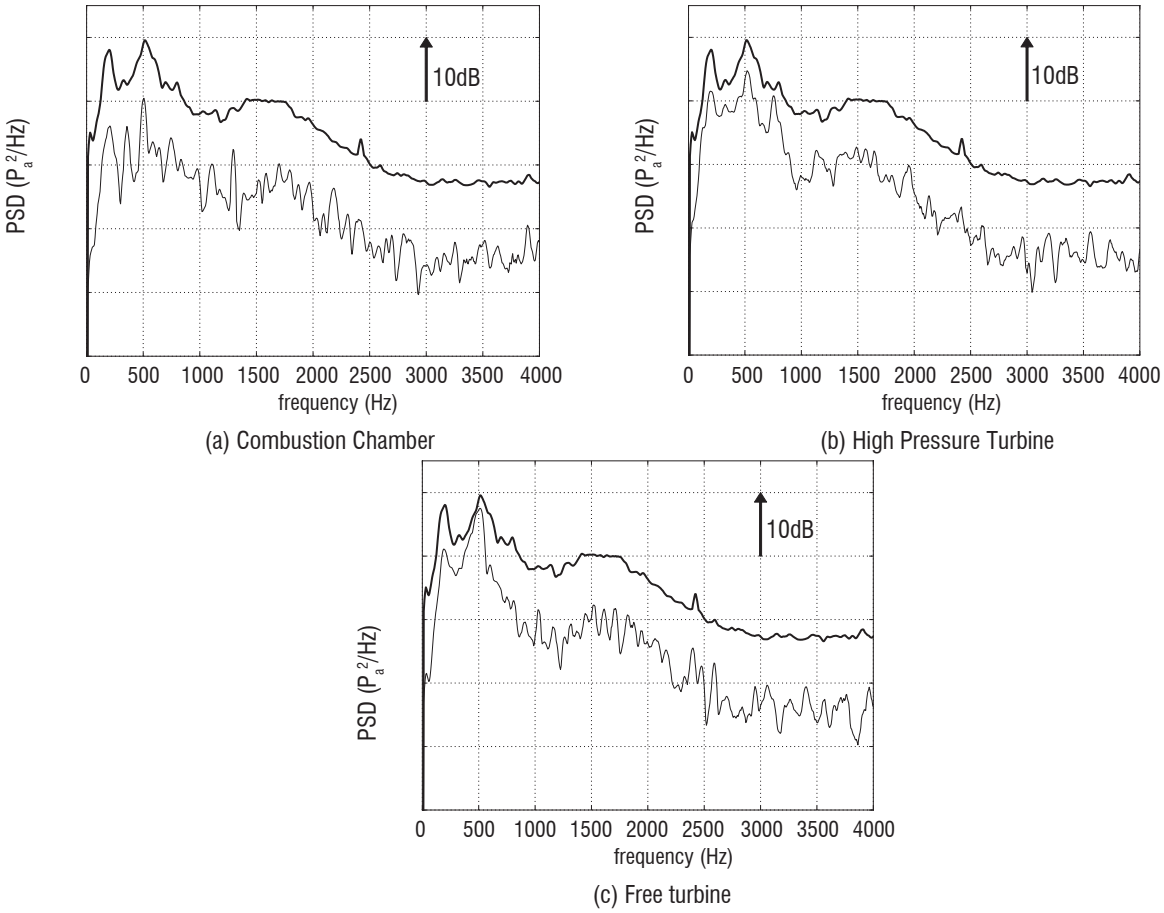

Figure 10 - Acoustic PSD (—) measured in the direction of maximum acoustic radiation at the far-field and coherent PSD of pressure fluctuations correlated between different locations within the engine and this reference microphone using the three-sensor techniques (—).

The experimental set-up consists of an entire Turbomeca engine, modified to install the instrumentation. A diagram of the configuration is shown in figure 8. Probes have been developed by the DLR to be adapted to the engine environment. Each pressure probe is a flush-mounted pin-hole with a remote microphone placed perpendicular to a semi-infinite tube, limiting standing wave effects [37]. To prevent microphone effects from hot combustion products, a cooling system injects a controlled air flow rate through the tube [12]. Temperature sensors were based on a twin thermocouple design, in order to be able to detect fluctuations of up to 700Hz. Since the project is aimed at identifying different noise sources, these sensors are placed in the combustion chamber, the high pressure turbine, the two free turbines and the exhaust nozzle. In total, 36 acoustic internal probes, 9 twin thermocouples and 18 far-field microphones were used. The harsh conditions, especially in the combustion chamber, required an original probe design and a cooling system, ensuring high-quality measurements.

Due to broadband nature of combustion noise, characterization of this contribution in the core noise requires broadband-noise breakdown techniques. In particular, it is possible to extract coherent power spectral density (PSD) of pressure fluctuations between three probes, using the three-sensor technique [54, 43, 6, 26] applied between two probes within the engine and a reference probe in the outlet nozzle, or in the far-field. Results are plotted in figures 9 and 10.

A narrowband coherent PSD is visible in figure 9(a) in the frequency interval [200Hz, 400Hz], between the combustion chamber and the outlet nozzle, which corresponds to the direct combustion noise, unlike the far-field reference microphone (figure 10(a)). On the other hand, the three-sensor technique applied in the high pressure turbine shows a global increase of coherent PSD in the interval [200 Hz, 1000Hz] in figures 9(b) and 10(b). However, the lack of noticeable spectral contents in temperature fluctuations in this frequency range does not allow indirect combustion noise to be clearly identified as major contributor. Finally, the three-sensor technique does not show an important contribution of the free turbine stages in the generation of coherent broadband PSD below 4000 Hz, as seen in figures 9(c) and 10(c).

Conclusions and perspectives

Combustion noise is a complex phenomenon involving at the same time combustion mechanisms, turbulence, chemistry, acoustics and turbomachinery. This noise source is not the main one in industrial aero-engines, though it has been shown to have a direct impact on helicopter certification levels. Its influence increases as other noise sources are reduced. At the same time, new low-NOx emission combustion chambers have been found to generate more combustion noise than their predecessors. For this reason, research is being carried out in order to predict this noise source and to develop noise-reduction methods. The dificulty of predicting combustion noise lies in its nature: direct noise is generated in the combustion chamber, but can be attenuated when propagating through turbine stages, while indirect noise is due to the acceleration of the entropy waves (generated in the combustion

chamber) when propagating through the blades. In this article, a hybrid method (CHORUS) is presented, in which large eddy simulations of the combustion chamber are combined with analytical solutions for the propagation of waves through turbine blades, in order to obtain the noise (direct and indirect) at the outlet of the aero-engine. The analytical method is based on strong assumptions, which must be validated with experimental data. With this purpose, the EWG experiment was performed, showing first the importance of indirect noise and allowing an experimental comparison with the analytical methods.

The TEENI experiment is also a good example of the progress being made by the combustion noise community. In this case, a complete turboshaft engine has been mounted and instrumented with state-of-the-art pressure and temperature probes, in order to identify combustion noise (and other sources) through detailed signal post-processing. These noise identification techniques are of great importance, since they allow the most significant noise sources to be identified. The objective is to later apply noise reduction technologies, such as acoustic liners, appropriately focused on the dominant source to obtain the largest possible noise reduction.

In the near future, the RECORD project (funded by the 7th FP of the European Commission) will further investigate combustion noise. In particular, the first part of the RECORD project will study the influence of the pulse nature on the generation of waves. At the same time, the RECORD project will focus on the noise sources inside experimental combustion chambers at high pressure (with an outlet nozzle), which will be then available for validation purposes, and on the propagation of acoustic and entropy waves through a real turbine stage, in order to validate the 2D analytical models ■

Nomenclature

c	Sound velocity	ξ	Vorticity
c_p	Specific heat at constant pressure	ρ	Density
c_v	Specific heat at constant volume	ρ_e	Excess density
J_k	Diffusion flux	γ	Ratio of specific heats
P	Pressure	τ_{ij}	Shear stress tensor
$\dot{Q}$	Unsteady heat release	$\omega_T^{\cdot}$	Heat release per unit volume
r	Specific gas constant	ω	Pulsation
s	Entropy	t	Total state
t	Time	i	Inlet
T	Temperature	o	Outlet
$\vec{u}$	Velocity vector	'	Fluctuation
w	Wave	∞	Far-field value
x	Axial component	+	Upstream
		-	Downstream

Acknowledgements

The authors would like to thank Nancy Kings and Friedrich Bake from the DLR for providing the EWG data and fruitful inputs. This work was partly funded by Snecma and Turbomeca.

References

[1] C. BAILLY, C. BOGEY, S. CANDEL - *Modelling of Sound Generation by Turbulent Reacting Flows*. International Journal of Aeroacoustics, 9(4):461-490, 2010.

[2] F. BAKE, C. RICHTER, B. MUHLBAUER, N. KINGS, I. ROHLE, F. THIELE, B. NOLL - *The Entropy Wave Generator (EWG): a Reference Case on Entropy Noise*. J. Sound Vib. , pages 574-598, 2009.

[3] T.-D. BUTLER, P.-J. O'ROURKE - *A Numerical Method for Two-Dimensional Unsteady Reacting Flows*. Proc. Combust. Inst. , 16(1):1503-1515, 1977.

[4] S. CANDEL - *Acoustic Transmission and Reection by a Shear Discontinuity Separating Hot and Cold Regions*. J. Sound Vib. , 24:87-91, 1972.

[5] H. CHIU, M. SUMMERFIELD - *Theory of Combustion Noise*. Acta Astronautica , 1: 967-984, 1974.

[6] J.-Y. CHUNG - *Rejection of Flow Noise Using a Coherence Function Method*. Journal of the Acoustical Society of America, 62(2):388-395, 1977.

[7] O. COLIN, F. DUCROS, D. VEYNANTE, T. POINSOT - *A Thickened Flame Model for Large Eddy Simulations of Turbulent Premixed Combustion.* Phys. Fluids , 12(7):1843-1863, 2000.

[8] N.-A. CUMPSTY, F.-E. MARBLE - *The Interaction of Entropy Fluctuations with Turbine Blade Rows; a Mechanism of Turbojet Engine Noise*. Proc. R. Soc. Lond. A , 357:323-344, 1977.

[9] A. DOWLING, G.-J. BLOXSIDGE, N. HOOPER, P.-J. LANGHORNE - *Active Control of Reheat Buzz*. AIAA Journal, 26(7):783-790, July 1988. ISSN 0001-1452. doi: 10.2514/3.9970. URL http://doi.aiaa.org/10.2514/3.9970.

[10] I. DURAN, S. MOREAU - *Solution of the Quasi One-Dimensional Linearized Euler Equations Using Flow Invariants and the Magnus Expansion*. Journal of Fluid Mechanics, 723: 190-231, May 2013.

[11] I. DURAN, S. MOREAU, T. POINSOT - *Analytical and Numerical Study of Combustion Noise Through a Subsonic Nozzle*. AIAA Journal, 51(1):42-52, 2013.

[12] U.-M.-F. BAKE, I. ROEHLE - *Investigation of Entropy Noise in Aero-Engine Combustors.* Proceedings of the ASME Turbo Expo 2006, 2006.

[13] R.-D. GIAMMAR, A.-A. PUTNAM - *Combustion Roar of Turbulent Diffusion Flames.* Journal of Engineering for Power, 92(2):157-165, April 1970.

[14] R.-D. GIAMMAR, A.-A. PUTNAM - *Combustion Roar of Premix Burners, Singly and in Pairs*. Combust. Flame , 18:435-438, 1972.

[15] A. GIAUQUE, M. HUET, F. CLERO - *Analytical Analysis of Indirect Combustion Noise in Subcritical Nozzles*. J. Eng. Gas Turbines Power, 134(11):111202, 2012.

[16] C.-S. GOH, A.-S. MORGANS - *Phase Prediction of the Response of Choked Nozzles to Entropy and Acoustic Disturbances*. Journal of Sound and Vibration, pages 1-15, June 2011. ISSN 0022460X. doi: 10.1016/j.jsv.2011.05.016. URL http://linkinghub. elsevier.com/retrieve/pii/S0022460X11004019.

[17] H. HASSAN - *Scaling of Combustion Generated Noise*. J. Fluid Mech. , 66:445-453, 1974.

[18] M.-S. HOWE - *The Generation of Sound by Aerodynamic Sources in an Homogeneous Steady Flow*. J. Fluid Mech. , 67(3):597-610, 1975.

[19] M.-S. HOWE - *Indirect Combustion Noise*. J. Fluid Mech. , 659:267-288, 2010.

[20] M. HUET, A. GIAUCQUE - *A Nonlinear Model for Indirect Combustion Noise Through a Compact Nozzle*. J. Fluid Mech. , 733:268-301, 2013.

[21] M. IHME, H. PITSCH - *On the Generation of Direct Combustion Noise in Turbulent Non-Premixed Flames*. International Journal of Aeroacoustics, 11(1):25-78, 2012.

[22] M. IHME, D. BODONY, H. PITSCH - *Towards the Prediction of Combustion-Generated Noise in Non-Premixed Turbulent Flames Using Large-Eddy Simulation*. CTR, pages 311-323, 2005.

[23] A.-R. KERSTEIN - *A linear Eddy Model of Turbulent Scalar Transport and Mixing*. Combust. Sci. Tech. , 60:391, 1988.

[24] M. KOSTKA, H. PITSCH - *Direct Approach to the Prediction of Indirect Combustion Noise*. Technical report, 2010.

[25] S. KOTAKE - *On Combustion Noise Related to Chemical Reactions*. J. Sound Vib. , 42: 399-410, 1975.

[26] E.-A. KREJSA - *Combustion Noise from Gas Turbine Aircraft Engines Measurement of Far-Field Levels*. Technical Report NASA Technical Report 88971, NASA, 1987.

[27] M. LEYKO - *Mise en œuvre et analyse de calculs aéroacoustiques de type SGE pour la prévision du bruit de chambres de combustion aéronautiques.* Phd thesis, INP Toulouse, 2010.

[28] M. LEYKO, F. NICOUD, S. MOREAU, T. POINSOT - *Numerical and Analytical Investigation of the Indirect Noise in a Nozzle*. Proc. of the Summer Program, pages 343-354, Center for Turbulence Research, NASA AMES, Stanford University, USA, 2008.

[29] M. LEYKO, S. MOREAU, F. NICOUD, T. POINSOT - *Numerical and Analytical Investigation of the Indirect Combustion Noise in a Nozzle*. Comptes Rendus Mécanique, 337(6-7): 415-425, 2009a.

[30] M. LEYKO, F. NICOUD, T. POINSOT - *Comparison of Direct and Indirect Combustion Noise Mechanisms in a Model Combustor*. AIAA Journal , 47(11):2709-2716, 2009b.

[31] M. LEYKO, S. MOREAU, F. NICOUD, T. POINSOT - *Numerical and Analytical Modeling of Entropy Noise in a Supersonic Nozzle with a Shock*. J. Sound Vib. , 330(16, 1): 3944-3958, 2011.

[32] M.-J. LIGHTHILL - *On Sound Generated Aerodynamically*. i. general theory. Proc. R. Soc. Lond. A , Mathematical and Physical Sciences, 211(1107):564-587, 1952.

[33] F.-E. MARBLE, S. CANDEL - *Acoustic Disturbances from Gas Nonuniformities Convected Through a Nozzle*. J. Sound Vib. , 55:225-243, 1977.

[34] M. MATALON, B.-J. MATKOWSKY - *Flames as Gas Dynamic Discontinuities*. J. Fluid Mech. , 124:239, 1982.

[35] W. MOASE, M. BREAR, C. MANZIE - *The Forced Response of Choked Nozzles and Supersonic Diffusers*. Journal of Fluid Mechanics, 585:281-304, 2007. ISSN 0022- 1120. doi: 10.1017/S0022112007006647. URL http://journals.cambridge.org/ abstract_S0022112007006647.

[36] M. MUTHUKRISHNAN, W. STRAHLE, D. NEALE - *Separation of Hydrodynamic, Entropy, and Combustion Noise in a Gas Turbine Combustor*. AIAA Journal, 16(4):320-327, 1978.

[37] S. PERENNES, M. ROGER - *Aerodynamic Noise of a Two-Dimensional Wing with High-Lift Devices*. AIAA Journal, 1998.

[38] O.-M. PHILLIPS - *On the Generation of Sound by Supersonic Turbulent Shear Layers*. J. Fluid Mech. , 9:1-28, 1960.

[39] G.-F. PICKETT - *Core Engine Noise Due to Temperature Fluctuations Convecting Through Turbine Blade Rows*. 2nd AIAA Aeroacoustics Conference - AIAA 1975-528, 1975.

[40] T. POINSOT, D. VEYNANTE - *Theoretical and Numerical Combustion*. Third Edition (www.cerfacs.fr/elearning), 2011.

[41] R. RAJARAM, T. LIEUWEN - *Acoustic Radiation from Turbulent Premixed Flames*. Journal of Fluid Mechanics, 637:357-385, 2009. ISSN 0022-1120.

[42] T. SCHONFELD, M. RUDGYARD - *Steady and Unsteady Flows Simulations Using the Hybrid Flow Solver AVBP*. AIAA Journal , 37(11):1378-1385, 1999.

[43] B.-N. SHIVASHANKARA - *Gas Turbine Core Noise Source Isolation by Internal-to-Far-Field Correlations*. J. Aircraft , 15(9):597-600, 1978.

[44] Y. SINAI - *The Generation of Combustion Noise by Chemical Inhomogeneities in Steady, Low-Mach-Number Duct Flows*. Journal of Fluid Mechanics, 99, 1980.

[45] S. STOW, A. DOWLING, T. HYNES - *Reflection of Circumferential Modes in a Choked Nozzle*. Journal of Fluid Mechanics, 467:215-239, 2002. ISSN 0022-1120. doi: 10.1017/S0022112002001428.

[46] W.-C. STRAHLE - *On Combustion Generated Noise*. J. Fluid Mech. , 49:399-414, 1971.

[47] W.-C. STRAHLE - *Some Results in Combustion Generated Noise.* J. Sound Vib. , 23(1): 113-125, 1972.

[48] N. SWAMINATHAN, G. XU, A. P. DOWLING, R. BALACHANDRAN - *Heat Release Rate Correlation and Combustion Noise in Premixed Flames*. Journal of Fluid Mechanics, 681:80-115, 2011. ISSN 0022-1120. doi: 10.1017/jfm.2011.232.

[49] M. TALEI, M. J. BREAR, E. R. HAWKES - *Sound Generation by Laminar Premixed Flame Annihilation*. Journal of Fluid Mechanics, 679:194-218, Apr. 2011. ISSN 0022-1120. doi: 10.1017/jfm.2011.131.

[50] C.-K. TAM, S.-A. PARRISH, J. XU, B. SCHUSTER - *Indirect Combustion Noise of Auxiliary Power Units*. AIAA Conference, number June, Colorado Springs, 2012.

[51] C.-K. TAM, S.-A. PARRISH, J. XU, B. SCHUSTER - *Indirect Combustion Noise of Auxiliary Power Units.* Journal of Sound and Vibration, 332(17):4004-4020, Aug. 2013. ISSN 0022460X. doi: 10.1016/j.jsv.2012.11.013. URL http://linkinghub.elsevier.com/ retrieve/pii/S0022460X12008619.

[52] H.-S. TSIEN - *The Transfer Functions of Rocket Nozzles.* J. American Rocket Society , 22 (3):139-143, 1952.

[53] J.-E.-F. WILLIAMS, M. HOWE - *The Generation of Sound by Density Inhomogeneities in Low Mach Number Nozzle Flows*. Journal of Fluid Mechanics, 70(3):605-622, 1975.

[54] P.-H. WIRSCHING, T.-L. PAEZ, K. ORTIZ - *Random Vibrations : Theory and Practice*. Dover publications, 2006.

[55] P. WOLF, G. STAFFELBACH, R. BALAKRISHNAN, A. ROUX, T. POINSOT - *Azimuthal Instabilities in Annular Combustion Chambers*. In N. A. U. Center for Turbulence Research, editor, Proc. of the Summer Program , pages 259-269, 2010.

Acronyms

CHORUS	(complete hybrid computation chain)
EWG	(Entropy Wave Generator)
FP7	(Framework Program)
HAT	(Hot Acoustic Testrig)
LES	(Large Eddy Simulations)
PSD	(Power Spectral Density)
RANS	(Reynolds-Averaged Navier-Stokes)
TEENI	(Turboshaft Engine Exhaust Noise Identification)

AUTHORS

Ignacio Duran graduated from Universidad Politécnica de Madrid (UPM) and Ecole Nationale Supérieure d'Ingénieurs de Constructions Aéronautiques (Ensica) in 2011 and received his Ph. D. Degree in Energetics in 2013. His Ph. D. thesis was focused on the prediction of combustion noise in modern aero engines combining Large Eddy Simulations and analytical methods at CERFACS and financed by Snecma.

Stéphane MOREAU graduated from Ecole Nationale Supérieure d'Aéronautique de l'Espace (now Isae) in 1988 and received his PhD in Mechanical Engineering (with a minor in Aeronautics & Astronautics) from Stanford University in 1993. He joined the AC2 start-up on plasma propulsion in 1994. He then worked in the Integration department at Snecma, Safran group in 1995. He then worked for Valeo, the Tier-1 automotive supplier on engine cooling fan systems, where he managed the research group from 1996 to 2008. He later joined the Mechanical Engineering faculty at Université de Sherbrooke in Québec, Canada, where is now a full professor

Franck Nicoud graduated in 1990 from the National School of Engineering for Hydraulics, Electronics, Electrotechnics and Informatics in Toulouse (ENSEEIHT). He then received a Fellowship from the French Space Agency (Cnes) to do a PhD thesis at the French Aerospace Lab (Onera), under the guidance of Prof. Ha Minh. After defending his experimental/numerical work about the prediction of heat transfers within solid rocket motors in 1993, he was hired by the European Center for Research and Advanced Training in Scientific Computing (Cerfacs) as a post-doctoral researcher. He became a senior scientist at Cerfacs in 1995 and participated in the development of Large Eddy Simulation tools for reacting compressible flows in complex geometries. He then accepted a research fellowship at the Center for Turbulence Research (CTR) of Stanford University and Nasa/Ames in 1998 and was appointed Professor at University Montpellier in 2001. While his research activity at Montpellier is now mainly focused on computational cardiovascular biomechanics and the development of the YALES2BIO solver, he is still working in close connection with Cerfacs, addressing issues related to combustion noise, thermo-acoustic instabilities and wall modeling.

Thomas Livebardon obtained his engineering degree from Ensma (Ecole Nationale Supérieure de Mécanique et d'Aérotechnique) and his Master's Degree in 2011. He is a PhD student working on the modeling of combustion noise in turboshaft engines at Cerfacs. This thesis is funded by TURBOMECA.

Éric Bouty: After a degree in lightning, acoustics and air conditioning, (Maîtrise de Sciences et Techniques, now ESIP) from Poitiers University, Éric Bouty graduated from Le Mans University in Acoustics (DEA) in 1987. He joined Gaz de France as a research engineer and then Snecma in 1989. He worked mainly on fan noise, proposing innovative OGV designs. He participated in many European projects, including SILENCE(R), for which he acted as the Coordinator Technical Deputy. He has led the acoustic group of Turbomeca since 2006, with a recent focus on combustion noise.

Thierry Poinsot received his PhD thesis in heat transfer from Ecole Centrale Paris in 1983 and his Thèse d'Etat in combustion in 1987. He is a research director at CNRS, head of the CFD group at Cerfacs, senior research fellow at Stanford University and a consultant for various companies. After his thesis at Ecole Centrale Paris and after two years of post-doctoral work at Stanford, he started combustion activities at Cerfacs in 1992 and his group (60 persons in 2010) has produced a significant part of the recent research in the field of LES of turbulent combustion in gas turbines. He teaches numerical methods and combustion at many schools and universities (Ecole Centrale Paris, ENSEEIHT, Ensica, Supaero, UPS, Stanford, Von Karmann Institute, CEFRC Princeton and Beijing). He has authored more than 150 papers in refereed journals and 200 communications. He is the co-author of the textbook "Theoretical and numerical combustion" together with Dr D. Veynante and an associate editor of "Combustion and Flame". He received the first Cray prize in 1993, the BMW prize in 2002, the Grand Prix of the French Academy in 2003 and an ERC advanced grant in 2013.

C. Bailly, B. André, T. Castelain
(Université de Lyon)
C. Henry, G. Bodard
(Snecma)
M. Porta
(Airbus)

E-mail: christophe.bailly@ec-lyon.fr

DOI : 10.12762/2014.AL07-06

An analysis of shock noise components

Screech and broadband shock-associated noise linked to the presence of a shock-cell structure in supersonic jets are reviewed in this paper. Only underexpanded supersonic circular jets issued from a convergent nozzle are considered here. An overview of the flow and of these two noise components is presented, based on recent experimental and numerical work. Flight effects on broadband shock-associated noise are also introduced, within the framework of aeronautical applications.

Introduction

The purpose of this introductory paper is to provide an overview of shock noise generated by underexpanded supersonic jets. This additional component to the mixing noise produced by turbulence is associated with the presence of a shock-cell structure in the jet supersonic core. Shock noise is composed of screech tones and a broadband shock-associated noise (BBSAN). Flight effects on the BBSAN are also discussed, within the context of aeronautical applications. The secondary stream of commercial engines is indeed underexpanded during the climb and cruise phases of a flight. While BBSAN comes alongside screech in model laboratory jets, the latter is not observed on civil aircraft engines, since the nozzle is not axisymmetric. Screech is however known to have a strong impact on the turbulent jet dynamics. Screech suppression is therefore an essential effort for studying BBSAN. This analysis of shock noise components is also based on recent experimental and numerical work carried out by the authors. Several methods have been successfully implemented to characterize the jet flow and its acoustic field: high-speed Schlieren technique, crossed Schlieren apparatus, static pressure measurements and velocimetry (LDV, PIV), as well as acoustic measurements. A statistical modelling of BBSAN using a steady solution of averaged Navier-Stokes equations is also assessed.

The paper is organized as follows. A brief description of underexpanded jets is first given. An analysis of Screech and BBSAN is then proposed. Flight effects on BBSAN are finally discussed and concluding remarks are drawn.

Underexpanded supersonic jets

A jet issuing from a converging nozzle is sonic for a nozzle pressure ratio greater than a critical value, where the nozzle pressure ratio (NPR) is defined as the reservoir or stagnation pressure p_t divided by the ambient pressure p_∞, $\mathrm{NPR} \equiv p_t / p_\infty$. For an air flow, this critical value is given by $[(\gamma+1)/2]^{\gamma/(\gamma-1)} \simeq 1.89$, where γ is the specific heat ratio.

A perfectly expanded jet, that is, a shock-free jet, is then obtained for this particular value since the exit pressure p_e is equal to the ambient pressure p_∞, noting also that a converging nozzle is characterized by a design Mach number M_d equal to unity at the nozzle exit.

For higher values of NPR, the Mach number at the nozzle exit is still equal to unity, but the exit pressure p_e no longer matches the ambient pressure p_∞. As a result, a weak shock-cell structure appears inside the transonic jet jet to adapt the jet pressure field to this ambient pressure and the jet is said to be underexpanded, since $p_e > p_\infty$. The fully expanded jet Mach number M_j defined by

$$M_j = \sqrt{\frac{2}{\gamma-1}\left(\mathrm{NPR}^{\frac{\gamma-1}{\gamma}} - 1\right)} \qquad (1)$$

is also often used to define the jet operating point. This Mach number corresponds to the design Mach number M_d of a convergent-divergent nozzle, which should be considered to obtain a shock-free jet at this given NPR.

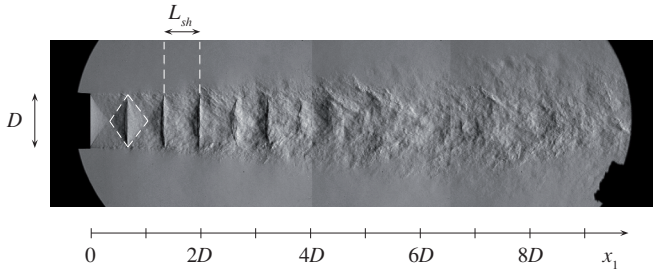

Figure 1 - Spark Schlieren visualization (conventional Z-type system, 4 μs time exposure) of an underexpanded jet at $M_j = 1.15$ and stagnation temperature $T_t = T_\infty$, issued from a notched (to avoid screech, see André et al. [6]) convergent nozzle of diameter D. The Reynolds number is $Re_D = u_j D/\nu = 1.27\times10^6$. Longitudinal density gradients are visualized here thanks to the orientation of the knife-edge, light and dark regions corresponding respectively to expansion and compression regions for the flow in shock cell diamond patterns [5].

As an illustration, an instantaneous view of a supersonic jet at M_j=1.15 is shown in figure 1. The quasi-periodic diamond pattern associated with expansion and compression waves trapped inside the jet plume is clearly visible from the nozzle exit, as well as the developing turbulent flow. The NPR is not high enough to observe a Mach disk inside the first shock cell in this case [1], but it can be seen at $M_j = 1.5$, for instance [5]. Various experimental techniques can be used to obtain an accurate picture of the jet flow development [7]. The longitudinal and transverse mean velocity components of the underexpanded jet at $M_j = 1.10$ obtained from particle image velocimetry, are displayed in figure 2. The axial mean velocity increases during expansion stages, which occur within light right-pointing triangles of the Schlieren view shown in figure 1, and decreases during compression stages associated with dark left-pointing triangles. It thus reaches a maximum corresponding to axial edges of shock-cell diamond patterns. Expansion and compression zones are also clearly identifiable by looking at the mean transverse velocity.

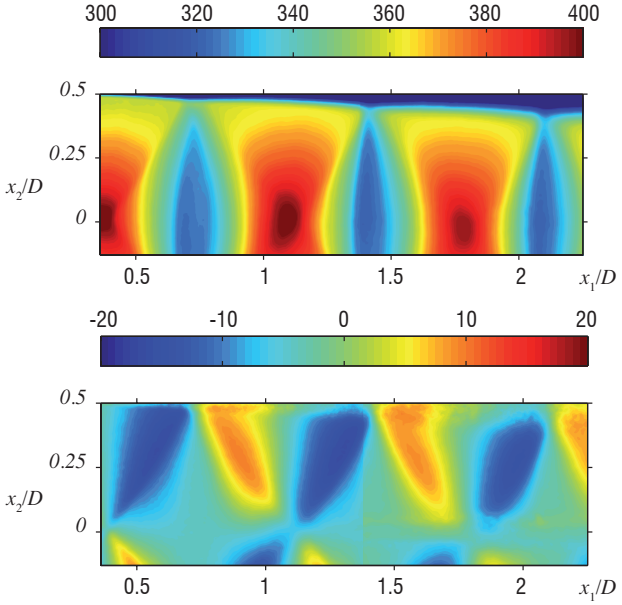

Figure 2 - Measured longitudinal (top) and transverse (bottom) mean velocity field (color scale in m.s^{-1}) in a plane containing the jet axis for M_j = 1.15, with a notched convergent nozzle and an additional slow coflow at $M_f = 0.05$ to ensure seeding of the supersonic jet surroundings. The PIV set-up leads to about 190 velocity vectors over one jet diameter. More details regarding the quality checks can be found in André [5,10].

The quasi-periodic shock-cell structure can be approximated by a vortex sheet model first introduced by Prandtl (1904) and modified by Pack (1950), as discussed in the review by Powell [28]. The corresponding axisymmetric pressure disturbance $p_s(x_1, x_\perp)$, where $x_\perp = (x_2^2 + x_3^2)^{1/2}$

$$p_{sh} / p_\infty = \sum_{n=1}^{\infty} A_n \phi_n(x_\perp) \cos(k_n x_1) \qquad (2)$$

is obtained as the solution of the Euler equations, linearized around a perfectly expanded supersonic jet, assuming that $p_e - p_\infty$ remains small. The complete expression for the amplitude A_n, the radial distribution of each mode ϕ_n and its wave number k_n can be found in Tam *et al.* [32,33]. One useful result of this simple model is the estimation of the shock-cell length, given by

$$L_{sh} \simeq 2\pi / k_1 \simeq 1.306 \beta D_j \qquad (3)$$

where D_j is the fully expanded jet diameter at M_j and the parameter β is defined as $\beta = (M_j^2 - 1)^{1/2}$. For weakly imperfectly expanded supersonic jets, it can been shown that $D_j / D = 1 + O(\beta^4)$. Therefore, the nozzle diameter D will be used as a reference length scale thereafter.

Narrow-band acoustic spectra measured in the far field for an underexpanded jet at $M_j = 1.10$ are plotted in figure 3, as a function of the Strouhal number $St = f D/u_j$, where $u_j = c_j M_j$ is the jet velocity defined from (1), and for different angular positions of the observer. There are three contributions to these spectra: mixing noise, screech and broadband shock-associated noise. Mixing noise is produced by jet flow turbulence and is the only component encountered in both subsonic and supersonic jets. It can thus be identified by continuation as M_j increases and forms the whole broadband part of the spectrum at $\theta = 30°$. This is discussed in detail by Bogey & Bailly [13] and the reader can refer to the review by Tam [34] for Mach waves. The tonal component and the subsequent harmonics are screech, indicated by arrows in figure 3, and broadband shock-associated noise (BBSAN), indicated by the dashed line, and corresponds to the broadband hump dominating mixing noise in the upstream direction. These last two components are linked to the presence of a shock-cell structure in the jet. At this stage, it is important to observe the high amplitude of screech, with an emergence of the fundamental peak of about 30 dB at $\theta = 130°$. While BBSAN comes alongside screech in model laboratory jets, the latter does not seem to be observed on civil aircraft engines. Screech is however known to have a strong impact on the turbulent jet dynamics [29], leading to a completely different jet development. Screech suppression is therefore essential for BBSAN study [6].

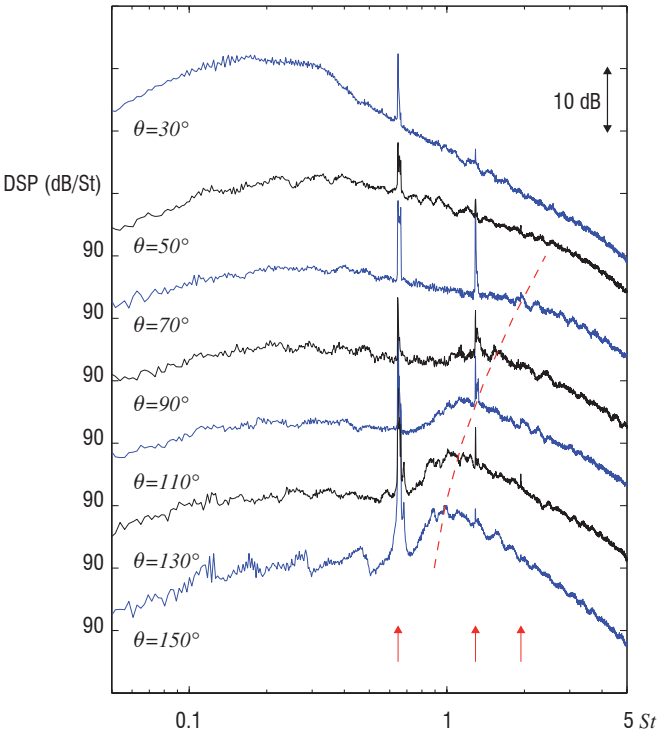

Figure 3 - Narrow-band acoustic spectra of M_j = 1.10 jet, measured at r/D = 53.2 as a function of the Strouhal number St, and for different angular positions. The angle θ is taken from the downstream jet axis. The red dashed line corresponds to relation (7) and the red arrows indicate the fundamental screech frequency and its two first harmonics. Data from André [5].

Screech

Screech is described as a feedback mechanism along the mixing layer of the jet, as studied at length by Powell [25–27] since the fifties for rectangular and round choked jets. Vortical structures are generated at the nozzle lip, and are convected downstream in the mixing layer. These perturbations interact with shock-cells and create acoustic waves that propagate upstream to the nozzle lip in the ambient medium and then trigger subsequent instability waves, which form new vortical structures along the shear layer bounding the jet. A simple acoustic model can be derived to explain the frequency selection. The pressure field resulting from a phased array of acoustic monopole sources by considering the axisymmetric mode as an illustration, each fixed source being located at the end of a shock-cell with a phase shift determined by the convection velocity, can be written as [22,30]

$$p(r,\theta,t) = \exp\left[\frac{i2\pi(c_\infty t - r)}{\lambda_s}\right] \times \sum_j \frac{S_j}{r_j} \exp\left[-i2\pi j \frac{L_{sh}}{\lambda_s}\left(\frac{1}{M_c} - \cos\theta\right)\right] \quad (4)$$

The observer position (r, θ) from the nozzle exit is assumed to be in the far field, the source to observer distance and strength of the j-th source are r_j and S_j, λ_s is the acoustic wavelength, $M_c = u_c / c_\infty$ is the convective Mach number and c_∞ the ambient speed of sound. The mechanism is sustained only if all of the acoustic waves reach the nozzle lip in phase, that is

$$\frac{L_{sh}}{\lambda_s}\left(\frac{1}{M_c} + 1\right) = n \quad \text{or} \quad \frac{n}{f_s} = \frac{L_{sh}}{u_c} + \frac{L_{sh}}{c_\infty} \quad (5)$$

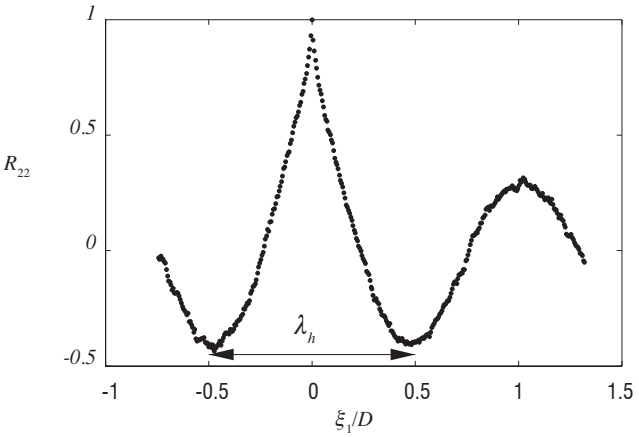

Figure 4 - Correlation function R_{22} measured by PIV at $x_1 = 3D$ along the lip line ($x_\perp = D/2$) for a screeching $M_j = 1.10$ jet, as a function of the axial separation ξ_1 normalized by the nozzle diameter. The length wave $\lambda_h = u_c / f_s \simeq D$ can be identified with $u_c = 0.65 u_j$ and $f_s = 5870$ Hz.

The sum of the convection time of vortical structures along the shear layer plus the acoustical return time to the nozzle lip is an integer of the screech oscillation periods. Using the value $u_c = 0.65 u_j$ indirectly measured [6], the Strouhal number associated with the fundamental mode $n = 1$ for the $M_j = 1.10$ jet is $St_s \cong 0.65$, in good agreement with experiments reported in figure 3. The screech frequency does not vary with the angular observer position. The directivity

$$D(\theta) = \lim_{r\to\infty} r^2 \overline{p'^2} / (\rho_\infty c_\infty^2)^2$$

of the phased array sources (4) presents a maximum in the upstream direction for this frequency. The simplicity of expression (5) should not hide the complexity of the physics involved. The structure of low-frequency instability waves and of the acoustic field can indeed take different modal forms [2, 27, 29, 30]. Screech for the $M_j = 1.1$ jet corresponds to the axisymmetric mode A_1, for instance.

Identification of shock-cells contributing to screech can be conducted through the examination of correlation functions among other quantities. The following two-point velocity correlation function,

$$R_{22}(\boldsymbol{x},\xi) = \frac{\overline{u'_2(\boldsymbol{x},t)\, u'_2(\boldsymbol{x}+\xi,t)}}{\overline{u'^2_2(\boldsymbol{x})}\ \overline{u'^2_{2'}(\boldsymbol{x}+\xi)}} \quad (6)$$

is shown in figure 4, as a function of the longitudinal separation coordinate $\xi = (\xi_1, 0, 0)$, and for a reference point x along the lip line. The wavelength $\lambda_h = u_c / f_s$ associated with Powell's model (5) can be clearly identified. By examining R_{22} and the integral length scale, a particular behavior can be identified along the five first shock cells for the $M_j = 1.10$ jet, which could suggest that these cells are involved in the screech generation [5,23,24,31].

Broadband shock-associated noise

As mentioned previously, screech must be suppressed in small-scale studies. This tonal noise can be removed by means of a notched nozzle [6] in a less intrusive manner than by introducing a protrusion or tab on the nozzle lip [8] in a laboratory facility. Harper-Bourne & Fisher [14] were the first to model BBSAN by a phased array of monopole sources similar to (4). The far-field results from the interference of these sources, with a peak frequency for the hump given by

$$f_p = \frac{u_c}{\bar{L}_{sh}(1 - M_c \cos\theta)} \quad (7)$$

This relation is in agreement with experimental observations reported in figure (3), by adjusting the value of the mean shock-cell spacing $\bar{L}_{sh}$. Harper-Bourne & Fisher also noticed that over a wide range of β, the BBSAN intensity varies as $I \propto (M_j^2 - 1)^2$ for convergent nozzles. Another approach was developed later by Tam *et al.* [32,34], considering the interaction of instability waves $u_t \sim e^{i(\alpha x - \omega t)}$ where $\alpha \simeq \omega / u_c$, with the shock-cell structure (2), that is, $u_{sh} \sim \cos(k_{sh} x)$ with $k_{sh} = 2\pi / L_{sh}$. Perturbations are given by their product

$$u_t u_{sh} \sim \underbrace{e^{i[(\alpha - k_{sh})x - \omega t]}}_{W^-} + \underbrace{e^{i[(\alpha + k_{sh})x - \omega t]}}_{W^+} \quad (8)$$

The phase velocity of waves W^- is $v_\varphi^- = \omega / (\alpha - k_{sh})$. For values of k_{sh} slightly greater than α, this phase velocity is negative and can be greater than the ambient speed of sound c_∞. Mach waves are then generated in the upstream direction, as illustrated in figure 5, with an emission angle such that $\cos\theta = c_\infty / v_\varphi^-$. Note that expression (7) is recovered from this condition. Regarding waves W^+, the phase velocity can be written as $v_\varphi^+ = \omega / (\alpha + k_{sh}) = u_c \omega / (\omega + k_{sh} u_c)$ and is thus always smaller than the convection velocity u_c. For the jet conditions considered here, u_c and thus v_φ^+ remain subsonic. Moreover, Tam & Tanna [32] found that for a convergent-divergent nozzle of design Mach number M_d, the acoustic intensity of BBSAN is proportional to $I \propto (M_j^2 - M_d^2)^2$. This expression is compatible with

Harper-Bourne & Fisher's result for convergent nozzles, for which $M_d = 1$. Note also that expression (3) still holds for a convergent-divergent nozzle. Interaction between convected turbulence and the shock-cell structure is also experimentally investigated in Pao & Seiner [24], and a critical review of the previous models is provided.

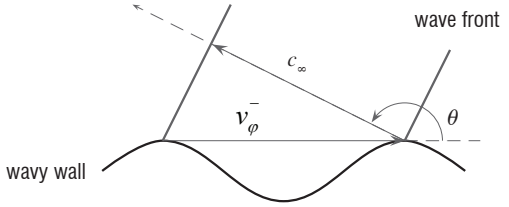

Figure 5 - Generation of Mach waves by a wavy wall moving at supersonic phase speed u_c, the direction of the radiation $\cos\theta = c_\infty / v_\varphi^-$ is obtained by matching the velocity trace along the flow direction. There is an analogy with the acoustic radiation of a vibrating plate for the reader familiar with vibroacoustics.

Morris & Miller [20] have developed a numerical model to predict BBSAN, in extending what has been done for mixing noise within the framework of statistical modelling [11, 21]. The inputs of such models are provided by a Reynolds-Averaged Navier-Stokes (RANS) solution. As a starting point, flow variables are split up among four contributions associated with the mean flow, the turbulent flow, the shock-cell structure and the fluctuations generated by the interaction between shocks and turbulence, including acoustic perturbations. For instance, the pressure term written as $\pi = (1/\gamma)\ln(p/p_\infty)$, is decomposed respectively into $\pi = \overline{\pi} + \pi_t + \pi_{sh} + \pi'$, where only π' is assumed to be unknown. For an isentropic flow, it can be shown that at the leading order, fluid dynamics equations can be reduced to the Euler equations linearized around the mean flow $(\overline{\pi}, \overline{\boldsymbol{u}})$, denoted hereafter by $\overline{\mathcal{L}}_i$ for $i = 0$ to 3. One has $\overline{\mathcal{L}}_0(\pi', \boldsymbol{u}') = 0$ for the energy equation written for the pressure variable here, and $\overline{\mathcal{L}}_i(\pi', \boldsymbol{u}') = f_i$ for the momentum equation ($i = 1$ to 3). The main source term for shock noise is given by $f = -\boldsymbol{u}_{sh} \bullet \nabla \boldsymbol{u}_t - \boldsymbol{u}_t \bullet \nabla \boldsymbol{u}_{sh}$ and corresponds to the source term already identified by Tam [34] for the interaction between turbulence and shocks. A vectorial Green function technique is introduced by Morris & Miller to solve this inhomogeneous linear system. The Green functions $(\Pi^n, \boldsymbol{V}^n)$, with $0 \le n \le 3$ linked to the number of scalar equations, must satisfy

$$\overline{\mathcal{L}}_i(\Pi^n, \boldsymbol{V}^n) = \delta(\boldsymbol{x} - \boldsymbol{y})\delta(t - \tau)\delta_{in} \tag{9}$$

for $i = 0, \ldots, 3$. Since there is no source term in the first equation for pressure ($i = 0$), one has $\Pi^0 \equiv 0$ and $V_i^0 \equiv 0$. The fluctuating pressure $p' = \rho_\infty c_\infty^2 \pi'$ is then directly related to the source term through the following integral

$$\pi'(x,t) = \sum_{n=1}^{3} \iint \Pi^n(\boldsymbol{x}, t; \boldsymbol{y}, \tau) f_n(\boldsymbol{y}, \tau) d\boldsymbol{y} d\tau \tag{10}$$

Assuming that the Π_n functions are known, this point is discussed in the next section, the pressure autocorrelation function $R_{pp}(\boldsymbol{x}, \tau)$, as well as the power spectral density $S_{pp}(\boldsymbol{x}, \omega)$, can be calculated under the assumption of an isotropic turbulence. The source term f is approximated by noting that $(\boldsymbol{u}_{sh})_i \sim \overline{u}_i \pi_{sh}$ and $\pi_{sh} = \rho_\infty c_\infty^2 p_{sh}$ and by assuming a local isotropy. In the end, $f_i(\boldsymbol{y}, \tau) = p_{sh}(\boldsymbol{y}) u_t(\boldsymbol{y}, \tau) / (\rho_\infty c_\infty l(\boldsymbol{y}))$, where $l(\mathbf{y})$ is a turbulent characteristic length scale. The final expression [16, 20] involves local turbulent characteristic scales, which are estimated from a RANS simulation. The static pressure p_{sh} associated with the shock-cell structure is also directly provided by the numerical solution.

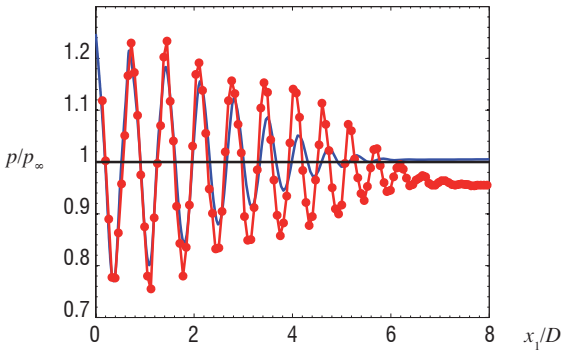

Figure 6 - Mean axial static pressure of the $M_j = 1.15$ jet normalized by p_∞, — RANS calculation [15], —•— measurements [7].

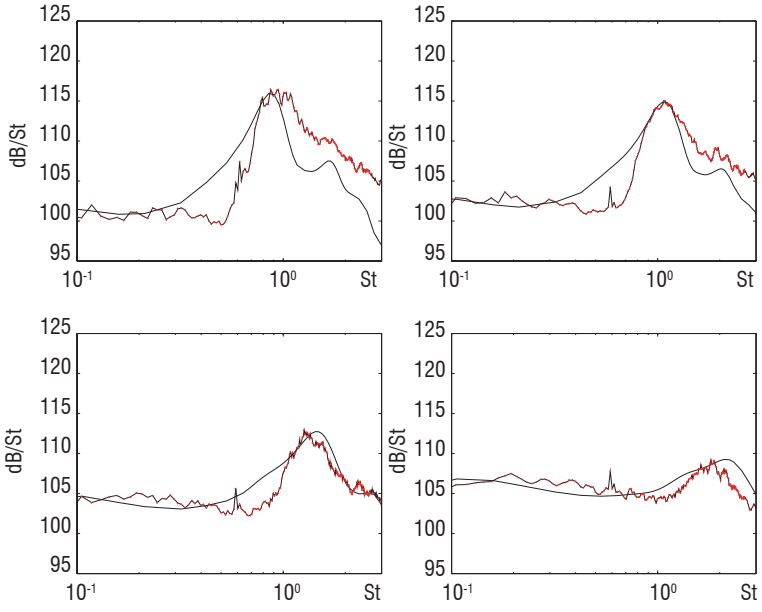

Figure 7 - Acoustic spectra in dB/St as a function of the Strouhal number $\mathrm{St} = fD/u_j$, of the $M_j = 1.15$ jet for an observer angle $\theta = 130°, 110°, 90°$ and $70°$; — measurements [5], — predicted BBSAN component [15], which is expected to dominate in the rear quadrant. The observer angle θ is taken from the downstream jet axis.

As an illustration, the computed mean axial static pressure is shown in figure 6 for the $M_j = 1.15$ jet, and is compared to measurements [5, 7]. The RANS calculations were done with the elsA CFD solver developed by Onera. A spatial Roe scheme was used and turbulence was modeled using the $k-\omega-SST$ model. The mesh contains approximately 150000 nodes with about 30 points in the first shock-cells in the axial direction and 20 points in the mixing layer for the radial direction. The shock locations are correctly predicted by the simulation and the overall agreement is quite satisfactory, though the shock damping is overestimated. The difference between calculations and experimental data for $x/D \geq 6$, where the flow becomes subsonic, stems from the pressure probe, which is designed to work at supersonic Mach numbers. The BBSAN component predicted by the statistical model is plotted in figure 7, as well as experimental results. The peak frequency f_p is correctly captured numerically and the emergence of BBSAN increases in the inlet direction ($\theta \to \pi$), as predicted by expression (7). The model is not expected to account for mixing noise and the good agreement observed at low frequencies ($\mathrm{St} \leq 0.5$) is rather a coincidence. Finally, this model makes BBSAN source distribution easy to study, through the examination of the integrand providing $S_{pp}(\boldsymbol{x}, \omega)$ at a given frequency. Close to the peak frequency f_p, sources are found to be widely spread along the shock-cell boundary in the mixing layer.

Flight effects on the BBSAN

The motivation for studying flight effects on the BBSAN is of course linked to aeronautical applications [17], as already mentioned in introduction. Figure 8 (top) illustrates the case of a dual-stream engine with a high bypass ratio. The central plug, the primary hot jet and the secondary cold and supersonic underexpanded jet can be identified. A RANS solution of a generic configuration is also shown. The shock-cell structure is confined between two shear layers [36], namely the inner shear layer between the primary and secondary stream and the outer layer between the secondary and the external stream.

It is not easy to reproduce this geometry in an anechoic wind tunnel, with a flight Mach number such as $0.8 \leq M_f \leq 0.9$. Moreover, amore basic configuration permits the role of key parameters to be better clarified. In this study, it has been chosen to set an underexpanded jet in the potential core of a larger subsonic jet to reproduce flight effects. As illustrated in Figure 8 (bottom), there is only one shear layer. The case of a free round underexpanded jet is thus recovered when the flight Mach number M_f goes to zero.

By referring to the work by Seiner [30], Tam [34] and Morris & Miller [20], the BBSAN source term is expected to be directly linked to the shock-cell strength and turbulence intensity, since BBSAN source term is proportional to pshut . From Schlieren visualizations and PIV data [5,9], the strength of the first shock cells, calculated as $(p_{max} - p_{min})/p_{min}$ inside each shock cell, has been consistently observed to become reduced in flight as M_f is increased. Moreover, an impressive expansion of the cell structure is observed with more shock cells visible. The evolution of each shock-cell length is reported in figure 9 for different flight Mach numbers. Except for the first cell, the shock length increases as Mf increases, in agreement with the vortex sheet model developed by Morris [19]. The external boundary layer thickness could slightly modulate this result by controlling the flow conditions at the nozzle exit, see figure 8 (bottom), but it is not easy to investigate this issue experimentally. Moreover, BBSAN acoustic sources are expected to be located downstream, unlike screech sources.

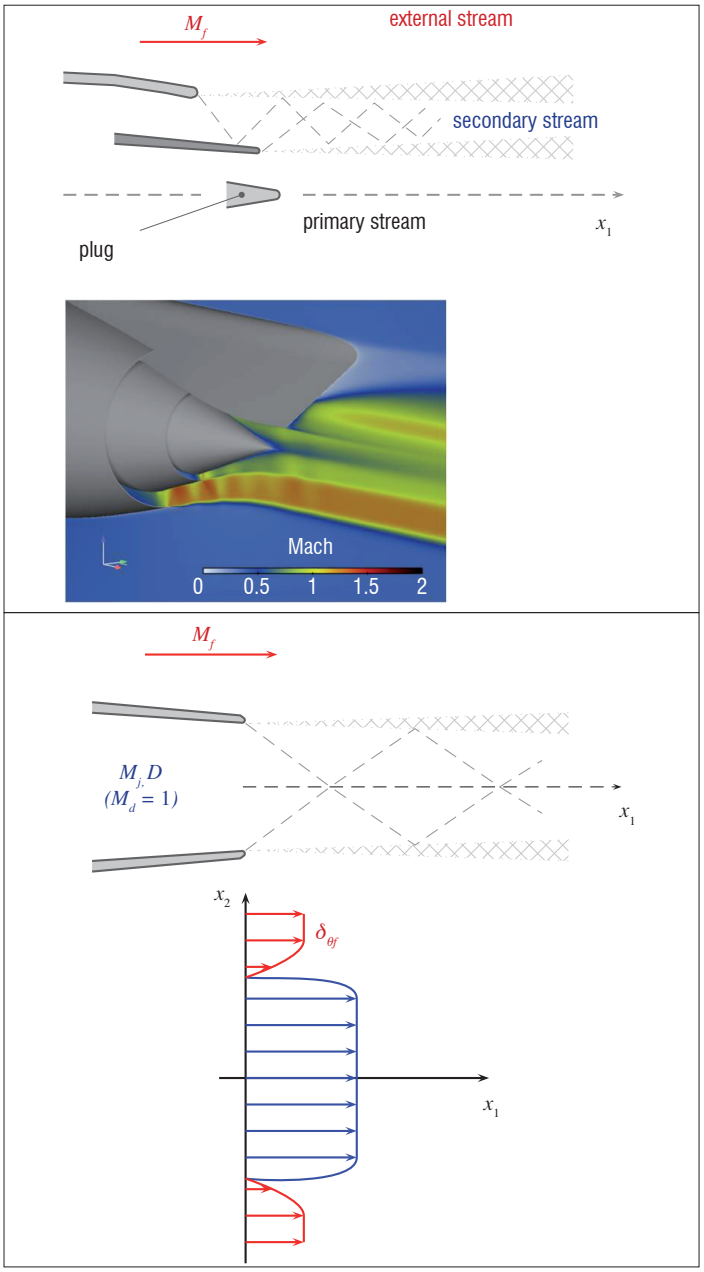

Figure 8 - Top – sketch of the exhaust of a commercial engine with a high bypass ratio, consisting of a central plug, the primary hot jet, the secondary cold underexpanded jet and the external stream characterized by its flight Mach number M_f. The Mach number field taken from a RANS simulation of a generic configuration is also shown [16]. The shock-cell structure in the secondary stream can be identified.
Bottom – sketch of the configuration to study flight effects in an anechoic wind-tunnel, with the shear layer between the supersonic stream and the external stream. The mean velocity profile induced at the nozzle exit is also shown, where $\delta_{\theta f}$ is the external boundary layer thickness.

Regarding velocity fluctuations, turbulence develops more slowly in space, since the mean velocity gradient is reduced, $\Delta u \sim u_j - u_f$, which can explain a small reduction of acoustic levels. In addition, the intrinsic time scale, that is, the integral time scale of turbulence in the convected frame, is found rather to be independent of M_f. Finally, examination of acoustic spectra [5] leads to the conclusions that the peak amplitude is practically not changed and that the overall amplitude is decreased by a few decibels.

The general formulation symbolized by expression (10) allows the inclusion of refraction effects in the BBSAN model of Morris and Miller [20]. This point is discussed in what follows. First, the vector Green functions can be analytically determined in the absence of a mean flow. The linearized Euler equations $\overline{\mathcal{L}}_i(\pi', \boldsymbol{u}') = f_i$ (with $f_0 = 0$) can indeed be reduced to a scalar wave equation $\partial_{tt}^2\pi' - c_\infty^2\nabla^2\pi' = -\nabla\bullet f$, for which the free space Green function is well-known. Therefore, it can be shown [16,20] that

$$\Pi^n(\boldsymbol{x},\boldsymbol{y},\omega) = \frac{ik_\infty}{4\pi c_\infty^2 x}\frac{x_n}{x}e^{-ik_\infty|\boldsymbol{x}-\boldsymbol{y}|} \qquad (11)$$

in the far field for $x \gg y$ and in the frequency domain with $k_\infty \equiv \omega / c_\infty$. The free space scalar Green function is however not known analytically in a more general context, but can be numerically determined by reformulating the problem for the adjoint Green function [35], for instance.

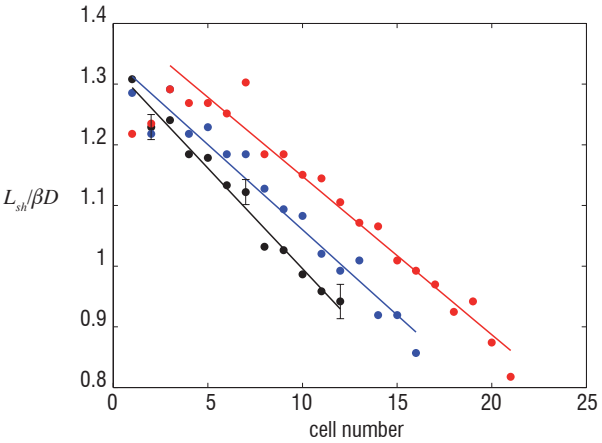

Figure 9 - Individual shock cell length L_{sh} normalized by βD as a function of the cell number and for three flight Mach numbers, • $M_f = 0$, • $M_f = 0.22$, • $M_f = 0.39$. The experimental data are obtained from Schlieren visualizations for the $M_j = 1.10$ jet [5,9].

An alternative approach is to account for mean flow effects using geometrical acoustics, since the associated assumptions are quite well satisfied by BBSAN [15,16]. Ray-tracing is an efficient and intuitive way to compute mean flow effects. The guiding idea consists in writing that each elementary volumetric source term $\delta W = W(\boldsymbol{y},\omega)\delta v$ of the BBSAN model radiates a fraction of this energy in a ray tube connecting the source $\boldsymbol{y}$ to the observer position $\boldsymbol{x}$, where $W(\boldsymbol{y},\omega)$ is the power spectral density per unit volume of the BBSAN source term. The conservation of energy along this ray tube permits the pressure fluctuation to be expressed at $\boldsymbol{x}$ and the scalar Green function to be identified. The link between this scalar Green function and the Π^n functions is more difficult to establish. In Henry et al. [15, 16], the mean flow is assumed to be parallel, in order to consider the third-order wave equation of Lilley [18] and to express this relation analytically [12]. Finally, the direct determination of eigen rays from the source at $\boldsymbol{y}$ to the observer at $\boldsymbol{x}$ is not very efficient. To compute BBSAN at a given position $\boldsymbol{x}$, an adjoint problem is considered by reversing the mean flow and by shooting from an observer position $\boldsymbol{x}$ to the source domain, as illustrated in figure 10.

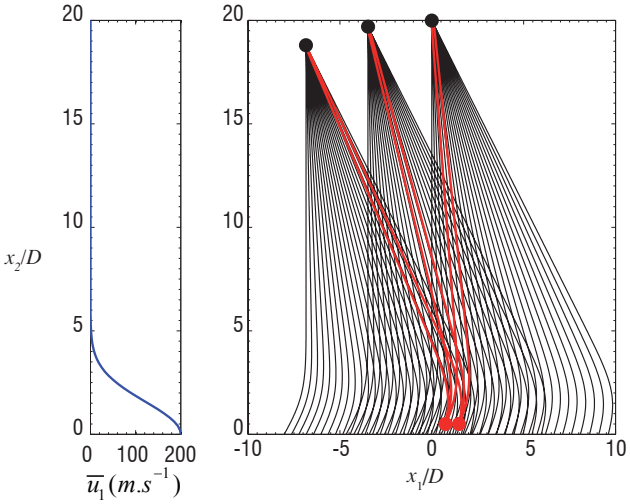

Figure 10 - Illustration of ray-tracing in the direct and adjoint problems, • observer positions, • source, — adjoint ray to the source domain at a given $\boldsymbol{x}$, — direct ray from the source $\boldsymbol{y}$ to the observer location $\boldsymbol{x}$.

Conclusion

Some properties of shock noise generated by underexpanded round jets issued from a convergent nozzle are briefly introduced in this paper. They are illustrated by experimental and numerical results from two recent studies [5, 16]. The work is aimed at developing a complete view of noise induced by a shock-cell structure, including flight effects. It can be emphasized that the characterization of flight effects on broadband shock-associated noise illustrates the good combination between experimental and numerical approaches, to complete the experimental test matrix for high subsonic flight Mach numbers, for instance. Identification of shock-cells contributing to screech and broadband shock-associated noise, characterization of the receptivity at the nozzle lip, or more quantitative analyzes of high-speed Schlieren images are topics that still require research efforts ■

Acknowledgment

This work was supported by the Labex CeLyA of Université de Lyon, operated by the French National Research Agency (ANR-10-LBX-0060/ ANR-11-IDEX-0007).

Acronyms

BBSAN	(BroadBand Shock-Associated Noise)
CFD	(Computational Fluid Dynamics)
LDV	(Laser Doppler Velocimetry)
NPR	(Nozzle Pressure Ratio)
PIV	(Particle Image Velocimetry)
RANS	(Reynolds-Averaged Navier-Stokes)

References

[1] M. ABBETT - *Mach Disk in Underexpanded Exhaust Plumes.* AIAA Journal, Vol. 9, N°. 3, 512-514, 1971.

[2] B. ANDRÉ, T. CASTELAIN, C. BAILLY - *Experimental Study of Flight Effects on Screech in Underexpanded Jets*. Phys. Fluids, Vol. 23, 126102, 1-14, 2011.

[3] B. ANDRÉ, T. CASTELAIN, C. BAILLY - *A Shock Tracking Procedure for Studying Screech Induced Oscillations*. AIAA Journal, Vol. 49, N°. 7, 1563-1566, 2011.

[4] B. ANDRÉ, T. CASTELAIN, C. BAILLY - *Shock Oscillations in a Supersonic Jet Exhibiting Antisymmetrical Screech*. AIAA Journal, vol. 50, N°. 9, 2017-2020, 2012.

[5] B. ANDRÉ - *Etude expérimentale de l'effet du vol sur le bruit de choc de jets supersoniques.* Ph.D. Thesis, ECL - N°. 2012-42, 2013.

[6] B. ANDRÉ, T. CASTELAIN, C. BAILLY - *Broadband Shock-associated Noise in Screeching and Non-Screeching Underexpanded Supersonic Jets*. AIAA Journal, Vol. 51, N°. 3, 665-673, 2013.

[7] B. ANDRÉ, T. CASTELAIN, C. BAILLY - *Experimental Investigation of Underexpanded Supersonic Jets.* To appear in Shock Waves, 2013.

[8] B. ANDRÉ, T. CASTELAIN, C. BAILLY - *Effect of a Tab on the Aerodynamical Development and Noise of an Underexpanded Supersonic Jet.* C. R.Méc., Acad. Sci. Paris, to appear, 2013.

[9] B. ANDRÉ, T. CASTELAIN, C. BAILLY - *Experimental Study of Flight Effects on Slightly Underexpanded Supersonic Jets.* 19th AIAA/CEAS Aeroacoustics Conference, AIAA Paper 2013-2079, 2013.

[10] B. ANDRÉ, T. CASTELAIN, C. BAILLY - *Investigation of the Mixing Layer in a Slightly Underexpanded Supersonic Jet by Particle Image Velocimetry*. Proceedings of the Eighth International Symposium on Turbulence and Shear Flow Phenomena (TSFP-8), 2013.

[11] C. BAILLY, P. LAFON, S. CANDEL - *Subsonic and Supersonic Jet Noise Predictions from Statistical Source Models*. AIAA Journal, Vol. 35, N°. 11, 1688-1696, 1997.

[12] C. BAILLY, C. BOGEY, S. CANDEL - *Modelling of sound Generation by Turbulent Reacting Flows*. International Journal of Aeroacoustics, Vol. 9, N°. 4-5, 461- 489, 2010.

[13] C. BOGEY, C. BAILLY - *An Analysis of the Correlations Between the Turbulent Flow and the Sound Pressure Field of Turbulent Jets*. J. Fluid Mech., Vol. 583, 71-97, 2007.

[14] M. HARPER-BOURNE, M.-J. FISHER - *The Noise from Shock Waves in Supersonic Jets*. Noise Mechanisms, N°. 131, 1973.

[15] C. HENRY, C. BAILLY, G. BODARD - *Statistical Modeling of BBSAN Including Refraction Effects*. 18th AIAA/CEAS Aeroacoustics Conference, AIAA Paper 2012-2163, 1-18, 2012.

[16] C. HENRY - *Prediction of Broadband Shock-associated Noise in Static and Flight Conditions*. Ph.D. Thesis, ECL - N°. 2012-60, 2012.

[17] J. HUBER, A. SYLLA, V. FLEURY, J. BULTÉ, K. BRITCHFORD, E. LAURENDEAU, D. LONG - *Understanding and Reduction of Cruise Jet Noise at Model and Full Scale*. 15th AIAA/CEAS Aeroacoustics Conference, AIAA Paper 2009-3382, 2009.

[18] G.-M. LILLEY - *The Generation and Radiation of Supersonic Jet Noise*. Vol. IV - Theory of Turbulence Generated Jet Noise, Noise Radiation from Upstream Sources, and Combustion Noise. Part II: Generation of Sound in a Mixing Region, AFAPL-TR-72-53, Vol. 4, 1972.

[19] P.-J.MORRIS - *A Note on the Effect of Forward Flight on Shock Spacing in Circular Jets*. J. Sound Vib., Vol. 121,N°. 1, 175-177, 1988.

[20] P.-J. MORRIS, A.-E. MILLER - *Prediction of Broadband Shock-associated Noise Using Reynolds-averaged Navier-Stokes Computational Fluid Dynamics.* AIAA Journal, Vol. 48, N°. 12, 2931-2944, 2010.

[21] P.-J. MORRIS, F. FARASSAT - *Acoustic Analogy and Alternative Theories for Jet Noise Predictions.* AIAA Journal, Vol. 40, N°. 4, 671-680, 2002.

[22] T.D. NORUM - *Screech Suppression in Supersonic Jets*. AIAA Journal, Vol. 21, N°. 2, 235-240, 1983.

[23] J. PANDA - *An Experimental Investigation of Screech Noise Generation.* J. Fluid Mech., Vol. 378, 71-96, 1999.

[24] S. PAO, J. SEINER - *Shock Associated Noise in Supersonic Jets.* AIAA Journal, Vol. 21, N°. 5, 687-693, 1983.

[25] A. POWELL - *On the Noise Emanating from a Two Dimensional Jet Above the Critical Pressure.* Aeronautical Quarterly, Vol. 4, 103-122, 1953.

[26] A. POWELL - *On the Mechanism of Choked Jet Noise*. Proc. Phys. Soc. London, Sect. B66, 1039-1057, 1953.

[27] A. POWELL, Y. UMEDA, R. ISHII - *The Screech of Round Jets, Revisited.* 13th AIAA Aeroacoustics Conference, AIAA Paper 90-3980, 1990.

[28] A. POWELL - *On Prandtl's Formulas for Supersonic Jet Cell Length*. Int. Journal of Aeroacoustics, Vol. 9, N°. 1 & 2, 207-236, 2010.

[29] G. RAMAN - *Advances in Understanding Supersonic Jet Screech: Review and Perspective.* Prog. Aerospace Sci., Vol. 34, 45-106, 1998.

[30] J.-M. SEINER - *Advances in High Speed Jet Aeroacoustics*. 9th Aeroacoustics Conference, AIAA Paper 84-2275, 1984.

[31] T. SUZUKI, S. LELE - *Shock Leakage Through an Unsteady Vortex-laden Mixing Layer: Application to Screech Jet*. J. Fluid Mech., Vol. 490, 139-167, 2003.

[32] C.-K.-W. TAM, H.-K. TANNA - *Shock Associated Noise of Supersonic Jets from Convergent-divergent Nozzles.* J. Sound Vib., Vol. 81, N°. 3, 337-358, 1982.

[33] C.-K.-W. TAM, J.-A. JACKSON, J.-M. SEINER - *A Multiple-scales Model of the Shock-cell Structure of Imperfectly Expanded Supersonic Jets*. J. Fluid Mech., Vol. 153, 123-149, 1985.

[34] C.-K.-W. TAM - *Supersonic Jet Noise*. Annu. Rev. Fluid Mech., Vol. 27, 17-43, 1995.

[35] C.-K.-W. TAM, L. AURIAULT - *Mean Flow Refraction Effects on Sound Radiated from Localized Sources in a Jet*. J. Fluid Mech., Vol. 370, 149-174, 1998.

[36] C.-K.-W. TAM, N.-N.PASTOUCHENKO, K. VISWANATHAN - *Broadband Shock-cell Noise from Dual Stream Jets*, J. Sound Vib., Vol. 324, N°. 3-5, 861-891, 2009.

AUTHORS

Christophe Bailly. Professor at Ecole Centrale de Lyon (ECL), associated with Institut Universitaire de France (2007-2012). Background: PhD from Ecole Centrale Paris in 1994, joined Centre Acoustique of the Laboratoire de Mécanique des Fluides et d'Acoustique (LMFA UMR CNRS 5509) at ECL in 1995.

Benoît André. CFD engineer at ebm-papst St. Georgen (Germany). Background: Graduated from Ecole des Ponts ParisTech (2009), PhD from Ecole Centrale de Lyon (2012).

Thomas Castelain. Assistant Professor at Université Lyon I. Background: PhD from Ecole Centrale de Lyon (2006). Main interests include subsonic and supersonic jet noise, microjets for noise reduction, experimental flow control.

Cyprien Henry. Rotor dynamics engineer at Snecma. Background: PhD from Ecole Centrale de Lyon (2012) in collaboration with Snecma, Master of Sciences from ECL in 2009 (in Aeronautics).

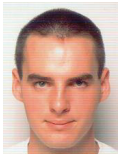

Guillaume Bodard. Engineer in Acoustics at Snecma. Background: Graduated from ENSMA (Ecole Nationale Supérieure de Mécanique et d'Aérotechnique de Poitiers, 2006), PhD fromEcole Centrale de Lyon (2009).

Mauro Porta. Jet noise specialist at Airbus Operations SAS Toulouse. Degree in aerospace engineering at Politecnico di Milano, 2003. PhD on Large Eddy Simulation for combustion chambers at INP Toulouse - Cerfacs, 2007.

S. Redonnet
(Onera)

E-mail : stephane.redonnet@onera.fr

DOI : 10.12762/2014.AL07-07

Aircraft Noise Prediction via Aeroacoustic Hybrid Methods - Development and Application of Onera Tools over the Last Decade : Some Examples

This article focuses on advanced noise prediction methodologies, in regard to aircraft noise mitigation. More precisely, the so-called aeroacoustic hybrid methodology is first recalled here, before illustrating its potentialities through several examples of application to realistic aircraft noise problems. Among other things, this paper highlights how Onera has contributed to the development of reliable computational methodologies over the last decade, which can now help in solving aircraft noise issues.

Introduction

A few years ago, noise annoyance by aircraft was officially identified as the major obstacle to sustainable air traffic growth. Therefore, all stakeholders involved in the development of aircraft systems or components are now focusing on practical ways to reduce the acoustic signature left by their products. On the other hand, since acoustics is a complex discipline, they are often bound to make intensive use of numerical simulation, which constitutes a powerful tool for R&D, when combined with experimentation. This, however, requires a continuous development and a proper application of advanced modeling and solving techniques, which are mandatory for simulating the noise generation and/or propagation phenomena occurring in realistic situations.

Aircraft noise prediction via aeroacoustic hybrid methodologies

Aircraft noise prediction

The noise signature of aircraft includes two main contributions, respectively of propulsive and non-propulsive origins. The first one, namely the *engine noise*, is due to all engine propulsive devices (turbofan or turboprop), whereas the second one, namely the *airframe noise*, is induced by the airframe and its appendages (fuselage, wings, slats, flaps, landing gear, cavities, etc.). Although the engine noise accounts for a dominant portion of the overall aircraft noise during take-off, the airframe noise component becomes equally important during the approach for landing, when the engine thrust is considerably reduced.

From a more phenomenological point of view, such a distinction between engine and airframe noises vanishes at some point, since both components result from the contribution and combination of a large number of acoustic sources and phenomena. Indeed, noise originates from numerous source mechanisms, such as structural vibrations, fluidic motions, flow interactions with structures, gas combustions or explosions, and so on. Once they have been generated by these sources, acoustic waves propagate within the surrounding environment, which is generally constituted by one or several media of various complexity (e.g., comprising solid bodies and/or medium heterogeneities, etc.). During this propagation phase, acoustic waves may be subjected to numerous and important alterations in terms of amplitude, phase or frequency. Such effects all result from mechanisms as diverse as reflection and diffraction effects by solid structures, convection by fluidic motions, refraction by the medium heterogeneities, diffusion by the medium turbulence, absorption by the medium viscosity and so on.

Many of the acoustic generation processes and most of the acoustic propagation mechanisms are relevant to the physics of fluid dynamics and can thus be simulated by numerically solving the Navier-Stokes equations. At the present time, however, and despite the continuous development of computational tools and resources, it is still extremely challenging to solve aeroacoustic problems following a direct manner, that is to say, via a single calculation. Indeed, except in particular situations (e.g., simplistic configurations, academic cases, etc.), it is nearly impossible to simulate at the same time the noise generation and its subsequent propagation, whose underlying mechanisms

greatly differ by their intrinsic characteristics (e.g., energy, length scales, etc...). As an example, most of the noise annoyances due to modern aircraft come from the so-called aerodynamic noise, which results from either the interaction of airflow with the structure itself (e.g., airframe noise), or from its ingestion by the engines (e.g., fan and/or turbine noises, etc...). On the other hand, the aerodynamic noise physics is made up of complex phenomena covering a broad range of spatiotemporal scales, with noise generation processes that are driven by turbulent structures of high amplitude and small space-time correlations, while propagation ones are associated with sound waves of low amplitudes and large space-time correlations. Thus, and although both phenomena are ruled by the same compressible Navier-Stokes equations, they cannot be easily predicted via a single calculation, because the computational resources required to resolve all of the relevant scales would be far too high.

Therefore, to make the numerical approach tractable in a practical context, the overall acoustic problem is usually broken down into a set of coupled sub-problems that focus on individual sub-regions of the overall spatial domain. Each sub-problem has a specific range of amplitudes and physical scales that can be addressed using a numerical method that is customized to the dominant physics occurring at this stage. Thus, methods involving a mix of techniques are classified as *hybrid* approaches for the acoustic prediction.

Aeroacoustic hybrid approach for aircraft noise prediction

In general, aeroacoustic hybrid methods are comprised of two to three stages (see figure 1), which are respectively devoted to :

- the noise generation and near-field propagation (over regions where the aerodynamic flow is unsteady, e.g., turbulent) ;
- the mid-field propagation (over regions where the aerodynamic flow is steady but heterogeneous) ;
- the far-field propagation (over regions where the aerodynamic flow is steady and virtually homogeneous).

The acoustic generation and early propagation (Stage #1) can be simulated with a compressible unsteady CFD approach, whether it involves DNS (Direct Numerical Simulation), LES (Large Eddy Simulation), unsteady RANS (Reynolds Averaged Navier-Stokes equations), or a judicious mix of these techniques, such as DES (Detached Eddy Simulation). The main advantage offered by these CFD techniques is that they are very close to the physics, with an accuracy level that is proportional to the costs that they entail (in terms of computational time and memory consumption)*.

The acoustic far-field radiation (Stage #3) can be predicted with an Integral Method (IM), such as those relying on Kirchhoff [25], Lighthill [29] or Ffowcs-Williams & Hawkings (FWH) [21] integration techniques. The main advantage offered by these methods is that they are relatively cheap (in terms of computational resources), while being rigorously exact - provided however that their underlying hypotheses are strictly verified. Indeed, these various IM techniques all assume that the acoustic propagation phase can be modeled by an elementary Green function, which allows meshing and computing the propagation medium to be avoided - and, thus, offers to greatly lower the computational time and memory requirements.

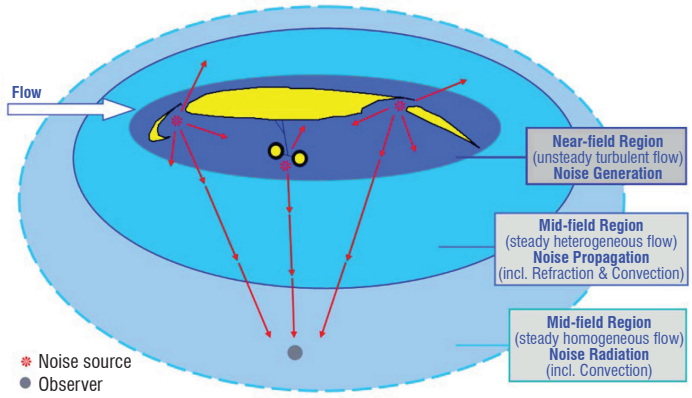

Figure 1 - Aircraft noise emissions by high lift wing and undercarriage systems; sketch of the overall problem and splitting of the latter into several distinct sub-problems, to be addressed following an aeroacoustic hybrid approach

Concerning now the acoustic mid-field propagation (Stage #2), this step can be neglected in particular situations, such as for instance when the noise source radiates in an unbounded medium at rest. This step cannot however be ignored when the noise emission is to be followed by other phenomena, such as acoustic reflection / diffraction effects by solid obstacles or acoustic refraction effects by the medium, which is something likely to occur in many aircraft noise problems [47]. As an example (see figure 1), when installed under a wing, landing gear is located within a region where acoustic waves may be subjected to both strong reflection effects (induced by the undersurface of the wing) and non-negligible refraction effects (induced by the mean flow gradients, which generally extend up to one chord away from the wing surface). As mentioned above, due to the variety and complexity of all of the physical phenomena involved, numerically simulating such a propagation phase is not a trivial task*. In particular, although they do not need to account for turbulent fluctuations nor viscous effects, computational techniques required for handling this noise propagation step must accurately simulate the propagation of acoustic waves over relatively large distances across possibly heterogeneous media, while accounting for the possible presence of solid obstacles (e.g., when the configuration is installed). This may typically be accomplished with higher fidelity acoustic propagation approaches, such as a Computational Aeroacoustics (CAA†) method relying on the Euler equations, or a linearized version thereof [43, 44]. Indeed, one can here recall that only a CAA method‡ can simultaneously account for both

* Here, one can notice that, in some situations, the acoustic near-field generation can also be mimicked with less sophisticated (and, thus, less accurate / expensive) methods, such as those relying on semi-empirical models (to be calibrated through experiments), or on stochastic/statistical techniques [39, 27, 6, 26]. These alternative approaches are however of more restrictive use, since their underlying assumptions generally narrow their range of validity and/or applicability.

* Although this would constitute an ideal solution, this mid-field acoustic propagation phase cannot be incorporated within Stage #1, because of the increased cost of extending the viscous, nonlinear CFD computations to include refraction by the medium heterogeneities and reflection by solid obstacles away from the noise source region(s).

† Here, it should be noted that the generic name “CAA” was first introduced to denote this young and rapidly growing discipline devoted to the numerical simulation of acoustic propagation within complex aerodynamic flows. This specific label is now often used in a wider sense and has been extended to simpler techniques, such as Integral Methods (e.g., Acoustic Analogy). Such extension could be seen as inappropriate, since most of these techniques belong more to the linear acoustic domain than to the non-linear aero-acoustic one, which CAA originally comes from.

‡ Whether it relies on high-order Finite Difference (FD) schemes operating on multi-block structured grids [28, 30, 56, 57] or on the so-called Discontinuous Galerkin Method (DGM) [1], which is based on unstructured grids.

the reflection/diffraction effects by solid obstacles and the refraction effects by the medium heterogeneities, contrary to other techniques that can only model the former (such as the Boundary Element Method, BEM), or even none of them (such as Integral Methods, IM).

Coupling processes of the aeroacoustic hybrid methodology

A critical aspect of developing aeroacoustic hybrid methodologies corresponds to the coupling process, i.e., the information exchange occurring between the various stages respectively associated with the individual sub-problems.

The nature of this coupling is problem dependent, because of significant variations in the inter-dependencies between the various stages from one problem to another. However, except in problems involving acoustic feedback (e.g., screech tones, in jet aeroacoustics), the coupling between these stages is weak, i.e., primarily unidirectional. Under this scenario, feedback from a given stage to the previous one can be ignored and the successive stages of an aeroacoustic hybrid calculation can be coupled in a *weak* sense, all possible retro-actions from a given step to the previous one being then neglected [47].

Such a weak coupling process occurring between two successive stages of an aeroacoustic hybrid approach is constituted with a data transfer, whose role is to transmit all of the acoustic information gathered at each step to the next level. Needless to say, such an operation must be properly achieved, so that it does not degrade the acoustic signal information to be transferred. This requires the weak coupling technique to both rely on sound physical principles and offer sufficient numerical robustness, especially in regard to an application within a realistic context [47, 12].

Two- to three-stage aeroacoustic hybrid methods

When circumstances allow the acoustic mid-field propagation (Stage #2) to be neglected, one ends up with the so-called two-step aeroacoustic hybrid method, which addresses only Stages #1 and #3 via a weak coupling of CFD and IM calculations (see top of figure 2).

Over the last decades, such 2-step aeroacoustic hybrid approach became one of the most popular techniques for simulating applied problems of external noise and use is now often made of 2-step hybrid calculations that couple CFD and IM modules, whether the latter IM module is based on the Acoustic Analogy by Lighthill (e.g., for an isolated jet) or by Ffowcs-Williams and Hawkings (e.g., for an isolated rotor). In particular, over the past decade, Onera widely promoted such a 2-step aeroacoustic hybrid approach by jointly developing CFD solvers (such as the *elsA* platform [3, 4]) and IM tools (such as the *KIM* code [41, 40]), which it later applied to realistic aircraft noise problems, as will be partially illustrated in the following paragraphs.

On the other hand, more recently, the three-step aeroacoustic hybrid approach also emerged, which combines Stages #1, #2 and #3 via a weak coupling of CFD, CAA and IM calculations (see bottom of figure 2). As was mentioned, and although it is more complicated to handle, such a 3-step aeroacoustic hybrid approach allows more complex problems to be simulated, since its CAA-based propagation stage can account for refraction and/or scattering effects that may occur in the midfield. As an illustration, the internal noise propagation problems that occur in nacelle and exhaust ducts of engines can be exemplified. Indeed, here, once their generation has been properly

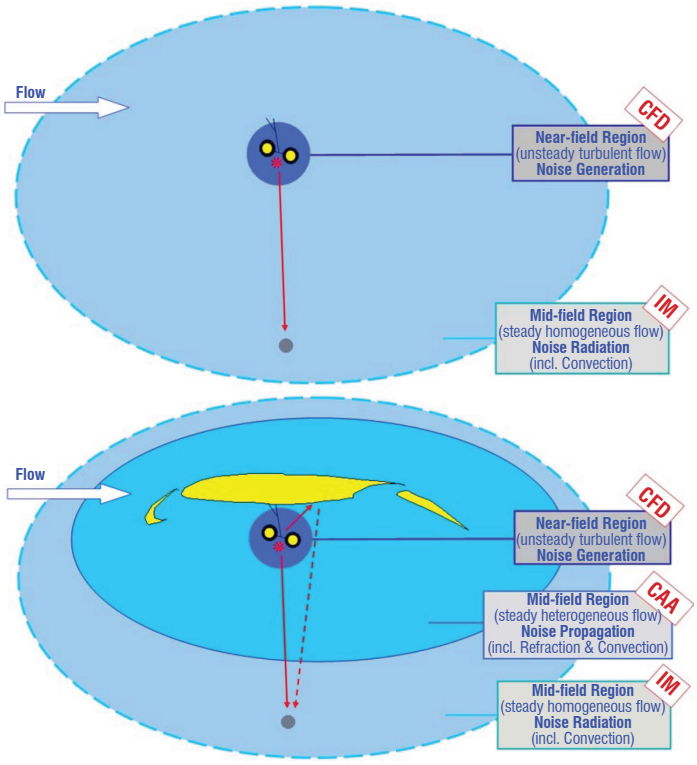

Figure 2 - Numerical prediction of the noise emission by landing gear in isolated (top) or installed (bottom) configuration, via either a 2-step (CFD-IM, top) or a 3-step (CFD-CAA-IM, bottom) aeroacoustic hybrid approach.

simulated via a numerical method (e.g., Computational Fluid Dynamics, CFD) or modeled by analytical means (e.g., duct mode theories [61]), acoustic waves can then be transferred to a CAA solver, for the latter to propagate them through the duct, while accounting for all internal effects to be possibly induced by the presence of flows, solid devices or any other disturbing elements (such as noise absorbing panels, etc.). Another typical situation for which an aeroacoustic hybrid approach relying on a CAA-based Stage #2 is mandatory concerns those external noise problems whose propagation phase occurs within a complex environment, such as for instance the airframe noise emissions by aircraft appendages (e.g., landing gear, etc.). Indeed, here again, once their generation has been properly simulated (usually via an unsteady compressible CFD method), acoustic waves can then be transferred to a CAA solver, for the latter to propagate them up to the far-field, while accounting for all of the installation effects induced by either the aircraft structure (e.g., reflection/diffraction) or the air flow surrounding the latter (e.g., convection/refraction).

Here too, over the past decade, Onera largely promoted such a 3-step aeroacoustic hybrid approach, by both i) developing the CAA solver *sAbrinA* [43, 44, 46, 50, 42, 6], before ii) allotting it with proper CFD-CAA weak coupling features [43, 44, 58, 47, 48] and iii) applying it to various (either isolated or installed) aircraft noise problems (see the next paragraphs). At this stage, one can recall that alternative three-step aeroacoustic hybrid approaches also exist, such as those based on the combination of CFD, CAA and BEM methods. In this case, the IM stage is simply replaced with a BEM one, which allows the far-field noise to be predicted, while taking into account additional scattering agents located in the far field region. This approach was also promoted by Onera, through dedicated joint projects [45, 37] conducted in collaboration with Airbus.

Two-step aeroacoustic hybrid method : noise predictions based on CFD and IM calculations

A few examples of aircraft noise predictions that were achieved following a two-step hybrid approach relying on CFD and IM weakly coupled calculations are presented hereafter. The latter were all conducted with the help of Onera tools; more precisely, the CFD calculations (Stage #1) were handled with either *elsA* [3, 4] or CEDRE [5] codes, which are two unsteady compressible CFD solvers that operate on structured and unstructured grids, respectively. On the other hand, the far-field noise extrapolations (Stage #3) were all achieved with the help of the KIM code [41, 40], which relies on a time domain IM (Integration Method) based on the FWH acoustic analogy [21]. Please note that the few examples presented hereafter are here for illustration purpose only; in particular, they do not claim at presenting the entire portfolio of application works that were achieved thanks to the two-step hybrid approach and tools developed at Onera.

Noise emission by an isolated CROR engine, via CFD (uRANS)-IM(FWH) weakly coupled calculations

Within the framework of an Airbus/Rolls-Royce project whose long term objective is to assess the sustainability of CROR*-powered aircraft with respect to noise regulations, a dedicated action was recently conducted by Colin et al. (Airbus). The aim here was to further assess and validate existing CROR-noise prediction methodologies, in regard to a use within an industrial context. With that view, joint experimental measurements and numerical calculations were performed, in order to characterize the aeroacoustics of a CROR engine, which was allotted either a high or a low speed flight condition; the aeroacoustic test campaign was performed at DNW†, whereas its numerical counterpart was performed at Airbus. All computations relied on a 2-step aeroacoustic hybrid approach and consisted in CFD-IM weakly coupled calculations [7-9].

The CFD computations were achieved with the help of a structured unsteady RANS approach, for which the Onera solver *elsA* was used. Some of these CFD(uRANS) calculations were handled via a full 3D approach relying on a Chimera technique (that is, with overlapping grids), which allowed part of the experimental set-up to be accounted for (see figure 3, left side) and, thus, its potential aerodynamic installation effects to be assessed. On the other hand, alternative CFD(uRANS) computations were performed using a chorochronic technique ‡ (see figure 3, right side), which permitted the meshing / computing efforts to be lessened, but however prevented any of the test set-up devices (and subsequent installation effects) from being accounted for.

Concerning now far-field acoustic extrapolations, all IM calculations were achieved following a FWH approach, for which use of Onera's solver KIM was made.

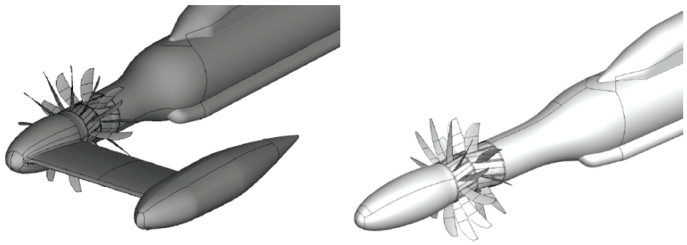

Figure 3 - CROR engine considered under either a facility installed (left) or an isolated (right) configuration. Reproduced from [9] with permission. Courtesy of Airbus

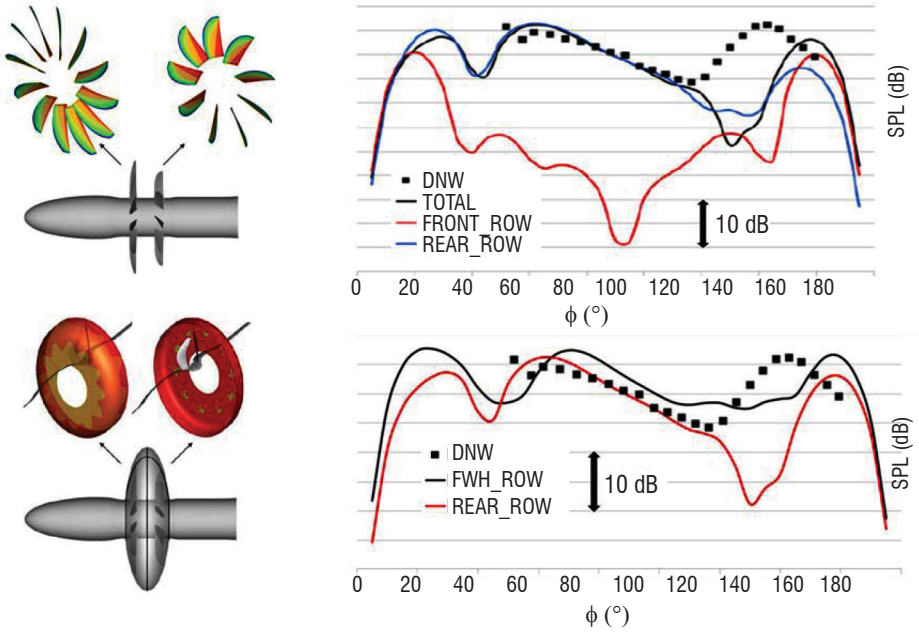

Figure 4 - Noise emission by an isolated CROR engine at take-off, predicted via a CFD(uRANS)-IM(FWH) hybrid calculation based on either a solid (top left) or a porous (bottom left) surface integration. Right side; far-field radiation of noise emissions associated with the BPF (Blade Passing Frequency) and its first harmonic, as extrapolated in a 'solid' (top: black line, bottom: 'FWH-SOL') or a 'porous' (bottom; 'FWH_PERM') surface sense. Numerical (solid lines) against experimental (black dots) results. Reproduced from [9] with permission. Courtesy of Airbus

* Counter-Rotating Open Rotor

† German-Dutch Wind Tunnels, established by the German Aerospace Center (DLR) and the Dutch National Aerospace Laboratory (NLR)

‡ that is, relying on space/time azimuthal periodicity

Some of these IM (FWH) computations were based on the *solid* surface approach, with only the noise emission coming from the blades (loading noise, etc.) being accounted for (see top of figure 4). On the other hand, alternative IM (FWH) calculations relied on the porous (or permeable) surface strategy, with all noise emissions coming from the immediate vicinity of blades being integrated also (see bottom of figure 4). As one can see in figure 4, results delivered by these CFD(uRANS)-IM(FWH) weakly coupled computations were favorably compared to experimental data.

In addition to this, specific parametric and/or comparative studies were conducted, which provided key insight of either phenomenological or methodological nature; concerning in particular methodological aspects and regarding first the CFD stage, results have shown that, whenever installation effects are to be accounted for, making use of the full 3D approach is mandatory, despite the increased meshing/computing costs that such an approach may involve. On the other hand, making use of the (lighter and cheaper) chorochronic approach is effectively to be privileged, as long as installation effects can be considered as negligible enough. Regarding now the IM stage, results have shown that the FWH porous (or permeable) surface integration approach allows far-field acoustic extrapolations to fulfill a higher degree of fidelity to the physics, since it incorporates additional effects*, compared to its solid surface counterpart. The latter, however, appears to be more flexible to use, since it avoids some of the issues of the former†, whereas it allows the noise generation mechanisms to be investigated further (here, by discriminating the various radiating parts of blades). For more details about this study, the reader is referred to [7-9].

Noise emission by a double stream jet with pylon, via CFD(LES)-IM(FWH) weakly coupled calculations

The so-called AITEC research project focused on the jet noise emissions by a double stream nozzle (of By-Pass Ratio value 9), which i) included a pylon and ii) was running under high power conditions. Within this context, near-field aerodynamic and far-field acoustic measurements had been gathered during a dedicated dual aero+acoustic campaign, which was conducted in the Onera wind tunnel *CEPRA 19*.

The configuration was then simulated by Vuillot et al. following a 2-step aeroacoustic hybrid approach, that is, via weakly-coupled CFD and IM calculations [62] ; the CFD computation consisted in an unstructured LES, which was achieved with the help of the Onera solver *CEDRE*, whereas the far-field noise was IM-extrapolated using a time domain/porous FWH calculation, for which the Onera code *KIM* was used.

As can be seen in figure 5, both aerodynamic and acoustic predictions were very favorably compared to experimental data. In particular, and although the turbulent transition was not perfectly reproduced by the CFD calculation, the latter succeeded in correctly capturing the aerodynamic installation effects (such as the flow deviation) due to the pylon's presence. More importantly, the latter's effect on acoustic far field radiation was properly predicted, both in terms of directivities and amplitude (absolute levels). In addition, despite the fact that the CFD grid had induced some filtering of the near-field acoustics, its low frequency content $(St < 1)$ could be correctly captured by the FWH extrapolation. Finally, a proper investigation of the latter results allowed the tonal noises observed to be related to the pairing of jet vortices. For more details about this study, the reader is referred to [62].

Noise emission by a nose landing gear, via CFD(ZDES)-IM(FWH) weakly coupled calculations

To better predict the physical mechanisms associated with landing gear noise emissions, the so-called LAGOON research program was initiated by Airbus a few years ago. The objective of the project was to acquire an extensive experimental database associated with elementary landing gear configurations, so that computational methods dedicated to landing gear noise predictions could be accurately and thoroughly validated.

Within this framework, combined experimental and computational campaigns were thus carried out, focusing on both the aerodynamics and the acoustics of a simplified nose landing gear (see figure 6). The model geometry was that of a nose gear of an Airbus A320 aircraft, with a scale factor of 1:2.5 and with only the main elements (leg, wheels, etc.) considered. Such geometry was taken as isolated, and allotted either a take-off or an approach flight condition.

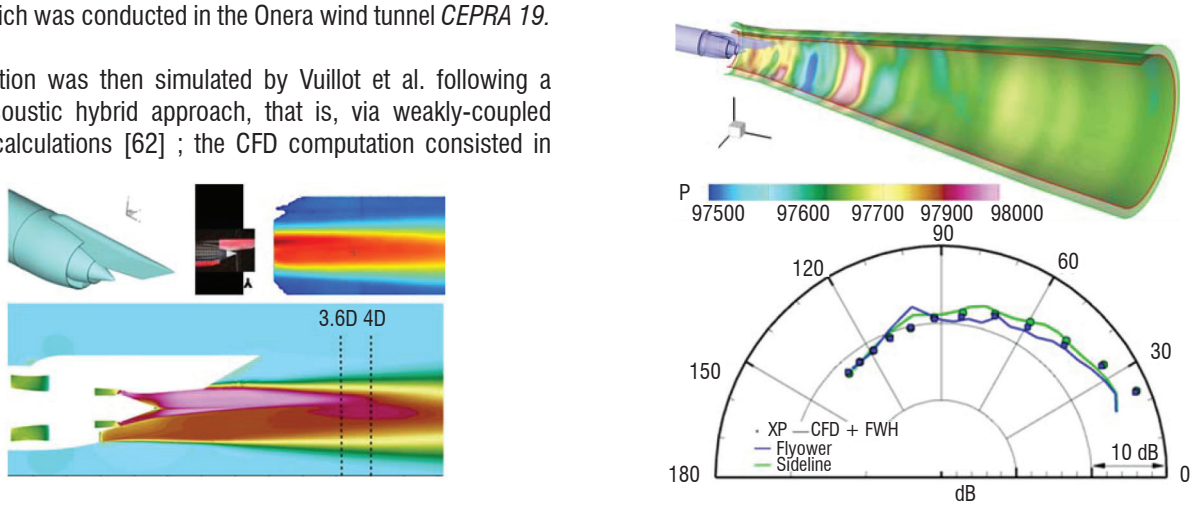

Figure 5 - Noise emission by a double stream jet, via a CFD(LES)-IM(FWH) hybrid calculation. Left : steady flow, as measured (top) and CFD-computed (bottom). Right side : far-field acoustics, as measured (dots) and IM-extrapolated (lines) from the CFD-IM weak-coupling surface (top). Reproduced from [62] with permission

* such as the so-called quadrupolar noise sources, the near-field flow refraction phenomena, etc...

† such as spurious noise sources due to an improper handling of wake vortices convected downstream from the blades

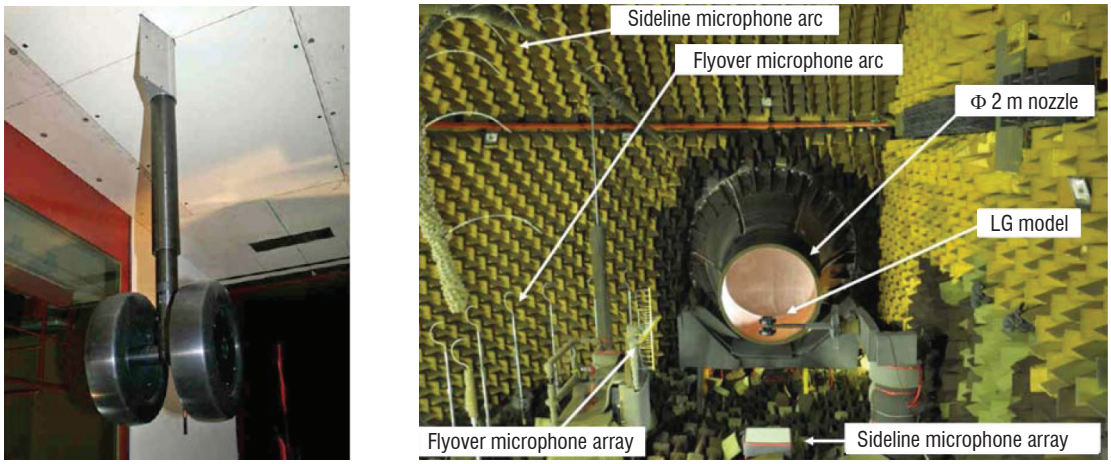

Figure 6 - Noise emission by a simplified nose landing (NLG) under approach flight conditions (LAGooN program). NLG model (seen from behind), as installed in both the aerodynamic facility (left side) and the open jet anechoic wind tunnel (right side) of Onera. Reproduced from [55] with permission. Courtesy of Airbus

The aero+acoustic dual experiments were performed by Manoha et al. in Onera's aerodynamic (*F2*) and anechoic (*CEPRA 19*) facilities, respectively [32, 33] (see figure 6).

The computational counterpart of this aero+acoustic experimental campaign was conducted at Onera, following a 2-step aeroacoustic hybrid approach [55]; unsteady aerodynamics predictions (Stage #1) relied on structured CFD calculations that were based on a ZDES approach [18, 19] and that were conducted by Ben Khelil et al. using the Onera solver *elsA* (see left side of figure 7). As can be seen on the left/bottom side of figure 7, those calculations were favorably compared with the aerodynamic measurements through direct comparison of near-field results (this, to the exception of mismatches over the low and high frequency ranges, which can be reasonably attributed to the high pass filtering induced by the experimental acquisition and the numerical simulation techniques, respectively). In particular, both experimental and numerical outputs exhibited tonal noises (with frequencies of approx. 1 kHz and 1.5 kHz), whose emission was inferred to be associated with resonances coming from the inner cavities of the wheels.

These unsteady CFD results were then acoustically extrapolated to the far-field by Sanders et al. via an IM(FWH) approach, which was based on either a porous or a solid surface integration and for which the Onera code *KIM* was used. These CFD-FWH weakly coupled calculation results were also favorably compared to the experimental measurements recorded in the far-field (see right/bottom of figure 7). Depending on the far-field location, however, an overestimation of acoustic levels could be observed for results that had been obtained via IM(FWH) calculations relying on a porous (rather than a solid) surface integration, this being due to side-effects coming from the FWH-integration of vortices convected by the wake of the landing gear. More details about this study can be found in [55].

Three-step aeroacoustic hybrid method : noise predictions based on CFD and/or CAA calculations

A few examples of aircraft noise predictions that were achieved following a 3-step hybrid strategy, that is, via CFD and/or CAA calculations are presented hereafter. These computations were mostly conducted with the help of Onera solvers. In particular, all CAA calculations were handled with the help of the Onera solver *sAbrinA* [43, 44, 46, 50], which is a highly-accurate time-domain CAA solver operating on multi-block structured grids. Here again, please, note that the application examples presented hereafter constitute a non exhaustive list excerpted from the range of works that were achieved thanks to the three-step hybrid approach and tools developed at Onera.

Aft fan noise emission by an engine at take-off, via CAA calculations

Fan noise is a major harmful aircraft sound source, especially during take-off and approach flight phases. For a long time, engine or aircraft manufacturers mainly focused on the numerical prediction of fan noise upstream components, which are emitted by the air intake of the engine. Over the past few years, however, they have also focused on the more complex problem of predicting their downstream counterparts, which propagate through the exhaust and its highly heterogeneous jet flow.

Within such framework, several collaborative Airbus-Onera studies were carried out, which consisted in performing out computations following the 3-step aeroacoustic hybrid philosophy, with a noise generation step (Stage #1) that was handled via analytical means (based on the modal theory* [61]), whereas the noise propagation step (Stage #2) was conducted using CAA calculations.

Among others, a study was conducted by Redonnet et al. a few years ago [50], with the purpose of assessing how far a time domain structured CAA method (such as the one underlying *sAbrinA* solver) could predict the noise propagation phase associated with aft fan noise emissions by a realistic bypass exhaust. Besides its realistic geometry (which incorporated the pylon and internal bifurcations of the nozzle), such exhaust was assigned representative thermodynamic conditions (take-off conditions) and relevant fan noise contents. The latter were analytically derived according to the modal theory* [61], being then CAA-forced at the upstream of the secondary exhaust, for the CAA solver (*sAbrinA*) to numerically propagate them up through the bypass exhaust.

* which delivers the elementary solutions of the acoustic propagation problem within an infinite annular rigid duct and a homogenous medium, with these solutions being characterized by an azimuthal periodicity of order m and a given radial distribution of order n [61].

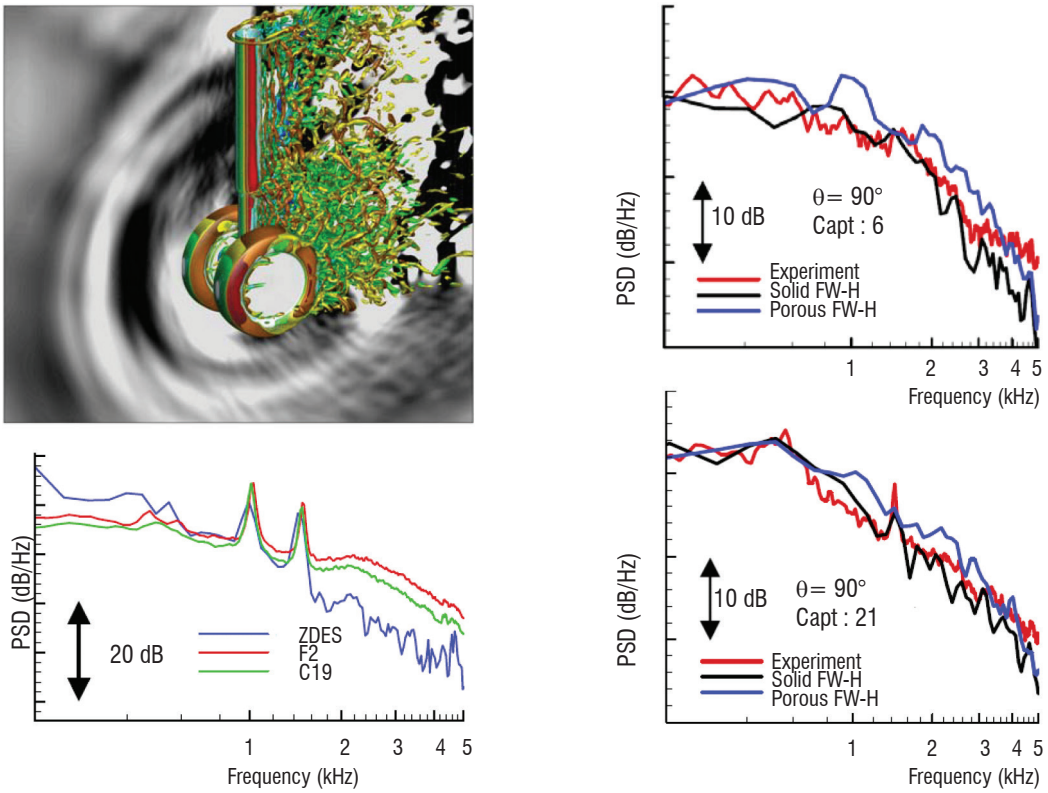

Figure 7 - Noise emission by an isolated nose landing gear (NLG) under approach flight conditions, via a CFD(ZDES)-IM(FWH) hybrid calculation. Left side: near-field aerodynamic results (top: Q-criterion iso-surfaces colored by the stream wise velocity component and instantaneous pressure fluctuation field), with validation (bottom) via direct comparison of the Power Spectral Density (PSD) computed by CFD (in blue) and recorded in the experiments (in red and green), for a probe of the right wheel. Right side; validation of the far-field acoustic results, via direct comparison of the PSD predicted by CFD-FWH (black and blue) and measured in the experiments (red), for two microphones located at 90° from the model in the flyover (top) and side line (bottom) directions. Reproduced from [55] with permission

As an illustration, figure 8 provides the acoustic field radiated by the exhaust at take-off, as CAA-predicted for an aft fan noise mode of azimuthal / radial orders $(m, n) = (13,1)$ emitted at the Blade Passing Frequency (BPF).

First, from a phenomenological point of view, this study allowed the installation effects to which acoustic waves may be subjected when propagating inside and outside an exhaust to be numerically characterized, thus highlighting how far the geometry and/or flow of a turbofan engine can affect its fan noise emissions. This conclusion is of importance, since it shows that a high fidelity to reality is required for numerically predicting the acoustic signature of an engine.

Secondly, and from a more methodological point of view, this study also proved that a time domain *structured* CAA method could be accurate and robust enough to offer both a high fidelity and a minimal flexibility, when applied to realistic engine noise problems. Indeed, for this study, special emphasis was placed on the validation stage, for which the results delivered by each CAA calculation were very favorably compared against those coming from alternative numerical techniques (BEM or DGM, see details in [50]). For more details about this work, the reader is referred to [50].

Here, it is worth mentioning that this particular study opened up the way to an intense applied research activity that was conducted at Onera since half a decade, and that aimed at numerically characterizing both the aft fan noise radiation in itself [50, 42], but also its possible mitigation via passive noise reduction devices - whether the latter relies on innovative installation concepts [45, 46, 38], novel exhaust designs [49, 37] or use of absorbing materials [52]. For instance, as a direct continuation of this study, more recently, alternative CAA calculations were conducted by Redonnet et al., to numerically assess the effect of acoustic absorbing materials on aft fan noise emission by realistic exhausts [52]. Indeed, nowadays, most of the engine noise reduction is achieved thanks to noise absorbing panels, which are set up inside intake and exhaust ducts. Therefore, the lined exhaust counterpart of the previous (rigid nozzle) simulation was conducted, with acoustic liner panels being modeled at end of the secondary exhaust (see top / left side of figure 9). The right side of figure 9 depicts the acoustic power emitted by both the rigid and the lined exhausts; as can be seen, the latter radiates much weaker acoustic levels than the former*, which obviously comes from the noise attenuation occurring within the downstream part of the secondary duct, due to the absorbing material.

* with, in this particular case, a Sound Pressure Level radiated by the lined exhaust of approx. 6dB lower than the one emitted by its rigid counterpart [52]

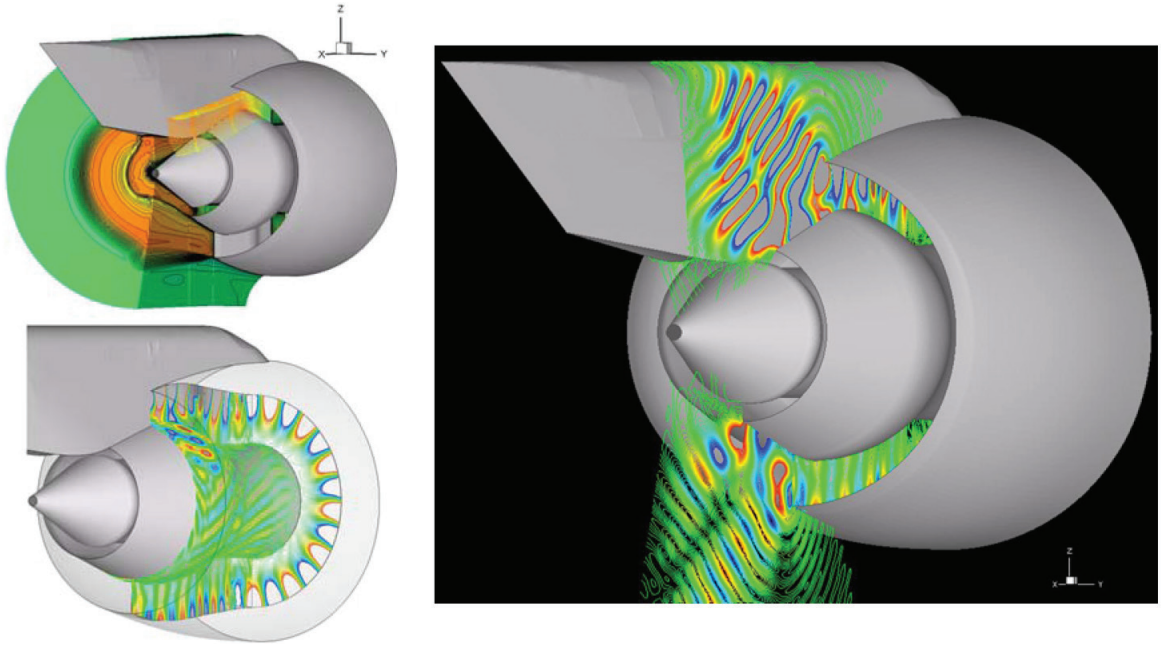

Figure 8 - Aft fan noise emission by an isolated exhaust at take-off, via a CAA calculation forced with analytical source contents. Counter-clockwise, from top left: steady mean flow field (axial velocity), internally propagated and externally radiated instantaneous perturbed pressure fields

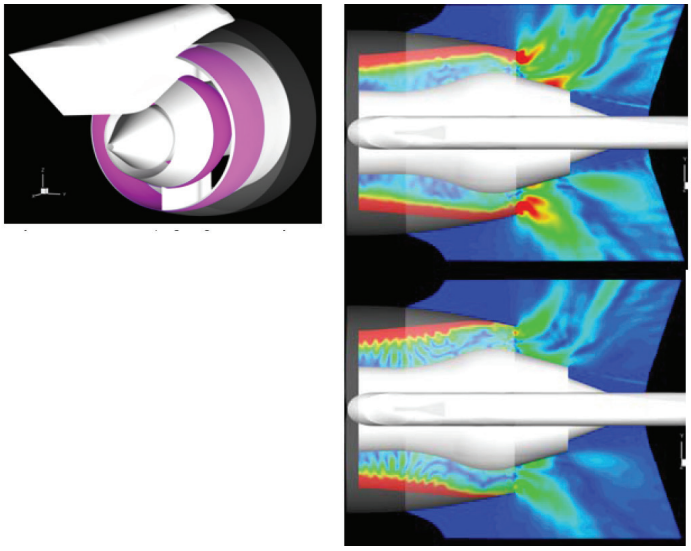

Figure 9 - Aft fan noise emissions by a possibly lined exhaust at take-off. Top left ; acoustic liner panels (in pink). Right side : Root Mean Square perturbed field radiated by the rigid (top) and the lined (bottom) exhausts

This alternative study allowed the efficiency of passive noise reduction technologies to be better highlighted, in regard to their application to engine noise problems. From a methodological point of view, this study has also shown that, once associated with proper post-processes, a CAA method could advantageously be employed to not only predict, but also to investigate some of the mechanisms that underlie the physics of acoustic liners (e.g., effects by ruptures of impedance or grazing flows - see [52]). Additional details about this study can be found in [52].

Aft fan noise emission by a partly installed engine, via CAA calculations

Over the past few years, several French national and European projects have been aimed at assessing how the aft fan noise emitted by engines could possibly be attenuated through the installation effects

Figure 10 - Low Noise Aircraft based on the Rear Fuselage Nacelle concept (courtesy of Airbus)

(or acoustic shielding) offered by structural elements (wing, empennage, fuselage) of non-conventional airplanes. As an illustration, figure 10 depicts an Airbus concept for a low noise aircraft, with the engines installed in RFN (Rear Fuselage Nacelle) configuration, so that the aft fan noise radiated through the exhaust is shielded by the rear fuselage and empennage.

Within this framework, several experimental and numerical studies were conducted at Onera [46, 45, 37], all aimed at characterizing the shielding effect provided by a simplified empennage wing on the aft fan noise of a coaxial exhaust under take-off conditions. Some of the computations performed were achieved by Redonnet et al. [40] following the 3-step aeroacoustic hybrid philosophy, with a noise generation step (Stage #1) relying on analytical means [61], whereas the noise propagation one (Stage #2) was handled via CAA calculations (*sAbrinA* solver). The latter calculations directly benefited from an advanced Chimera technique developed by Desquesnes et al. [20] relying on the use of overlapping grids; this technique greatly helped in lightening the meshing tasks, while allowing the entire configuration to be simulated through simultaneously and strongly coupled CAA-CAA calculations.

First, the overall methodology was carefully validated by considering the installed exhaust as emitting within a quiescent medium, calculation results being then very favorably compared to those delivered by a reference BEM computation (see details in [46]). Then, the actual configuration (take-off flight conditions) was addressed, allowing the relevance of the RFN concept to be highlighted. As an illustration, figure 11 shows the instantaneous perturbed pressure field associated the acoustic emission of an aft fan noise mode (2, 2) emitting at one half of the BFP. By observing what occurs in the lower part of the domain (under the airfoil), one can observe that the empennage wing actually acts as an efficient shield, since only a fraction of the sound emitted in the aft direction succeeds in diffracting around the airfoil and propagating towards the ground.

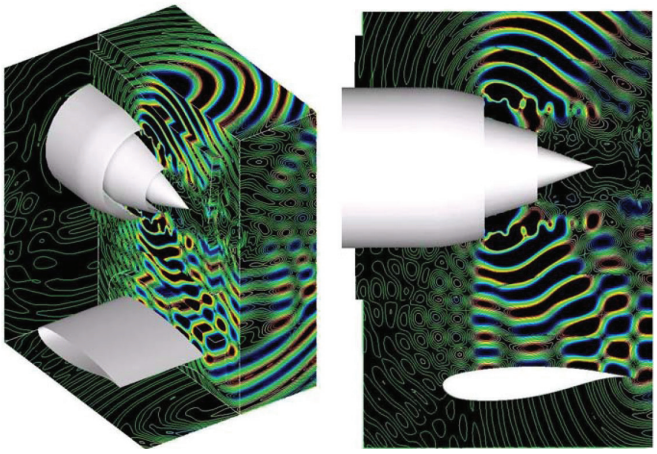

Figure 11 - Aft fan noise emission by a coaxial exhaust installed over an empennage airfoil, via a CAA calculation (fed with analytical source contents)

From a phenomenological point of view, the conclusions of this study were that RFN configurations are particularly efficient in regard to aft fan noise reduction, thus constituting a promising approach for diminishing acoustic signatures by aircraft. From a more methodological point of view, this study had further shown that a time domain structured CAA approach could allow realistic engine noise problems to be handled in an accurate and flexible manner, as long as some of its intrinsic constraints (e.g., meshing effort) could be relaxed through additional features (e.g. the Chimera-based CAA-CAA strong coupling technique used here). Main outcomes and conclusions of such work (which details can be found in [46]) were further confirmed by subsequent Onera studies devoted to the numerical and experimental characterization of the RFN concept [37].

Noise emission by the slat cove noise of a high lift wing, via partly decoupled CFD and CCA calculations

The leading edge slat is known as a major airframe noise source on large transport aircraft. Its underlying mechanisms are complex, as shown by several attempts to characterize slat noise emissions via unsteady CFD techniques [52, 2, 17-19].

Among other works, a few years ago, a dedicated research action was jointly conducted by Onera and Airbus; the computational tasks were based on a 3D-zonal unsteady CFD(LES) approach [36], calculations being performed by Ben Khelil et al. over the slat region of a 2D high-lift wing, which was considered in an as-like approach flight configuration [2]. Once they were properly post-processed by means of spectral analyses, the unsteady CFD results acquired over the slat region revealed the presence of strong local tonal sources within the cove area (see figure 12).

Although the final objective was to simulate the complete slat cove noise production chain following a 3-step hybrid aeroacoustic strategy based on a CFD-CAA weakly coupled calculation, the latter was first replaced by a analytical-CAA one; indeed, post-processes of the unsteady CFD data had delivered enough information about the noise generation stage for equivalent sources to be able to be analytically synthesized, based on the characteristics (location, frequency, relative magnitude, etc.) of the principal tonal emissions occurring within the cove area. Based on these elementary sources (harmonic monopoles), several CAA calculations [20] were then conducted by Desquesnes et al., enabling an interesting qualitative study to be achieved at a reasonable cost. Here, one can notice that, as for the computations presented in the previous paragraph, these CAA calculations directly benefited from the chimera-based CAA-CAA strong coupling technique (which was however used here in its *one way* version).

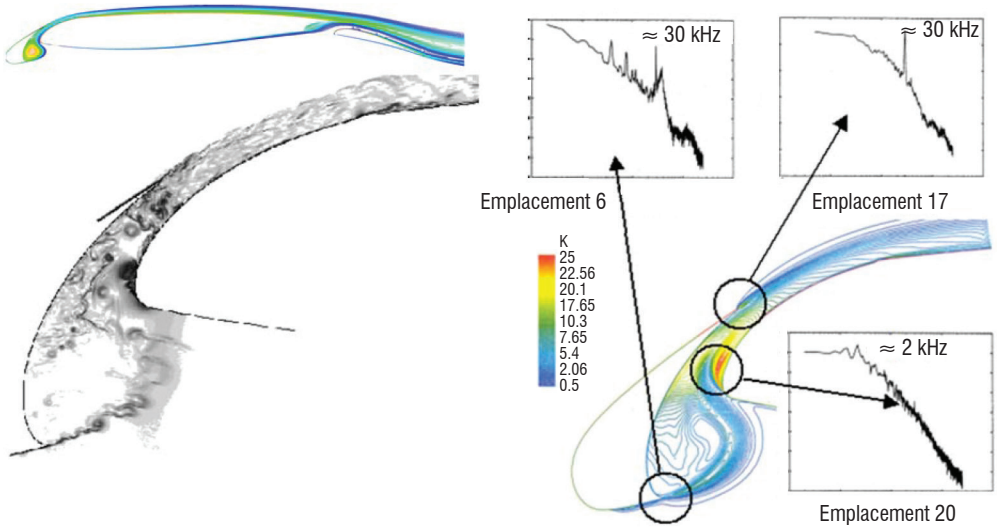

Figure 12 - Noise generation by a slat cove of a high lift wing at approach, via an unsteady CFD (zonal RANS/LES) calculation. Left side ; steady (top) and unsteady (bottom) aerodynamic fields. Right side : turbulent kinetic energy and acoustic spectra within the slat cove

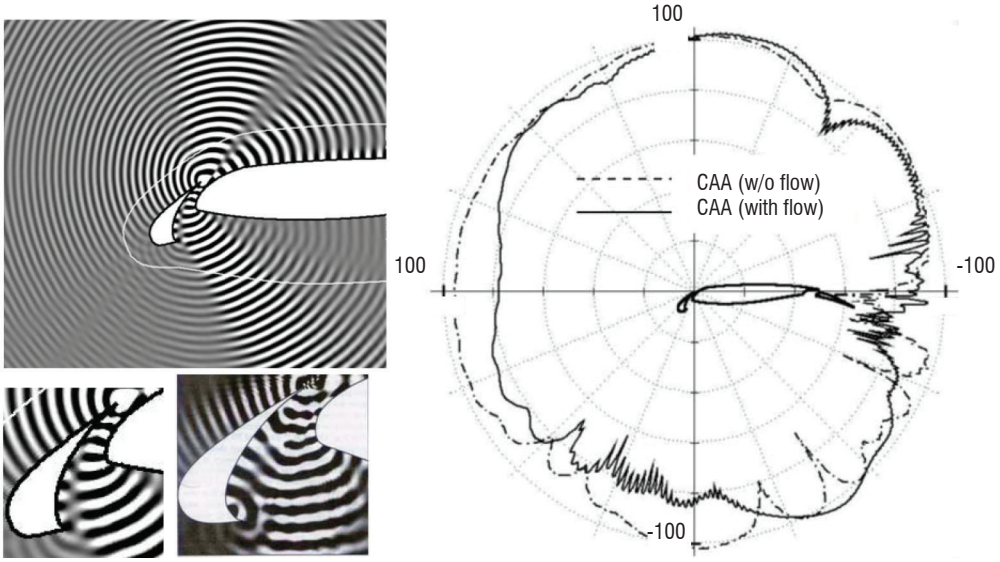

Figure 13 - Noise radiation by the slat cove trailing edge of a high lift wing at approach, as predicted by a CAA calculation based on an equivalent (analytical) source. Left side; instantaneous perturbed pressure field obtained over the domain (top) or within the slat cove (bottom left), to be compared with near-field CFD results obtained for an alternative configuration (bottom right, calculation by NASA). Right side; mid-field directivity diagram (in lines, to be compared with its quiescent medium radiation counterpart, in dashes). Reproduced from [20] with permission

Figure 13 presents the results associated with an (equivalent) noise source of 30 kHz, mimicking the acoustic emission by the slat trailing edge, due to the vortex shedding occurring at this location. As can be seen, the noise radiation patterns are very complex, resulting from the multiple interactions that occur between the acoustic waves and their environment; such interactions primarily come from the reflection/diffraction effects by the wing and the slat geometry, as was numerically highlighted here through a preliminary calculation conducted within a quiescent medium (whose results were very favorably compared to those delivered by a BEM computation, see [20]). These interactions also come from the convection/refraction effects by the associated steady flow, which were underlined here by comparison with results obtained for a quiescent medium (see right side of figure 13). Among other things, all of this leads the slat wing gap to act as an 'acoustic focal' device, which redirects part of the noise emission towards the ground direction in a very directive manner.

From a more methodological point of view, this study further showed the importance of accounting for realistic flows and associated refraction effects, when numerically predicting the acoustic propagation phase of airframe noise problems. This study also indirectly demonstrated the pertinence of handling such problems via a multi-stage aeroacoustic hybrid method based on *partly decoupled* CFD and CAA calculations, along with proper equivalent sources. For more details about this study and its outcomes, the reader is referred to [20].

Noise emission by truncated trailing edges, via weakly coupled CFD/CAA calculations

A few years ago, a couple of CFD-CAA weakly coupled computations were conducted, in order to assess the noise emission by airfoil truncated trailing edges; first, the numerical prediction of the noise emitted by the blunted trailing edge (TE) of an in-flight NACA0012 [35] was achieved by Manoha et al. following a 3-stages hybrid method strategy, via CFD-CAA-IM weakly coupled calculations [34, 59] (with an IM step consisting in a Kirchhoff extrapolation, see left side of figure 14).

Then, such TE noise simulation was extended to a thick plate configuration (see right side of figure 14), which was handled via a CFD-CAA weakly coupled calculation by Guenanff [22].

These studies first allowed an innovative CFD-CAA weak coupling procedure developed by Redonnet [43, 44] to be assessed and validated, in regard to its application to practical airframe noise problems. Beyond that, they also allowed specific key aspects of theoretical and methodological natures to be pinpointed, regarding the proper exploitation of unsteady CFD calculations via an acoustic-based method [34].

Lately, such aspects were addressed more thoroughly by Redonnet et al. [47, 48, 12, 13], which led to improving and optimizing the CFD-CAA weak coupling procedure, thus facilitating its application to real-life problems. As shown below, these recent works and associated outcomes helped to pave the way to the emergence of an accurate and robust 3-step aeroacoustic hybrid method.

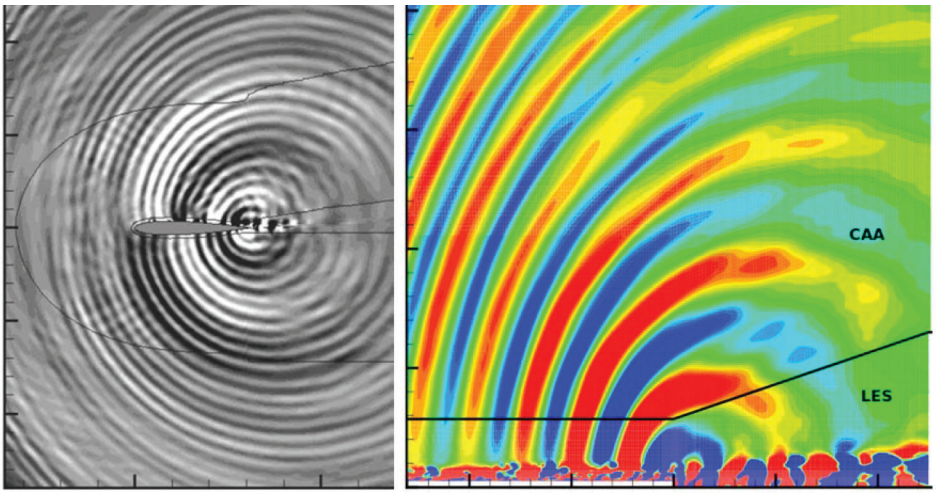

Figure 14 - Noise emission by either a blunted airfoil (left side) or a thick plate (right side) trailing edges, via a CFD-CAA-IM and a CFD-CAA weakly coupled computation, respectively. Right side image reproduced from [22] with permission

Noise emission by a facility installed tandem cylinder, via CFD-CAA weakly coupled calculations

With the view of better understanding landing gear noise sources, an experimental and numerical dual campaign was conducted by NASA Langley Research Center (LaRC), such campaign focusing on both the aerodynamics and the acoustics of a Tandem Cylinders (TC) configuration (see figure 15). To this end, extensive experimental data [24, 23] were collected, being then compared to results of CFD-IM weakly coupled computations [31] associated with a 2-step aeroacoustic hybrid method. Although such comparisons provided a very favorable experimental vs. numerical agreement, there was still concern about possible installation effects that could have been induced on acoustic data by the experimental set-up (see right side of figure 15), thus biasing such a validation exercise.

Therefore, a dedicated study was performed within the framework of a dedicated NASA-Onera collaboration*, whose objective was to numerically assess and investigate the various acoustic installation effects that could have been effectively induced by the experimental set up on the acoustic data gathered during NASA/LaRC experiments. To this end, several CFD-CAA weakly coupled calculations were conducted by Redonnet et al. [48], this being achieved through a weak coupling of (i) the CFD stage that had been performed by NASA/LaRC over the isolated TC and (ii) various CAA stages for which the TC configuration was considered as (either partly or fully) installed within the facility. All calculations relied on the so-called *Non Reflecting Interface* (NRI) [47, 54], which constitutes an improved version of the CFD-CAA weak coupling technique previously recalled, and whose non-reflective character allowed the acoustic backscattering effects that were expected to occur due to the facility devices (e.g., collector, side mounting plates, nozzle - see right side of figure 15) to be properly handled here. As an illustration, the right side of figure 16 displays the CFD-CAA results obtained for the fully installed TC configuration, which included all main devices of the facility, along with its confined and sheared jet flow.

All of these CFD-CAA calculations delivered results that were found to be closely consistent with outcomes previously acquired by NASA with the help of less advanced approaches, which either relied on the CFD-IM hybrid method previously recalled [31] or on alternative techniques (such as the so-called Equivalent Source Method, ESM – see [60]). On the other hand, compared to the latter approaches, the NRI-based CFD-CAA hybrid method allowed the fidelity of the TC noise

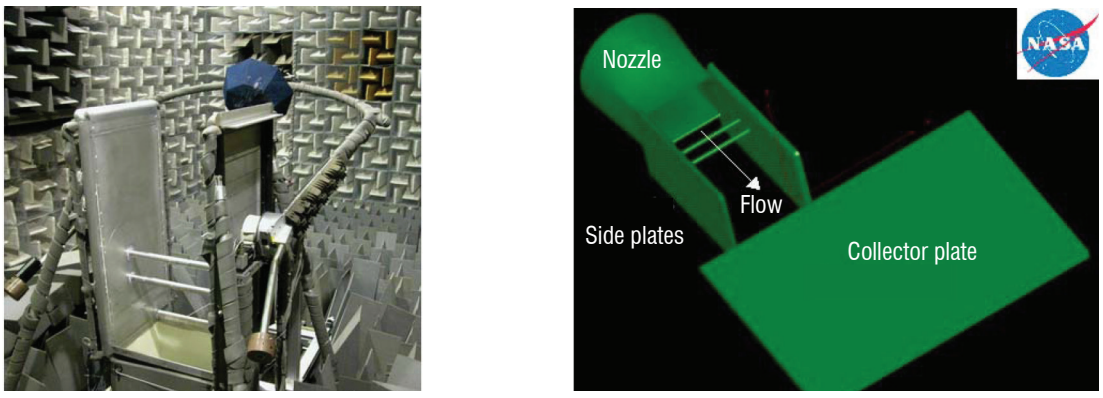

Figure 15 - Noise emission of a Tandem Cylinder (TC) installed within NASA/LaRC's Quiet Flow Facility (QFF). Left side: TC model, with some of the QFF devices (nozzle, mounting side plates). Right side: sketch of the whole installed TC set up, with all the QFF devices (nozzle, mounting side plates, collector plate). Courtesy of NASA

* namely, the International Agreement between NASA and Onera on "Understanding and Predicting the Source of Nose Landing Gear Noise"

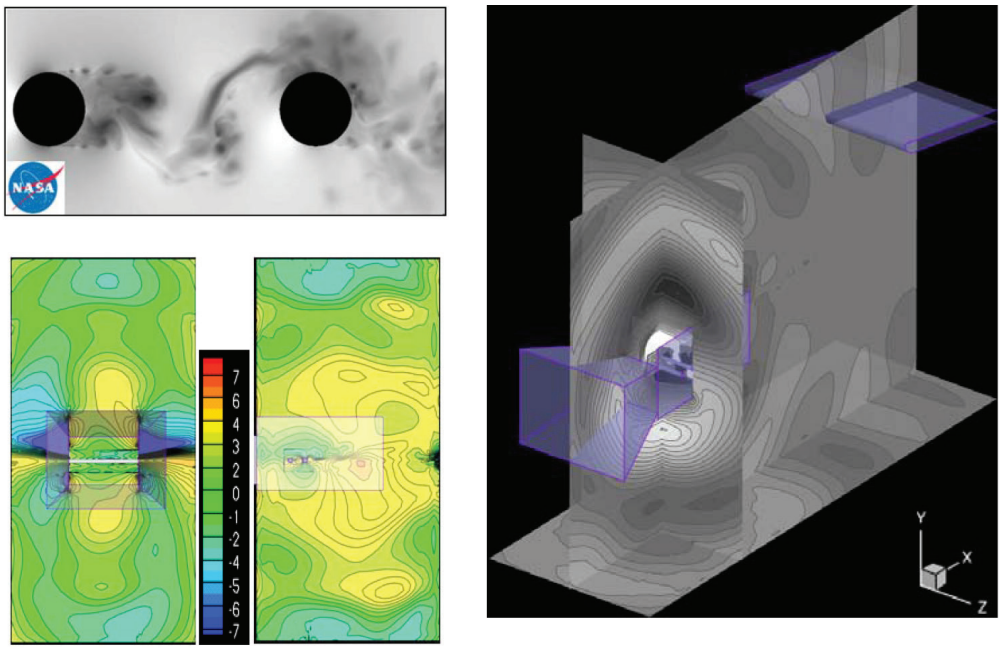

Figure 16 - Noise emission of a Tandem Cylinder (TC) installed within NASA/LaRC's anechoic facility QFF, via CFD-CAA weakly coupled computations. Clockwise, from top/left: instantaneous perturbed fields obtained via either i) the CFD calculation of the isolated TC or ii) the subsequent CFD-CAA computation of the QFF-installed TC, and iii) deltas (in dB) between the Sound Pressure Level fields associated with both configurations, as recorded in within two lateral planes (xy and yz)

propagation stage to be improved, by i) accounting for the acoustic emission that had been effectively predicted by the CFD stage (rather than by modeling it via equivalent sources, as is implicitly or explicitly done by IM or ESM techniques), as well as by ii) including the facility apparatus and associated (confined sheared) jet flow characterizing the experiment (rather than to consider a simplistic homogenous free field medium, as necessarily assumed by IM and ESM techniques).

As a result, this study primarily allowed the various acoustic installation effects that could have been effectively induced by the experimental apparatus on the acoustic data gathered during NASA/LaRC tests to be investigated (see left bottom of figure 16), highlighting not only the reflection / diffraction by the experimental set-up, but also the (partial) convection / refraction by its confined and sheared jet flow. From a more methodological point of view, the study allowed the innovative NRI-based CFD-CAA weak coupling procedure to be further assessed and validated, as well as making it possible to illustrate how far an aeroacoustic hybrid approach relying on the latter could effectively handle practical airframe noise problems involving installed configurations. More details about this work can be found in [48].

Noise emission by a nose landing gear, via CFD-CAA weakly coupled calculations

As was mentioned previously, the so-called LAGOON project [32, 33] focused on a simplified nose landing gear (NLG) in approach flight, in order to assess/validate the 2-step hybrid methodology by comparing to experiments the numerical results of CFD-IM weakly coupled calculations (see above).

Lately, such an assessment exercise was extended to the 3-step hybrid methodology, by completing these CFD-IM weakly coupled calculations with CFD-CAA ones. Here too, the objective was to further improve the fidelity of the acoustic propagation stage, by i) accounting for the acoustic emission that had been effectively predicted by the CFD stage (rather than to model it via equivalent sources, as implicitly done in the IM approach), as well as by ii) including the realistic jet flow characterizing the experiment (rather than to model it via a simplistic uniform mean flow, as is also done in the IM approach). To this end, CFD-CAA coupled calculations were conducted by Redonnet et al. [53], which were i) based on the unsteady aerodynamics data coming from the CFD computations previously achieved (see above), and ii) conducted with the help of the NRI-based CFD-CAA weak coupling technique.

First, CFD-CAA coupled calculation corresponded to an isolated NLG, that is, was allotted a computational set up similar to that of CFD-FWH computation (incorporating in particular a steady mean flow corresponding to a homogeneous free field). Such a calculation allowed the CFD-CAA outputs to be validated through direct comparison against both the numerical (CFD) and the experimental results, which had been acquired and/or processed under the same "homogeneous propagation medium" conditions*(see right side of figure 17). An alternative CFD-CAA calculation considered the NLG as installed in the anechoic wind tunnel, with a (heterogeneous) mean flow matching the sheared steady jet occurring in the facility. This alternative calculation (see left side of figure 17) made it possible to assess the sole mean flow effects that could have been induced by the facility jet on the experimental data.

* with experimental data that had been corrected from the refraction effects by the open jet shear layers

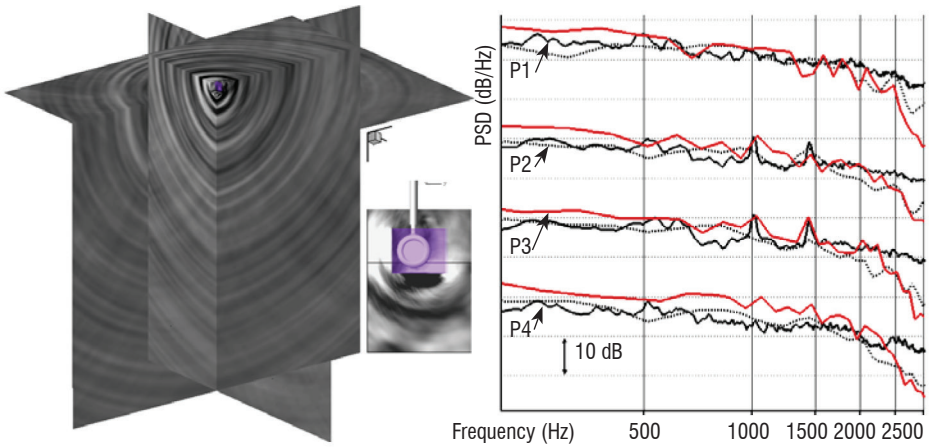

Figure 17 - Noise emission by Nose Landing Gear (NLG) installed within Onera's CEPRA19 anechoic facility, via CFD-CAA weakly coupled computations. Left side: instantaneous perturbed field radiated by the facility-installed NLG. Right side; validation of the isolated NLG calculation, via a cross-comparison of far-field results (Power Spectral Density recorded at four probes, P1-4) obtained for both the experiments (in black lines), the CFD-CAA (in red lines), and the CFD-FWH (in black dashes)

Here, it is worth mentioning that, beyond its sole applicative concerns, this study allowed the overall CFD-CAA coupled approach to be optimized further [11, 51, 12], so that it can be applied to realistic configurations in a safer and easier way. More precisely, the impact that its manipulation (sampling, interpolation, etc.) can have on an unsteady CFD dataset was studied from both a fundamental and a methodological point of view, allowing several innovative solutions to be proposed (including (i) specific guidelines for the preservation of aeroacoustic signals [13, 14], (ii) a novel interpolation method [10, 15] and (ii) a new class of finite difference derivative schemes [16]). Based on this, the CFD-CAA hybrid methodology was enhanced with key improvements (methodological guidelines, advanced methods, etc.), so that it can cope with all stringent constraints that are dictated by real-life problems without being jeopardized by some of their unavoidable side-effects (CFD data manipulation, acoustic signal degradation, etc.). For additional details about this work, the reader is referred to [53].

Conclusion and perspectives

This article focused on the so-called aeroacoustic hybrid approach, whose ultimate objective is the numerical prediction of realistic aircraft noise problems. More precisely, here, we recalled some of the efforts deployed over the last decade at Onera to improve aeroacoustic hybrid methods, through both the development of computational tools and their subsequent application to practical problems of aircraft noise.

With that view, it was first recalled here what aeroacoustic hybrid methods are about, whether the latter methods are composed of two or three stages. Their potentialities were then highlighted through various examples of application to practical problems of engine or airframe noise.

All this illustrates well the facts that i) two-stage aeroacoustic hybrid approaches (which rely more on Integral Methods) have now became the most popular means for numerically predicting the noise emission by aircraft components, whereas ii) their three-stage counterparts (which rely more on Computational Aeroacoustics techniques) now offer an even more promising alternative, thanks to the higher fidelity that they bring to the propagation phase of the hybrid scenario. Therefore, it turns out that, at the present date, aeroacoustic hybrid approaches constitute the best viable alternative to Direct Numerical Simulation, which is known to be inapplicable to industrial problems because of the excessive CPU time and memory requirements that it involves.

One can thus expect to see aeroacoustic hybrid approaches being more and more intensively applied to aircraft noise problems over the coming years. At that stage, there is no doubt that Onera will play a key role in helping these advanced noise prediction methods and underlying techniques to flourish within industrial environments ■

Acknowledgements

The studies presented above were achieved within several frameworks of various natures, such as research actions, contractual services, multi-entity collaborations, PhD theses, etc. Likewise, these studies were supported by funding of various origins, such as contracts by industry partners, support by national government agencies, Onera internal funds, etc. Since these are too numerous to be listed here, the author gratefully acknowledges all of the stakeholders (whether individuals or corporate entities) that enabled and/or achieved these R&D works. Credit primarily goes to the authors of all associated references, who are gratefully thanked for their contributions and permission to reproduce results.

Acronyms

AITEC	French national project (supported by DGAC) devoted to jet aeroacoustics)
BEM	Boundary Element Method
BPF	Blade Passing Frequency
CAA	Computational AeroAcoustics
CEDRE	Onera's CFD solver (unstructured approach)
CEPRA19	Onera's anechoic facility
CFD	Computational Fluid Dynamics
CROR	Counter-Rotating Open Rotor
dB	Decibel
DES	Detached Eddy Simulation
DGM	Discontinuous Galerkin Method
DLR	German Aerospace Center
DNS	Direct Numerical Simulation
DNW	German-Dutch Wind Tunnels
elsA	Onera's CFD solver (structured approach
ESM	Equivalent Source Method
F2	Onera's aerodynamic facility
FWH	Ffowcs-Williams & Hawkings
IM	Integral Method
KIM	Onera's IM solver
kHz	Kilohertz
LAGOON	Transantional project (supported by Airbus), devoted to landing gear aeroacoustics
LaRC	Langley Research Center (NASA)
LES	Large Eddy Simulation
NACA	Airfoil profile geometry
NASA	National Aeronautics and Space Administration (USA)
NLG	Nose Landing Gear
NLR	Dutch National Aerospace Laboratory
NRI	Non Reflecting Interface
Pa	Pascal
PSD	Power Spectral Density
Q-criterion	Positive 2nd invariant of Jacobian
QFF	NASA/LaRC's anechoic facility
RANS	Reynolds Averaged Navier-Stokes
RFN	Rear Fuselage Nacelle
R&D	Research & Development
sAbrinA	Onera's CAA solver (structured approach)
St	Strouhal number
TC	Tandem Cylinder
TE	Trailing edge
uRANS	Unsteady RANS
ZDES	Zonal DES

References

[1] H. L. ATKINS - *Continued Development of the Discontinuous Galerkin Method for Computational Aeroacoustic Applications.* AIAA Paper 1997-1581, May 1997.

[2] S. BEN KHELIl - *Large Eddy Simulation of Flow Around a Slat with a Blunt Trailing Edge*. Proceedings of ICCFD3, July 2004.

[3] L. CAMBIER and M. GAZAIX - *elsA : an Efficient Object Oriented Solution to CFD Complexity*. AIAA Paper 2002-108, January 2002.

[4] L. CAMBIER, S. HEIB and S. PLOT - *The Onera elsA CFD Software: input from Research and Feedback from Industry*. Mechanics & Industry, Vol 14 (3), pp 159-174, January 2013.

[5] P. CHEVALIER, B. COURBET, D. DUTOYA, P. KLOTZ, E. RUIZ, J. TROYES and P. VILLEDIEU - *CEDRE : Development and Validation of a Multiphysic Computational Software*. Proceedings of the 1st EUCASS Congress, July 2005, Moscow, Russia.

[6] V. CLAIR, C. POLASCEK, T. LE GARREC, G. REBOUL, M. GRUBER and P. JOSEPH - *Experimental and Numerical Investigation of Turbulence-Airfoil Noise Reduction Using Wavy Edges*. AIAA Journal, Vol. 51 n°11, November 2013

[7] Y. COLIN, A. CARAZO, B. CARUELLE, T. NODÉ-LANGLOIS, A.B. PARRY - *Computational Strategy for Predicting CROR Noise at Low-Speed, Part I: Review of the Numerical Methods*. AIAA paper 2012-2221, June 2012.

[8] Y. COLIN, F. BLANC, B. CARUELLE, F. BARROIS, N. DJORDJEVIC - *Computational Strategy for Predicting CROR Noise at Low-Speed, Part II: Investigation of the Noise Sources Computation with the Chorochronic Approach.* AIAA paper 2012-2222, June 2012.

[9] Y. COLIN, B. CARUELLE, A.B. PARRY - *Computational Strategy for Predicting CROR Noise at Low-Speed, Part III : Investigation of Noise Radiation with the Ffowcs-Williams Hawkings analogy.* AIAA paper 2012-2223, June 2012.

[10] G. CUNHA and S. REDONNET - *An Innovative Interpolation Technique for Aeroacoustic Hybrid Methods.* AIAA Paper n° 2011-2483, June 2011.

[11] G. CUNHA and S. REDONNET - *Towards a Robust and Accurate CFD-CAA Coupling Procedure for Hybrid Methods in Aeroacoustics - Part 1 : On the Optimization of CFD/CAA Coupled Calculations*. AIAA paper 2012-2063, June 2012.

[12] G. CUNHA - *Optimization of a Computational Aeroacoustics Methodology Based on the Weak Coupling of Unsteady Aerodynamic and Acoustic Propagation Approaches.* PhD Thesis, Toulouse University, October 2012.

[13] G. CUNHA and S. REDONNET - *On the Signal Degradation Induced by the Interpolation and the Sampling Rate Reduction in Aeroacoustics Hybrid Methods.* International Journal for Numerical Methods in Fluids, Vol. 71 (7), February 2013.

[14] G. CUNHA and S. REDONNET - *On the Effective Accuracy of Explicit Spectral-Like Optimized Finite-Difference Schemes for Computational Aeroacoustics*. Journal of Computational Physics, Vol. 263, April 2014.

[15] G. CUNHA and S. REDONNET - *An Innovative Optimization Methodology for Explicit High-Order Interpolation Schemes*. Submitted for publication in International Journal for Numerical Methods in Fluids (Spring 2014).

[16] G. CUNHA and S. REDONNET - *Low-Dispersion High-Order Explicit Finite-Difference Schemes for Computational Aeroacoustics*. submitted for publication in International Journal for Numerical Methods in Fluids, October 2013.

[17] S. DECK - *Zonal-Detached-Eddy Simulation of the Flow Around a High-Lift Configuration. AIAA Journal,* Vol. 43 (11), November 2005.

[18] S. DECK and R. LARAUFIE - *Numerical investigation of the flow dynamics past a three-element aerofoil*. Journal of Fluid Mechanics, Vol. 732, pp. 401-444, October 2013.

[19] S. DECK - *Recent improvements in the Zonal Detached Eddy Simulation (ZDES) formulation*. Theoretical and Computational Fluid Dynamics, Vol. 26, n° 6, pp 523-550, 2012.

[20] G. DESQUESNES, M. TERRACOL, E. MANOHA and P. SAGAUT - *On the use of High Order Overlapping Grid Method for Coupling in CFD/CAA*. Journal of Computational Physics, Vol. 220 (1), December 2006.

[21] J. E. FFOWCS-WILLIAMS, and D. L. HAWKINGS - *Sound Generation by Turbulence and Surfaces in Arbitrary Motion*. Philosophical Transactions of the Royal Society of London A, Vol. 342, 1969, pp. 264–321.

[22] R. GUENANFF - *Couplage instationnaire Navier-Stokes/Euler pour la génération et le rayonnement des sources de bruit aérodynamique*. PhD Thesis, Rennes University, 2004, n° 3138.

[23] F. V. HUTCHESON and T. F. BROOKS - *Noise Radiation from Single and Multiple Rod Configurations*. AIAA Paper 2006-2629, May 2006.
[24] L. N. JENKINS, M. R. KHORRAMI, M. M.CHOUDHARI, and C. B. MCGINLEY - *Characterization of Unsteady Flow Structures Around Tandem Cylinders for Component Interaction Studies in Airframe Noise*. AIAA Paper 2005-2812, May 2005.
[25] G. R. KIRCHHOFF - *Zur Theorie der Lichtstrahlen*. Annalen der Physik und Chemie, Vol. 18, 1883.
[26] A. LAFITTE, T. LE GARREC, C. BAILLY, and E. LAURENDEAU - *Turbulence Generation from a Sweeping-Based Stochastic Model.* AIAA Journal, Vol. 52 n°2 , February 2014
[27] T. LE GARREC, E. MANOHA and S. REDONNET - *Flow Noise Predictions Using RANS/CAA Computations.* AIAA Paper 2010-3756, June 2010.
[28] S.K. LELE - C*ompact Finite Difference Schemes with Spectral-Like Resolution*. Journal of Computational Physics, Vol 103, pp. 16-42, 1992.
[29] M.J. LIGHTHILL - *On Sound Generated Aerodynamically*. I. General theory / II. Turbulence as a source of sound", Proc. Roy. Soc. London, Vol. A 211, 1952 / Vol. A 222, 1954.
[30] D.P. LOCKARD, K.S. BRENTNER, H.L. ATKINS - *High Accuracy Algorithms for Computational Aeroacoustics*. AIAA Journal, Vol. 33, N° 2, pp. 246-251, 1995.
[31] D. P. LOCKARD, M. R. KHORRAMI, M. M.CHOUDHARI, F. V. HUTCHESON and T. F. BROOKS - *Tandem Cylinder Noise Prediction*. AIAA Paper 2007-3450, May 2007.
[32] E. MANOHA, J. BULTÉ and B. CARUELLE - *LAGOON : an Experimental Database for the Validation of CFD/CAA Methods for Landing Gear Noise Prediction.* AIAA paper 2008-2816, May 2008.
[33] E. MANOHA, J. BULTÉ, V. CIOBACA and B. CARUELLE - *LAGOON : Further Analysis of Aerodynamic Experiments and Early Aeroacoustics Results.* AIAA paper 2009-3277, May 2009.
[34] E. MANOHA, C. HERRERO, P. SAGAUT and S. REDONNET - *Numerical Prediction of Airfoil Aerodynamic Noise*. AIAA Paper n°2002-2573, June 2002.
[35] E. MANOHA, P. DELAHAY, P. SAGAUT, I. MARY, S. BEN KHELIL and P. GUILLEN - *Numerical Prediction of the Unsteady Flow and Radiated Noise from a 3D Lifting Airfoil*. AIAA Paper n° 2001-2133, May 2001.
[36] I. MARY and P. SAGAUT - *Large Eddy Simulation of Flow Around an Airfoil*. AIAA paper 2001-2559, June 2001
[37] C. MINCU, E. MANOHA, C.PARZANI, J. CHAPPUIS, S.REDONNET, R. DAVY and M. ESCOUFLAIRE - *Numerical and Experimental Characterization of Aft Fan Noise for Isolated and Installed configurations.* AIAA Paper n° 2010-3918, June 2010.
[38] C. MINCU, E. MANOHA, G. REBOUL, S. REDONNET and S. PASCAL - *Numerical simulation of broadband aft fan noise radiation for turbofan with scarfed nozzle*. AIAA paper 2011-2941, June 2011.
[39] M. OMAIS, B. CARUELLE, S. REDONNET, E. MANOHA and P. SAGAUT - J*et Noise Prediction Using RANS CFD Input*. AIAA Paper 2008-2938, May 2008.
[40] J. PRIEUR and G. RAHIER - *Aeroacoustic Integral Methods, Formulation and Efficient Numerical Implementation*. Aerospace Science and Technology, Vol. 5 (7), October 2001, pp. 457-468.
[41] G. RAHIER and J. PRIEUR - *An Efficient Kirchhoff Integration Method for Rotor Noise Prediction Starting Indifferently from Subsonically or Supersonically Rotating Meshes*. Proceedings of the 53rd Annual Forum of the American Helicopter Society, Virginia Beach, VA, April-May 1997.
[42] G. REBOUL and C. POLACSEK - *Towards Numerical Simulation of Fan Broadband Noise Aft Radiation from Aero-engines*. AIAA Journal, Vol 48 n° 9, September 2010.
[43] S. REDONNET, E. MANOHA and P. SAGAUT - *Numerical Simulation of Propagation of Small Perturbations interacting with Flows and Solid Bodies*. AIAA Paper 2001-2223, May 2001.
[44] S. REDONNET - *Simulation de la propagation acoustique en présence d'écoulements quelconques et de structures solides, par résolution numérique des équations d'Euler*. PhD Thesis, Université Bordeaux I, December 2001.
[45] S. REDONNET, C. PARZANI, E. MANOHA and D. LIZARAZU - *Numerical Study of 3D Acoustic Installation Effects through a Hybrid Euler/BEM method*. AIAA Paper 2007-3500, May 2007.
[46] S. REDONNET, G. DESQUESNES, E. MANOHA and C. PARZANI - *Numerical Study of Acoustic Installation Effects with a CAA Method*. AIAA Journal, Vol. 48 n° 5, May 2010.
[47] S. REDONNET - *On the Numerical Prediction of Aerodynamic Noise via a Hybrid Approach - Part 1 : CFD/CAA Surfacic Coupling Methodology, Revisited for the Prediction of Installed Airframe Noise Problem*. AIAA Paper 2010-3709, June 2010.
[48] S. REDONNET, D. P. LOCKARD, M. R. KHORRAMI and M. M. CHOUDHARI - *CFD-CAA Coupled Calculations of a Tandem Cylinder Configuration to Assess Facility Installation Effects*. AIAA Paper 2011-2841, June 2011.
[49] S. REDONNET, E. MANOHA and O. KENNING - *Numerical Simulation of the Downstream Fan Noise of 3D Coaxial Engines*. AIAA Paper n° 2005-2816, May 2005.
[50] S. REDONNET and Y. DRUON - *Computational AeroAcoustics of Realistic Co-Axial Engines*. AIAA Journal, Vol. 50 (5), May 2012.
[51] S. REDONNET and G. CUNHA - *Towards a Robust and Accurate CFD-CAA Coupling Procedure for Hybrid Methods in Aeroacoustics - Part 2 : On the Application of the CFD-CAA Surface Weak Coupling Methodology to Realistic Aircraft Noise Problems.* AIAA paper 2012-2191, June 2012.
[52] S. REDONNET - *Computational Aeroacoustics of the Aft Fan Noise Emission by a Lined Realistic Exhaust.* Proceedings of Internoise Congress, Paper IN 2012-1284, August, 2012.
[53] S. REDONNET, G. CUNHA and S. BEN KHELIL - *Numerical Simulation of Landing Gear Noise via Weakly Coupled CFD-CAA Calculations*. AIAA paper 2013-2068, 19th AIAA/CEAS Aeroacoustics Conference, Germany, June 2013.
[54] S. REDONNET, D. P. LOCKARD, M. R. KHORRAMI and M. M. CHOUDHARI - *The Non Reflective Interface: An Innovative Forcing Technique for Computational Acoustics Hybrid Methods*. To be submitted for publication in International Journal for Numerical Methods in Fluids (2014).
[55] L. SANDERS, E. MANOHA, S. BEN KHELIL and C. FRANÇOIS - *LAGOON: New Mach Landing Gear Noise Computation and Further Analysis of the CAA Process*. AIAA paper 2012-2281, June 2012.
[56] C.K.W. TAM and J.C. WEBB - *Dispersion-Relation-Preserving Finite Difference Schemes for Computational Acoustics*. Journal of Computational Physics, Vol. 107 n° 8, 1993.
[57] C.K.W. TAM - *Computational Aeroacoustics; Issues and Methods*. AIAA Journal, Vol. 33, N° 10, pp. 1788-1796, 1995.
[58] M. TERRACOL et al - *Numerical Simulation of the 3D Unsteady Flow in a Slat Cove for Noise Prediction.* AIAA Paper 2003-3110, May 2003.
[59] M. TERRACOL, E. MANOHA, C. HERRERO, E. LABOURASSE, S. REDONNET and P. SAGAUT - *Hybrid Methods for Airframe Noise Numerical Prediction.* Theoretical and Computational Fluid Dynamics, Vol. 19, n° 3, July 2005.
[60] A. F. TINETTI and M. H. DUNN - *Acoustic Simulations of an Installed Tandem Cylinder Configuration.* AIAA Paper 2009-3158, May 2009.
[61] J. M. TYLER and T. G. SOFRIN - *Axial Flow Compressor Noise Studies*. Transactions of the SAE, Vol. 70, 1962, pp. 309–332.
[62] F. VUILLOT, N. LUPOGLAZOFF, M. HUET - *Effect of a Pylon on Double Stream Jet Noise from Hybrid CAA Computations.* AIAA paper 2010-4029, June 2010.

AUTHOR

Stephane Redonnet After graduating with a double degree in Applied Mathematics and Mechanics, S. Redonnet conducted his PhD at Onera in the field of Computational AeroAcoustics (CAA). Then, he joined Onera's Acoustic team permanently as a Research Engineer. As a CAA specialist, he first took the leading role in the development of Onera's CAA solver *sAbrinA*, before applying the latter code to various applied research problems of aircraft noise mitigation. More recently, he spent one year and a half in residence at NASA Langley Research Center, dedicating himself to the further development of advanced aeroacoustic prediction methods relying on both CFD (Computational Fluid Dynamics) and CAA. S. Redonnet is now the person responsible on the national level for the French roadmap devoted to the development of numerical techniques for aircraft noise prediction/mitigation.

D.C. Mincu, E. Manoha
(Onera)

E-mail: daniel-ciprian.mincu@onera.fr

DOI : 10.12762/2014.AL07-08

Numerical and Experimental Characterization of Fan Noise Installation Effects

Within the context of the two major European Research Projects, NACRE and OPENAIR, the potential of acoustic installation effects on the aft fan noise radiated by innovative installations of coaxial turbofans are evaluated. Three different installation concepts are considered: a semi-buried engine, a rear-fuselage nacelle and, finally, a scarfed nozzle. The main objective of these concepts is to reduce the acoustic radiation of fan noise through the engine nozzle towards the ground, without significant losses in the aerodynamic performance. This evaluation relies on numerical simulations achieved with Onera's solvers, namely sAbrinA-V0 (CAA) and BEMUSE (BEM). The nozzle configurations are typical of coaxial turbofans with a large bypass ratio, including 3D effects from the internal bifurcation and, possibly, the external pylon or fuselage. To obtain a representative fan noise effect, several levels of complexity are used to numerically model the fan noise sources. The most advanced acoustic computations rely on Random Phase Multi-modal Injection (RPMI), an innovative technique based on the optimization of the modal phases, in order to obtain, with a minimum number of CAA computations, the contribution of all cut-on modes with evenly distributed acoustic power, summed in an un-correlated way. Noise propagation also accounts for the refraction effects, due to the large velocity gradients in the coaxial flow. For this purpose, non-homogeneous RANS mean flows were computed by Onera, AIRBUS and SNECMA respectively, for the reference (isolated) and the installed configurations, allowing their respective aerodynamic performances to be checked. For all three configurations, the installation effect is evaluated as a combination of the result of the CAA computation in the near-field and an extrapolation in the far-field, using the BEM or Kirchhoff integral methods to take into account the acoustic scattering on different fuselage parts. Undeniable benefits in noise reduction by the use of such installations are demonstrated. However, additional studies are still required to confirm these benefits, especially by improving the modeling of the fan noise sources and optimizing the acoustic shielding process.

Introduction

After decades of continuous reduction of the noise radiated by aeronautic powerplant systems, and especially by modern turbofans with high by-pass ratio, further improvements are now expected from engine installation effects, which means by using the airframe (fuselage, wing, empennage), or even the nacelle itself, as noise shielding surfaces through innovative engine integrations.

Current acoustic studies of innovative engine installations rely on combining numerical predictions and experiments, mostly at model scale. Moreover, the development of innovative numerical methods must rely on a dedicated experimental database, achieved on academic configurations for validation. This was the case, for example, in the European project NACRE (New Aircraft Concepts Research in Europe, 2005-2010) where Airbus recently led studies relating to the RFN concept [1, 2, 3] (Task 3.1 "Rear Fuselage Nacelle", see figure 1b) combining experiments performed in Onera's CEPRA19 aeroacoustic open-jet windtunnel and several up-to-date numerical prediction methods for isolated/installed jet and fan noise from a turbofan engine. In the case of the Payload Driven Aircraft (PDA) or "flying wing" configuration [4, 5, 6] (figure 1a), also studied in NACRE

(Task 3.2 “Radical Engine Integration” coordinated by Onera), radical solutions were tested [7, 8, 9] with the engine installed as close as possible to the airframe, or even partly buried inside, following interests expressed by the airframer (reduced pitching moment, weight, and noise).

a) Payload Driven Aircraft

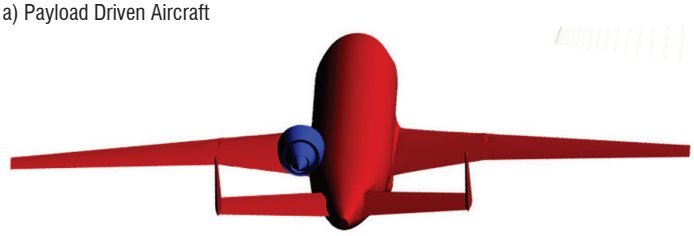

b) Rear Fuselage Nacelle

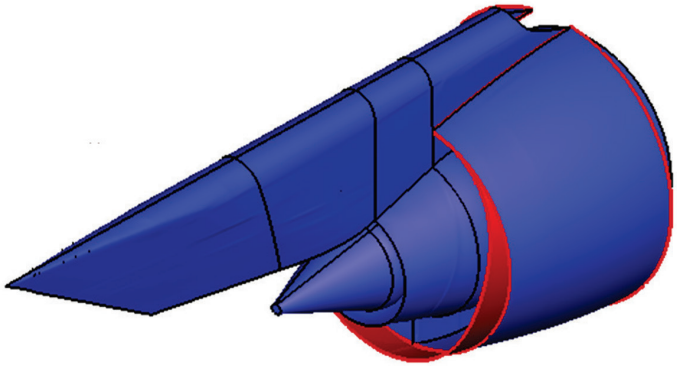

c) Scarfed aft-fan

Figure 1 - Configurations tested to evaluate the potential of acoustic shielding effect

Although less revolutionary, the nacelle itself can be used to generate acoustic installation effects on fan noise, as is already the case for nacelles equipped with a scarfed air inlet. Indeed, on several aircraft, the positive scarf of the inlet (the upper part of the lip is upstream from the lower part) offers optimum aerodynamic flow properties for high incidence angles at takeoff, but tends to increase the fan noise level radiated to the ground. A decade ago, studies performed by Airbus France [10], within the European research project SILENCER, on scarfing the lower part of the lip [11] (Negatively Scarfed Intake – NSI) showed, as expected, opposite effects on acoustics with benefits of up to 1.4 EPNdB under both take off and approach conditions, but with major drawbacks on aerodynamics. The central conclusion of several studies [12, 13, 14] addressed to counterbalance this drawback was that both acoustics and aerodynamics must be accounted for conjunctively, from the beginning of the design process. Within the European project OPENAIR (OPtimization for low Environmental Noise impact), the “scarfing” (Scarfed Aft-Fan – SAF) concept is tentatively applied to the downstream nozzle of the turbofan (figure 1c), with the objective of decreasing fan noise levels radiated towards the ground through the turbofan nozzle [15].

However, major issues can arise from these types of installations ; for example :

- structure “fatigue” problems may arise with the RFN concept;
- for the scarfed configuration, the thrust axis may be deviated and the mass-flow affected ;
- for a semi-buried engine, the proximity of the airframe surface may result in a strong distortion of the intake flow ;
- for extreme configurations, the possible ingestion of the thick airframe boundary layer may occur.

In addition, certification issues can become critical, especially for the case of engine burst events and, for this purpose, material and energy absorption analysis must be considered.

The numerical prediction of engine acoustic installation effects is very complex, because it requires the combination of:

- the simulation of the noise generation by the engine and the near-field acoustic propagation of this noise in a complex flow ;
- the acoustic scattering over the aircraft surface and propagation up to the observer ;
- finally, the possible strong coupling between the two previous approaches, through the retroaction of the acoustic field on the noise generation mechanisms.

One possible simplification, applied in this paper, is to rely on a hybrid methodology, which deliberately neglects this possible retroaction (figure 2). The successive steps are the following:

Step 1 - The noise generation and propagation from the isolated engine up to a near-field control surface is predicted, for example, by using an accurate CAA (Computational AeroAcoustics) solver.

Step 2 - The acoustic field collected on the control surface is used to compute an incident acoustic field on the aircraft scattering surface and at the observer position, for example, by the use of a Kirchhoff method (note that this step is also able to provide the noise radiated by the isolated engine to a far-field observer).

Step 3 - The acoustic field scattered by the aircraft surface is computed by solving a Helmholtz equation (possibly accounting for the convection by a uniform mean flow) with specific surface boundary conditions, which can be done by another acoustic method, for example based on the BEM (Boundary Element Method).

Step 4 - Finally, the total acoustic field at any observation point is the sum of the incident and the scattered fields.

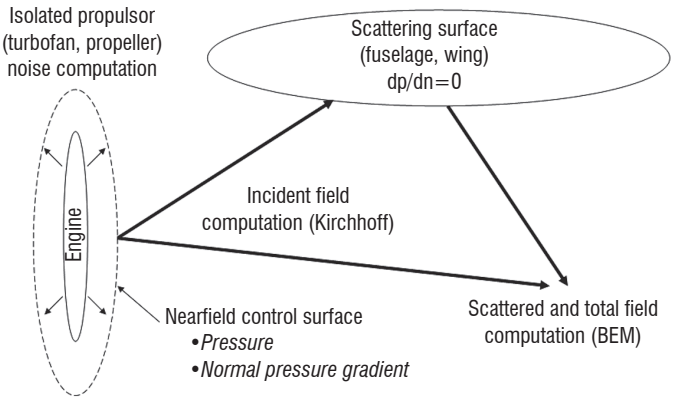

Figure 2 - Simplified strategy based on a hybrid methodology for the prediction of engine noise installation effects

For several years, Airbus, SNECMA and Onera have collaborated on the development of such hybrid methodology for the prediction of isolated/installed fan noise propagating in the aft direction [16, 17].

This collaboration recently continued within the framework of the NACRE and OPENAIR programs, with the objective of validating this hybrid methodology against available fan noise experimental databases. In NACRE, the acoustical measurements were collected during Onera's above-mentioned CEPRA19 campaign, in which a turbofan nacelle equipped with a TPS (Turbine Powered Simulator) was tested in RFN configuration, with an Airbus model at scale 1/11 (figure 3). The NACRE program ended in early 2010, but the collaboration on this approach between Airbus and Onera continued using their own funding. Regarding the OPENAIR program, an experimental campaign took place in 2012, at QinetiQ, in the NTF open-jet acoustic wind tunnel. In this campaign, fan noise was simulated with in-duct loudspeakers rings, instead of the TPS used in NACRE.

NACRE fan noise experiment

The NACRE experimental fan noise campaign was conducted in CEPRA 19 (figure 3). Realistic interaction fan noise generation was performed by using a scaled TPS placed along the WT axis and attached to the side wall of the chamber by a symmetrical wing profile covered by acoustic absorbing foam. Real aircraft geometry (a commercial single aisle Airbus aircraft model at scale 1/11) was used to account for the installation effects. The aircraft model was mounted on a trolley support allowing 3D positioning around the TPS position. This set-up was ideally designed to allow the validation of the numerical prediction of a real fan noise source with a complex scattering object. The test matrix included the survey of three TPS regimes (approach, cutback and take-off conditions) and various external flow Mach numbers and relative positions of the aircraft w.r.t. the TPS. The influence of individual airframe components (wing, empennage) and also parameters such as the slat and flap settings were also evaluated.

In this work, we only considered the configuration corresponding to the approach regime and the $M = 0$ case, either isolated or installed with the complete aircraft model with retracted slats and flaps. Other cases with non-zero external flows were not considered because, at that time, the BEM solver BEMUSE was not able to account for a non-zero mean flow. Since then, this capability has been implemented using the formulation proposed by [18].

The characterization of the acoustic field inside the bypass duct of the nacelle was performed using an azimuthal array located just upstream of the exhaust, made of 54 Kulite unsteady pressure transducers. The far-field acoustic measurements mainly relied on a circular array with a diameter of 5 m containing 48 microphones (azimuthal step 7.5°), circling the wind tunnel open jet, and centered on the jet axis. This circular array could be moved in the axial direction over a distance of approximately one meter, providing the acoustical field along a circular cylinder.

Figure 3 (bottom) shows typical results obtained with the circular array of Kulite wall pressure sensors located inside the nacelle. On the upper plot, the RMS pressure at the BPF (Blade Passing Frequency) measured by the sensors show strong oscillations in the azimuthal direction, over an amplitude larger than 10 dB. These oscillations of the RMS pressure are generated by the non-axisymmetry of the bypass duct, and especially by the bifurcation, which generates azimuthal standing waves by interaction with spinning modes. The lower plot displays a decomposition in azimuthal modes, also at the BPF, of this wall pressure field. The strongest mode ($m = -8$) corresponds to the fan-OGV interaction mode.

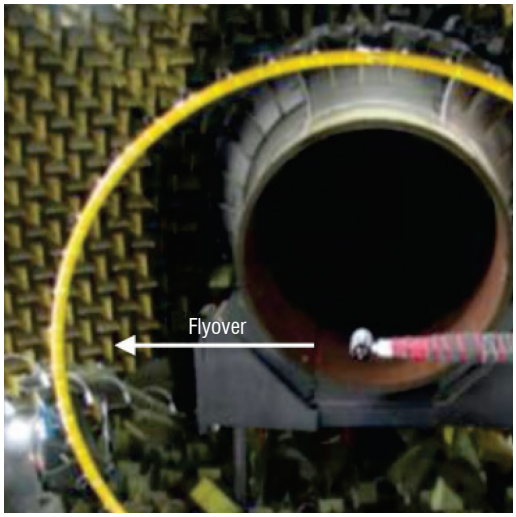

a) isolated TPS with the ϕ 5 m circular microphone array

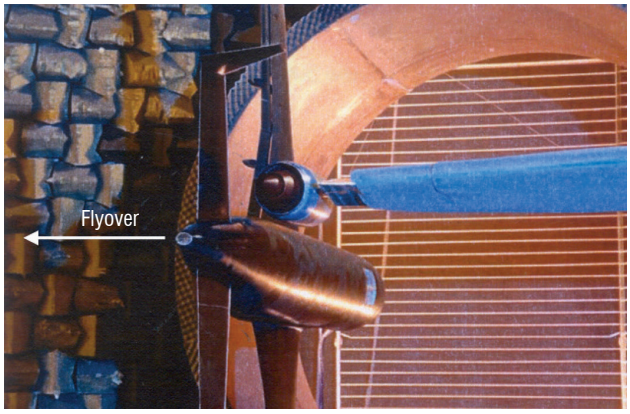

b) TPS in RFN configuration with the aircraft model

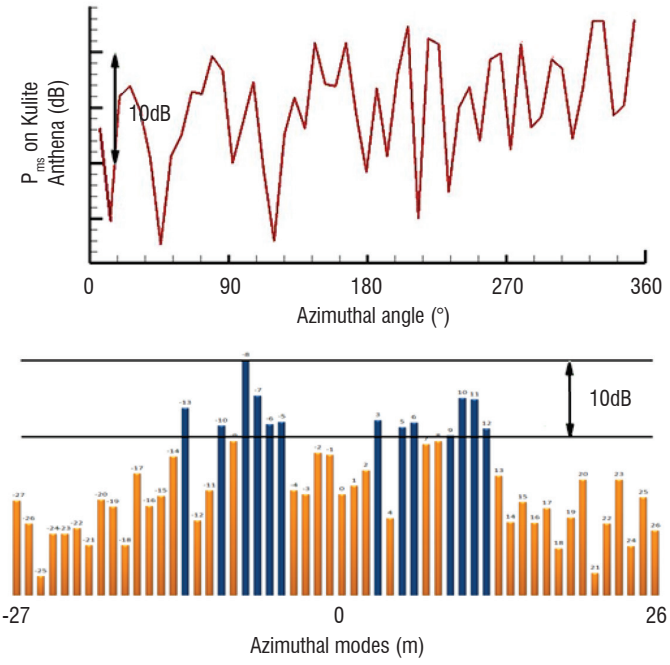

c) Wall pressure fluctuations at the BPF measured by the internal array of Kulite transducers located inside the bypass duct. Top: RMS on each Kulite sensor. Bottom: azimuthal Fourier transforms

Figure 3 - Views of the NACRE experiment in CEPRA 19

Figure 4 (top) compares the far-field RMS pressure field measurement at the BPF, for the TPS either isolated or installed with the aircraft model, measured with the circular array of diameter 5 m displaced in the axial direction. In these plots, the bifurcation and the pylon of the TPS are oriented at the azimuthal angle of 180°, whereas the flyover direction, which is mainly of interest for aircraft noise, is located at 0° (mixed dash-dot lines). Note that all measurements are projected on a sphere of radius 6 m. The plot on the right side of the figure compares the RMS pressure in the flyover direction, showing a shielding factor by the aircraft of about 10 dB.

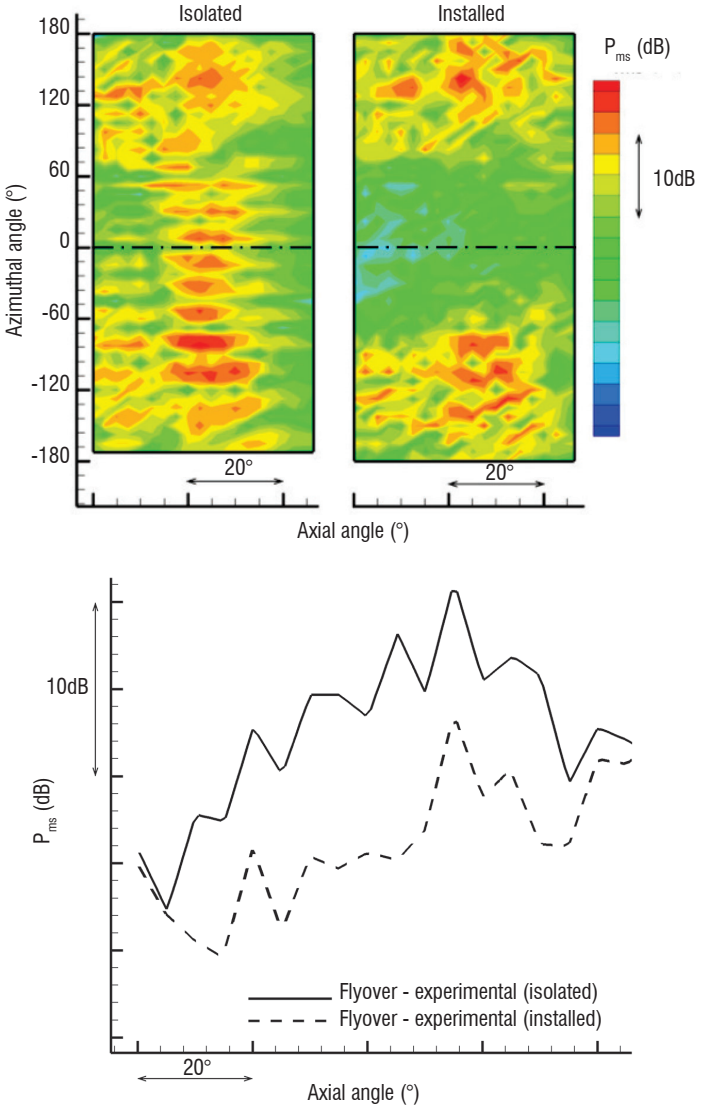

Figure 4 - RMS sound field of the isolated/installed TPS, measured by the circular array of 48 microphones (diameter 5 m, extrapolated to r = 6 m). Top : azimuthal/axial distribution. Bottom: cut in the flyover direction.
Note: the internal bifurcation is located at the azimuthal angle 0°/360°

Numerical methodology based on experimental measurements

Selection of numerical methods

Returning to the 4-step process described in § "Introduction", numerical methods that meet the constraints must be selected at each step.

The first step is the propagation of fan noise from the fan plane, inside the nacelle secondary duct and nozzle, then through the external highly non-homogenous coaxial mean flow, up to a near-field control surface. Even though the engine is considered as "isolated" at this stage, this is a very challenging computation that must take into account significant acoustic refraction effects, due to the strong velocity and temperature gradients in this region. This constraint assumes that Euler equations are solved locally on a grid with sufficient resolution to propagate acoustic waves without dissipation and realistically model the flow gradients, which involves relying on CAA techniques, for example solving (non-linearized) Euler equations in perturbations with high-order finite difference scheme on block structured grids.

Steps 2 and 3 assume that an incident field can be derived (from step 1) over the scattering surface, an then a scattered field can computed from this incident field using boundary conditions on the surface. The CAA technique used for step 1 could obviously provide this result, at the price of including the scattering surface in the CAA grid, which would be too expensive in most cases and, moreover, unnecessary as long as the flow gradients can be neglected at the vicinity of the scattering surface, which is often the case. With these restrictions, integral methods are much more straightforward, for example the Kirchhoff integral for the computation of the incident field and the BEM for computing the scattered field.

sAbrinA-V0 solver

The initial CAA computations of the fan noise propagation through the non-uniform mean flow in the by-pass duct, are achieved with Onera's CAA parallelized solver sAbrinA-V0 [19], which solves, in the time domain, the full (non-linear) Euler equations in conservative and perturbation form, using high-order finite difference and spatial filtering schemes (6^{th} order spatial derivatives and 10^{th} order filters) and RK3 Runge-Kutta time marching scheme, on structured multiblock meshes. sAbrinA-V0 benefits from Onera's significant progress in High Power Computing provided by a parallel supercomputer, SGI Altix ICE 8200 EX, equipped with Intel "Nehalem-EP" quadriprocessors at 2.8 GHz, with a total of 3072 nodes.

BEMUSE solver

Modern numerical methods for the solution of BEM equations provide an approximation of the solution, by solving a perturbed linear system where the associated matrix is easier to handle. Onera's BEM BEMUSE [20] code uses a Brakhage-Werner [21] integral formulation, an algebraic approach of the kernel approximation based on the Adaptive Cross Approximation (ACA) method initially published by Bebendorf [22] for asymptotically smooth kernel operators, and improved by Grasedyck [23]. Thanks to the algebraic approach, the ACA method can be used as a "black box", computing a low–rank approximation of appropriate matrix blocks, independent on the kernel operator. The size of the final matrix to be solved, within the above considerations, is largely diminished from an N^2 to an N•logN order.

Computational global parameters

Semi-buried engine for the Payload Driven Aircraft concept

The main entry data are grids containing the geometries and the RANS mean flows computed by Onera's Applied Aerodynamics Department. One of the objectives of these aerodynamic computations was to evaluate the influence of the "offset level", corresponding to the vertical distance between the fuselage level and

the lowest position of the engine fan plane, divided by the fan diameter. Two different nacelle shapes (figure 5, left) have been designed by Onera, with the offset level targets of 8 % (shape 1) and 15 % (shape 2). This "offset level" difference induces slight differences in the upper lip shape. For both shapes, the fan plane is located at $x = 1.23R$ (where R is the fan radius or internal nacelle radius) from the inlet lip. For both nacelle shapes 1 and 2, CAA structured multi-block grids were derived from the RANS grid with specific criteria based on homogeneous cell size, depending on the acoustic wave length to be propagated. The grid is adapted to acoustic "in-flow" computations. In these cases, the flight Mach number considered is rather low (approach, $M = 0.25$), but the flow inside the nacelle can be much higher (up to $M = 0.8$ in the fan plane), so the acoustic waves in the nacelle travel against a strong adverse flow with very small apparent acoustic wavelength. This leads to a considerable increase in the grid resolution in this region. The final grid was obtained by using the mesh generator GAMBIT and contains 4.9 millions points.

Rear Fuselage Nacelle concept

CAA Computation

The 3D acoustic mesh used for these computations is presented in Figure 5 (center), showing the split blocks for parallel computing on 256 processors. The geometry of the aft TPS with its axisymmetrical non-homogenous mean flow was provided by Airbus. sAbrinA-V0 is used to compute the propagation of fan noise modes, through the nacelle bypass duct and the turbofan exhaust, up to a cylindrical control ("Kirchhoff") surface surrounding the engine. In order to "acoustically" take into account the three-dimensionality of the by-pass duct, an internal bifurcation was added inside the duct, between the fan plane and duct exit, with the same axial extent as in the actual TPS. For simplicity sake (the mean flow remains axisymmetrical), the bifurcation was modeled as a rigid wall (Wall Boundary Condition) with zero thickness. The final grid contains a total of approximately 10 million cells. Each computation was performed on 256 processors, the steady state being reached after 60 acoustical periods in about 10 CPU hours.

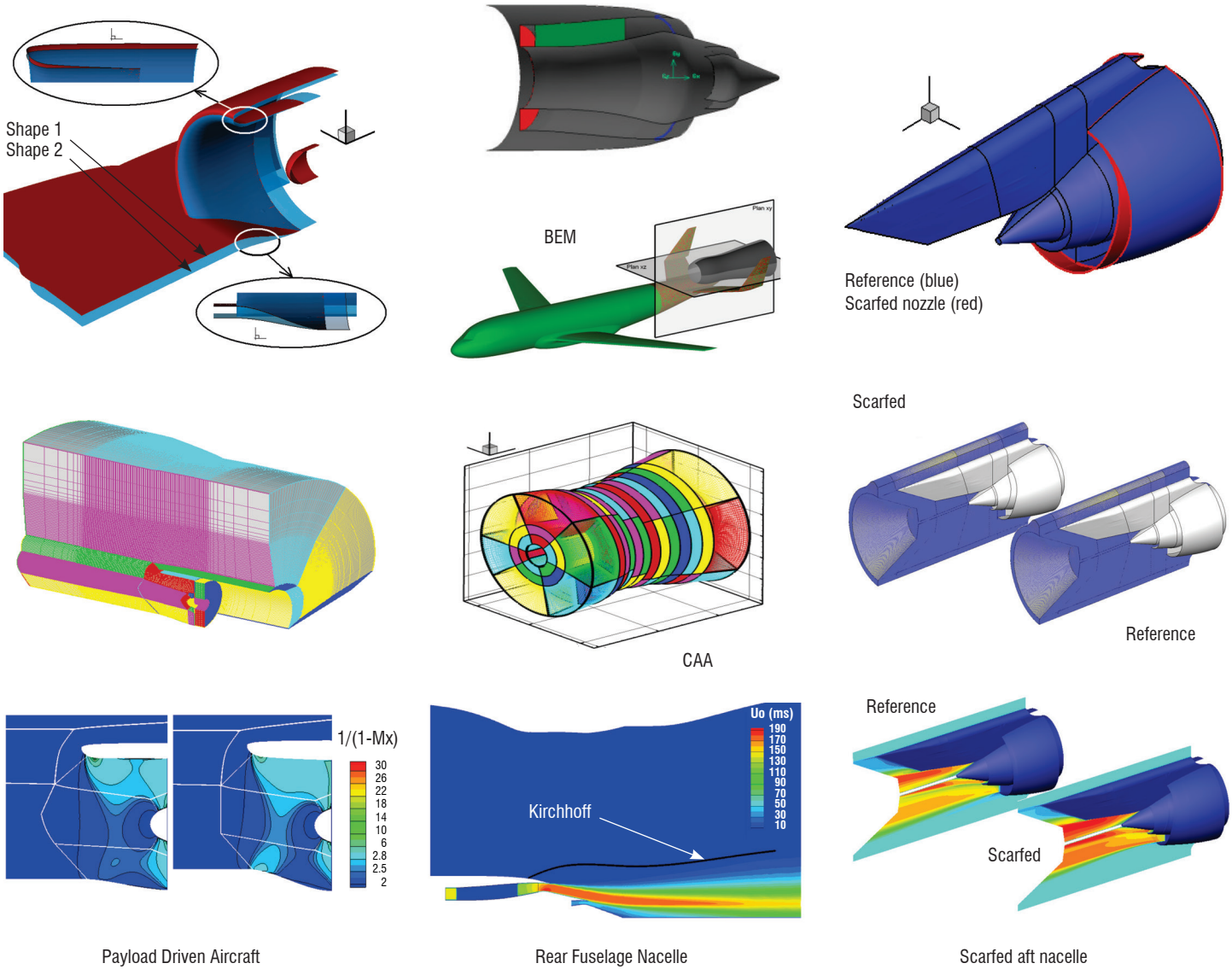

Figure 5 - From top to bottom: (1) geometries, (2) acoustical grids and (3) mean flows used in the CAA computations

BEM Computation

The final objective is to use Onera's BEM solver BEMUSE to compute acoustic installation effects from the acoustic fields collected on the Kirchhoff surface. The position of the control surface is critical. It must be close enough to the nozzle so that the grid stretching in the radial direction does not induce significant numerical dissipation, but not too close, in order to avoid mean flow gradients on the surface. This optimal position was generated with GAMBIT and the acoustic field for each computation was simply interpolated using the graphic solver TECPLOT. The radiation surface was discretized, within classical BEM constraints (6 p.p.w.), with an unstructured grid of about 135000 points. The objective of this work is to simulate the acoustic installation effects of the TPS in the presence of the aircraft model. Figure 5 (top, center) shows the configuration that is targeted to investigate this problem. The complete aircraft geometry is drawn in green and the control ("Kirchhoff") surface, which is used to compute the incident field, is shown in grey (corresponding to the black line in the respective CFD plot). Considering the TPS aft fan noise directivity, with a main lobe directed in the downstream direction, and with a view to considerably lighten the BEM computation, only the rear part of the aircraft (shown in green/red in figure 5, top-center) will be considered in the simulations of installation effects (note that this part contains about 25% of the elements of the entire aircraft, about 118 000 points).

Scarfed aft-fan (SAF)

The acoustical grid of the reference case for the CAA computation was designed by scaling the one described in references [24, 25] and modifying it to propagate all cut-on helicoidal modes in the outer field with at least 16 ppw (points per wavelength). The aerodynamic optimization process of the scarfed nacelle geometry was performed by SNECMA and the final configuration was proposed for the acoustical numerical computation. The scarfing of the nozzle was performed by distorting the reference CAA grid into the prescribed shape, keeping the same grid topology. The final CAA computational mesh is composed of about 24 million cells. The RANS stationary mean flow (Figure 3, right, bottom) for both configurations was also performed by SNECMA (using Onera's Navier-Stokes code *elsA*), using the same inflow conditions as for the reference case. As was expected, preserving the mass flow rate through a smaller section involves flow acceleration in the axial direction, as can be observed in figure 5 (right, bottom), where the longitudinal velocity component is presented in the symmetry plane. One interesting point is that the flow is highly accelerated in the engine axis vicinity and in the downstream part of the pylone, where the acoustical waves generated by the fan are less energetical.

Fan noise sources

In an infinite annular duct with uniform flow, any acoustic field can be decomposed as a sum of rotating mode patterns with circumferential and radial (order m and n) pressure distributions, which are the elementary solutions of the convected Helmholtz equation with rigid wall boundary conditions. For real wave numbers, the modes are "cut-on", which means that they propagate in the upstream and/or the downstream directions. Fan tonal noise is generated by rotating forces on blades and periodic load fluctuations due to the wake interaction between the fan rotor and stator and the interaction of the fan with the ingested part of the stationary non-uniform mean flow. Note that fan noise also includes a broadband noise with two main components; firstly, the interaction noise [26] due to the turbulence ingested by the rotating fan (low frequency) and secondly the trailing edge noise (or self-noise) [27] generated by the turbulent boundary layer developed on the blade (and vane) surface (high frequency). However, this broadband noise is beyond the scope of this work. In sAbrinA-v0, the modes are injected, in terms of the usual boundary condition (BC), by imposing the downstream analytical solution in fictitious cells at each time step and taking into account the phase dependency.

For the PDA concept, the acoustical cut-on modes in the fan plane were prescribed by MTU at the first harmonic of the BPF (harmonic index $n = 1$) corresponding to the normalized frequency $kR = 2\pi fR/c = 22.30$. A total number of 16 modes were injected, representing:

- the rotor/stator interaction (according to Tyler and Sofrin [28], the interaction of a fan with B blades with a stator with V vanes generates modes at the frequency n BPF with azimuthal index $m = nB+kV$ with $k = \ldots -2, -1, 0, 1, 2 \ldots$) ;
- the inflow distortion / rotor interaction. The objective of this study was to compare the acoustical noise emitted in the upward direction by both configurations (Shape 1 & 2), using a limited number of simulations. According to the computing capacities at that time, a "coherent broadband" source was used, meaning that all considered cut-on modes were accounted for together in a coherent way, with amplitudes prescribed by MTU (figure 6a).

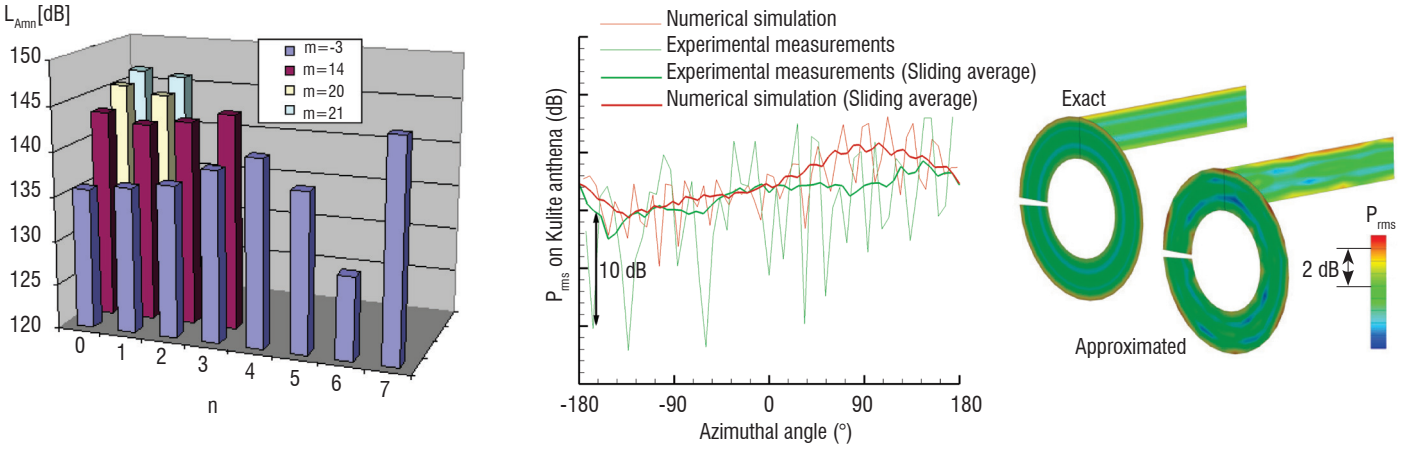

a) Payload Driven Aircraft b) Rear Fuselage Nacelle c) Scarfed aft-fan nacelle

Figure 6 - Modal content injected into the CAA computations.
From left to right: PDA (MTU predictions), RFN (reconstructed amplitudes on Kulite positions), SAF (RPMI technique)

Lately, within the RFN program, this assumption has been revisited. The acoustic radiation resulted from the un-correlated sum of "cut-on" modes and the Kulite circular array was assumed to provide a good approximation of this modal distribution. From the experimental mode detection shown in figure 2, we only retained 13 azimuthal modes within a dynamics (or level range) of 10 dB below the maximum (shown in blue in figure 3), each contributing with one or two "cut-on" radial modes ($n = 1$ and $n = 2$). Finally, 23 different computations were performed for individual modes with an arbitrary amplitude of unity. Then, for each mode, a Kirchhoff integral method was used to derive the far-field noise from the control ("Kirchhoff") double layer surface, with a section as indicated with a black line in figure 5.

The experimental in-duct detection does not provide any information on the relative power of two different radial modes having the same azimuthal order, as was the case with the MTU prescriptions. For this reason, in the final summation, the amplitudes of the $(m, 1)$ and $(m, 2)$ modes were arbitrarily adjusted to have the same acoustic power. In the process of summing the contributions of all 23 modes, each injected mode distributes its own energy to many other azimuthal (and probably radial) modes, due to the presence of the bifurcation. In order to solve this amplitude problem, the assumption of acoustic linearity was considered. The modal detection process was applied to the acoustic field radiated by all 23 individual modes and these results contributed to building a matrix problem that is used to find the source modal distribution (again, assuming that radial modes $n = 1$ and $n = 2$ have identical power) generating the experimental modal detection. These amplitudes were finally used to combine all modes and obtain estimations of the acoustic near-field and far-field. The near-field results are presented in figure 6b, in the form of the distribution of the RMS pressure at the positions of the Kulite sensors, compared to corresponding experimental data. The raw data (in thin lines) shows that there is a fair qualitative and quantitative agreement between the simulation and the measurement, although the amplitude of the oscillations is larger for the measurements. The same results are shown after applying a sliding average (thick lines), showing a good agreement (maximum difference inferior to 4 dB) between the numerical fitting and the experimental measurements.

The approach used to simulate the source in the RFN configuration was possible because the acoustical modal content was well known and the number and acoustical properties of modes were available. When experimental data on the in-duct modal content does not exist, which is the case in the scarfed nozzle configuration studied in OPENAIR, all cut-on modes must be considered, generally with amplitudes that are scaled with the assumption of evenly distributed acoustic power. This approach is often denoted as "broadband sum", although the context remains in the "tonal noise", at frequencies harmonics of the BPF. Using this approach involves an important number of numerical simulations. On the other hand, if all modes are injected simultaneously (coherent sum), strong interactions will occur between modes and the final solution may not be representative of the physics.

In this context, the RPMI (Random Phase Multi-modal Injection) method was developed [29, 30] to associate a random phase to each duct mode and to launch a limited number of independent simulations, or "RPMI events", much smaller than the original number "n" of modes, preserving the non-interaction effects. Finally, a hundred azimuthal/radial cut-on modes are injected simultaneously, their amplitude being set to obtain the same acoustic power for each mode. Using this RPMI technique, only 10 different simulations were needed to achieve duct convergence.

Results

Payload Driven Aircraft concept

For the "coherent broadband" case (figure 7, top), there is an integration (or averaging) of the effects by all superimposed modes and the level difference between both shapes is less pronounced, although in favor of shape 2. For this case, it is interesting to notice that, whatever the nacelle shape, either n° 1 or n° 2, the radiated noise field is not symmetrical with respect to the nacelle median plane $(y = 0)$. In these figures, we compare iso-contours of the RMS pressure, in horizontal and vertical planes. This very different acoustic behavior for shape 1 and shape 2 is not easily explained. It makes sense that, in the case of shape 2, the steeper slope at the lower part of the nacelle increases the proportion of acoustic energy that is reflected back, in the inward direction. These reflected waves should combine with the incident waves and produce some weak "standing waves" and a close examination of the RMS field inside the nacelles actually shows slight oscillations, which are more pronounced for shape 2 than for shape 1. However, those reflected waves are rapidly convected downstream and should fully reflect on the fan plane, where the acoustic mode is injected (a surface that acts as a rigid boundary for the waves coming from within the computational domain). One last unknown point is how much acoustic energy can be dissipated through the acoustic propagation in strong mean flow gradients.

Rear Fuselage Nacelle concept

In this part, installation effects have been computed with BEMUSE for all individual modes, from their own surface pressure fields individually computed with sAbrinA-V0 on the control surface. Then, the total (scattered + direct) acoustic field was computed as an uncorrelated sum of all mode contributions. The results are presented in Figure 7 (bottom). On the left side (bottom), we compare the experimental result to the numerical result obtained with BEMUSE. From a qualitative point of view, the comparison is satisfying, especially with a shadow zone that is shifted towards the positive azimuthal angles, due to the relative engine aircraft position. However, a detailed comparison of the levels, either observed or computed, in the flyover direction (right-side plot) shows that the computation underestimates the experimental level by 7-8 dB. Two points are still very encouraging. It can be observed that the same modulation is preserved between the simulation and the experiments, and also the same slope of directivity. Within these considerations, the engine can be now moved in its axial direction to find the optimum position. In the future, the differences between the prediction and the measurement for this axial position may be reduced by increasing the amount of cut-on modes, which is limited in this simulation, and propagating them over a more realistic internal mean flow (the bifurcation thickness is not taken into account in the CFD). The recent implementation of the mean flow in the BEM solver now allows some flow gradients to be taken into account. Finally, a supplementary effect could be added, by also taking into account the inlet fan propagation, as shown in [31].

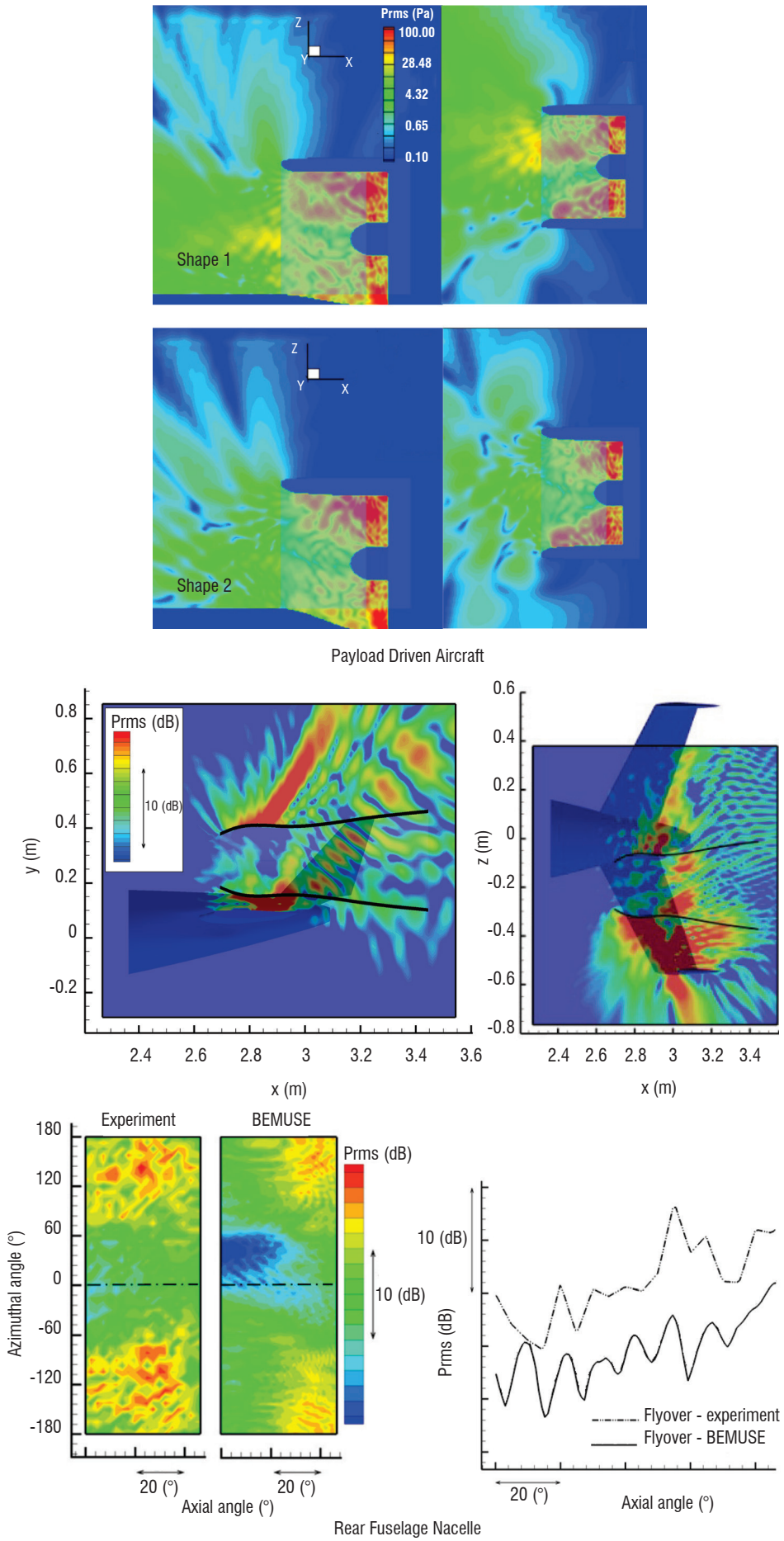

Figure 7 - Acoustical results for global evaluation of shielding effects. PDA: transversal and lateral RMS pressure distribution. RFN: noise scattered by the rear empennage (top), RMS pressure comparisons between measurements and numeric results (bottom).

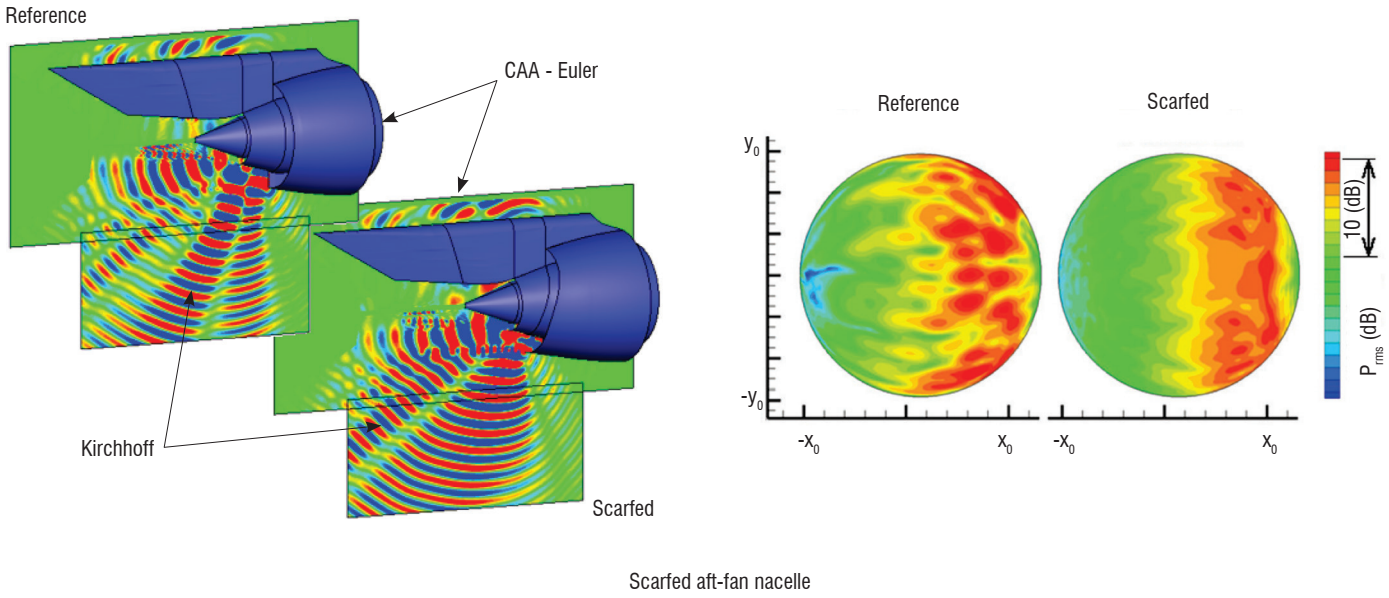

Scarfed aft-fan nacelle

Figure 8 - SAF: instantaneous view of pressure fluctuations (left), far-field directivity (right).

Scarfed aft-fan concept

The instantaneous view of near-field pressure fluctuations (figure 8, left) shows the acoustic pattern, but does not provide a global evaluation in the far-field domain. To overcome this problem, a semi-spherical observation surface was placed at a distance of about $400\ R$ from the centre of the fan exhaust plane. The far-field results were averaged in an un-correlated way between the 10 simulated RPMI events. In Figure 8 (right), the angular extension of the observation surface around the engine is represented. In this view, it is clear that the scarfed nozzle globally radiates lower levels. In order to quantify this overall noise reduction, an azimuthal integration of the RMS pressure levels over the semi-spherical surface was computed, showing that, for almost all axial angular positions, the attenuation is of between 1 and 3 dB.

Conclusions

Based on three concepts of future innovative aircraft, this work offers insight on current possibilities of numerically investigating the potential of installation effects for aircraft noise reduction. Most of the acoustical tools presented have now reached some maturity and can be successfully used for industrial cases. For all three studied configurations, the shielding effects obtained by different rigid surfaces can be considered as effective (of course, with possible consequences for other aircraft performances). For example, in the case of the scarfed nozzle, a small extension of the lower nacelle may induce significant noise reduction, according to predictions [32]. In all numerical simulations, one critical point is the description of the noise sources, an issue that is particularly addressed in this study, mainly based on assumptions driven by experimental data. Comparisons with analytical solutions or simplified configurations also allowed phenomena to be isolated and understood (see references 1-15). In the case of the RFN configuration, the proposed hybrid methodology is particularly suited to parametric studies of installation effects, especially the relative position of the engine and the aircraft. For this purpose, the NACRE fan noise experimental database remains a valuable tool for further validations of numerical codes and methods. This will also be the case in OPENAIR, where specific measurements will be devoted to the investigation of installation effects ■

Acknowledgements

The authors deeply acknowledge the helpful contributions from their colleagues at Onera, Cyril Polacsek, Thomas le Garrec and Gabriel Reboul (Aeroacoustics Team) and Xavier Juvigny (High Performance Computing Team), for fruitful discussions about the modal description of sound fields in nacelles and the computational process.

The research presented in this paper has received funding from the European Commission under OPENAIR Grant Agreement No. 234313 (FP7) and NACRE Grant Agreement No. 516068 (FP6).

The authors are grateful to Onera's focal points Franck Cléro for the OPENAIR project, Alain Julienne for NACRE Task 3.1 on the Rear Fuselage Nacelle and Jean-Luc Godard for NACRE Task 3.2 on Payload Driven Aircraft).

References

[1] D.C. MINCU, E. MANOHA, C. PARZANI, J. CHAPPUIS, S. REDONNET, R. DAVY, M. ESCOUFLAIRE - *Numerical and Experimental Characterization of Aft - Fan Noise for Isolated and Installed Configurations.* AIAA-2010-3918, 16th AIAA/CEAS Aeroacoustics Conference, Stockholm, Sweden, June 2010.
[2] S. BARRÉ, S. LEMAIRE, L. DAUMAS, V. LEVASSEUR - *Prédiction des effets de l'installation motrice sur le bruit généré par un avion d'affaire.* 43rd 3AF Applied Aerodynamics Conference, 10, 11 and 12 March 2008, Poitiers (France).
[3] J. DIERKE, R. EWERT, J. CHAPPUIS, S. LIDOINE, J. RICOUARD - *The Influence of Realistic 3-D Viscous Mean Flow on Shielding of Engine-Fan Noise by a 3-Element High-Lift Wing.* AIAA-2010-3917, 16th AIAA/CEAS Aeroacoustics Conference, Stockholm, Sweden, June 2010.
[4] E. MANOHA, D.C. MINCU - *Numerical Simulation of the Fan Noise Radiated Through a Semi-Buried Air Inlet.* AIAA Paper No. AIAA-2009-3293, AIAA/CEAS Aeroacoustics Conference, Miami, June, 2009.
[5] G. EFRAIMSSON, N. FORSBERG, J. JAN NORDSTROM - *Simulations of Acoustic Waves in a Turbo-Fan Engine Air Intake.* AIAA-2010-3717, 16th AIAA/CEAS Aeroacoustics Conference, Stockholm, Sweden, June 2010.
[6] R.H. LIEBECK, M.A. PAGE, B.K. RAWDON - *Blended Wing Body Subsonic Commercial Transport.* 36th AIAA Aerospace Sciences Meeting & Exhibit, January 12-15, 1998, Reno (NV), USA, AIAA 98-0438.
[7] B. MIALON, T. FOL, C.BONNAUD - *Aerodynamic Optimization of Subsonic Flying Wing Configurations.* 20th AIAA Applied Aerodynamics Conference, June 24-26, 2002, Saint Louis (TN), USA, AIAA 2002-2931.
[8] J. FROTA - *Novel Concepts for Aircraft Component Technologies: The NACRE European Integrated Project.* 25th ICAS Congress, September 3-8, 2006, Hamburg, Germany, ICAS 2006-1.6-1.
[9] A.P. PLAS, M.A. SARGEANT, V. MADANI, D. CRICHTON, E.M. GREITZER, T.P. HYNES, C.A. HALL - *Performance of a Boundary Layer Ingesting (BLI) Propulsion System.* 45th AIAA Aerospace Sciences Meeting & Exhibit, January 8-11, 2007, Reno (NV), USA, AIAA-2007-450.
[10] F. MONTÉTAGAUD. S. MONTOUX - *Negatively Scarfed Intake: Design and Acoustic Performance*" AIAA Paper No. AIAA-2005-2944, AIAA/CEAS Aeroacoustics Conference, Monterey, May, 2005.
[11] L.R. CLARK, R.H. THOMAS, R.P. DOUGHERTY, F. FARASSAT, C.H. GERHOLD - *Inlet Shape Effects on the Far-Field Sound of a Model Fan.* AIAA-97-1589, 1997.
[12] M.M. CURTIN M, R.P. DOUGHERTY, J.M. MCCONACHIE, M.L. SANGWIN - *WO Patent 99/61316: Biplanar Scarfed Nacelle Inlet.* 1999.
[13] J.M. ABBOTT, J.W. SLATER - *Computational Study of the Aerodynamic Performance of Three-Dimensional Subsonic Inlets.* AIAA-2001-3886, 2001.
[14] C.H. GERHOLD, L.R. CLARK, R.T. BIEDRON - *Control of inflow distortion in a scarf inlet.* AIAA-2002-2432, 2002.
[15] D.C. MINCU, E. MANOHA, G. REBOUL, S. REDONNET, S. PASCAL - *Numerical Simulation of Broadband Aft Fan Noise Radiation for Turbofan with Scarfed Nozzle.* AIAA-2011-2941, 17th AIAA/CEAS Aeroacoustics Conference, Portland, USA, June 2011.
[16] S. REDONNET, G. DESQUESNES, E. MANOHA, E. MANOHA, C. PARZANI - *Numerical Study of Acoustic Installation Effects with a CAA Method.* AIAA-Journal Vol. 48, n°5, May 2010.
[17] C. POLACSEK, S. BURGUBURU, S. REDONNET, M. TERRACOL - *Numerical Simulations of Fan Interaction Noise using a Hybrid Approach.* AIAA Journal Vol. 44, No.6, June 2006.
[18] A. AGARWAL, A. DOWLING - *The Calculation of Acoustic Shielding of Engine Noise by the Silent Aircraft Airframe.* AIAA-2005-2996, 17th AIAA/CEAS Aeroacoustics Conference, Monterey, USA, May 2005.
[19] S. REDONNET, E. MANOHA, P. SAGAUT - *Numerical Simulation of Propagation of Small Perturbation Interacting with Flows and Solid Bodies.* AIAA-Paper 2007-3493, 7th AIAA/CEAS Aeroacoustics Conference, May 2001, Maastricht (Netherlands)
[20] X. JUVIGNY - *A Fast Algebraic Boundary Integral Solver.* Eccomas Paper, Venise, 1998.
[21] V. ROKHLIN - *Rapid Solution of Integral Equations of Classical Potential Theory.* Journal of Computational Physics, 60, 187–207 (1985)
[22] M. BEBENDORF - *Approximation of Boundary Element Matrices.* Numer. Math. 86, 565-589 (2000).
[23] L. GRASEDYCK - *Adaptive Recompression of H-matrix for BEM.* Technical Report 17, Max-Planck- Institut fur Mathematik in den Naturwissenschaften, Leipzig (2004)
[24] S. REDONNET, D.C. MINCU, G. DELATTRE - *Computational AeroAcoustics of a Realistic Co-Axial Engine, Possibly Equipped with Acoustic Liners.* AIAA-2010-3717, 16th AIAA/CEAS Aeroacoustics Conference, Stockholm, Sweden, June 2010.
[25] S. REDONNET, Y. DROUN - *Computational Aeroacoustics of Aft Fan Noises Characterizing a Realistic Coaxial Engine.* AIAA Journal, Vol. 50, Issue 5, pp. 1029-1046, 2012
[26] V. CLAIR, C. POLACSEK, T. LE GARREC, G. REBOUL, M. GRUBER, P.JOSEPH - *Experimental and Numerical Investigation of Turbulence-Airfoil Noise Reduction Using Wavy Edges.* AIAA Journal, Vol. 51, No. 11, November 2013
[27] Y. ROZENBERG, M. ROGER, S. MOREAU - *Rotating Blade Trailing-Edge Noise: Experimental Validation of Analytical Model.* AIAA Journal, Vol. 48, 951-962, 2010.

[28] J.M. TYLER, T.G. SOFRIN - *Axial Flow Compressor Noise Studies.* Trans. SAE, No. 70, pp. 309-332, 1962.
[29] C. POLACSEK, G. DESQUESNES, G. REBOUL - *An Equivalent-Source Model for Simulating Noise Generation in Turbofan Engines.* J. Sound Vib., Vol. 323, Issues 3-5, pp 697-717 (2009).
[30] G. REBOUL, C. POLACSEK - *Towards Numerical Simulation of Fan Broadband Noise Aft Radiation from Aero-engines.* AIAA Journal, 2010, Vol. 48, No. 9, pp. 2038-2048.
[31] C. POLACSEK, R. BARRIER - *Numerical simulation of counter-rotating fan aeroacoustics.* 13th AIAA/CEAS Aeroacoustics Conference, Rome (Italy), 21-23, May 2007.
[32] *Scarf nozzle for a jet engine and method of using the same*. US Patent Application No. 2004/0140,397

Acronyms

ACA	(Adaptive Cross Approximation)
BC	(Boundary Condition)
BEM	(Boundary Element Method)
BPF	(Blade Passing Frequency)
CAA	(Computational AeroAcoustics)
CFD	(Computational Fluid Dynamics)
MTU	(Michigan Technological University)
NACRE	(New Aircraft Concepts Research in Europe)
OPENAIR	(OPtimization for low Environmental Noise impact)
PDA	(Payload Driven Aircraft)
RANS	(Reynolds Averaged Navier Stokes)
RFN	(Rear Fuselage Nacelle)
RMS	(Root Mean Square)
RPMI	(Random Phase Multi-modal Injection)
SAF	(Scarfed Aft-Fan)
TPS	(Turbine Powered Simulator)

AUTHORS

Daniel-Ciprian Mincu has been working as a research engineer at Onera (the French Aerospace Lab) since 2009, in the Aeroacoustics Research Unit of the Computational Fluid Dynamics and Aeroacoustics Department, on activities such as the aerodynamics, the airframe noise or the acoustic installation effects of civil aircraft. He obtained his PhD in Aeroacoustics in 2010 at Provence University (Marseilles, France). Before joining Onera, he worked as a Helicopter Operation and Maintenance Ground Technical Officer for the Romanian Air Force.

Eric Manoha obtained his PhD in Fluid Mechanics at University Pierre et Marie Curie (Paris, France) in 1993. Since 1989, he has been working as a research engineer at Onera (the French Aerospace Lab), initially in the Hydro-Acoustics Division, where he contributed to understanding and reducing submarine self-noise and propeller noise. Since 1997, he has been working on aeronautical applications in the Flow Noise Research Unit (which was included in the Aeroacoustics Research Unit in 2007), his main domain of interest being the numerical simulation of airframe noise and engine acoustic installation effects.

P. Malbéqui
(Onera)

E-mail : patrice.malbequi@onera.fr

DOI : 10.12762/2014.AL07-09

Capabilities of the High-Order Parabolic Equation to Predict Sound Propagation in Boundary and Shear Layers

The so-called parabolic equation (PE) has proved its capability to deal with the long range sound propagation as an alternative to the ray model. It was shown that the High-Order Parabolic Equation (HOPE), based on a Padé expansion, significantly increases the aperture angle of propagation, compared to the standard PE and the wide-angle PE. As a result, for the in-duct propagation it allows us an accurate prediction close to the cut-off frequency. This paper concerns the propagation using the HOPE in heterogeneous flows, including a boundary layer above a hard wall and in shear layers. The thickness of the boundary layer is some dozens of centimeters while, outside of it, the Mach number can reach 0.5. The flow effects are investigated showing the refraction effects at a propagation distance of 30 meters, up to a few kilohertz. Significant discontinuities in the directivity patterns occur in the shear layer. Comparisons with the Euler solution are considered, including configurations beyond the theoretical limits of the HOPE.

Introduction

The propagation of waves in a heterogeneous medium is a problem widely encountered in aero-acoustics for the prediction of the noise radiated by an aircraft. For instance, the fan noise radiation from the aero-engine represents a significant acoustical source during take-off. The optimization of absorbent liners on the nacelle walls and the design of the nacelle shape are efficient means to reduce the noise. The modeling of this configuration includes the liner absorption and the flow effects. To deal with such a problem in the very large frequency range of interest, from a few dozen Hertz to few a kilo-Hertz (i.e., a reduced wave number $k_0 a$ varying from 1 to 100, where k_0 is the wave-number and a is the duct radius), several complementary methods are required. Recent progress in Computational Aero-Acoustics (CAA) allows us to analyze wave propagation in a complex medium for realistic configurations, solving the Euler's equations with a high-order finite difference scheme. Among the CAA techniques, the latter are the less restrictive regarding the flow properties. They can handle a rotational flow such as the one that evolves in an exhaust jet. However, at present time, they are still limited to the low frequency range, due to the CPU time requirement. The Boundary Element Method (BEM) is applicable over almost the entire frequency range of interest, assuming a homogeneous flow in the radiated far-field [12]. As an approximation to the BEM, the fast multi-pole method allows realistic configurations in aero-acoustics to be modeled, including the shielding effects [8]. The coupled FEM/BEM and the FEM/Infinite elements can be used to take into account a potential flow [18], [1] in the low and mid frequency range. The ray-model is widely used in the high-frequency approximation. In addition to propagation in a heterogeneous medium, it has been applied for predicting the propagation of broadband fan-noise and to analyze the effect of scarfing on the radiation from an intake [11]. However, taking into account both an obstacle and a non-uniform flow is difficult, especially integrating the ray equations together with the implementation of the scattering effects and creeping waves on the obstacle surface. There is a need for the modeling of wave propagation in the high frequency range. This paper is aimed at illustrating that the High-Order Parabolic Equation (HOPE) is a candidate for computing propagation in the mid and high frequency range.

The Parabolic Equation (PE) is used in many domains, such as electromagnetic propagation, seismic waves, underwater acoustics and long range sound propagation in the atmosphere [4]. Numerical solutions of wave scattering problems in the parabolic approximation are presented in [5], for instance, the scattering of plane waves by a refraction index inhomogeneity with an elliptical cross–section and the scattering of plane waves by a viscous core vortex, which are of interest for problems such as propagation in a shear layer of a free jet. These situations may occur for internal noise radiating from the jet engine pipe, or in anechoic open wind tunnel facilities used to simulate the forward flight effects. The solutions are in good agreement with the Born approximation, including on the right hand-side an index of refraction and its derivative in the incidence direction.

This paper describes sound propagation in the presence of refractions. It starts with a brief derivation of the High-Order Parabolic Equation. Its application to propagation in boundary and shear layers is then presented. The results are compared to reference solutions.

Theoretical background

The PE is derived from the elliptic wave equation in a heterogeneous medium. Neglecting the back-scattered field, the PE uses a marching method to efficiently solve the forward propagating field. The PE involves an approximation of the square root operator, including a second order derivative of the pressure field.

The PE is currently used for outdoor propagation and underwater acoustics. Few applications are also devoted to duct acoustics, to predict the noise radiated from an aeroengine nacelle. In the past, Baumeister [3] proposed the numerical spatial marching techniques for in-duct propagation, where he examined the stability problem of the finite difference technique. Dougherty [9] developed a method based on the parabolic approximation to the convected Helmholtz equation in an orthogonal curvilinear coordinate system, to analyze the effects on sound propagation in non-uniform, softwall ducts. Nark et *al.* [15] coupled the duct propagation in the parabolic approximation with the radiation technique in the far-field based on the Ffwocs Williams-Hawkings approach.

In the past, Onera developed the PARABOLE code based on the Wide-Angle PE (WAPE) for outdoor propagation, taking into account the temperature and the wind gradients, the sound absorption by the ground and the soil topography [13]. The HOPE is based on the Padé expansion, using a high order to approximate the square root operator. The theoretical background of the HOPE was analyzed by Bamberger et *al.* [2]. It has been used by Collins [7] for underwater acoustics in presence of an elastic bottom and by Malbéqui [14] for duct acoustics, to take into account scattering effects at very large angles, allowing the propagation close to the cut-off frequency to be predicted accurately. This latter work has also shown the interest and the capabilities of the PE for applications on the aeroacoustics problems and has motivated this study dealing with the propagation in heterogeneous flows.

Wave equation in a heterogeneous medium

It is not straightforward to appreciate the validity and the limitations of the PE. Making use of reference cases and of increasing progress in CAA to solve the Euler's equations, it is convenient to examine its validity domain.

Starting from the Lighthill equations and assuming a medium characterized by velocity fluctuations much smaller than the sound celerity $(u/c_0 << 1)$, temperature fluctuations much smaller than the ambient temperature $(T'/T_0 << 1)$ and a low mean flow Mach number $(M_0 = u_0/c_0 << 1)$, the propagation of a weak acoustic field in the medium may be described by the following wave equation [5]:

$$\Delta p - \frac{1}{c_0^2}\frac{\partial^2 p}{\partial t^2} = -\frac{\partial}{\partial x_i}\left(\frac{T'}{T_0}\frac{\partial p}{\partial x_i}\right) - 2\rho_0 \frac{\partial^2 u_i v_j}{\partial x_i \partial x_j} \qquad (1)$$

where T_0, ρ_0, c_0 are the mean temperature, density and sound velocity, T' and u_i represent the temperature and velocity fluctuations in the medium, and P and v_j are the perturbations associated to the acoustic field.

In the case of the propagation of a monochromatic sound field ($k_0 = \omega/c_0$ with $a\,exp^{(-i\omega t)}$ time dependence) in an almost time independent medium, Eqn. (1) is transformed into an elliptical wave equation.

Parabolic equation

We consider the sound propagation in two-dimensional cylindrical coordinates (r, z), where r is the range and z is the altitude. For compactness, the linear partial differential $[P]$ and $[Q]$ operators are introduced:

$$[P] = \frac{\partial}{\partial r} \qquad (2a)$$

$$[Q] = [1+X]^{1/2} \qquad (2b)$$

$$[X] = \left[N^2 - 1 + \frac{1}{k_0^2}\frac{\partial^2}{\partial z^2}\right] \qquad (2c)$$

Assuming small variations of the index of refraction $N = c_0/(c+u_r)$ along the main direction of propagation , where u_r is the horizontal component of the flow velocity, after a certain amount of algebra, the elliptical wave equation can be factored into forward and backward propagating components :

$$[P + ik_0 Q][P - ik_0 Q]\,p = 0 \qquad (3)$$

The paraxial approximation consists in neglecting the backward field. The pressure field P is written in the form $p(r,z) = \psi(r,z)\exp(ik_0 r)$, using a plane wave assumption, $\exp(ik_0 r)$ and an envelope function with slow variations with respect to the phase of the wave, $\psi(r, z)$. Thus, equation (3) can be transformed into :

$$[P]\psi = ik_0[Q-1]\psi \qquad (4)$$

Finally, to obtain a parabolic equation, the square root operator Q is approximated. The simpler approximation, based on the Taylor expansion of the first order in X, provides the standard PE [10]. The High-Order Parabolic Equation (HOPE) is derived, using an approximation of Q with a Padé expansion of order n :

$$[Q] = \left[1 + \sum_{j=1}^{n} \frac{a_{j,n}X}{1+b_{j,n}X}\right] + O(X^{2n+1}) \qquad (5)$$

When n equals 1, the so-called wide-angle parabolic Equation proposed by Claerbout is obtained [6].

Numerical method

The PE is solved using a finite difference technique and a Crank-Nicholson scheme. We consider $\Psi^l{}_m$ the field at point $(l\Delta r, m\Delta z)$, where Δr and Δz denote the steps with respect to r and z. The second derivative $\partial^2/\partial z^2$ is estimated with a central difference of order $O(\Delta z^2)$. At each marching step, from $l\Delta z$ to $(l+1)\Delta r$, the discretization of the PE leads to a linear tri-diagonal system. For its numerical implementation, the HOPE associated to the Padé expansion

of order n is transformed into a set of n successive PEs. For compactness, we set :

$$L_{j,n} = \frac{a_{j,n} X}{1 + b_{j,n} X} \tag{6}$$

and the HOPE becomes

$$[P]\psi = ik_0 \left[\sum_{j=1}^{n} L_{j,n} \right] \psi \tag{7}$$

Applying the Cranck-Nicholson finite difference scheme on the P operator, Eqn. (7) can be transformed into a set of n successive PEs, using the alternating directions technique. The j^{th} PE is written as:

$$\left[1 - ik_0 \frac{\Delta r}{2} \sum_{j=1}^{n} L_{j,n} \right] \psi^{l+j/n} = \left[1 + ik_0 \frac{\Delta r}{2} \sum_{j=1}^{n} L_{j,n} \right] \psi^{l+(j-1)/n} \tag{8}$$

The first PE, when $j = 1$, makes use of the known field y^l at range r, and the last one, when $j = n$, provides the expected field ψ^{l+1} at the range $r + \Delta r$.

Boundary conditions

For the numerical implementation of the PE, a Gaussian function is generally used as the starting field, at $r = r_0$. This reduces the aperture angle of the field, in agreement with the paraxial approximation. Using the HOPE, allowing a larger aperture angle of propagation, a spherical radiation from a monopole source can be used (in presence of the image source for the configuration of the boundary layer above a wall).

Two techniques are available to avoid artificial numerical reflections in the upper part of the mesh, at $z = z_{Max}$: to fix the wave impedance of the field on the boundary, or to mesh additional absorbing layers. The first one has been successfully applied for the long range sound propagation in the atmosphere. The wave impedance of the acoustics field, at $z = z_{Max}$, is obtained from the pressure and acoustical velocity, approximated from the solution of spherical waves in a homogeneous medium. In comparison with the absorbing layers, this reduces the mesh size and the CPU time, but for the configurations of interest in this paper with significant gradients it is not efficient. The second technique, with a sponge domain, is applied. Its thickness corresponds to about 50 % of the domain where the sound field is computed. In practice, in the absorbing layers, we add an imaginary part $ig(z)$ to the real wave-number k_0, where $g(z)$ is proportional to z^2, introducing a damping of the field according to a law $exp(-g(z))$.

Using the PE, no boundary condition is required at the end of the mesh, $r = r_{Max}$, avoiding here the tricky problem of the implementation of a non-reflective boundary condition.

Propagation in a boundary layer

For the Euler solution, the code Sabrina developed by Onera including a high-order finite difference scheme is used [17]. The mesh is regular in the domain of interest and stretches in a sponge region to avoid artificial numerical reflections on the boundaries. The solution is time dependent, with a time step Δt of 6.10 $^{-5}$ s. A few millions of grid points are required to simulate the propagation up to 1 kHz, in a range propagation of 30 meters, corresponding to about one hundred acoustical wavelengths, and an altitude of 15 meters.

For the PE solution, the spatial steps in both vertical and horizontal directions are of about a tenth of the wavelength, and the Padé number is 5.

Figures 1, 2, 4 and 5 (next page) compare the PE and the Euler solutions, for various flow conditions. The pressure is plotted in a vertical plane $(0, r, z)$ in decibels and referenced to 0 dB at the distance of 1 m from the point source. It must be noted that, for the Euler method, the point source in the fluid is approximated by a normalized Gaussian-distribution [16], while for the PE a starting field modeling is considered. As a result, level differences are observed very close to the source between the PE and Euler solutions.

The PE and the Euler solutions are plotted in figures 1 and 2 for a Mach number 0.01 and 0.5, in the case of a homogeneous flow. The pressure is plotted in a vertical plane $(0, r, z)$ in decibels. A quite good agreement is shown, including the expected interference pattern between direct and reflected fields (a good agreement is also found with the analytical solution derived from the direct field and reflected fields).

For the sound propagation in the boundary layer, the Mach number profile is defined by : $M(z) = M_0 z/(z + \alpha)$, where M_0 represents the Mach number limit when z goes to infinity and M_0/α is the slope of the profile at $z = 0$ (figure 3).

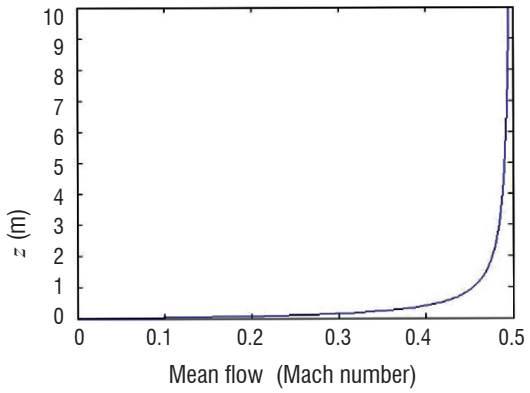

Figure 3 - Profile of the boundary layer above a wall : $M_0 = 0.5$, $\alpha = 0.1$.

Figure 4 shows the directivity pattern in presence of the boundary layer $(M_0 = 0.5, \alpha = 0.1)$. The point source is located at 4 m above the wall, where the gradient of the flow velocity is weaker, so no significant difference is observed between the uniform and the heterogeneous configurations. However, as expected with refraction, the energy tends to be bent towards the wall. A satisfactory agreement between the two solutions is obtained, while the flow velocity and its fluctuations are beyond the theoretical PE assumptions.

Figure 5 illustrates the comparisons at 2 kHz in presence of the boundary layer, where a satisfactory agreement between the Euler and the PE solutions is found.

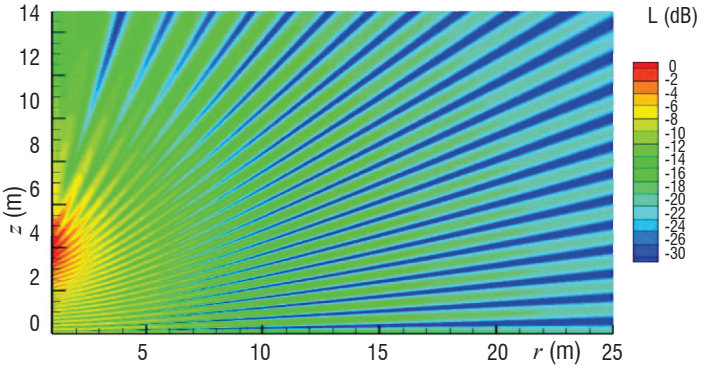

a) Parabolic solution

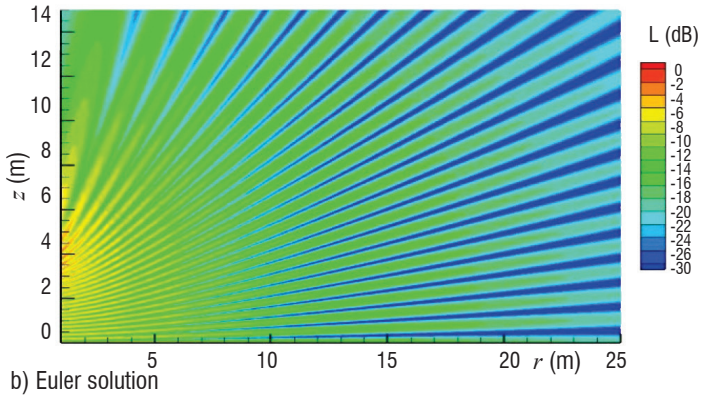

b) Euler solution

Figure 1 - Propagation above a rigid wall, in a uniform flow, $M = 0.01$, f = 1 kHz

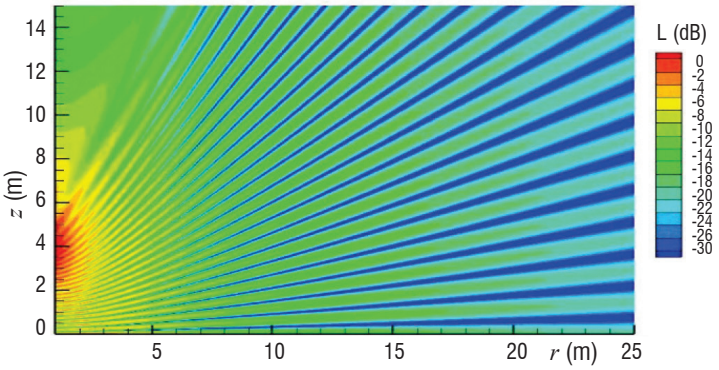

a) Parabolic solution

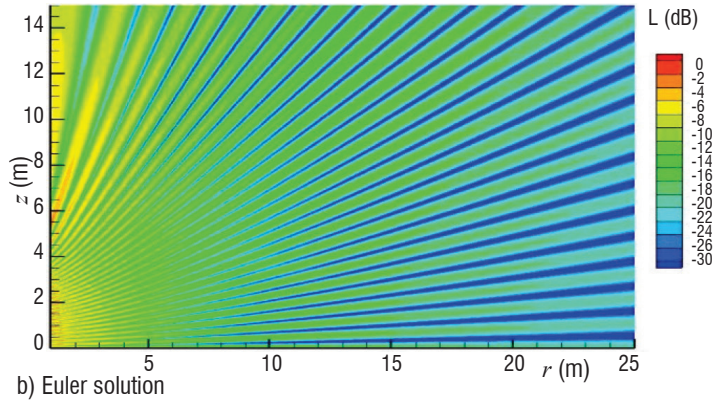

b) Euler solution

Figure 2 - Propagation above a rigid wall in a uniform flow, $M = 0.5$, f = 1 kHz

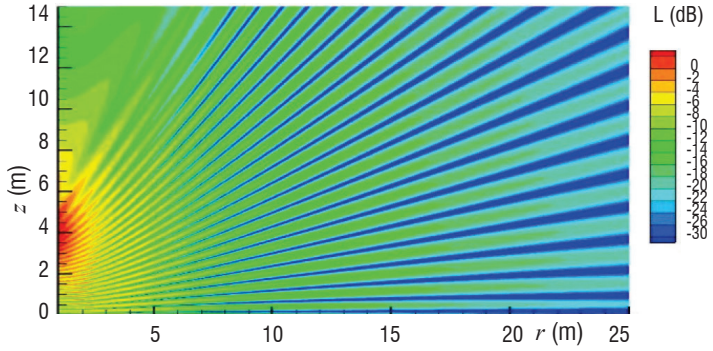

a) Parabolic solution

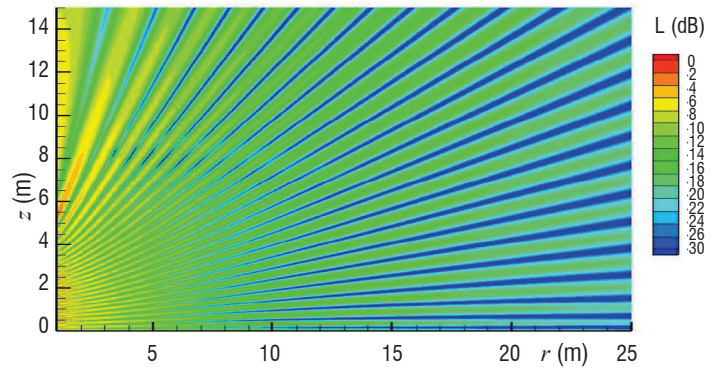

b) Euler solution

Figure 4 - Propagation above a rigid wall in a boundary layer $M_0 = 0.5$, $\alpha = 0.1$, f = 1 kHz

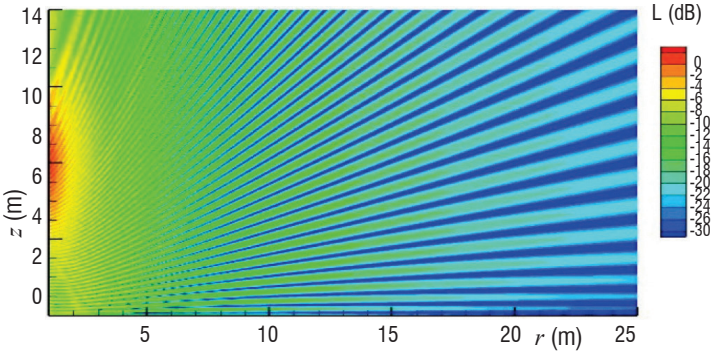

a) Parabolic solution

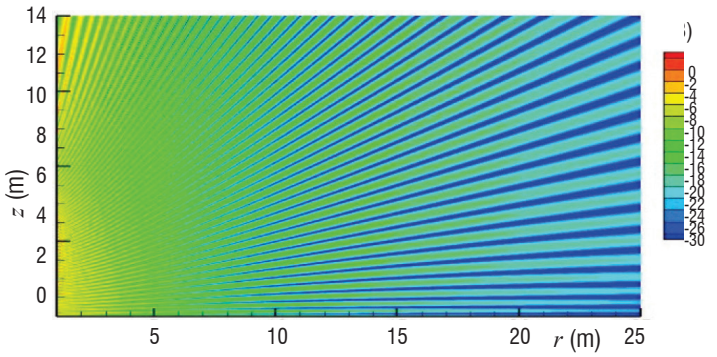

b) Euler solution

Figure 5 - Propagation above a rigid wall, in a boundary layer $M_0 = 0.5$, $\alpha = 0.1$, f = 2 kHz

Propagation in a shear layer

For the propagation in the shear layer, the Mach number profile is defined by :

$$M(z) = M_0 - M_0^- z/(z-\beta), \text{ if } z < 0 \quad (9a)$$

$$M(z) = M_0 + M_0^+ z/(z+\beta), \text{ if } z > 0 \quad (9b)$$

where M_0^- and M_0^+ represent the Mach number limits when z goes to ± infinity, M_0 equals $(M_0^+ + M_0^-)/2$ and $M_0^{\pm}/\beta$ is the slope of the profile at $z = 0$, see figure 6.

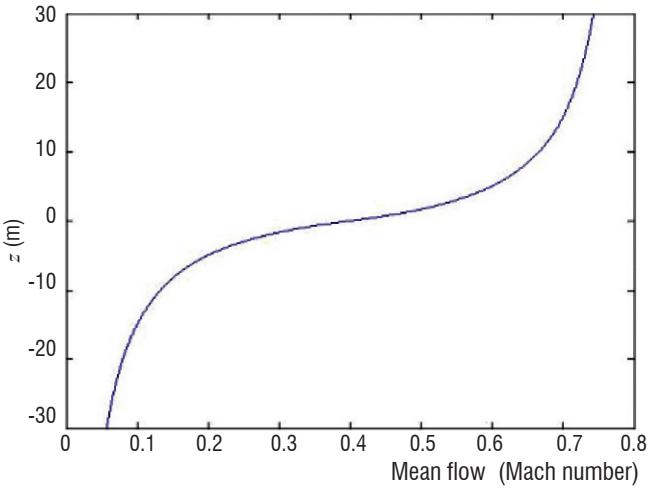

Figure 6 - Profile of the shear layer : $M_0^- = 0.0$, $M_0^+ = 0.8$ and $\beta = 0.5$

We first consider in figure 7 the propagation of a spherical wave in a homogenous medium, with the two Mach numbers 0.1 and 0.8. The directivity pattern shows the HOPE limitation at a very large aperture angle, where a false increase of the pressure level appears from about 75°, when the Mach number reaches 0.8.

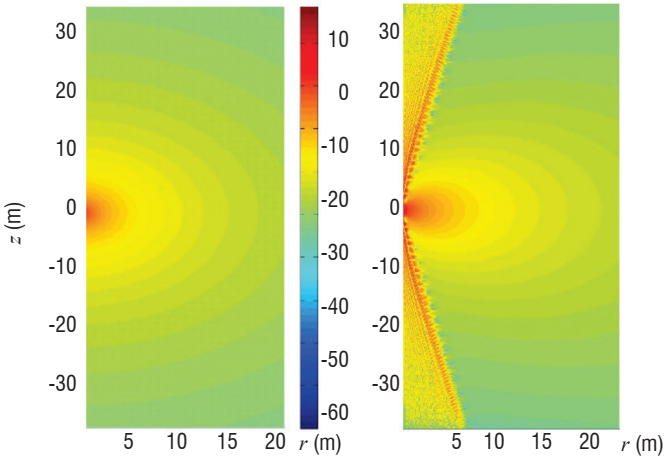

a) $M_0 = 0.1$ b) $M_0 = 0.8$

Figure 7 - Propagation in a uniform flow with the Parabolic Equation, f = 1 kHz

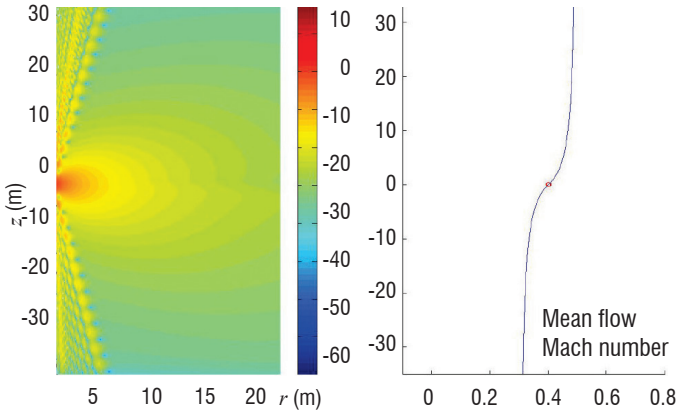

a) $M_0^- = 0.3$, $M_0^+ = 0.5$, $\beta = 5$, $z = 0$

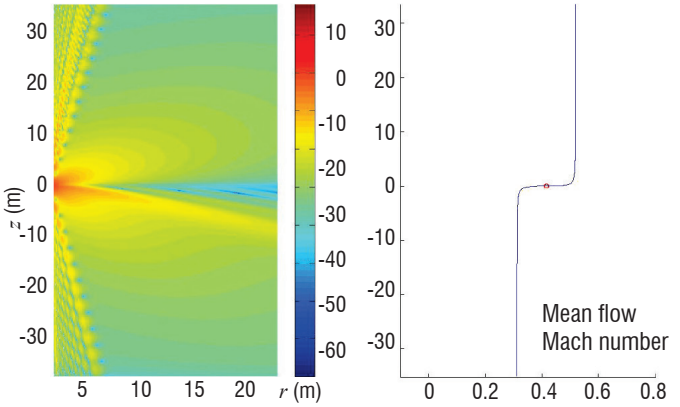

b) $M_0^- = 0.3$, $M_0^+ = 0.5$, $\beta = 0.1$, $z = 0$

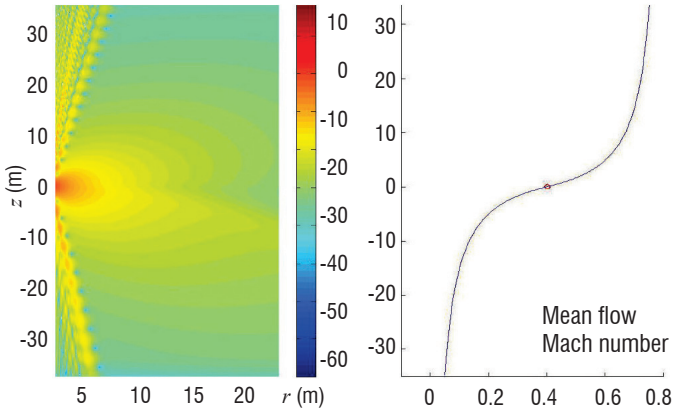

c) $M_0^- = 0.0$, $M_0^+ = 0.8$, $\beta = 5$, $z = 0$

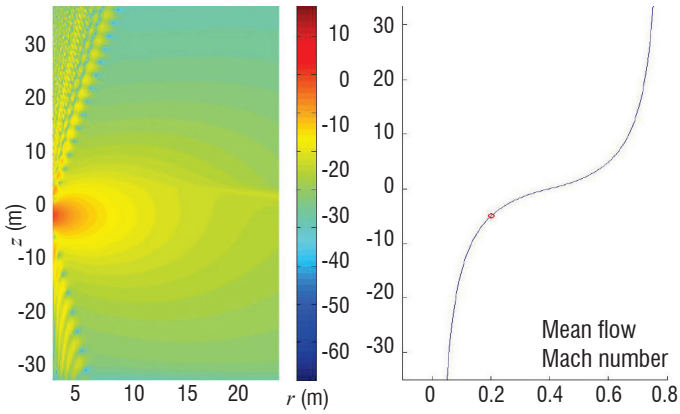

d) $M_0^- = 0.0$, $M_0^+ = 0.8$, $\beta = 5$, $z = -5$ m

Figure 8 - Propagation in a shear flow with the Parabolic Equation, f = 1 kHz

Figure 8 plots, on the left hand-side, the directivity pattern and on the right-hand side the profile of the shear flow (the red point indicates the source location). First, the pattern at the aperture angle of about 75°, where the solution is not valid arises, as observed in figure 7. Figure 8a and figure 8b show the influence of the shape of the shear layer on the sound radiation, when the source is located at the origin. It is found that the increase of the slope variations in the flow modifies the directivity pattern, in particular, it accentuates the differences between the radiation in the upper $(z > 0)$ and the lower half planes $(z < 0)$. Figures 8c and 8d compare the results with the same shear flow profile at two source locations. As expected, when the source gets closer to the origin, the wave refraction becomes more intense.

Figure 9 superimposes the PE solution (constant contour lines) and the Euler solution (scale of color levels) for a shear flow with $M_0^- = 0.4$, $M_0^+ = 0.5$, $\beta = 5$, when the source is located at $z = -5\ m$. A marked influence of the shear layer appears on the pressure field. A convenient agreement is obtained between the two solutions in the lower half plane, but differences occur on the upper half plane. It must be noted that, in addition to the constitutive equations, the problems solved with the PE and Euler are not exactly the same : as a starting field, the PE solution assumes the radiation of a spherical wave, while in the Euler solution the source radiation modified by the shear layer is no longer a spherical wave.

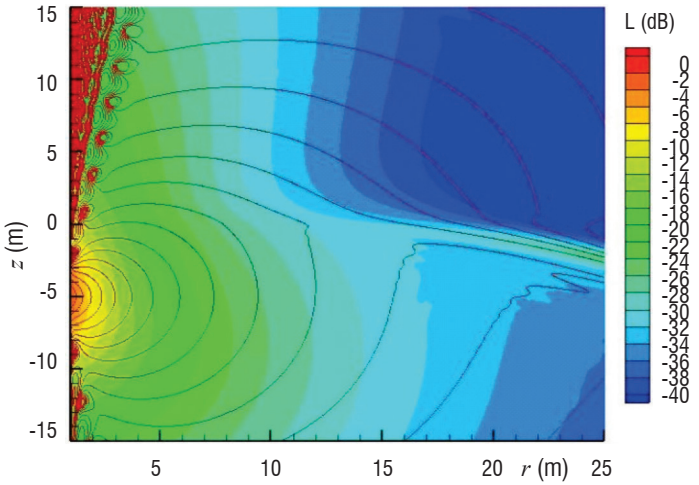

Figure 9 - Propagation in a shear flow, $f = 1$ kHz. Constant contour lines : parabolic solution ; scale of color levels : Euler solution.

Conclusion

The High-Order Parabolic Equation (HOPE) is derived from the wave equation under successive assumptions to predict sound propagation in a heterogeneous flow, within a short CPU time. It is solved with a finite difference scheme, together with the alternating direction method. The HOPE includes an approximation of a square operator using a rational function with a Padé expansion. It is then possible to overcome the limitation of the aperture angle, when using a high Padé order. It seems that neglecting the back-scattered field is not too restrictive, especially in the high frequency range. The PE being derived from the wave equation, its more restrictive assumption concerns the propagation in a potential flow. The PE results are in good agreement with the Euler solution for propagation in a boundary layer above a rigid wall. Differences between the two solutions occur in the case of the shear layer, but the starting fields are not the same. Using the PE, a boundary condition is introduced in the far-field. When solving the Euler equation, a monopolar acoustical source is modeled in the fluid and the modification of its radiation pattern in the near field by the heterogeneous flow is taken into account through the computation.

The PE saves significant computational time compared to the exact solution of the Euler equation, remaining attractive nowadays, especially for applications in the high frequency range, such as the design of a liner on the intake walls of an aeroengine nacelle and, more generally, optimization problems.

Further studies concern the parabolic computations using the Euler solution as starting field, with the application of the HOPE to more realistic geometries using an implementation with a system of curvilinear coordinates. Numerical developments are also required for the extension from 2D to 3D modelization ■

Acknowledgments

The author acknowledges AIRBUS-France for fruitful discussions and for supporting this study. He would also like to thank D. Simon-Christien, Master Student at Paris Sud XI, for his contribution in the study and D. Mincu, from the Onera CFD and aero-acoustics Department, for his guidance in providing the Euler solution.

Acronyms

BEM	(Boundary Element Method)
CAA	(Computational Aero-Acoustics)
FEM	(Finite Element Method)
HOPE	(High Order Parabolic Equation)
PE	(Parabolic Equation)
WAPE	(Wide-Angle Parabolic Equation)

References

[1] R. J. ASTLEY - *A Finite Element, Wave Envelope Formulation for Acoustical Radiation in Moving Flows*. Journal of Sound and Vibration, 103, 471-485, 1985.
[2] A. BAMBERGER, B. ENGQUIST, L. HALPERN AND P. JOLY - *Parabolic Wave Equation Approximations in Heterogeneous Media*. SIAM J. Appl. Math., 48(1), 99-128, 1988.
[3] K. J. BAUMEISTER and K. L. KREIDER - *Finite Difference Time Marching in the Frequency Domain : a Parabolic Formulation for Aircraft Acoustic Nacelle Design*. NASA Technical Memorandum 10689, 1995.
[4] PH. BLANC-BENON, L. DALLOIS, D. JUVÉ - *Long Range Sound Propagation in a Turbulent Atmosphere Within the Parabolic Approximation.* Acta Acustica united with Acustica, 87, 659-669, 2001.
[5] S. M. CANDEL - *Numerical Solution of Wave Scattering Problems in the Parabolic Approximation*. Journal of Fluid Mechanics, 19, 1978.
[6] J. F. CLAERBOUT - *Fundamentals of Geophysical Data Processing.*McGraw-Hill, New York, 1976.
[7] M. D. COLLINS - *A Higher-Order Parabolic Equation for Wave Propagation in an Ocean Overlying an Elastic Bottom*. J. Acoust. Soc. Am. 86, 1459-1464, 1989.
[8] A. DELNEVO AND S. LE SAINT, G. SYLVAND and I. TERASSE - *Numerical Methods : Fast Multipole Method for Shielding Effects*. AIAA Paper 2005-2971, 2005.
[9] R. P. DOUGHERTY - *A Parabolic Approximation for Flow Effects on Sound Propagation in Nonuniform, softwall, ducts*. AIAA Paper 99-1822, 1999.
[10] R. H. HARDIN and F. D. TAPPERT - *Application of the Split-Step Fourier Method to Resolution of Non-Linear and Variable Coefficient Wave Equations*. SIAM, Rev. 15, 423, 1973.
[11] A. J. KEMPTON - *Ray Theory to Predict the Propagation of Broadband Fan-Noise*. AIAA Paper 80-0968, 1980.
[12] P. MALBÉQUI, C. GLANDIER, C. REYNIER - *Sound Propagation in a Curved Duct.* AIAA Journal, 34, 1778-1784, 1996.
[13] P. MALBÉQUI - *Atmospheric Sound Propagation Using the Wide-Angle Parabolic Equation.* Proceedings of the. 7th Int. Symp. on Long-Range Sound Propagation, Lyon, France, 1996.
[14] P. MALBÉQUI - *Duct Propagation Using a Higher Order Parabolic Equation*. Proceeding of the 11th International Congress on Sound and vibration, Saint Petersburg, Russia, 2004.
[15] D. M. NARK, F. FARASSAT, D. S. POPE, V. VATSA - *The Development of the Ducted Fan Noise Propagation and Radiation Code CDUCT-LARC*. AIAA paper 2003-3242, 2003.
[16] C. POLACSEK, G. DESQUESNES, G. REBOUL - *An Equivalent-Source Model for Simulating Noise Generation in Turbofan Engines*. Journal of Sound and Vibration, 323, 697–717, 2009.
[17] S. REDONNET, E. MANOHA, O. KENNING - *Numerical Simulation of the Downstream Noise of 3D Coaxial Engines*. AIAA Paper 2005-2816, 2005.
[18] P. ZHANG, T. W. WU and L. LEE - *A Coupled FEM/BEM Formulation for Acoustical Radiation in Moving Flows*. Journal of Sound and Vibration, 192, 333-347, 1996.

AUTHOR

Patrice Malbéqui graduated from TELECOM ParisTech in 1983. He is at present responsible for "Environment and Propagation" in the CFD and Aeroacoustics department at Onera, where he is involved in aircraft noise modelling and in the acoustical environment of launchers at lift-off. As a specialist on sound propagation, he developed a model based on the parabolic equation together with assessment against experimental results. He has some experience in other fields, such as signal processing, duct acoustics, experiments in wind tunnels and liner optimization.